รายงานวิจัยฉบับสมบูรณ์

โครงการธรรมชาติทางกายภาพของฟังก์ชันเสริมในรูปแบบใหม่ของสมการนาเวียร์-สโตกส์

โดย กัญญุตา ภู่ชินาพันธุ์

กันยายน 2561

สัญญาเลขที่ MRG5580217

รายงานวิจัยฉบับสมบูรณ์

โครงการธรรมชาติทางกายภาพของฟังก์ชันเสริมในรูปแบบใหม่ของสมการนาเวียร์-สโตกส์

ผู้วิจัย กัญญุตา ภู่ชินาพันธุ์
ต้นสังกัด คณะวิทยาศาสตร์ มหาวิทยาลัยเชียงใหม่

สนับสนุนโดยสำนักงานกองทุนสนับสนุนการวิจัย
และมหาวิทยาลัยเชียงใหม่

บทคัดย่อ

ในโครงการวิจัยนี้ได้เสนอระเบียบวิธีเชิงตัวเลขเพื่อประมาณค่าคำตอบของการไหลแบบ axisymmetric ขั้นตอนวิธีที่ได้สามารถนำไปใช้ศึกษาโครงสร้างของปัญหาการไหลอัดไม่ได้แบบ axisymmetric ในสามมิติ ซึ่งสามารถอธิบายได้ด้วยสมการนาเวียร์-สโตกส์ ทำการแก้ปัญหาของชุดสมการนาเวียร์-สโตกส์โดยการลดรูปลงมาพิจารณาในสองมิติได้ โดยใช้รูปแบบใหม่ของสมการนาเวียร์-สโตกส์คิดขึ้นโดย Aristov and Pukhnachev (2004) ฟังก์ชันเสริมที่ปรากฏในระบบสมการดังกล่าวสัมพันธ์กับความดัน และรูปแบบใหม่ของสมการนี้มีความคล้ายกับรูปแบบของฟังก์ชัน vorticity-stream แบบจำลองเชิงตัวเลขของรูปแบบใหม่ของสมการนาเวียร์-สโตกส์สำหรับการเคลื่อนที่แบบ axisymmetric ของของไหลที่มีความหนืดแบบอัดตัวไม่ได้ อาจจะได้ผลที่แตกต่างจากรูปแบบของฟังก์ชัน vorticity-stream ซึ่งเป็นผลมาจากธรรมชาติทางฟิสิกส์ของการรวมตัวกันของฟังก์ชัน การพัฒนาขั้นตอนเชิงตัวเลขในโครงการนี้สามารถลดเวลาในการคำนวณและประยุกต์ใช้ได้กับของไหลที่มีรูปแบบที่ซับซ้อน

รหัสโครงการ: MRG5580217

ชื่อโครงการ: ธรรมชาติทางกายภาพของฟังก์ชันเสริมในรูปแบบใหม่ของสมการนาเวียร์-สโตกส์

ชื่อนักวิจัย: ดร.กัญญุตา ภู่ชินาพันธุ์ คณะวิทยาศาสตร์ มหาวิทยาลัยเชียงใหม่

E-mail Address: kanyuta@hotmail.com

ระยะเวลาโครงการ: 2 ปี

คำสำคัญ: Navier-Stokes equations, Incompressible fluid flow, Finite difference method

Abstract

In this project, we propose and analyze the numerical methods for the approximation of axisymmetric flows as well as algorithms suitable for the solution of fluid structure. This work deals with the three-dimensional axisymmetric fluid problem based on the incompressible Navier-Stokes equations (NSEs) which are solved on the two-dimensional problem. We then introduce a new form of the NSEs for axisymmtric flow derived according to Aristov and Pukhnachev (2004). The new function is introduced that is related to the pressure and a system similar to the vorticity-stream function formulation is derived. The new form of the NSEs for the axisymmetric motion of a viscous incompressible fluid offers the possibility to create a different numerical model. Because of the physical nature of the coupling function, the model may have different mathematical properties than the vorticity-stream function formulation. We account for large deformations of the fluid structure and we show how existing algorithms may be improved to reduce the computational time. Moreover, the developed method can be applied to numerical simulation for more complicated flow problems. Further investigation of developed methods is encouraged. The success can be attributed to the adequate physical nature of the auxiliary function.

Project Code: MRG5580217

Project Title: Physical Nature of the Auxiliary function in New Form of the Navier-Stokes Equations

Investigator: Dr. Kanyuta Poochinapan, Faculty of Science, Chiang Mai University

E-mail Address: kanyuta@hotmail.com

Project Period: 2 years

Keywords: Navier-Stokes equations, Incompressible fluid flow, Finite difference method

Introduction to the research problem and its significance:

Axisymmetric-rotating flows have been studied for a variety of reasons. Their technological applications are many (e.g., centrifugal pumps, cyclone separators and so on). Their importance to geophysical flows is indicated over a large range of scales (e.g., tornadoes, hurricanes, ocean circulations).

These flows have been treated by representing the Navier-Stokes equations in cylindrical coordinates. The stream function or the velocity and pressure field is used to numerical simulation in many researches. Methods of the approximate solutions of the Navier-Stokes equations have been investigated rather extensively in the past.

The practical estimation of any scheme can be rather different from the theoretical estimation because of the nonlinearity of the Navier-Stokes equations and the implicit nature of the continuity condition. This is correct specifically for very high Reynolds numbers. Different schemes perform better in different situations. There is no single scheme can be best in every aspects. The above reason causes the creation of new methods in the past several years.

In 2003, Aristov and Pukhnachev [1] proposed new form of the Navier-Stokes equations. The advantage of the new form of the equations is the following:

a) The system is weakly coupled system of two parabolic second-order equations, for which the first initial boundary value problem is stated, and one linear elliptic fourth-order equation, for which a Neumann-type problem is stated.

b) The boundary conditions for unknown functions are uncoupled, in contrast to the traditional approach, where the proper derivation of the boundary values for the vorticity is a difficult computational problem.

The Navier-Stokes equations for a viscous incompressible fluid are

$$\frac{d\bar{v}}{dt} = -\frac{1}{\rho}\nabla p + \nu \nabla^2 \bar{v} \tag{1}$$

$$\nabla \cdot \bar{v} = 0 \tag{2}$$

where p is the pressure, ρ is the density, and ν the kinematic viscosity ($\nu = \frac{\mu}{\rho}$ where is dynamic viscosity). The density and the kinematic viscosity are assumed constant.

In two-dimensional flow, the incompressible Navier-Stokes equations can be formulated by introducing two scalar variables, the vorticity ω stream function ψ, in place of the primitive variables, the velocity $\bar{v}$ and pressure p. For fluid motions parallel to the plane xy, the scalar vorticity ω is the z-component of the vorticity vector $\bar{\omega} = \nabla \times \bar{v}$, normal to the plane, namely,

$$\omega = \nabla \times \bar{v} \cdot \bar{k} \tag{3}$$

where $\bar{\omega} = \nabla \times \bar{v}$ is the unit vector normal to the plane xy.

In two-dimensional, the condition of incompressibility $\nabla \cdot \bar{v} = 0$ can be satisfied by expressing $\bar{v}$ in term of stream function ψ according to

$$\bar{v} = \nabla \psi \times \bar{k} .$$

In conclusion, taking the curl of the momentum equation (1) and make use of the fact that the curl of a gradient of a scalar is zero (so that the pressure terms go away) leads to the vorticity transport equation

$$\frac{\partial \omega}{\partial t} + \frac{\partial \omega}{\partial x}\frac{\partial \psi}{\partial y} - \frac{\partial \omega}{\partial y}\frac{\partial \psi}{\partial x} = \nu \nabla^2 \omega .$$

On the other hand, substituting the expression $\bar{v} = \nabla \psi \times \bar{k}$ in to the vorticity definition (3) gives the following Poisson equation for the stream function

$$\nabla^2 \psi = -\omega .$$

The vorticity-stream function formulation of the Navier-Stokes equations for two-dimentional flow are

$$\frac{\partial \omega}{\partial t} + J(\omega, \psi) = \nu \nabla^2 \omega , \tag{4}$$

$$-\nabla^2 \psi = \omega , \tag{5}$$

where $J(\omega, \psi) = \dfrac{\partial(\omega, \psi)}{\partial(x, y)}$.

Substitution $\omega = -\nabla^2 \psi$ into the vorticity transport equation (4) gives the following time-dependent bi-harmonic problem

$$\frac{\partial \nabla^2 \psi}{\partial t} + J\left(\nabla^2 \psi, \psi\right) = \nu \nabla^4 \psi . \tag{6}$$

The Navier-Stokes equations for a viscous incompressible fluid can be written as

$$\frac{\partial v_r}{\partial t} + v_r \frac{\partial v_r}{\partial r} + \frac{v_\theta}{r}\frac{\partial v_r}{\partial \theta} + v_z \frac{\partial v_r}{\partial z} - \frac{{v_\theta}^2}{r} = -\frac{1}{\rho}\frac{\partial p}{\partial r} + \nu\left[\nabla^2 v_r - \frac{v_r}{r^2} - \frac{2}{r^2}\frac{\partial v_\theta}{\partial \theta}\right], \tag{7}$$

$$\frac{\partial v_\theta}{\partial t} + v_r \frac{\partial v_\theta}{\partial r} + \frac{v_\theta}{r}\frac{\partial v_\theta}{\partial \theta} + v_z \frac{\partial v_\theta}{\partial z} + \frac{v_r v_\theta}{r} = -\frac{1}{\rho r}\frac{\partial p}{\partial \theta} + \nu\left[\nabla^2 v_\theta - \frac{v_\theta}{r^2} + \frac{2}{r^2}\frac{\partial v_r}{\partial \theta}\right], \tag{8}$$

$$\frac{\partial v_z}{\partial t} + v_r \frac{\partial v_z}{\partial r} + \frac{v_\theta}{r}\frac{\partial v_z}{\partial \theta} + v_z \frac{\partial v_z}{\partial z} = -\frac{1}{\rho}\frac{\partial p}{\partial z} + \nu \nabla^2 v_z , \tag{9}$$

$$\frac{1}{r}\frac{\partial(r v_r)}{\partial r} + \frac{1}{r}\frac{\partial v_\theta}{\partial \theta} + \frac{\partial v_z}{\partial z} = 0 , \tag{10}$$

where the Laplace operator in cylindrical coordinates takes the form

$$\nabla^2 = \frac{1}{r}\frac{\partial}{\partial r}\left(r\frac{\partial}{\partial r}\right) + \frac{1}{r^2}\frac{\partial^2}{\partial \theta^2} + \frac{\partial^2}{\partial z^2} ,$$

and r, θ and z denote the radial, azimuthal and axial coordinates respectively and v_r, v_θ and v_z the respective components of the velocity vector.

Axisymmetric flow is most conveniently described in terms of cylindrical coordinates (r,θ,z). The assumption of axisymmetry implies that the velocity components and pressure are functions only of r and z. Therefore, the Navier-Stokes equations for a viscous incompressible fluid in case of axisymmetric flow can be written as

$$\frac{\partial v_r}{\partial t}+v_r\frac{\partial v_r}{\partial r}+v_z\frac{\partial v_r}{\partial z}-\frac{{v_\theta}^2}{r}=-\frac{1}{\rho}\frac{\partial p}{\partial r}+\nu\left[\frac{\partial^2 v_r}{\partial r^2}+\frac{1}{r}\frac{\partial v_r}{\partial r}-\frac{1}{r^2}v_r+\frac{\partial^2 v_r}{\partial z^2}\right], \tag{11}$$

$$\frac{\partial v_\theta}{\partial t}+v_r\frac{\partial v_\theta}{\partial r}+v_z\frac{\partial v_\theta}{\partial z}+\frac{v_r v_\theta}{r}=\nu\left[\frac{\partial^2 v_\theta}{\partial r^2}+\frac{1}{r}\frac{\partial v_\theta}{\partial r}-\frac{1}{r^2}v_\theta+\frac{\partial^2 v_\theta}{\partial z^2}\right], \tag{12}$$

$$\frac{\partial v_z}{\partial t}+v_r\frac{\partial v_z}{\partial r}+v_z\frac{\partial v_z}{\partial z}=-\frac{1}{\rho}\frac{\partial p}{\partial z}+\nu\left[\frac{\partial^2 v_z}{\partial r^2}+\frac{1}{r}\frac{\partial v_z}{\partial r}+\frac{\partial^2 v_z}{\partial z^2}\right], \tag{13}$$

$$\frac{1}{r}\frac{\partial(rv_r)}{\partial r}+\frac{\partial v_z}{\partial z}=0. \tag{14}$$

The stream function is defined such that the continuity equation is identically satisfied, which gives

$$v_r=-\frac{1}{r}\frac{\partial\psi}{\partial z} \qquad \text{and} \qquad v_z=\frac{1}{r}\frac{\partial\psi}{\partial r}. \tag{15}$$

The stream function is related only to the radial and axial velocity components and independent of azimuthal velocity component. The vorticity vector in axisymmetric flow is given by $\bar{\omega}=(\omega_r,\omega_\theta,\omega_z)$ such that

$$\omega_r=-\frac{\partial v_\theta}{\partial z}, \qquad \omega_\theta=\frac{\partial v_r}{\partial z}-\frac{\partial v_z}{\partial r}, \qquad \omega_z=\frac{1}{r}\frac{\partial(rv_\theta)}{\partial r}=\frac{\partial v_\theta}{\partial r}+\frac{v_\theta}{r}.$$

Now, we introduce the function $\Gamma=rv_\theta$. Using Eq.(15) vorticity vector can be represented in the following form

$$\bar{\omega}=(-\frac{1}{r}\frac{\partial\Gamma}{\partial z},-\frac{1}{r}\mathrm{E}\psi,\frac{1}{r}\frac{\partial\Gamma}{\partial r}),$$

where

$$\mathrm{E}=\frac{\partial^2}{\partial r^2}-\frac{1}{r}\frac{\partial}{\partial r}+\frac{\partial^2}{\partial z^2},$$

and the velocity vector is

$$\bar{v}=(v_r,v_\theta,v_z)=(-\frac{1}{r}\frac{\partial\psi}{\partial z},\frac{1}{r}\Gamma,\frac{1}{r}\frac{\partial\psi}{\partial r}).$$

The association between stream function ψ and vorticity function ω_θ is $-\mathrm{E}\psi=r\omega_\theta$. In term of ψ, ω_θ, and Γ, the axisymmetric Navier-Stokes equations become

$$D\Gamma = \nu \mathrm{E}\Gamma, \tag{16}$$

$$D\left(\frac{\omega_\theta}{r}\right) = \nu\left[\mathrm{E}\left(\frac{\omega_\theta}{r}\right) + \frac{4}{r}\frac{\partial}{\partial r}\left(\frac{\omega_\theta}{r}\right)\right] + \frac{\partial}{\partial z}\left(\frac{\Gamma^2}{r^4}\right), \tag{17}$$

$$-\mathrm{E}\psi = r\omega_\theta, \tag{18}$$

where

$$D = \frac{\partial}{\partial t} - \frac{1}{r}\frac{\partial \psi}{\partial z}\frac{\partial}{\partial r} + \frac{1}{r}\frac{\partial \psi}{\partial r}\frac{\partial}{\partial z}.$$

The substitution of Eq.(15) into Eq.(13) provides

$$\frac{\partial}{\partial r}\left(\frac{\partial \psi}{\partial t} - \frac{1}{r}\frac{\partial \psi}{\partial r}\frac{\partial \psi}{\partial z} - \nu \mathrm{E}\psi\right) + \frac{\partial}{\partial z}\left(r\frac{1}{\rho}p + \frac{1}{r}\left(\frac{\partial \psi}{\partial r}\right)^2\right) = 0. \tag{19}$$

Therefore, there is a function Φ satisfying the relations

$$\frac{1}{\rho}p = -\frac{1}{r^2}\left(\frac{\partial \psi}{\partial r}\right)^2 + \frac{1}{r}\frac{\partial \Phi}{\partial r}, \tag{20}$$

$$\frac{\partial \psi}{\partial t} - \frac{1}{r}\frac{\partial \psi}{\partial r}\frac{\partial \psi}{\partial z} + \frac{\partial \Phi}{\partial z} = \nu \mathrm{E}\psi. \tag{21}$$

The substitution of Eq. (15) into Eq. (12) provides

$$\frac{\partial \Gamma}{\partial t} - \frac{1}{r}\frac{\partial \psi}{\partial z}\frac{\partial \Gamma}{\partial r} + \frac{1}{r}\frac{\partial \psi}{\partial r}\frac{\partial \Gamma}{\partial z} = \nu \mathrm{E}\Gamma. \tag{22}$$

Differentiating Eq. (20) and Eq. (21) with respect to r and z, respectively, and substituting the resulting expressions into Eq.(11), where v_r and v_z are expressed in term of ψ, we obtain

$$\mathrm{E}\Phi = \frac{1}{r^2}\left(\Gamma^2 + \left(\frac{\partial \psi}{\partial z}\right)^2\right) + \frac{2}{r}\frac{\partial \psi}{\partial r}\mathrm{E}\psi. \tag{23}$$

Since, we do not know boundary conditions for the function Φ, which is needed to Eq. (23). Aristov and Pukhnachev [1], are shown that if apply operator E to Eq. (23) the boundary condition for new fourth-order equation can be derived easily. So, applying the operator E into Eq.(23) we get a fourth-order equation

$$\mathrm{E}^2\Phi = \mathrm{E}\left[\frac{1}{r^2}\left(\Gamma^2 + \left(\frac{\partial \psi}{\partial z}\right)^2\right) + \frac{2}{r}\frac{\partial \psi}{\partial r}\mathrm{E}\psi\right]. \tag{24}$$

In term of new variables ψ, Φ, and Γ, the axisymmetric Navier-Stokes equations become Eqs. (21), (22) and (24).

A typical boundary condition consists in prescribing the value of the velocity $\bar{v}$ on the boundary

$$\bar{v}\big|_S = \bar{b}(\bar{x}_S, t), \quad t \in [0, T], \tag{25}$$

where S is the boundary of the domain V occupied by the fluid, $\bar{b}$ is given function and $\bar{x}_S \in S$. When the boundary is a solid wall in contact with the fluid, the velocity boundary value $\bar{b}$ is equal to the velocity of the wall. The condition on the tangential components of velocity is known as the no-slip condition.

The initial condition consists in the specification of the velocity field $\bar{v}_0$ at the initial time, $t = 0$, namely,

$$\bar{v}\big|_{t=0} = \bar{v}_0(\bar{x}). \tag{26}$$

The boundary velocity $\bar{b}$ must satisfy, for all $t \geq 0$, the global condition

$$\oint \bar{n} \cdot \bar{b}\, ds = 0, \tag{27}$$

which follows from integrating the continuity equation over V and using the divergence theorem. The vector $\bar{n}$ denotes the outward unit normal to the boundary S. To determine the pressure uniquely additional requirement is needed

$$p(\bar{x}_0, t) = 0, \quad \forall t \in [0, T], \quad \bar{x}_0 \in V.$$

The boundary conditions supplementing the vorticity-stream function formulation of the Navier-Stokes problem for two-dimensional flow are deduced by separating the normal and tangential components of the velocity boundary condition $\bar{v}\big|_S = \bar{b}(\bar{x}_S, t)$. Here S represents the boundary of the two-dimensional domain V. Let $\bar{n}$ denotes the outward unit vector normal to the boundary S and $\bar{\tau}$ is the unit vector tangential to S. Finally, let s be the curvilinear coordinate along the boundary S. Then, the boundary condition for the normal component

$$\bar{n} \cdot \nabla\psi \times \bar{k}\big|_S = \bar{k} \times \bar{n} \cdot \nabla\psi = \bar{\tau} \cdot \nabla\psi = \left.\frac{\partial \psi}{\partial s}\right|_S = \bar{n} \cdot \bar{b},$$

and for the tangential component

$$\bar{\tau} \cdot \nabla\psi \times \bar{k}\big|_S = \bar{k} \times \bar{\tau} \cdot \nabla\psi = -\bar{n} \cdot \nabla\psi = -\left.\frac{\partial \psi}{\partial n}\right|_S = \bar{\tau} \cdot \bar{b}.$$

The first boundary condition, after integrating its right-hand side, provides a Dirichlet condition for ψ. So that the two conditions can be written as follows

$$\psi\big|_S = a, \qquad \left.\frac{\partial \psi}{\partial n}\right|_S = b \tag{28}$$

where $a = \int_{s_1}^{s} \bar{n} \cdot \bar{b}\, ds'$ and $b = -\bar{\tau} \cdot \bar{b}$. The initial data $\bar{v}_0$ and the boundary data $a(s,t)$ are assumed to satisfy the conditions

$$\nabla \cdot \bar{v}_0 = 0, \qquad \frac{\partial a(s,0)}{\partial s} = \bar{n} \cdot \bar{v}_0\big|_S. \tag{29}$$

The initial condition for the system of equations governing ω and ψ is concerned, the initial velocity field $\bar{v}_0$ provides the following initial condition for the vorticity

$$\omega\big|_{t=0} = \nabla \times \left(\bar{v}\big|_{t=0} \right) \cdot \bar{k} = \nabla \times \bar{v}_0 \cdot \bar{k} \,. \tag{30}$$

Let R^+ be the $r > 0$ half-plane of the (r, z) plane, Ω be the bounded domain in R^+, Σ be the boundary of Ω, $Q_T = \Omega \times (0, T)$, and $S_T = \Sigma \times (0, T)$. Assume the closure $\bar{\Omega}$ of domain Ω does not contain points lying on the z axis.

The boundary conditions for the system of Eqs. (21), (22), and (24) are considered only in the case where $v_r = v_\theta = v_z = 0$ are satisfied at the boundary of the flow domain. In term of the functions ψ and Γ, these conditions are represented in the form

$$\frac{\partial \psi}{\partial n} = 0 \,, \qquad (r, z, t) \in S_T \,, \tag{31}$$

$$\psi = 0 \,, \; \Gamma = 0 \,, \; (r, z, t) \in S_T \,, \tag{32}$$

where $\dfrac{\partial}{\partial n}$ means differentiation with respect to the normal to the Σ. The boundary condition (32) can be used for Eqs. (21) and (22), respectively. The initial conditions for the system of Eqs. (21), (22), and (24) are

$$\psi = \psi_0(r, z) \,, \quad (r, z) \in \bar{\Omega} \,, \quad t = 0 \,, \tag{33}$$

$$\Gamma = \Gamma_0(r, z) \,, \quad (r, z) \in \bar{\Omega} \,, \quad t = 0 \,. \tag{34}$$

Boundary conditions for the function Φ which is redundant for Eq. (21) is derived by using condition (31). To this end, by using operator E apply into Eq. (23) provides a fourth-order equation (24). One boundary condition for Eq. (24) follows immediately from Eqs. (23), (31), and (32)

$$\mathrm{E}\Phi = 0 \,, \qquad (r, z, t) \in S_T \,. \tag{35}$$

Applying the operator $\dfrac{\partial}{\partial n}$ to Eq. (23) and using Eqs. (31) and (32), then the second condition for Eq. (24) is following

$$\frac{\partial}{\partial n} \mathrm{E}\Phi = \frac{2}{r} \frac{\partial}{\partial n} \left(\frac{\partial \psi}{\partial r} \right) \mathrm{E}\psi \,, \qquad (r, z, t) \in S_T \,. \tag{36}$$

Concluding this section, Eq. (31) follows from Eqs.(23) and (36) under the additional condition

$$\frac{1}{r^2} \frac{\partial}{\partial n} \left(\frac{\partial \psi}{\partial z} \right) \cos\varphi + \frac{\partial}{\partial n} \left(\frac{1}{r} \mathrm{E}\psi \right) \sin\varphi \neq 0 \,, \qquad (r, z, t) \in S_T \,,$$

where φ is the angle between the z axis and the normal to the Σ. If the last condition is valid for $t = 0$, it is satisfied at least for small $T > 0$.

This new form of Navier-Stokes equations can attributed to the adequate physical nature of several phenomenon such as: axisymmetric rotating flows (For example, the hard disk drive (HDD) is one of the most important components in many

computers these days and it is the primary device, which provides storages space for software and data. In today's Thailand hard disk drive industry, the demand for higher recording density and higher rotating speed has become more and more stringent and this requires a good understanding of the airflow characteristics to achieve a highly accurate head positioning).

Literature review:

Couette flow (the flow between two concentric rotating cylinders) is simplest example of axisymmetric flow can be find in any handbook of fluid mechanics (see for example [2-3]). Axisymmetric flow is a subject of much interest in many areas of engineering and has been investigated by many researchers. There have been a number of experimental and numerical studies of these flow (e.g.,[4-28]).

Escudier [11] observe the flow produced in a cylindrical container by a rotating endwall. Observations made using the laser-induced fluorescence technique are presented of the steady swirling flow produced in a closed cylindrical container completely full of fluid by rotating one endwall. The oscillatory motion in certain swirling flows is observed by Chanaud [11]. A descriptive experimental study was made in both air and water of the temporally periodic motion that occurs in the vortex whistle and cyclone separator. A comparison between the experimental visualization and numerical simulations of the occurrence of vortex breakdown in laminar swirling flows is presented by Lopez [13]. The physical mechanisms for vortex breakdown is studied by Brown and Lopez [14]

A viscous incompressible fluid flow in cylindrical container with a rotating disk at the fluid surface is numerically investigated by [4,13-18,24-28]. Inamuro, Yamaguchi, and Ogino [4] solve the axisymmetric Navier-Stokes equations using a finite-volume method. The effect of the relative directions and magnitudes of disk and container rotations are studied. The numerical simulation for solving the axisymmetric unsteady incompressible Navier-Stokes equations using vorticity-velocity variables and a staggered grid is presented by Dexun and Yanwen [16]. The numerical results are also compared with experimental data. Lopez and Shen [17], studied about an efficient and accurate numerical scheme for the axisymmtric Navier-Stokes equations in primitive variables in a cylinder. Numerical solutions of the axisymmetric flow are used to study over a range of Reynolds numbers [$10^2 - 4\times10^3$] where the flow is observed to remain axisymmetric (e.g., [5,8,17-19]). The numerical simulation of the incompressible fluid

flows the appropriate mathematical formulation of the Navier-Stokes equations may be advantageous if the choice is according to the problem domain and boundary condition.

Reference:

[1] Aristov, S.N., and Pukhnachev, V.V. On the Equations of Axisymmetric Motion of a Viscous Incompressible. Doklady Physics (2004); 49(2): 112-115.

[2] Batchelor, G.K. An Introduction to Fluid Dynamics. Cambridge Mathematical Library (2000).

[3] Marshall, J.H. Inviscid Incompressible Flow (2001). USA: Wiley Inter-Science.

[4] Inamuro, T., Yamaguchi, A., and Ogino, F. Fluid Flow in a Rotating Cylindrical Container with a Rotating Disk at the Fluid Surface. Fluid Dynamics Research (1997); 21: 417-430.

[5] Iwatsu, R. Flow Pattern and Heat Transfer of Swirling Flows in Cylindrical Container with Rotating Top and Stable Temperature Gradient. International Journal of Heat and Mass Transfer (2004); 47: 2755-2767.

[6] Levit, C. Parallel Solution of Pentadiagonal Systems Using Generalized Odd-Even Elimination. ACM (1989). 11: 333-336.

[7] Lopez, J.M., and Shen, J. An Efficient Spectral-Projection Method for the Navier-Stokes Equations in Cylindrical Geometries. Journal of Computational Physics (1998); 139: 308-326.

[8] Stevens, J.L., Lopez, J.M., and Cantwell, B.M. Oscillatory Flow State in an Enclosed Cylinder with a Rotating Endwall. J. Fluid Mech (1999); 389: 101-118.

[9] Taylor, G.I. Stability of a Viscous Liquid Contained between Two Rotating Cylinder. Philosophical Transactions of the Royal Society of London. Series A. Containing papers of a Mathematical or Physical Character (1923); 223: 289-343.

[10] Mallock A. Experiments on Fluid Viscosity. Philosophical Transactions of the Royal Society of London. Series A. Containing papers of a Mathematical or Physical Character (1896); 187: 41-96.

[11] Escudier M.P. Observations of the Flow Produced in a Cylindrical Container by a Rotating Endwall. Experiment in Fluids (1984); 2: 189-196.

[12] Chanaud R.C. Observations of Oscillatory Motion in Certain Swirling Flows. J. Fluid Mech. (1996); 21(1): 111-127.

[13] Lopez J.M. Axisymmetric Vortex Breakdown Part I. Confined Swirling Flow. J. Fluid Mech. (1990); 221: 533-552.

[14] Brown G.L. and Lopez J.M. Axisymmetric Vortex Breakdown Part II. Physical Mechanisms. J. Fluid Mech. (1990); 221: 553-576.

[15] Coney J.E.R. and El-Shaarawi M.A.I. A Contribution to the Numerical Solution of Developing Laminar Flow in the Entrance Region of Concentric Annuli with Rotating Inner Walls. J. Fluids Engineer (1974); 96: 333-340.

[16] Li Y., Dexun F. and Yanwen M. Numerical Simulation of Axisymmetric Unsteady Incompressible Flow by a Vorticity-Velocity Method. Int. J. Numerical Method in Fluids (1995); 21: 401-411.

[17] Lopez, J.M., and Perry, A.D. Axisymmetric Vortex Breakdown. Part 3 Onset of Periodic Flow and Chaotic Advection. J. Fluid Mech (1992); 234: 449-471.

[18] Lopez, J.M., and Perry, A.D. Periodic Axisymmetric Voetrex Breakdown in a Cylinder with a Rotating End Wall. Phys.Fluids.A (1992); 4:1871.

[19] Quartapelle, L. Numerical Solution of the Incompressible Navier-Stokes Equations. Basel, Switzerland: Birkhauser Verlag (1993).

[20] Pfister G., Schmidt H. Cliffe K.A. and Mullin T. Bifurcation Phenomena in Taylor-Couette Flow in a Very Short Annulus. J. Fluid Mech. (1998); 191: 1-18.

[21] Benjamin T.B. Bifurcation phenomena in Steady Flows of a Viscous Fluid I. Theory. Proc. R. Soc. Lond. A. (1978); 359: 1-26.

[22] Benjamin T.B. Bifurcation phenomena in Steady Flows of a Viscous Fluid II. Experiments. Proc. R. Soc. Lond. A. (1978); 359: 27-43.

[23] Benjamin T.B. and Mullin T. Anomalous modes in the Taylor experiment. Proc. R. Soc. Lond. A. (1981); 377: 221-249.

[24] Cliffe K.A. Numerical Calculations of Two-Cell and Single-Cell Taylor Flows. J. Fluid Mech. (1983); 135: 219-233.

[25] Neitzel G.P. Numerical Computation of Time-Dependent Taylor-Vortex Flows in Finite-Length Geometries. J. Fluid Mech. (1984); 141: 51-66.

[26] Cliffe K.A. and Mullin T. A Numerical and Experimental Study of Anomalous Modes in the Taylor Experiment. J. Fluid Mech. (1985); 153: 243-258.

[27] Jones C.A. On Flow Between Counter-Rotating Cylinders. J. Fluid Mech. (1982); 120: 443-450.

[28] Lui D.C.S. and Chen C.F. Numerical Experiments on Time-Dependent Rotational Couette Flow. J. Fluid Mech. (1973); 59(1): 77-95.

Objectives:

- To derive a numerical method for approximate solutions of the NSEs in new variables proposed by Aristov and Pukhnachev (2004).
- The proposed technique can be used in the future for in-depth investigations of the phenomena in rotating flows.
- The developed method can be applied to a numerical simulation of more complicated flow problem such as, two-dimensional flow past circular cylinder.
- The success can be attributed to the adequate physical nature of the auxiliary function.

Methodology:

- Literature search and survey and study on the methodology used in this research.
- Problem formulation and construct of the mathematical model.
- Developed computer codes (FORTRAN code).
- Numerical solution of the particular problem.

Scope of research:

In this project, there are limitations on

- The fluid is viscous and incompressible.
- The axisymmetric flow problems are considered.
- Using the numerical methods for approximation solution.

Output:

- **K. Poochinapan** and N. P. Moshkin, Numerical Implementation for New Form of the Navier-Stokes Equations. (ติดโปสเตอร์ในงานประชุม สกว. ปี 2557)
- B. Wongsaijai, T. Mouktonglang, N. Sukantamala, and **K. Poochinapan**, Compact structure-preserving approach to solitary wave in shallow water modeled by the Rosenau-RLW equation, **Applied Mathematics and Computational**, 340: 84-100, (2019). **(Impact factor 2.3, Q1, Corresponding author)**
- S. Yimnet, B. Wongsaijai, T. Rojsiraphisal, **K. Poochinapan**, Numerical Implementation for solving the symmetric regularized long wave equation,

Applied Mathematics and Computation, 273: 809-825 (2016). **(Impact factor 2.3, Q1, Corresponding author**)

- B. Wongsaijai and **K. Poochinapan**, A three-level average implicit finite difference scheme to solve equation obtained by coupling the Rosenau–KdV equation and the Rosenau–RLW equation, **Applied Mathematics and Computational**, 245: 289-304, (2014). **(Impact factor 2.3, Q1, Corresponding author)**
- **K. Poochinapan**, B. Wongsaijai, and T. Disyadej, Efficiency of high-order accurate difference schemes for the Korteweg-de Vries equation, **Mathematical Problems in Engineering**, 2014, Article ID 862403, 8 pages (2014). **(Impact factor 1.145, Q2, Corresponding author)**
- J. Janwised, B. Wongsaijai, T. Mouktonglang, and **K. Poochinapan**, A Modified Three-Level Average Linear-Implicit Finite Difference Method for the Rosenau-Burgers Equation, **Advances in Mathematical in Physics**, 2014, Article ID 734067, 11 pages (2014). **(Impact factor 0.71, Q3, Corresponding author)**
- B. Wongsaijai, **K. Poochinapan**, and T. Disyadej, A Compact Finite Difference Method for Solving the General Rosenau-RLW Equation, **IAENG International Journal of Applied Mathematics**, 44 (4): (2014). **(Scopus, Q3, Corresponding author)**

Numerical Implementation for New Form of the Navier-Stokes Equations

Kanyuta Poochinapan[a,*], Nikolay Moshkin

[a] *Department of Mathematics, Faculty of Science, Chiang Mai University, Chiang Mai 50200, Thailand*

Abstract

In this project, we propose and analyze a numerical method for the approximation of flows as well as algorithms suitable for the solution of fluid structures. This work deals with fluid problems based on the incompressible Navier-Stokes equations which are solved on the two-dimensional problem. We then introduce a new form of the Navier-Stokes equations for flow derived according to Aristov and Pukhnachev (2003). A new function related to the pressure and a system similar to the vorticity-stream function formulation are derived. The new form of the Navier-Stokes equations for the motion of a viscous incompressible fluid offers the possibility to create a different numerical model. Because of the physical nature of the coupling function, the model may have different mathematical properties than the vorticity-stream function formulation. We account for large deformations of fluid structures. Moreover, the developed method can be applied to numerical simulation for more complicated flow problems. The success can be attributed to the adequate physical nature of the auxiliary function.

Keywords: Navier-Stokes equations, Incompressible flow, Finite difference method

1. Introduction

It may be worthwhile to briefly mention why the 2D flow is important. It has applications in the industry (e.g. progressive cavity pumps) and importance to the scientific world, specifically in fluid mechanics. In general, a viscous fluid flow inside a driven cavity has been a common experiment approach used to check or improve numerical techniques (see for example, Ghia et. al. 1982; Botella and Peyret, 1998; Spotz 1998; Christov and Marinava, 2001; Moshkin and Poochinapan, 2010).

Traditionally, the viscous incompressible flow has been treated by representing the NSEs in the Cartesian coordinates. The stream function, stream function/vorticity, or (alternatively) the velocity and pressure field can be used. First, we write the viscous incompressible flow in the Cartesian coordinate system (x, y),

$$u_t + uu_x + vu_y = -\frac{1}{\rho}p_x + \nu\big(u_{xx} + u_{yy}\big), \tag{1}$$

$$v_t + uv_x + vv_y = -\frac{1}{\rho}p_y + \nu\big(v_{xx} + v_{yy}\big), \tag{2}$$

$$u_x + v_y = 0, \tag{3}$$

where u and v are the velocity components in $x-$ and $y-$directions, respectively; p is the pressure, ρ is the fluid density, and ν is the kinematic viscosity. The fluid is subjected to potential external forces. In 2D, the constraint of incompressibility $\nabla \cdot \bar{v} = 0$ can be satisfied exactly by expressing the

*Corresponding author

Email address: kanyuta@hotmail.com (Kanyuta Poochinapan)

velocity vector in terms of the stream function ψ according to

$$u = \frac{\partial \psi}{\partial y}, \quad v = -\frac{\partial \psi}{\partial x}. \tag{4}$$

The aim of the present work is to develop and validate a finite-difference scheme for the approximate solution of governing equations (1)–(3) proposed in Pukhnachev (2004):

$$\psi_t - \psi_x \psi_y + \Phi_x = \nu \Delta \psi, \tag{5}$$

$$\Delta \Phi = 2 \psi_y \Delta \psi, \tag{6}$$

where $\Delta \stackrel{\text{def}}{=} \dfrac{\partial^2}{\partial x^2} + \dfrac{\partial^2}{\partial y^2}$ and a function Φ satisfies the relations

$$\frac{1}{\rho} p = -\psi_y^2 + \Phi_y.$$

The case of the no-slip conditions satisfied at the boundary of the flow domain will be considered only. In terms of the function ψ only, boundary conditions are

$$\psi = 0, \ \frac{\partial \psi}{\partial n} = b(x, y), \tag{7}$$

where $\dfrac{\partial \psi}{\partial n}$ means the derivative in the direction of the normal vector to the boundary. To complete the formulation of the problem, it is necessary to specify the initial conditions

$$\psi = \psi_0(x, y), \ \Phi = \Phi_0(x, y), \ t = 0. \tag{8}$$

The main difficulty in solving the system of equations for ψ and Φ is that two boundary conditions are specified for ψ while none is available for Φ. This difficulty is similar to the vorticity–stream function equations in two dimensions.

A schematic of the flow geometry is shown in the figure where parameters are defined: L_x is the width of the cavity, L_y is the height of cavity, and U is velocity of wall motion.

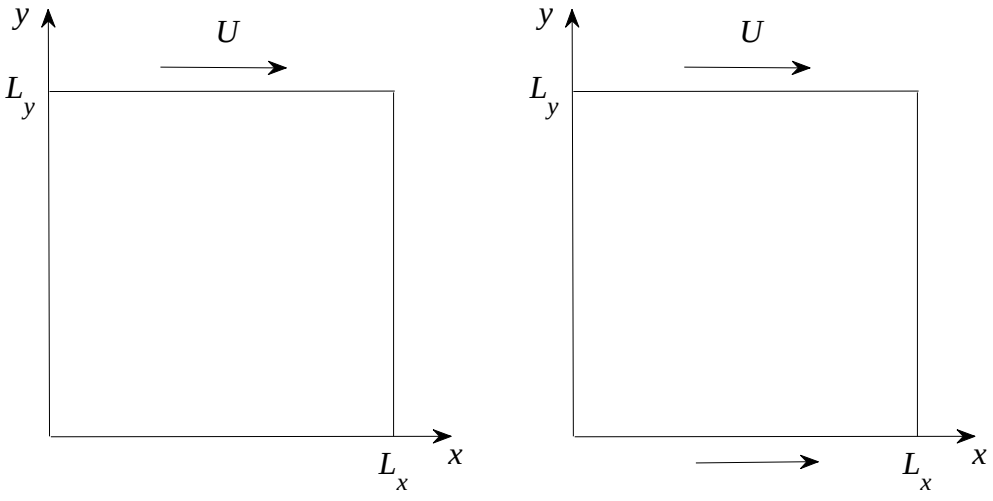

Figure 1: The flow geometry.

The non-dimensional parameters of the problem are

$$Re = \frac{L_x U}{\nu} \text{ and } \Gamma = \frac{L_y}{L_x},$$

where Re is the Reynolds number and Γ is the aspect ratio. The system of equations (1)–(3) is rendered dimensionless as follows:

$$x = \frac{x^*}{L_x}, \quad y = \frac{y^*}{L_x}, \quad t = \frac{t^*\nu}{L_x^2}, \quad u = \frac{u^*}{U}, \quad v = \frac{v^*}{U}. \tag{9}$$

2. Numerical method

The domain $Q = \{0 \leqslant x \leqslant 1,\ 0 \leqslant y \leqslant \Gamma\}$ is covered with a uniform staggered grid

$$Q_h = \left\{(x_i, y_j) | x_i = (i-1.5)h_x,\ y_j = (j-1.5)h_y,\ i = 1, \ldots, N_x,\ j = 1, \ldots, N_y\right\}$$

with spacings $h_x = \frac{1}{N_x - 2}$ and $h_y = \frac{1}{N_y - 2}$ in the $x-$ and $y-$directions, respectively. Such grid allows one to use the central differences to approximate boundary conditions with the second-order on two-point stencils.

The essential element of the proposed algorithm is that equations (5) and (6) for ψ and Φ are considered as a coupled system. Note that ψ and Φ are evaluated on the full-time steps. This formulation is based on the idea of considering the two boundary conditions for ψ as actual conditions for the $\psi - \Phi$ system. The second-order central-difference approximations for the operators in equations (5) and (6) are employed. The system of difference equations is

$$\frac{\psi_{i,j}^{n+1} - \psi_{i,j}^n}{\tau} - Re\frac{(\psi_{i+1,j}^n - \psi_{i-1,j}^n)(\psi_{i,j+1}^{n+1} - \psi_{i,j-1}^{n+1})}{8h_x h_y} - Re\frac{(\psi_{i+1,j}^{n+1} - \psi_{i-1,j}^{n+1})(\psi_{i,j+1}^n - \psi_{i,j-1}^n)}{8h_x h_y}$$
$$+ Re\frac{\left(\Phi_{i+1,1}^{n+1} - \Phi_{i-1,j}^{n+1}\right)}{2h_x} = \frac{1}{2}\left(\triangle\psi_{i,j}^{n+1} + \triangle\psi_{i,j}^n\right), \tag{10}$$

$$\triangle\Phi_{i,j}^{n+1} = \frac{1}{2h_y}\left[(\psi_{i,j+1}^n - \psi_{i,j-1}^n)\triangle\psi_{i,j}^{n+1} + (\psi_{i+1,j}^{n+1} - \psi_{i-1,j}^{n+1})\triangle\psi_{i,j}^n\right],$$
$$i = 2, \ldots, N_x - 1, \quad j = 2, \ldots, N_y - 1. \tag{11}$$

The boundary conditions are written in the following form

$$\begin{array}{ll}
\dfrac{\psi_{2,j}^{n+1} + \psi_{1,j}^{n+1}}{2} = 0, & \dfrac{\psi_{2,j}^{n+1} - \psi_{1,j}^{n+1}}{h_x} = 0, \\
\dfrac{\psi_{N_x,j}^{n+1} + \psi_{N_x-1,j}^{n+1}}{2} = 0, & \dfrac{\psi_{N_x,j}^{n+1} - \psi_{N_x-1,j}^{n+1}}{h_x} = 0, \\
\dfrac{\psi_{i,2}^{n+1} + \psi_{i,1}^{n+1}}{2} = 0, & \dfrac{\psi_{i,2}^{n+1} - \psi_{i,1}^{n+1}}{h_y} = 1, \\
\dfrac{\psi_{i,N_y}^{n+1} + \psi_{i,N_y-1}^{n+1}}{2} = 0, & \dfrac{\psi_{i,N_y}^{n+1} - \psi_{i,N_y-1}^{n+1}}{h_y} = 1,
\end{array} \quad \begin{array}{l} j = 1, \ldots, N_y, \\ \\ \\ i = 1, \ldots, N_x. \end{array} \tag{12}$$

To combine equations as a *single* linear system with a banded matrix, two new indices are introduced as follows:

$$\begin{aligned}
k_{(i,j)} &= 2(j-1)N_x + 2i - 1, \quad i = 1, \ldots, N_x, \\
m_{(i,j)} &= 2(j-1)N_x + 2i = k_{(i,j)} + 1, \quad j = 1, \ldots, N_y.
\end{aligned}$$

Now, the new grid function σ_k is introduced. It is defined on the composite grid where σ_k represents $\psi_{i,j}$ and $\sigma_m(=\sigma_{k+1})$ represents $\Phi_{i,j}$. Substituting σ_k instead of $\psi_{i,j}$ and σ_m instead of $\Phi_{i,j}$ into equations (10)–(11), the algebraic system can be recast as the following form

$$\frac{\sigma_k^{n+1}-\sigma_k^n}{\tau}+\frac{Re}{8h_xh_y}\Big[\left(\sigma_{k+2}^n-\sigma_{k-2}^n\right)\left(\sigma_{k+2N_x}^{n+1}-\sigma_{k-2N_x}^{n+1}\right)+\left(\sigma_{k+2}^{n+1}-\sigma_{k-2}^{n+1}\right)\left(\sigma_{k+2N_x}^n-\sigma_{k-2N_x}^n\right)\Big] - \frac{Re}{2h_x}\left(\sigma_{k+1}^{n+1}-\sigma_{k-3}^{n+1}\right)=\frac{1}{2}\left(\Delta\sigma_k^{n+1}+\Delta\sigma_k^n\right), \quad (13)$$

$$\Delta\sigma_m^{n+1}=\frac{(\sigma_{m+2N_x-1}^n-\sigma_{m-2N_x-1}^n)}{2h_y}\Delta\sigma_{m-1}^{n+1}+\frac{(\sigma_{m+2N_x-1}^{n+1}-\sigma_{m-2N_x-1}^{n+1})}{2h_y}\Delta\sigma_{m-1}^n, \quad (14)$$

where

$$\Delta\sigma_k=\frac{(\sigma_{k+2}-2\sigma_k+\sigma_{k-2})}{h_x^2}+\frac{(\sigma_{k+2N_x}-2\sigma_k+\sigma_{k-2N_x})}{h_y^2}.$$

We applied the developed numerical tool for investigating the mechanisms of the 2-sided lid driven cavity flow by using different values of the governing parameters. If the steady flow is needed then the algorithm can be considered as an iterative procedure. Iterations are terminated at the certain time $n=N$ when the following criterion is satisfied:

$$\frac{\max_{i,j}\left|\sigma_{i,j}^{N+1}-\sigma_{i,j}^N\right|}{\max_{i,j}\left|\sigma_{i,j}^{N+1}\right|}\leqslant 10^{-8}.$$

Note that the linear system for the coupled formulation of the $\psi-\Phi$ problem can be written as the following multi-diagonal system for the composite grid function σ

$$B_{l-2N_x-1}\sigma_{l-2N_x-1}^{n+1}+B_{l-2N_x}\sigma_{l-2N_x}^{n+1}+B_{l-3}\sigma_{l-3}^{n+1}+B_{l-2}\sigma_{l-2}^{n+1} + B_{l-1}\sigma_{l-1}^{n+1}+B_l\sigma_l^{n+1}+B_{l+1}\sigma_{l+1}^{n+1}+B_{l+2}\sigma_{l+2}^{n+1} + B_{l+2N_x-1}\sigma_{l+2N_x-1}^{n+1}+B_{l+2N_x}\sigma_{l+2N_x}^{n+1}+B_{l+2N_x+1}\sigma_{l+2N_x+1}^{n+1}=F_l, \quad (15)$$

where $l=1,\ldots,2N_yN_x$. The matrix of the linear system (15) is banded with $2N_x+1$ lower and upper bandwidths. The standard routings DGBSV and DGBSVX of the LAPACK routine are used to compute the solution of equation (15).

3. Results and comparisons

In this section we applied the developed numerical tool for investigating the mechanisms of the 2-sided lid driven cavity flow for different values of the governing parameters.

The dynamic of the flow when driven by the top and bottom lids was investigated for $Re\in[50,1700]$ and $\Gamma\in[2,3]$. For $Re=100$ and small to moderate Γ, the flow consists of two-eddy symmetrical to each other, created essentially by the parallel motion of the walls. As the relative length Γ increases, the two-eddy stationary flow is eventually replaced by the four-eddy structure. The further increase of the aspect ratio to $\Gamma=2.5$ leads to the vortex of the secondary streaming and $\Gamma=3$ marks the actual transition to a four-eddy structure, when the small two-eddy structure occurs between the two vortices and spans with the increase of Γ, the entire breath of the gap. As it should have been expected (see Fig. 6), the further increase of Γ allows the secondary vortices to grow and to become commensurate with the other two-eddy structure.

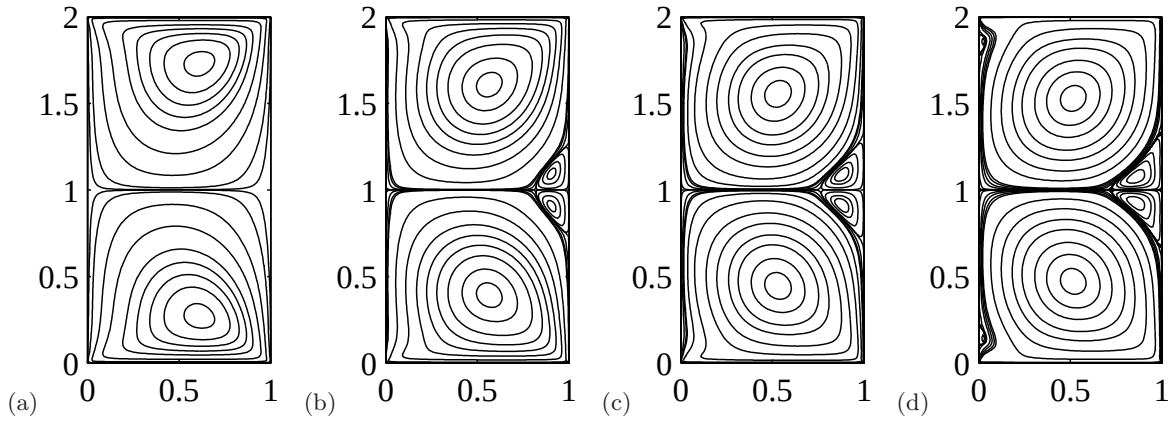

Figure 2: Stream function, Gamma 2: (a) $Re = 100$ (b) $Re = 300$ (c) $Re = 700$ (c) $Re = 1700$.

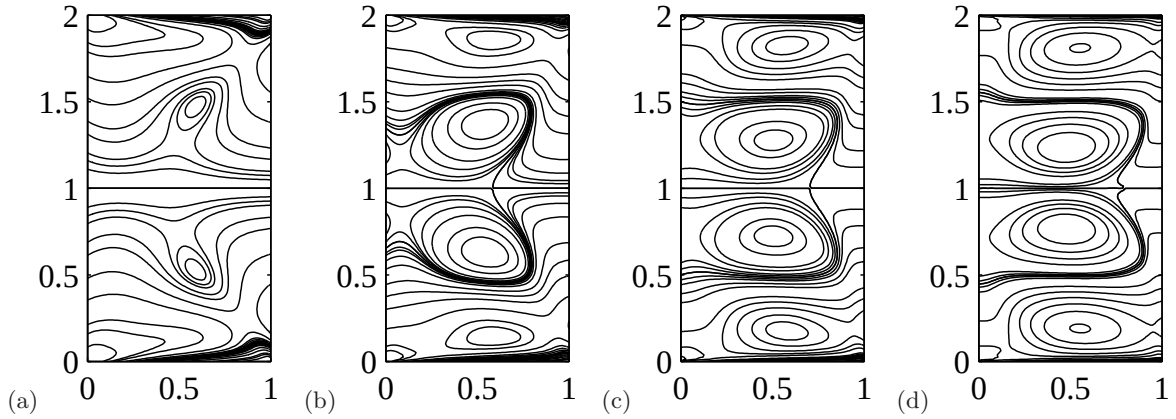

Figure 3: Φ function, Gamma 2: (a) $Re = 100$ (b) $Re = 300$ (c) $Re = 700$ (c) $Re = 1700$.

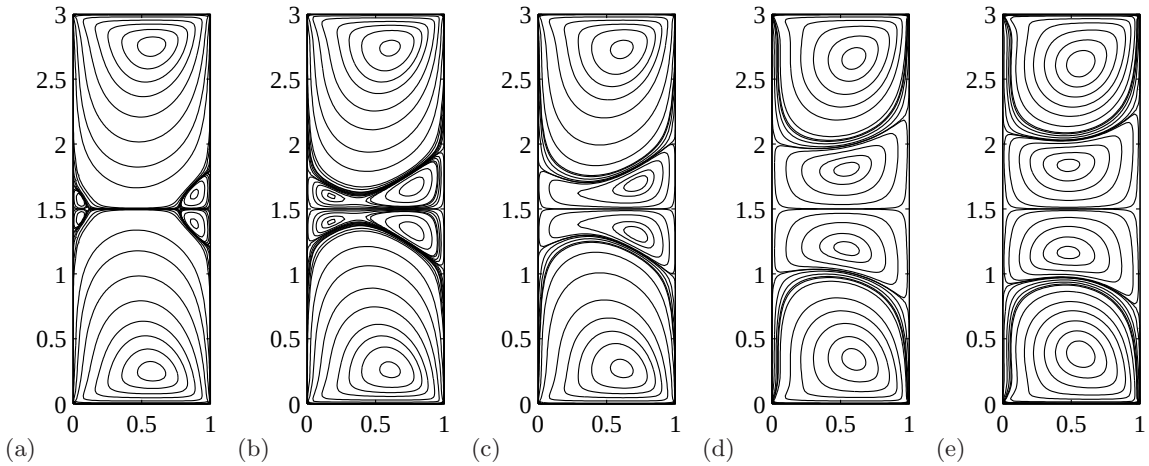

Figure 4: Stream function, Gamma 3: (a) $Re = 50$ (b) $Re = 85$ (c) $Re = 100$ (d) $Re = 200$ (e) $Re = 300$.

In order to understand better the role of nonlinearity in the process of transition from a four-eddy to a six-eddy, we chose $\Gamma = 5$ and $Re \in [100, 1500]$ which lies securely inside the region of parameters where the six-eddy structure is to be expected. After the flow is established for a particular

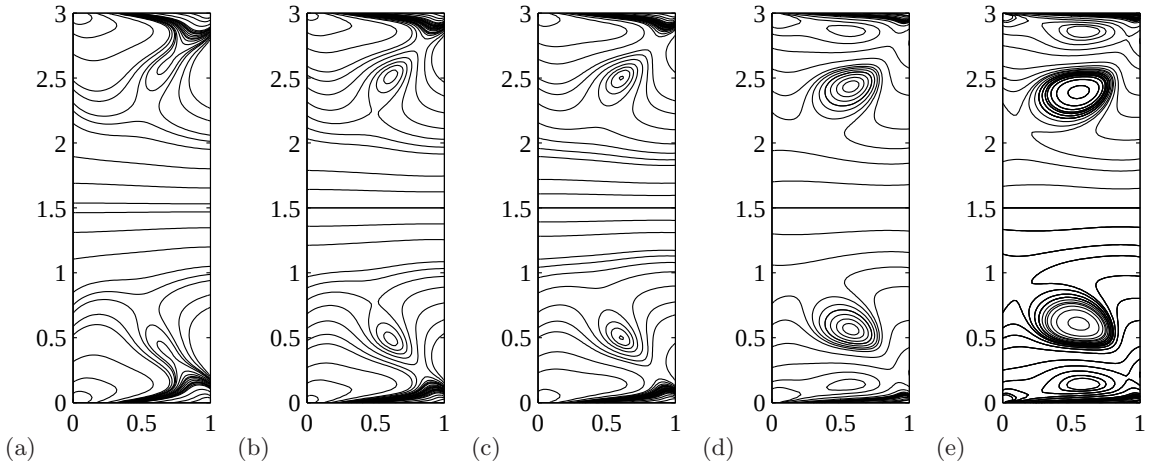

Figure 5: Φ function, Gamma 3: (a) $Re = 50$ (b) $Re = 85$ (c) $Re = 100$ (d) $Re = 200$ (e) $Re = 300$.

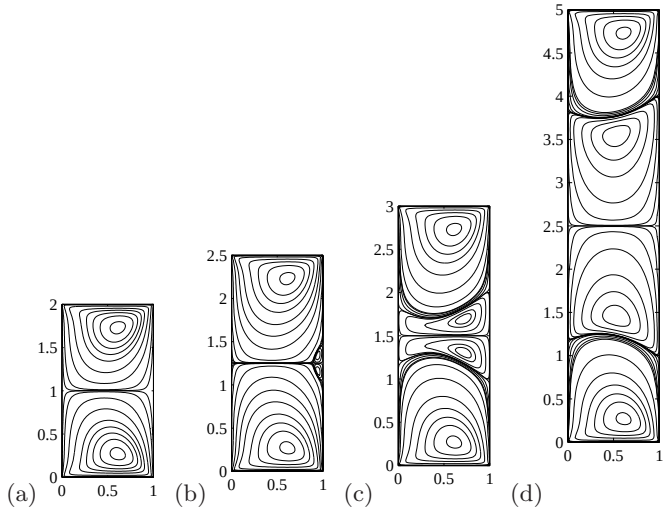

Figure 6: Stream function, Re=100: (a) $\Gamma = 2$ (b) $\Gamma = 2.5$ (c) $\Gamma = 3$ (d) $\Gamma = 5$.

Reynolds number (say, Re_0), we increase Re in small increments according to the formula $Re = Re_0(1 - exp(-0.05(n-1))))$, where $n = 1, 2, 3, ..., n_f$ is the time step. The number of n_f defines the value of Re, which has to be reached. Then we continue the time steps $n > n_f$ with the last value of Reynolds number until stationary regime is attained. Thus, we are able to proceed from one Reynolds number to another without imposing discontinuous initial condition. These precautions are needed in order to avoid artificial jumps that can make the solution end up in another bifurcated state. The steady states that we were able to reach with this algorithm are shown in Fig. 7. By slowly increasing Re reached $Re = 1500$ for which Reynolds number the flow changed from a four-eddy structure to a six-eddy structure.

4. Acknowledgments

This work was financially supported by the Commission on Higher Education (CHE), the Thailand Research Fund (TRF), Chiang Mai University (CMU), Project Number: MRG5580217.

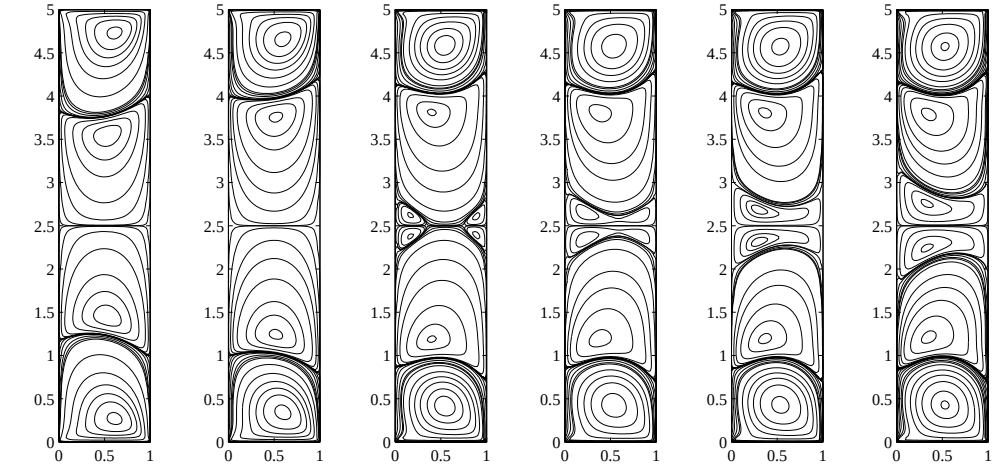

(a) (b) (c) (d) (e) (f)

Figure 7: Stream function, Gamma 5: (a) $Re = 100$ (b) $Re = 200$ (c) $Re = 500$ (d) $Re = 600$ (e) $Re = 700$ (f) $Re = 1500$.

References

[1] S.N. Aristov and V.V. Pukhnachev, *On the Equations of Axisymmetric Motion of a Viscous Incompressibl*, Doklady Physics 49(2) (2004) pp. 112–115.

[2] V.V. Pukhnachev, *Integrals of motion of an incompressible fluid occupying the entire space*, J. Appl. Mech. Tech. Phys. 45(2) (2004) pp. 167–171.

[3] U. Ghia, K.N. Ghia, and C.T. Shin, *High-resolutions for incompressible flow using the Navier-Stokes equations and multigrid method*, J. Comput. Phys. 48 (1982) pp. 387–411.

[4] O. Botella and R. Peyret, *Benchmark spectral results on the lid-driven cavity flow*, Comp. Fluids 27 (4) (1998) pp. 421–433.

[5] W.F. Spotz, *Accuracy and performance of numerical wall boundary conditions for steady, 2D, incompressible streamfunction vorticity*, Int. J. Numer. Methods Fluids 28 (1998) pp. 737–757.

[6] C.I. Christov and R.S. Marinova, *Implicit vectorial operator splitting for incompressible Navier-Stokes equations in primitive variables*, J. Comput. Tech. 6(4) (2001) pp. 92–119.

[7] N.P. Moshkin, K. Poochinapan, and C.I. Christov *Numerical Implementation of Aristov-Pukhnachev's Formulation for Axisymmetric Viscous Incompressible Flows*, Int. J. Numer. Methods Fluids 62(10) (2010) pp. 1063–1080.

[8] N.P. Moshkin and K. Poochinapan, *Finite Difference Scheme for the Numerical Solution of Two-Dimensional Incompressible Navier- Stokes Equations*, Int. J. Numer. Anal. Model. 7(2) (2010) pp. 321–329.

Applied Mathematics and Computation 340 (2019) 84–100

Contents lists available at ScienceDirect

Applied Mathematics and Computation

journal homepage: www.elsevier.com/locate/amc

Compact structure-preserving approach to solitary wave in shallow water modeled by the Rosenau-RLW equation

B. Wongsaijai[a,b], T. Mouktonglang[a,b], N. Sukantamala[a,b], K. Poochinapan[a,b,*]

[a] Center of Excellence in Mathematics and Applied Mathematics, Department of Mathematics, Faculty of Science, Chiang Mai University, Chiang Mai 50200, Thailand
[b] Centre of Excellence in Mathematics, CHE, Si Ayutthaya Rd. Bangkok 10400, Thailand

ARTICLE INFO

Keywords:
Solitary wave
Shallow water
Rosenau-RLW equation
Compact finite difference method

ABSTRACT

A mass-preserving scheme, a nonlinear algorithm based on modification of a finite difference method to the Rosenau-RLW equation, is proposed subject to homogeneous boundary conditions. The key feature of the method for improving the accuracy of approximate solutions is to develop a compact higher-order scheme together with an iterative algorithm for solving the nonlinear implicit scheme. The derivatives for space discretization are approximated by using the algorithm dealing with a five-point stencil. In addition, a three-level average difference technique is used to perform time discretization. The conservation of mass and both the existence and uniqueness of the numerical solution are proved. The stability and convergence of the numerical solution with order $O(\tau^4 + \tau^2 h^2 + h^4)$ are also confirmed. For efficiency analysis, numerical results show that the computational efficiency of the compact scheme is much higher than that of non-compact schemes. Moreover, long-time behavior is also used to validate the capability of the present method.

1. Introduction

An ocean surface disturbance generally resulted from undersea earthquakes that shift the seafloor generating tsunami wave and ocean acoustic fields has been severe topics of scientists for a long time [1,2]. Tsunami is nearshore propagating waves which have enormous amplitudes and long wavelengths. Then, the possibility for migration into land and devastation to properties are substantial. In the past, the observation of wave forms and wave trains, with either leading elevated waves or leading depressed waves has been performed. In terms of producing any catastrophes for humans, the amplitude and wavelength range of these types of wave are very considerable. That is, climate changes and global warming are several examples of such very huge natural disasters seen previously. Nowadays, heat waves, flooding, earlier spring arrival, sea-level rising, melting glaciers, coral reef bleaching, and the spread of disease are obvious signs of climate changes. However, alternative energy sources for the near future can be generated by utilizing these giant waves if essential technology is applied.

A natural phenomenon is the interesting field of scientific study, which in the past many researchers have investigated in mathematical models by using various nonlinear evolution equations. In the learning internal mechanism of dynamic of nonlinear phenomena, finding of the exact traveling wave solution to nonlinear evolution equations plays an important role.

* Corresponding author at: Center of Excellence in Mathematics and Applied Mathematics, Department of Mathematics, Faculty of Science, Chiang Mai University, Chiang Mai 50200, Thailand.
E-mail address: poochinapan@gmail.com (K. Poochinapan).

https://doi.org/10.1016/j.amc.2018.06.009
0096-3003/

Various potent methods create analytical and approximate solutions of these nonlinear evolution equations. Furthermore, with the assistance of analytical solutions, nonlinear evolution equations have been used to approximate, to comprehend better, and to criticize such wave behaviors. Nevertheless, analytical solutions of these equations are barely feasible while nonlinear terms are implicated. Hence, a numerical solution of these nonlinear evolution equations is significantly essential because only limited types of the equations are solvable by analytical methods.

The mathematical models of water wave have drawn attention for a long time. These models aim to describe from smaller-scale waves, such as ripples on the water surface to larger-scale waves, such as tsunami waves. The examples of mathematical models that explain the dynamic of waves are the KdV equation (Korteweg-de Vries equation) [3], the RLW equation (Regularized Long-Wave equation) [4,5], and the Rosenau equation [6,7]. Boussinesq and Korteweg & de Vries applied the KdV equation to investigate shallow waves, ion sound waves, and longitudinal astigmatic waves [8–10]. Although the KdV equation has an analytical solution, but it is numerically unstable. On the other hand, the KdV equation has been numerically solved by various techniques, such as the finite difference method (FDM), the collocation method, the finite element method, the Galerkin method, and the spectral method.

Initially suggested by Peregrine [4,5], the RLW equation provides a presentation on a different situation of a nonlinear dispersive wave from the more classical KdV equation. The RLW equation is one of models which are used to study in many areas, e.g. ion-acoustic plasma waves, magnetohydrodynamic plasma waves, and shallow water waves. Shallow water wave that is observed at the beach is generally applied in oceanography and atmospheric science. Besides, the RLW equation can also explain soliton motion through optical fibers in a telecommunication system. The equation cannot explain the interaction between wave-wave and wave-wall, but it is suitable for modeling a small-amplitude long wave in a channel. For the dynamic of dense discrete systems, the interaction between wave-wave and wave-wall can be explained by the Rosenue equation. Early studies attempted to find both theoretical and numerical techniques on the equation [6,7,11–15]. The results from Park [11,12] showed the existence and uniqueness of the solution for the Rosenau equation. In the field, the solitary wave's behavior of the equation has been well numerically studied for the past years.

For an additional examination of nonlinear behaviors of waves, a viscous term u_{xxt} needs to be included in the Rosenau equation. The equation is commonly called the general Rosenau-RLW

$$u_t + u_{xxxxt} - u_{xxt} + u_x + \alpha(u^p)_x = 0, \tag{1}$$

where $p \geq 2$ is an integer and α is a constant. If $p = 2$ and $\alpha = \frac{1}{2}$, then Eq. (1) is called the usual Rosenau-RLW equation. If $p = 3$, then Eq. (1) is called the modified Rosenau-RLW equation. It is to be decorated that such type of the equation frequently arises in various branches of physics and applied sciences. In the recent period, many methods were settled and proposed for finding the exact solution of the Rosenau-RLW equation, such as the sech ansatz method and sine-cosine method. However, solutions of the Rosenau-RLW equation are not analytically solved in general. For this reason, numerical techniques are important to be developed in order to get much more understanding solution behaviors.

Most of numerical methods for solving the usual Rosenau-RLW and general Rosenau-RLW are based on the FDM [16–24]. In [16], Zuo et. al. have proposed the Crank-Nicolson FDM for the generalized Rosenau-RLW and also discussed its convergence and stability of the proposed scheme. Later, Pan and Zhang [17] developed and studied an average three-level linearized conservative FDM. Very recently, Wang et. al. [18] presented a three-level finite difference scheme (FDS) by introducing two weighted parameters appeared on a first order derivative in both time and space variables. A critical review of using finite difference techniques shows that several approaches have been developed for the structure-preserving schemes with an order of accuracy $O(\tau^2 + h^2)$. However, Hu et. al. [24] attempted to provide a linear there-level higher-order FDM by using the Richardson extrapolation idea, but it is a non-compact scheme due to the number of grid stencils.

A method to conquer the conflict among stability, accuracy, and computational cost is the improvement of a high-order compact difference scheme since the stability, accuracy, and computational cost, which are in conflict with each other, are the desired properties of the FDS. Implicit approximation is required in order to reach the stability of the FDS. The stencil becomes wider with increasing order of accuracy for a high-order method of a conventional scheme. Furthermore, the solution of an algebraic system for equations with extensive bandwidth is resulted by using an implicit method. It is supposed to improve schemes that have a broad range of stability and high order of accuracy.

Generally, previous research highlights that the higher-order compact difference method performs better solutions when compared with non-compact or low-order methods on the same grid stencils (see [21,22,25–29]). At present, there are few results on a higher-order compact FDM for solving the Rosenau-RLW type equation. In [21], the authors proposed a linear three-level compact FDM for the generalized Rosenau-RLW equation derived via standard Taylor expansion, where the method achieves the truncation error of order $O(\tau^2 + h^4)$. Moreover, a compact conservative nonlinear FDS is considered by Wang et. al. [18]. The recent work of Li [23] analyzed a compact conservative FDM for solving the 3D Rosenau-RLW equation. There are currently detailed studies of an iterative algorithm for solving the nonlinear system generated by the scheme.

The benefit of characterizing order of accuracy in time is that quite strong statement can be made on how the order of accuracy ultimately evolves. It appears obvious that there are other important factors for improving the efficiency and reducing the computation cost of a finite difference technique. However, most past studies have correlated with the second-order of accuracy in time. Therefore, a new compact finite difference technique with order of accuracy $O(\tau^4 + \tau^2 h^2 + h^4)$ is applied to the solution of the generalized Roseanu-RLW equation in this research. Then, we consider the generalized

Rosenau-RLW equation with an initial condition

$$u(x,0)=u_0(x),\quad x_l\le x\le x_r, \tag{2}$$

and boundary conditions

$$u(x_l,t)=u_x(x_l,t)=u_{xx}(x_l,t)=0,\ u(x_r,t)=u_x(x_r,t)=u_{xx}(x_r,t)=0,\quad 0\le t\le T. \tag{3}$$

When x_l and x_r are large enough, the initial-boundary value problem (1)–(3) is consistent, so the boundary conditions (3) are reasonable.

The main purpose of this paper is to create a compact FDS for the Rosenau-RLW equation with initial and boundary conditions. Some preliminary lemmas and discrete norms are given, and the invariant property Q^n is proved in Section 2. We discuss about the priori estimate and boundedness of the solution in Section 3. The solvability of the FDS and the existence and uniqueness of the solution are also proved in Section 4. Section 5 presents complete proofs on the convergence and stability of the proposed method with convergence rate $O(\tau^4+\tau^2h^2+h^4)$. Within this study, the iterative algorithm for solving the nonlinear implicit scheme is described in Section 6. The outcomes of the numerical experiments are presented in Section 7, where we make a detailed comparison with available data to confirm and illustrate our theoretical analysis. Finally, conclusions are drawn in Section 8.

2. Compact finite difference scheme

This section is devoted to a complete description of how the compact structure-preserving method can be developed for the Rosenau-RLW equation. Here, the description about a computational domain will be discovered. First, we introduce the solution domain to be

$$Q=\{(x,t)|\ x_l\le x\le x_r,\ 0\le t\le T\},$$

which is covered by a uniform grid

$$Q_h=\{(x_i,t_n)|\ x_i=x_l+ih,\ t_n=n\tau,\ i=0,\dots,M,\ n=0,\dots,N\}.$$

We discretize the time domain uniformly identified by $t_n=n\tau$, here τ is a time increment. In addition, the spatial domain $[x_l,x_r]$ is discretized by using function values on a finite set of the points $\{x_i\}_{i=0}^{M}\subset[x_l,x_r]$, where the grid size $h=(x_r-x_l)/M$ is a uniform distance between two points. Points can be located according to values of i and n, so difference equations are usually written in term of the point $(i,\ n)$. Then, u_i^n will be called, in this paper, the grid function of u at the point $(x_l+ih,n\tau)$, and the space Z_h^0 is introduced:

$$Z_h^0=\{u=(u_i)|\ u_{-1}=u_0=u_1=u_{M-1}=u_M=u_{M+1}=0,\ i=-1,0,1,\dots,M-1,M,M+1\}.$$

For completeness, the following notations will be used:

$$(u_i^n)_t=\frac{u_i^{n+1}-u_i^n}{\tau},\quad (u_i^n)_{\bar t}=\frac{u_i^n-u_i^{n-1}}{\tau},\quad (u_i^n)_{\hat t}=\frac{u_i^{n+1}-u_i^{n-1}}{2\tau},$$
$$(u_i^n)_x=\frac{u_{i+1}^n-u_i^n}{h},\quad (u_i^n)_{\bar x}=\frac{u_i^n-u_{i-1}^n}{h},\quad (u_i^n)_{\hat x}=\frac{u_{i+1}^n-u_{i-1}^n}{2h},$$
$$\bar u_i^n=\frac{u_i^{n+1}+u_i^{n-1}}{2},\quad (u^n,v^n)=h\sum_{i=1}^{M-1}u_i^nv_i^n,\quad \|u^n\|^2=(u^n,u^n),$$

and $\|u^n\|_\infty=\max\limits_{1\le i\le M-1}|u_i^n|$. Now, we give a description of a finite difference scheme and an algorithm for the formulation of the problem (1). By setting $w=-u_x-\alpha(u^p)_x$, Eq. (1) can be written as $w=u_t-u_{xxt}+u_{xxxxt}$. Using the Taylor expansion in the variable t, we obtain

$$w_i^n=\left[\left(u_i^n\right)_{\hat t}-\frac{\tau^2}{6}\left(\partial_t^3u\right)_i^n\right]-\left[\left(\partial_x^2u_i^n\right)_{\hat t}-\frac{\tau^2}{6}\left(\partial_x^2\partial_t^3u\right)_i^n\right]+\left[\left(\partial_x^4u_i^n\right)_{\hat t}-\frac{\tau^2}{6}\left(\partial_x^4\partial_t^3u\right)_i^n\right]+O\left(\tau^4\right). \tag{4}$$

From definition of w, Eq. (4) may be arranged as

$$w_i^n+\frac{\tau^2}{6}\left(\partial_t^2w\right)_i^n=\left(u_i^n\right)_{\hat t}-\left(\partial_x^2u_i^n\right)_{\hat t}+\left(\partial_x^4u_i^n\right)_{\hat t}+O\left(\tau^4\right). \tag{5}$$

The standard central difference approximations are used in order to obtain corresponding higher order convergence rates, which imply

$$w_i^n+\frac{\tau^2}{6}\left(\partial_t^2w\right)_i^n=\left(u_i^n\right)_{\hat t}-\left[\left(u_i^n\right)_{x\bar x\hat t}-\frac{h^2}{12}\left(\partial_x^4u_i^n\right)_{\hat t}\right]+\left[\left(u_i^n\right)_{xx\bar x\bar x\hat t}-\frac{h^2}{6}\left(\partial_x^6u_i^n\right)_{\hat t}\right]+O(\tau^4+h^4). \tag{6}$$

Unless additional terms in the Taylor expansion are included, this approach is at most the fourth-order accurate in time and space. Moreover, using the Taylor expansion in the variable x, we obtain

$$w_i^n = -\left[\left(u_i^n\right)_{\hat{x}} - \frac{h^2}{6}\left(\partial_x^3 u\right)_i^n\right] - \alpha\left[\left[(u_i^n)^p\right]_{\hat{x}} - \frac{h^2}{6}\left(\partial_x^3 u^p\right)_i^n\right] + O(h^4). \tag{7}$$

Inspection of Eq. (5) shows that the higher-order derivative term can be eliminated by presenting

$$\left(\partial_x^6 u_i^n\right)_{\hat{t}} = \left(\partial_x^4 u_i^n\right)_{\hat{t}} - \left(\partial_x^2 u_i^n\right)_{\hat{t}} - \left(\partial_x^3 u\right)_i^n - \alpha\left(\partial_x^3 u^p\right)_i^n + O(\tau^2). \tag{8}$$

This approach is the second-order accurate. By using Eqs. (7)–(8), Eq. (6) can be rewritten as

$$\left(u_i^n\right)_{\hat{t}} - \left(1 - \frac{h^2}{6}\right)\left(u_i^n\right)_{x\bar{x}\hat{t}} + \left(1 - \frac{h^2}{12}\right)\left(u_i^n\right)_{xx\bar{x}\bar{x}\hat{t}} + \left(u_i^n\right)_{\hat{x}} + \alpha\left[(u_i^n)^p\right]_{\hat{x}} - \frac{\tau^2}{6}\left(\partial_t^2 w\right)_i^n = O(\tau^4 + h^2\tau^2 + h^4). \tag{9}$$

To illustrate the higher order finite difference scheme, we use an appropriate form to approximate the term $\left(\partial_t^2 w\right)_i^n$:

$$\left(\partial_t^2 w\right)_i^n = -(u_i^n)_{\hat{x}t\bar{t}} - \frac{\alpha p}{p+1}[(u_i^n)^{p-1}(u_i^n)_{\hat{x}} + [(u_i^n)^p]_{\hat{x}}]_{t\bar{t}} + O(\tau^2 + h^2).$$

For convenience, $\psi_p(u_i^n)$ may be decomposed as

$$\psi_p(u_i^n) = \frac{\alpha p}{(p+1)}[(u_i^n)^{p-1}(u_i^n)_{\hat{x}} + [(u_i^n)^p]_{\hat{x}}].$$

After discretizing Eqs. (1)–(3) in time and space, they can be regarded as the compact fourth-order scheme

$$\left(u_i^n\right)_{\hat{t}} - s_1\left(u_i^n\right)_{x\bar{x}\hat{t}} + s_2\left(u_i^n\right)_{xx\bar{x}\bar{x}\hat{t}} + \left(u_i^n\right)_{\hat{x}} + \alpha\left[(u_i^n)^p\right]_{\hat{x}} + \frac{\tau^2}{6}(u_i^n)_{\hat{x}t\bar{t}} + \frac{\tau^2}{6}[\psi_p(u_i^n)]_{t\bar{t}} = 0; \quad 1 \le i \le M-1,\ 1 \le n \le N-1, \tag{10}$$

$$u_i^0 = u_0(x_i), \quad 0 \le i \le M, \tag{11}$$

$$u_0^n = u_M^n = 0,\ (u_0^n)_{\hat{x}} = (u_M^n)_{\hat{x}} = 0,\ (u_0^n)_{x\bar{x}} = (u_M^n)_{x\bar{x}} = 0, 1 \le n \le N, \tag{12}$$

where $s_1 = 1 - \frac{h^2}{6}$ and $s_2 = 1 - \frac{h^2}{12}$.

Theorem 1. *Suppose $u_0 \in H_0^2[x_l, x_r]$. If $p = 2$, then the finite difference scheme(10)–(12) is conservative for discrete mass in sense:*

$$Q^n = \frac{h}{2}\sum_{i=1}^{M-1}\left(u_i^{n+1} + u_i^n\right) = Q^{n-1} = \cdots = Q^0. \tag{13}$$

Proof. By multiplying Eq. (10) by h, summing up for i from 1 to $M-1$ and considering the boundary conditions (12), we approach our point

$$\frac{h}{2}\sum_{i=1}^{M-1}\left(u_i^{n+1} - u_i^{n-1}\right) + \frac{h\tau^2}{6}\sum_{i=1}^{M-1}[\psi_p(u_i^n)]_{t\bar{t}} = 0.$$

Due to the equality

$$\sum_{i=1}^{M-1}[\psi_p(u_i^n)] = \frac{2\alpha}{3}\sum_{i=1}^{M-1}\left[u_i^n(u_i^n)_{\hat{x}} + [(u_i^n)^2]_{\hat{x}}\right] = 0,$$

finally, we arrive to our aim giving Eq. (13), which completes the proof. □

The following lemma is some properties of the above FDS which can be directly obtained from the definition. It is essential for existence, uniqueness, convergence, and stability of our numerical solution.

Lemma 2. *For any two mesh functions $u, v \in Z_h^0$, we have*

$$(u_{\hat{x}}, v) = -(u, v_{\hat{x}}), \qquad (u_{x\bar{x}}, v) = -(u_x, v_x), \qquad (u_{xx\bar{x}\bar{x}}, v) = (u_{x\bar{x}}, v_{x\bar{x}}),$$

then one has

$$(u_{x\bar{x}}, u) = -(u_x, u_x) = -\|u\|^2, \qquad (u_{xx\bar{x}\bar{x}}, u) = (u_{x\bar{x}}, u_{x\bar{x}}) = \|u_{x\bar{x}}\|^2.$$

3. Priori estimate

We now investigate the priori estimate of the compact FDM proposed through Eq. (10).

Lemma 3. *(discrete Sobolev's inequality [30]). There exist two constants C_1 and C_2 such that*

$$\|u^n\|_\infty \le C_1\|u^n\| + C_2\|u_x^n\|.$$

Theorem 4. *Suppose $u_0 \in H_0^2[x_l, x_r]$, then the solution u^n satisfies $\|u^n\| \le C$, $\|u_x^n\| \le C$ and $\|u_{x\bar{x}}^n\| \le C$, which yields $\|u^n\|_\infty \le C$ and $\|u_x^n\|_\infty \le C$.*

Proof. It follows from the initial condition, and that is $u^0 \le C$. The first level of a scheme u^1 can be computed by an available fourth-order method. Hence, the following estimate is gotten about $\|u^1\| \le C$, $\|u_{x\bar{x}}^1\| \le C$, and $\|u^1\|_\infty \le C$. Now, we use an induction argument to prove the theorem. Assuming that

$$\|u^k\|_\infty \le C, \quad \text{for } k = 2, 3, \ldots, n. \tag{14}$$

Taking the inner product of Eq. (10) with $2\bar{u}^n\big(i.e.\ u^{n+1} + u^{n-1}\big)$ and using Lemma 2, we obtain

$$\begin{aligned}&\Big(\|u^{n+1}\|^2 - \|u^{n-1}\|^2\Big) + s_1\Big(\|u_x^{n+1}\|^2 - \|u_x^{n-1}\|^2\Big) + s_2\Big(\|u_{x\bar{x}}^{n+1}\|^2 - \|u_{x\bar{x}}^{n-1}\|^2\Big)\\ &+2\tau\big(u_{\hat{x}}^n, 2\bar{u}^n\big) + \alpha\big([(u^n)^p]_{\hat{x}}, 2\bar{u}^n\big) + \frac{\tau^3}{3}\big(u_{\hat{x}t\bar{t}}^n, 2\bar{u}^n\big) + \frac{\tau^3}{3}\big([\psi_p(u_i^n)]_{t\bar{t}}, 2\bar{u}^n\big) = 0.\end{aligned} \tag{15}$$

According to the Cauchy-Schwarz inequality, the boundary conditions (12) provide inequalities

$$\|u_{\hat{x}}^n\| \le \|u_x^n\| \tag{16}$$

and

$$\big(u_{\hat{x}}^n, 2\bar{u}^n\big) \le \Big(\|u_x^n\|^2 + \frac{1}{2}\|u^{n+1}\|^2 + \frac{1}{2}\|u^{n-1}\|^2\Big). \tag{17}$$

Next, we turn to the inner product of Eq. (10) with $2\bar{u}^n$, that is

$$\big([(u^n)^p]_{\hat{x}}, 2\bar{u}^n\big) = -h\sum_{i=1}^{M-1}(u_i{}^n)^p\big(u_i^{n+1} + u_i^{n-1}\big)_{\hat{x}} \le C\Big(\|u^n\|^2 + \frac{1}{2}\|u_x^{n+1}\|^2 + \frac{1}{2}\|u_x^{n-1}\|^2\Big), \tag{18}$$

$$\begin{aligned}\big(u_{\hat{x}t\bar{t}}^n, 2\bar{u}^n\big) &= \frac{h}{\tau^2}\sum_{i=1}^{M-1}\big((u_i^{n+1})_{\hat{x}} - 2(u_i^n)_{\hat{x}} + (u_i^{n-1})_{\hat{x}}\big)(u_i^{n+1} - u_i^{n-1})\\ &\le \frac{2}{\tau^2}\big(\|u^{n-1}\|^2 + \|u^{n+1}\|^2 + \|u_x^{n-1}\|^2 + \|u_x^n\|^2 + \|u_x^{n+1}\|^2\big)\end{aligned} \tag{19}$$

and

$$\begin{aligned}\Big([\psi_p(u^n)]_{t\bar{t}}, 2\bar{u}^n\Big) &= \frac{\alpha p}{(p+1)}\Big[\big([(u^n)^{p-1}(u^n)_{\hat{x}}]_{t\bar{t}}, 2\bar{u}^n\big) - \big([(u^n)^p]_{t\bar{t}}, 2\bar{u}_{\hat{x}}^n\big)\Big]\\ &= \frac{\alpha ph}{\tau^2(p+1)}\Bigg[\sum_{i=i}^{M-1}\Big(\big(u_i^{n+1}\big)^{p-1}\big(u_i^{n+1}\big)_{\hat{x}} - 2\big(u_i^n\big)^{p-1}\big(u_i^n\big)_{\hat{x}} + \big(u_i^{n-1}\big)^{p-1}\big(u_i^{n-1}\big)_{\hat{x}}\Big)\big(u_i^{n+1} + u_i^{n-1}\big)\\ &\quad - \sum_{i=1}^{M-1}\Big(\big(u_i^{n+1}\big)^p - 2\big(u_i^n\big)^p + \big(u_i^{n+1}\big)^p\Big)\big(u_{\hat{x}}^{n+1} + u_{\hat{x}}^{n-1}\big)\Bigg]\\ &\le \frac{C}{\tau^2}\big(\|u^{n-1}\|^2 + \|u^n\|^2 + \|u^{n+1}\|^2 + \|u_x^{n-1}\|^2 + \|u_x^n\|^2 + \|u_x^{n+1}\|^2\big),\end{aligned} \tag{20}$$

where Eq. (14), the Cauchy-Schwarz inequality, the boundary conditions (12), Eq. (16), and Lemma 2 are used, respectively. Due to inequalities (17)–(20), Eq. (15) can be rewritten as

$$\begin{aligned}&\Big(\|u^{n+1}\|^2 - \|u^{n-1}\|^2\Big) + s_1\Big(\|u_x^{n+1}\|^2 - \|u_x^{n-1}\|^2\Big) + s_2\Big(\|u_{x\bar{x}}^{n+1}\|^2 - \|u_{x\bar{x}}^{n-1}\|^2\Big)\\ &\quad\le 2\tau C\big(\|u^{n-1}\|^2 + \|u^n\|^2 + \|u^{n+1}\|^2 + \|u_x^{n-1}\|^2 + \|u_x^n\|^2 + \|u_x^{n+1}\|^2\big).\end{aligned} \tag{21}$$

Next, the function B^n is presented:

$$B^n = \|u^n\|^2 + \|u^{n-1}\|^2 + s_1\Big(\|u_x^n\|^2 + \|u_x^{n-1}\|^2\Big) + s_2\Big(\|u_{x\bar{x}}^n\|^2 + \|u_{x\bar{x}}^{n-1}\|^2\Big) \tag{22}$$

and, turning to Eq. (21), we express it in terms of a function defined in Eq. (22) as follows:

$$B^{n+1} - B^n \le \tau C\big(B^{n+1} + B^n\big).$$

If τ is sufficiently small which satisfies $\tau \le \dfrac{k-2}{kC}$ and $k>2$ then

$$B^{n+1} \le \frac{(1+\tau C)}{(1-\tau C)} B^n \le (1+\tau kC)B^n \le \exp(CT)B^0. \tag{23}$$

Thus, B^{n+1} in the left-hand side in Eq. (23) is bounded, which immediately provides $\|u^n\| \le C$, $\|u_x^n\| \le C$ and $\|u_{x\bar{x}}^n\| \le C$. Next, we are ready to estimate $\|u^n\|_\infty \le C$ and $\|u_x^n\|_\infty \le C$ where Lemma 3 is used. □

4. Existence and uniqueness

At present, we prove the solvability of the solution to the scheme (10) that guarantees the existence and uniqueness of our numerical solution. To prove the existence of the solution to the scheme (10)–(12), the Browder fixed point theorem will be used for the proof.

Lemma 5 (Browder fixed point theorem [31]). *Let H be a finite dimensional inner product space. Suppose that g: $H \to H$ is continuous, and there exists an $\alpha > 0$ such that $(g(x), x) > 0$ for all $x \in H$ with $\|x\| = \alpha$. Then, there exists $x^* \in H$ such that $g(x^*) = 0$ and $\|x^*\| \le \alpha$.*

Lemma 6. *Let $v \in Z_h^0$. Then $(\psi_p(v), v) = 0$.*

Proof. The direct calculation of the inner product gives

$$\begin{aligned}(\psi_p(v), v) &= \frac{\alpha ph}{(p+1)} \sum_{i=1}^{M-1} [(v_i)^{p-1}(v_i)_{\hat{x}} + [(v_i)^p]_{\hat{x}}]v_i \\ &= \frac{\alpha p}{2(p+1)} \sum_{i=1}^{M-1} [v_{i+1}(v_i)^p - v_{i-1}(v_i)^p + v_i(v_{i+1})^p - v_i(v_{i-1})^p] \\ &= 0,\end{aligned}$$

which completes the proof. □

Theorem 7. *The finite difference scheme (10)–(12) is solvable.*

Proof. To prove the theorem, we proceed by the mathematical induction. We assume that $u^0, u^1, \ldots, u^n$ satisfy the difference scheme (10) for $1 \le n \le N-1$. Indeed, u^1 can be computed by an available method. Next, we prove that there exists u^{n+1} satisfied Eq. (10). Define an operator $g: Z_h^0 \to Z_h^0$ as the following form

$$\begin{aligned}g(v) = v - u^{n-1} &- s_1\left(v_{x\bar{x}} - u_{x\bar{x}}^{n-1}\right) + s_2\left(v_{xx\bar{x}\bar{x}} - u_{xx\bar{x}\bar{x}}^{n-1}\right) + 2\tau(u^n)_{\hat{x}} + 2\tau\alpha[(u^n)^p]_{\hat{x}} \\ &+\frac{\tau}{3}\left((v)_{\hat{x}} - 2(u^n)_{\hat{x}} + (u^{n-1})_{\hat{x}}\right) + \frac{\tau}{3}\left(\psi_p(v) - 2\psi_p(u^n) + \psi_p\left(u^{n-1}\right)\right).\end{aligned}$$

In order to apply the Browder fixed point theorem, we need to show that there exists a positive α such that $(g(v), v) > 0$ for all $v \in Z_h^0$ with $\|v\| = \alpha$. Let us consider

$$\begin{aligned}(g(v), v) =& \|v\|^2 + s_1\|v_x\|^2 + s_2\|v_{x\bar{x}}\|^2 - (u^{n-1}, v) - s_1(u_x^{n-1}, v_x) - s_2(u_{x\bar{x}}^{n-1}, v_{x\bar{x}}) \\ &+ 2\tau\alpha([(u^n)^p]_{\hat{x}}, v) + \frac{\tau}{3}\left(4u_{\hat{x}}^n + u_{\hat{x}}^{n-1}, v\right) + \frac{\tau}{3}\left(\psi_p(v) - 2\psi_p(u^n) + \psi_p\left(u^{n-1}\right), v\right) \\ \ge& \|v\|^2 + s_1\|v_x\|^2 + s_2\|v_{x\bar{x}}\|^2 - \|v\| \cdot \|u^{n-1}\| - s_1\|v_x\| \cdot \|u_x^{n-1}\| \\ &- s_2\|v_{x\bar{x}}\| \cdot \|u_{x\bar{x}}^{n-1}\| - \frac{\tau}{3}\left(4\|u_x^n\| \cdot \|v\| + \|u_x^{n-1}\| \cdot \|v\|\right) \\ &+ 2\tau\alpha([(u^n)^p]_{\hat{x}}, v) + \frac{-2\tau}{3}(\psi_p(u^n), v) + \frac{\tau}{3}\left(\psi_p\left(u^{n-1}\right), v\right)\end{aligned} \tag{24}$$

where we apply the Cauchy-Schwarz inequality, Lemma 2, Lemma 6, and Eq. (16). Using Theorem 4, Eq. (16), and the Young's inequality, which immediately obtain inequalities

$$\begin{aligned}([(u^n)^p]_{\hat{x}}, v) &= -h\sum_{i=1}^{M-1}(u_i^n)^p(v_i)_{\hat{x}} \le C\|u^n\| \cdot \|v\| \le C\tau\|u^n\|^2 + \frac{1}{24\alpha\tau}\|v\|^2, \\ (\psi_p(u^n), v) &= \frac{\alpha ph}{(p+1)} \sum_{i=1}^{M-1}[(u_i^n)^{p-1}(u_i^n)_{\hat{x}} + [(u_i^n)^p]_{\hat{x}}]v_i \le hC\left(\sum_{i=1}^{M-1}\left|(u_i^n)^{p-1}(u_i^n)_{\hat{x}}\right||v_i| + \sum_{i=1}^{M-1}\left|u_i^n\right|^p|(v_i)_{\hat{x}}|\right) \\ &\le C\tau\left(\|u^n\|^2 + \|u_x^n\|^2\right) + \frac{1}{8\tau}\|v\|^2 + \frac{s_1}{4\tau}\|v_x\|^2.\end{aligned}$$

Next, we calculate $\left(\psi_p(u^{n-1}), v\right)$ which is similar to the above:

$$\left(\psi_p(u^{n-1}), v\right) \le C\tau\left(\|u^{n-1}\|^2 + \|u_x^{n-1}\|^2\right) + \frac{1}{4\tau}\|v\|^2 + \frac{s_1}{2\tau}\|v_x\|^2.$$

Again by using the Young's inequality with the remaining terms in Eq. (24), we have

$$\begin{aligned}
\|u^{n-1}\| \cdot \|v\| &\le 3\|u^{n-1}\|^2 + \frac{1}{12}\|v\|^2,\\
\|u^{n-1}\| \cdot \|v_x\| &\le \frac{3}{2}\|u_x^{n-1}\|^2 + \frac{1}{6}\|v_x\|^2,\\
\|u_{x\bar{x}}^{n-1}\| \cdot \|v_{x\bar{x}}\| &\le \frac{1}{2}\|u_{x\bar{x}}^{n-1}\|^2 + \frac{1}{2}\|v_{x\bar{x}}\|^2,\\
\|u_x^n\| \cdot \|v\| &\le 4\tau\|u_x^n\|^2 + \frac{1}{16\tau}\|v\|^2,\\
\|u_x^{n-1}\| \cdot \|v\| &\le \tau\|u_x^n\|^2 + \frac{1}{4\tau}\|v\|^2.
\end{aligned}$$

Then Eq. (24) can be estimated by

$$\begin{aligned}
(g(v), v) \ge& \frac{1}{2}\left(\|v\|^2 + s_1\|v_x\|^2 + s_2\|v_{x\bar{x}}\|^2\right) - C\left(\|u^{n-1}\|^2 + \|u_x^{n-1}\|^2 + \|u_{x\bar{x}}^{n-1}\|^2\right)\\
&- C\tau^2\left(\|u^{n-1}\|^2 + \|u_x^{n-1}\|^2 + \|u^n\|^2 + \|u_x^n\|^2\right)\\
\ge& \frac{1}{2}\|v\|^2 - (1+\tau^2)C\left(\|u^{n-1}\|^2 + \|u_x^{n-1}\|^2 + \|u_{x\bar{x}}^{n-1}\|^2 + \|u^n\|^2 + \|u_x^n\|^2\right).
\end{aligned}$$

That is $(g(v), v) \ge 0$, for all $v \in Z_h^0$ with

$$\|v\| = 2(1+\tau^2)C\left(\|u^{n-1}\|^2 + \|u_x^{n-1}\|^2 + \|u_{x\bar{x}}^{n-1}\|^2 + \|u^n\|^2 + \|u_x^n\|^2\right) + 1.$$

Finally, it follows from the Browder fixed point theorem that there exists $v^* \in Z_h^0$ which satisfies $g(v^*) = 0$. This implies the existence of the solution to the scheme (10)–(12). This completes the proof. □

Theorem 8. *Suppose τ is sufficiently small. The finite difference scheme (10)–(12) is unique.*

Proof. Suppose that u^{n+1} and w^{n+1} are two solutions of the scheme (10)–(12). We denote $\rho^{n+1} = u^{n+1} - w^{n+1}$. Then,

$$\rho_i^{n+1} - s_1\left(\rho_i^{n+1}\right)_{x\bar{x}} + s_2\left(\rho_i^{n+1}\right)_{xx\bar{x}\bar{x}} + \frac{\tau}{3}(\rho_i^{n+1})_{\hat{x}} + \frac{\tau}{3}[\psi_p(u_i^{n+1}) - \psi_p(w_i^{n+1})] = 0. \tag{25}$$

Taking the inner product of Eq. (25) with ρ^{n+1} leads to

$$\left\|\rho^{n+1}\right\|^2 + s_1\left\|\rho_x^{n+1}\right\|^2 + s_2\left\|\rho_{x\bar{x}}^{n+1}\right\|^2 + \frac{\tau}{3}\left(\psi_p(u^{n+1}) - \psi_p(w^{n+1}), \rho^{n+1}\right) = 0, \tag{26}$$

where Lemma 2 is used. The inner product, $\left(\psi_p(u^{n+1}) - \psi_p(w^{n+1}), \rho^{n+1}\right)$, may be arranged as

$$\begin{aligned}
\left(\psi_p(u^{n+1}) - \psi_p(w^{n+1}), \rho^{n+1}\right) &= h\sum_{i=1}^{M-1}\left(\psi_p(u_i^{n+1}) - \psi_p(w_i^{n+1})\right)\rho_i^{n+1}\\
&= \frac{\alpha p h}{(p+1)}\sum_{i=1}^{M-1}\left((u_i^{n+1})^{p-1}(u_i^{n+1})_{\hat{x}} - (w_i^{n+1})^{p-1}(w_i^{n+1})_{\hat{x}}\right)\rho_i^{n+1}\\
&\quad + \frac{\alpha p h}{(p+1)}\sum_{i=1}^{M-1}\left([(u_i^{n+1})^p]_{\hat{x}} - [(w_i^{n+1})^p]_{\hat{x}}\right)\rho_i^{n+1}.
\end{aligned}$$

Next, we apply Theorem 4, the Cauchy-Schwarz inequality, and Eq. (16), giving

$$\begin{aligned}
&h\sum_{i=1}^{M-1}\left(\left(u_i^{n+1}\right)^{p-1}\left(u_i^{n+1}\right)_{\hat{x}} - \left(w_i^{n+1}\right)^{p-1}\left(w_i^{n+1}\right)_{\hat{x}}\right)\rho_i^{n+1}\\
&= h\sum_{i=1}^{M-1}\left(\left(u_i^{n+1}\right)^{p-1}\left(\rho_i^{n+1}\right)_{\hat{x}} + \rho_i^{n+1}\left(w_i^{n+1}\right)_{\hat{x}}\sum_{j=0}^{p-2}\left(u_i^{n+1}\right)^{p-j-2}\left(w_i^{n+1}\right)^j\right)\rho_i^{n+1}\\
&= hC\sum_{i=1}^{M-1}\left(|(\rho_i^{n+1})_{\hat{x}}| + |\rho_i^{n+1}|\right)|\rho_i^{n+1}|\\
&\le C\left(\|\rho^{n+1}\|^2 + \|\rho_x^{n+1}\|^2\right),
\end{aligned}$$

and

$$h\sum_{i=1}^{M-1}\left([(u_i^{n+1})^p]_{\hat{x}}-[(w_i^{n+1})^p]_{\hat{x}}\right)\rho_i^{n+1}=-h\sum_{i=1}^{M-1}\left((u_i^{n+1})^p-(w_i^{n+1})^p\right)(\rho_i^{n+1})_{\hat{x}}$$
$$=-h\sum_{i=1}^{M-1}\left(\rho_i^{n+1}\sum_{j=0}^{p-1}\left(u_i^{n+1}\right)^{p-j-1}\left(w_i^{n+1}\right)^j\right)(\rho_i^{n+1})_{\hat{x}}$$
$$\le hC\sum_{i=1}^{M-1}\left|\rho_i^{n+1}\right|\left|(\rho_i^{n+1})_{\hat{x}}\right|\le C\left(\|\rho^{n+1}\|^2+\|\rho_x^{n+1}\|^2\right),$$

respectively. Hence, the inner product appearing in Eq. (26) may be reduced to the relation

$$\left(\psi_p(u^{n+1})-\psi_p(w^{n+1}),\rho^{n+1}\right)\le C\left(\|\rho^{n+1}\|^2+\|\rho_x^{n+1}\|^2\right).$$

Using the above inequality, Eq. (26) can be estimated as

$$\left\|\rho^{n+1}\right\|^2+s_1\left\|\rho_x^{n+1}\right\|^2+s_2\left\|\rho_{x\bar{x}}^{n+1}\right\|^2\le\tau C\left(\left\|\rho^{n+1}\right\|^2+\left\|\rho_x^{n+1}\right\|^2\right).$$

Provided that τ is sufficiently small such that $s_2-\tau C>0$, then we obtain inequality

$$(1-\tau C)\left\|\rho^{n+1}\right\|^2+s_1\left\|\rho_x^{n+1}\right\|^2+(s_2-\tau C)\left\|\rho_{x\bar{x}}^{n+1}\right\|^2\le 0. \tag{27}$$

Finally, Eq. (27) implies that

$$\left\|\rho^{n+1}\right\|=\left\|\rho_x^{n+1}\right\|=\left\|\rho_{x\bar{x}}^{n+1}\right\|=0.$$

That is, Eq. (25) has only a trivial solution. Therefore, the scheme (10)–(12) determines u^{n+1} uniquely, as in required, which completes the proof. □

5. Convergence and stability

In this section, we prove the convergence and stability of the scheme (10)–(12). Let $e_i^n=v_i^n-u_i^n$, where v_i^n and u_i^n are the solutions of (1)–(3) and (10)–(12), respectively. We then obtain the following error equations

$$r_i^n=\left(e_i^n\right)_{\hat{t}}-s_1\left(e_i^n\right)_{x\bar{x}\hat{t}}+s_2\left(e_i^n\right)_{xx\bar{x}\bar{x}\hat{t}}+\left(e_i^n\right)_{\hat{x}}+\alpha\left[(v_i^n)^p\right]_{\hat{x}}-\alpha\left[(u_i^n)^p\right]_{\hat{x}}$$
$$+\frac{\tau^2}{6}(e_i^n)_{\hat{x}t\bar{t}}+\frac{\tau^2}{6}[\psi_p(v_i^n)]_{t\bar{t}}-\frac{\tau^2}{6}[\psi_p(u_i^n)]_{t\bar{t}}, \tag{28}$$

where r_i^n denotes the truncation error. By using Taylor expansion, we easily obtain that $r_i^n=O\left(\tau^4+h^2\tau^2+h^4\right)$ holds as τ, $h\to 0$.

The following lemmas are well known and useful for the proof of convergence and stability.

Lemma 9 (discrete Gronwall's inequality [30])**.** *Suppose that $\omega(k)$ and $\rho(k)$ are nonnegative functions, and $\rho(k)$ is nondecreasing. If $C>0$ and*

$$\omega(k)\le\rho(k)+C\tau\sum_{l=0}^{k-1}\omega(l),\quad\forall k$$

then

$$\omega(k)\le\rho(k)e^{C\tau k},\quad\forall k.$$

Lemma 10. *Suppose that $u_0\in H_0^2[x_l,x_r]$, then the solution u^n of Eqs. (1)–(3) satisfies*

$$\|u\|_{L_2}\le C,\quad\|u_x\|_{L_2}\le C,\quad\|u\|_{L_\infty}\le C,\quad\|u_x\|_{L_\infty}\le C.$$

The following theorem guarantees the convergence of our scheme with the convergence rate $O(\tau^4+\tau^2h^2+h^4)$.

Theorem 11. *Suppose $u_0\in H_0^2[x_l,x_r]$, then the solution u^n of the scheme (10)–(12) converges to the solution of the problem (1)–(3) in the sense of $\|\cdot\|_\infty$, and the rate of convergence is $O(\tau^4+h^2\tau^2+h^4)$.*

Proof. Taking the inner product of Eq. (28) and $2\bar{e}^n$(*i.e.* $e^{n+1}+e^{n-1}$) leads to

$$\left(\left\|e^{n+1}\right\|^2-\left\|e^{n-1}\right\|^2\right)+s_1\left(\left\|e_x^{n+1}\right\|^2-\left\|e_x^{n-1}\right\|^2\right)+s_2\left(\left\|e_{x\bar{x}}^{n+1}\right\|^2-\left\|e_{x\bar{x}}^{n-1}\right\|^2\right)+2\tau\left(e_{\hat{x}}^n,2\bar{e}^n\right)$$
$$+\alpha\left(\left[(v^n)^p-(u^n)^p\right]_{\hat{x}},2\bar{e}^n\right)+\frac{\tau^3}{3}\left(e_{\hat{x}t\bar{t}}^n,2\bar{e}^n\right)+\frac{\tau^3}{3}\left([\psi_p(v^n)]_{t\bar{t}}-[\psi_p(u^n)]_{t\bar{t}},2\bar{e}^n\right)-2\tau\left(r^n,2\bar{e}^n\right)=0, \tag{29}$$

where Lemma 2 is used. The quantity appearing in Eq. (29) may be reduced to relations

$$\|e^n_{\hat{x}}\|^2 \le \|e^n_x\|^2, \tag{30}$$

$$\left(e^n_{\hat{x}}, 2\bar{e}^n\right) \le \|e^n_x\|^2 + \frac{1}{2}\left(\|e^{n+1}\|^2 + \|e^{n-1}\|^2\right), \tag{31}$$

$$(r^n, 2e^n) \le \|r^n\|^2 + \frac{1}{2}\left(\|e^{n+1}\|^2 + \|e^{n-1}\|^2\right). \tag{32}$$

By using Lemma 2, Lemma 10, and Theorem 4, we see that

$$\begin{aligned}
\left(e^n_{\hat{x}t\bar{t}}, 2\bar{e}^n\right) &= \frac{h}{\tau^2}\sum_{i=1}^{M-1}\left((e_i^{n+1})_{\hat{x}} - 2(e_i^n)_{\hat{x}} + (e_i^{n-1})_{\hat{x}}\right)(e_i^{n+1} - e_i^{n-1}) \\
&\le \frac{2}{\tau^2}\left(\|e^{n-1}\|^2 + \|e^{n+1}\|^2 + \|e_x^{n-1}\|^2 + \|e_x^n\|^2 + \|e_x^{n+1}\|^2\right) \\
\left(\left[(v^n)^p - (u^n)^p\right]_{\hat{x}}, 2\bar{e}^n\right) &= -h\sum_{i=1}^{M-1}\left(\left(v_i^n\right)^p - \left(u_i^n\right)^p\right)(\bar{e}_i^n)_{\hat{x}} \\
&= -h\sum_{i=1}^{M-1}\left(e_i^n\sum_{j=0}^{p-1}\left(v_i^{n+1}\right)^{p-j-1}\left(u_i^{n+1}\right)^j\right)(\bar{e}_i^n)_{\hat{x}} \\
&\le hC\sum_{i=1}^{M-1}\left|e_i^n\right|\left|(\bar{e}_i^n)_{\hat{x}}\right| \\
&\le C\left(\|e^n\|^2 + \|e_x^{n-1}\|^2 + \|e_x^{n+1}\|^2\right).
\end{aligned} \tag{33}$$

Next, we turn to the inner product, $\left([\psi_p(v^n)]_{t\bar{t}} - [\psi_p(u^n)]_{t\bar{t}}, 2\bar{e}^n\right)$ in Eq. (29), and we have

$$\left([\psi_p(v^n)]_{t\bar{t}} - [\psi_p(u^n)]_{t\bar{t}}, 2\bar{e}^n\right) = \frac{\alpha p}{(p+1)}[(M_1, 2\bar{e}^n) - (M_2, 2\bar{e}^n)]$$

where

$$M_1 = \left[(v^n)^{p-1}(v^n)_{\hat{x}}\right]_{t\bar{t}} - \left[(u^n)^{p-1}(u^n)_{\hat{x}}\right]_{t\bar{t}},$$
$$M_2 = \left[(v^n)^p\right]_{\hat{x}t\bar{t}} - \left[(u^n)^p\right]_{\hat{x}t\bar{t}},$$

are used. According to Lemma 2, Theorem 4, Lemma 10, the Cauchy-Schwartz inequality and Eq. (30), we arrive at

$$\begin{aligned}
\left((v^n)^{p-1}(v^n)_{\hat{x}} - (u^n)^{p-1}(u^n)_{\hat{x}}, 2\bar{e}^n\right) &= 2h\sum_{i=1}^{M-1}\left[\left(v_i^n\right)^{p-1}\left(v_i^n\right)_{\hat{x}} - \left(u_i^n\right)^{p-1}\left(u_i^n\right)_{\hat{x}}\right]\bar{e}_i^n \\
&= 2h\sum_{i=1}^{M-1}\left[\left(v_i^n\right)^{p-1}\left(e_i^n\right)_{\hat{x}}\bar{e}_i^n\right] + 2h\sum_{i=1}^{M-1}\left[\left(v_i^n\right)^{p-1} - \left(u_i^n\right)^{p-1}\right]\left(u_i^n\right)_{\hat{x}}\bar{e}_i^n \\
&= 2h\sum_{i=1}^{M-1}\left[\left(v_i^n\right)^{p-1}\left(e_i^n\right)_{\hat{x}}\bar{e}_i^n\right] + 2h\sum_{i=1}^{M-1}\left[e_i^n\sum_{k=0}^{p-2}\left(v_i^n\right)^{p-2-k}\left(u_i^n\right)^k\right]\left(u_i^n\right)_{\hat{x}}\bar{e}_i^n \\
&\le C\left(\|e^{n-1}\|^2 + \|e^n\|^2 + \|e^{n+1}\|^2 + \|e_x^n\|^2\right).
\end{aligned} \tag{34}$$

This leads to the inequality

$$(M_1, 2\bar{e}^n) \le \frac{C}{\tau^2}\left(\|e^{n-1}\|^2 + \|e^n\|^2 + \|e^{n+1}\|^2 + \|e_x^{n-1}\|^2 + \|e_x^n\|^2 + \|e_x^{n+1}\|^2\right). \tag{35}$$

Here, we also have

$$(M_2, 2\bar{e}^n) \le \frac{C}{\tau^2}\left(\|e^{n-1}\|^2 + \|e^n\|^2 + \|e^{n+1}\|^2 + \|e_x^{n-1}\|^2 + \|e_x^{n+1}\|^2\right) \tag{36}$$

which is similar to the proof of Eq. (33). Instead of Eqs. (30)–(36), Eq. (29) becomes

$$\begin{aligned}
&\left(\|e^{n+1}\|^2 - \|e^{n-1}\|^2\right) + s_1\left(\|e_x^{n+1}\|^2 - \|e_x^{n-1}\|^2\right) + s_2\left(\|e_{x\bar{x}}^{n+1}\|^2 - \|e_{x\bar{x}}^{n-1}\|^2\right) \\
&\quad \le C\tau\left(\|e^{n-1}\|^2 + \|e^n\|^2 + \|e^{n+1}\|^2 + \|e_x^{n-1}\|^2 + \|e_x^n\|^2 + \|e_x^{n+1}\|^2\right) + 2\tau\|r^n\|^2.
\end{aligned} \tag{37}$$

Let B^n be defined as follows:

$$B^n = \left(\|e^n\|^2 + \|e^{n-1}\|^2\right) + s_1\left(\|e_x^n\|^2 + \|e_x^{n-1}\|^2\right) + s_2\left(\|e_{x\bar{x}}^n\|^2 + \|e_{x\bar{x}}^{n-1}\|^2\right)$$

and, turning to Eq. (37), we easily obtain that

$$B^{n+1} - B^n \le 2\tau\|r^n\|^2 + \tau C\left(B^{n+1} + B^n\right).$$

Therefore,

$$(1 - C\tau)\left(B^{n+1} - B^n\right) \le 2\tau\|r^n\|^2 + 2C\tau B^n.$$

Provided that τ is sufficiently small satisfying $1 - C\tau > 0$, then

$$B^{n+1} - B^n \le C\tau\|r^n\|^2 + \tau C B^n.$$

By summing up from 0 to $n-1$, we have

$$B^n \le B^0 + C\tau\sum_{k=0}^{n-1}\|r^k\|^2 + C\tau\sum_{l=0}^{n-1}B^k. \tag{38}$$

The properties of the operator norm and Eq. (28) yield

$$\tau\sum_{k=0}^{n-1}\|r^k\|^2 \le n\tau\max_{0\le k\le n-1}\|r^k\|^2 \le T\cdot O\left(\tau^4 + \tau^2h^2 + h^4\right)^2$$

and $e^0 = 0$. Now, we are ready to estimate

$$B^n \le O\left(\tau^4 + \tau^2h^2 + h^2\right)^2 + C\tau\sum_{k=0}^{n-1}B^k,$$

where $B^0 = O\left(\tau^4 + \tau^2h^2 + h^4\right)^2$. According to Lemma 9 , we obtain the inequality $B^n \le O\left(\tau^4 + \tau^2h^2 + h^4\right)^2$, that is

$$\|e^n\|^2 \le O\left(\tau^4 + \tau^2h^2 + h^4\right)^2, \quad \|e_x^n\|^2 \le O\left(\tau^4 + \tau^2h^2 + h^4\right)^2,$$

and $\|e_{x\bar{x}}^n\|^2 \le O\left(\tau^4 + \tau^2h^2 + h^4\right)^2$, respectively. Finally, we arrive at our aim

$$\|e^n\|_\infty \le C\|e^n\| + C\|e_x^n\| \le O\left(\tau^4 + \tau^2h^2 + h^4\right),$$

due to Lemma 3, which completes the proof. □

Theorem 12. *Under the conditions of Theorem 11, the solution of scheme (10)–(12) is stable by* $\|\cdot\|_\infty$.

6. Iterative algorithm

This section gives an iterative algorithm for solving the nonlinear implicit higher-order compact three-level scheme (10)–(12). Inspired by the techniques in Sun and Zhu [32], the nonlinear term can be solved by the following iterative algorithm, for $s = 0, 1, 2, \ldots,$:

$$\begin{aligned}&\frac{1}{2\tau}\left(u_i^{(n+1)(s+1)} - u_i^{n-1}\right) - \frac{s_1}{2\tau}\left(u_i^{(n+1)(s+1)} - u_i^{n-1}\right)_{x\bar{x}}\\ &\quad + \frac{s_2}{2\tau}\left(u_i^{(n+1)(s+1)} - u_i^{n-1}\right)_{xx\bar{x}\bar{x}} + \left(u_i^n\right)_{\hat{x}} + \alpha\left[(u_i^n)^p\right]_{\hat{x}} + \frac{1}{6}\left(u_i^{(n+1)(s+1)} - 2u_i^n + u_i^{n-1}\right)_{\hat{x}}\\ &\quad + \frac{1}{6}\left[\psi_p\left(u_i^{(n+1)(s)}\right) - 2\psi_p\left(u_i^n\right) + \psi_p\left(u_i^{n-1}\right)\right] = 0; \quad 1 \le i \le M-1,\ 1 \le n \le N-1,\end{aligned} \tag{39}$$

$$u_i^0 = u_0(x_i), \quad 0 \le i \le M, \tag{40}$$

$$u_0^n = u_M^n = 0,\ (u_0^n)_x = (u_M^n)_x = 0,\ (u_0^n)_{x\bar{x}} = (u_M^n)_{x\bar{x}} = 0,\ 1 \le n \le N, \tag{41}$$

where

$$u_i^{(n+1)(0)} = 2u_i^n - u_i^{n-1}.$$

Before proving the convergence of the iterative algorithm (39)–(41), we let

$$\varepsilon_i^{(s)} = u_i^{(n+1)} - u_i^{(n+1)(s)}.$$

Note that

$$\begin{aligned}\varepsilon_i^{(0)} &= u_i^{n+1} - 2u_i^n + u_i^{n-1}\\ &\le \left(u_i^{n+1} - v_i^{n+1}\right) - 2\left(u_i^n - v_i^n\right) + \left(u_i^{n-1} - v_i^{n-1}\right) + v_i^{n+1} - 2v_i^n + v_i^{n-1}\\ &\le O(h^4 + h^2\tau^2 + \tau^4) + O(\tau^2) = O(\tau^2 + h^4).\end{aligned} \tag{42}$$

Similarly, we also have

$$\left(\varepsilon_i^{(0)}\right)_x \le O(\tau^2 + h^4), \quad \left(\varepsilon_i^{(0)}\right)_{x\bar{x}} \le O(\tau^2 + h^4). \tag{43}$$

Theorem 13. *Let τ and h be sufficiently small. Then, the iterative algorithm (39)–(41) converges to the solution of the higher-order compact difference scheme (10)–(12).*

Proof. Let τ and h be sufficiently small. We have

$$\|\varepsilon^{(0)}\|_\infty \le \frac{1}{2}.$$

Suppose

$$\|\varepsilon^{(s)}\|_\infty \le \frac{1}{2} \text{ and } \|\varepsilon_x^{(s)}\|_\infty \le \frac{1}{2}. \tag{44}$$

By Theorem 4 and the assumption (44), we see that

$$\|u^{(n+1)(s)}\|_\infty \le \|u^{n+1}\|_\infty + \|\varepsilon^{(s)}\|_\infty \le C.$$

Subtracting Eqs. (39)–(41) from Eqs. (10)–(12), we have

$$\frac{1}{2\tau}\varepsilon_i^{(s+1)} - \frac{s_1}{2\tau}\left(\varepsilon_i^{(s+1)}\right)_{x\bar{x}} + \frac{s_2}{2\tau}\left(\varepsilon_i^{(s+1)}\right)_{xx\bar{x}\bar{x}} + \frac{1}{6}\left(\varepsilon_i^{(s+1)}\right)_{\hat{x}} + \frac{1}{6}\left[\psi_p\left(u_i^{(n+1)(s+1)}\right) - \psi_p\left(u_i^{n+1}\right)\right] = 0. \tag{45}$$

Taking the inner product of Eq. (45) with $\varepsilon^{(s+1)}$, by using Lemma 2, we have

$$\left\|\varepsilon^{(s+1)}\right\|^2 + s_1\left\|\varepsilon_x^{(s+1)}\right\|^2 + s_2\left\|\varepsilon_{x\bar{x}}^{(s+1)}\right\|^2 + \frac{\tau}{3}\left(\psi_p\left(u^{(n+1)(s)}\right) - \psi_p\left(u^{n+1}\right), \varepsilon^{(s+1)}\right) = 0. \tag{46}$$

The inner product, $\left(\psi_p\left(u^{(n+1)(s)}\right) - \psi_p\left(u^{n+1}\right), \varepsilon^{(s+1)}\right)$, appearing in Eq. (46) may be reduced to the relation

$$\left(\psi_p\left(u^{(n+1)(s)}\right) - \psi_p\left(u^{n+1}\right), \varepsilon^{(s+1)}\right) = \frac{\alpha p}{(p+1)}\left[\left(M_3, \varepsilon^{(s+1)}\right) - \left(M_4, \varepsilon^{(s+1)}\right)\right], \tag{47}$$

where

$$M_3 = \left(u^{(n+1)(s)}\right)^{p-1}\left(u^{(n+1)(s)}\right)_{\hat{x}} - \left(u^{n+1}\right)^{p-1}\left(u^{n+1}\right)_{\hat{x}},$$
$$M_4 = \left(u^{(n+1)(s)}\right)^{p} - \left(u^{n+1}\right)^{p}.$$

Turning to Eq. (47), we express inner product terms as

$$\begin{aligned}\left(M_3, \varepsilon^{(s+1)}\right) &= \left(\left(u^{(n+1)(s)}\right)^{p-1}\left(u^{(n+1)(s)}\right)_{\hat{x}} - \left(u^{n+1}\right)^{p-1}\left(u^{n+1}\right)_{\hat{x}}, \varepsilon_i^{(s+1)}\right)\\ &= h\sum_{i=1}^{M-1}\left[\left(u_i^{(n+1)(s)}\right)^{p-1}\left(u_i^{(n+1)(s)}\right)_{\hat{x}} - \left(u_i^{n+1}\right)^{p-1}\left(u_i^{n+1}\right)_{\hat{x}}\right]\varepsilon_i^{(s+1)}\\ &= h\sum_{i=1}^{M-1}\left(u_i^{(n+1)(s)}\right)^{p-1}\left(\varepsilon_i^{(s)}\right)_{\hat{x}}\varepsilon_i^{(s+1)} + h\sum_{i=1}^{M-1}\left[\left(u_i^{(n+1)(s)}\right)^{p-1} - \left(u_i^{n+1}\right)^{p-1}\right]\left(u_i^{n+1}\right)_{\hat{x}}\varepsilon_i^{(s+1)}\\ &= h\sum_{i=1}^{M-1}\left[\left(u_i^{(n+1)(s)}\right)^{p-1}\left(\varepsilon_i^{(s)}\right)_{\hat{x}}\varepsilon_i^{(s+1)}\right] + h\sum_{i=1}^{M-1}\left[\varepsilon_i^{(s)}\sum_{k=0}^{p-2}\left(u_i^{(n+1)(s)}\right)^{p-2-k}\left(u_i^{n+1}\right)^k\right]\left(u_i^{n+1}\right)_{\hat{x}}\varepsilon_i^{(s+1)}\\ &\le C\left(\|\varepsilon^{(s)}\|^2 + \|\varepsilon_x^{(s)}\|^2 + \|\varepsilon^{(s+1)}\|^2\right),\end{aligned} \tag{48}$$

and

$$\begin{aligned}\left(M_4, \varepsilon_{\hat{x}}^{s+1}\right) &= h\sum_{i=1}^{M-1}\left(\left(u_i^{(n+1)(s)}\right)^{p} - \left(u_i^{n+1}\right)^{p}\right)\left(\varepsilon_i^{(s+1)}\right)_{\hat{x}}\\ &= -h\sum_{i=1}^{M-1}\left(\varepsilon_i^{(s)}\sum_{j=0}^{p-1}\left(u_i^{(n+1)(s)}\right)^{p-j-1}\left(u_i^{n+1}\right)^j\right)\left(\varepsilon_i^{(s+1)}\right)_{\hat{x}}\\ &\le C\left(\|\varepsilon^{(s)}\|^2 + \|\varepsilon_x^{(s+1)}\|^2\right),\end{aligned} \tag{49}$$

by according to Lemma 2, Theorem 4, the Cauchy-Schwartz inequality and Eq. (16). From Eq. (46), we have

$$\|\varepsilon^{(s+1)}\|^2 + s_1\|\varepsilon_x^{(s+1)}\|^2 + s_2\|\varepsilon_{x\bar{x}}^{(s+1)}\|^2 \le \tau C\left(\|\varepsilon^{(s)}\|^2 + \|\varepsilon_x^{(s)}\|^2 + \|\varepsilon^{(s+1)}\|^2 + \|\varepsilon_x^{(s+1)}\|^2\right),$$

where the estimates in Eqs. (48) and (49) are used. Let τ be sufficiently small $s_2 - \tau C > 0$, then the above inequality is arranged as

$$\begin{aligned}\|\varepsilon^{(s+1)}\|_\infty^2 + \|\varepsilon_x^{(s+1)}\|_\infty^2 &\le \tau C\left(\|\varepsilon^{(s)}\|^2 + \|\varepsilon_x^{(s)}\|^2\right)\\ &\le \tau C\left(\|\varepsilon^{(s)}\|_\infty^2 + \|\varepsilon_x^{(s)}\|_\infty^2\right),\end{aligned} \tag{50}$$

where Lemma 3 is used. Again, let ε is sufficiently small to obtain

$$\|\varepsilon^{(s+1)}\|_\infty^2 + \|\varepsilon_x^{(s+1)}\|_\infty^2 \le \frac{1}{2}\left(\|\varepsilon^{(s)}\|_\infty^2 + \|\varepsilon_x^{(s)}\|_\infty^2\right).$$

By the induction principle, we see that $\|\varepsilon^{(s+1)}\|_\infty \le \frac{1}{2}$ and $\|\varepsilon_x^{(s+1)}\|_\infty \le \frac{1}{2}$. Then

$$\|\varepsilon^{(s+1)}\|_\infty \le \frac{1}{2}\|\varepsilon^{(s)}\|_\infty \le \frac{1}{2^{s+1}}\|\varepsilon^{(0)}\|_\infty,$$

which completes the proof. □

7. Numerical experiments

As the first step, the efficiency of the proposed scheme is analyzed by using test cases $p = 2$ and $p = 4$ compared with available data. Next, the consistency of numerical results compared with previous published studies is assessed. The algorithm is finally applied through long-time behavior of a solitary wave to confirm the performance of the present method. To investigate the form and shape of an incident wave, many metrics could be used. It is significant to specify measures which do not alter or barely alter. The evolution of solitary wave amplitude is often described using the Rosenau-RLW equation. In this equation, there are invariants and it specifically shows that

$$Q^n = \int_{x_l}^{x_r} u(x,t)dx \approx h\sum_{i=1}^{M-1} u_i^n, \tag{51}$$

$$\begin{aligned}E^n &= \int_{x_l}^{x_r} u^2(x,t) + u_x^2(x,t) + u_{xx}^2(x,t)dx\\ &\approx h\sum_{i=1}^{M-1}\left(\left(u_i^n\right)^2 + \left[\left(u_i^n\right)_{\hat{x}}\right]^2 + \left[\left(u_i^n\right)_{x\bar{x}}\right]^2\right),\end{aligned} \tag{52}$$

which are related to the conservative of mass and energy, respectively. The benefit of characterizing the wave shape in terms of Q^n and E^n is to investigate on how the wave ultimately evolves. Moreover, the accuracy of the scheme will be monitored by the comparison of numerical data with analytical data by using $\|\cdot\|$ and $\|\cdot\|_\infty$ norms defined by

$$\begin{aligned}\|e^n\| &= \left\|u^{\text{exact}} - u^n\right\| = \left(h\sum_{i=1}^{M-1}\left|u_i^{\text{exact}} - u_i^n\right|^2\right)^{1/2},\\ \|e^n\|_\infty &= \left\|u^{\text{exact}} - u^n\right\|_\infty = \max_{1\le i\le M-1}\left|u_i^{\text{exact}} - u_i^n\right|.\end{aligned}$$

Example 1. Consider the following usual Rosenau-RLW equation in the case of $p = 2$, $\alpha = 0.5$

$$u_t - u_{xxt} + u_{xxxxt} + u_x + uu_x = 0 \tag{53}$$

with an initial condition

$$u(x,0) = \frac{15}{19}\operatorname{sech}^4\left(\frac{\sqrt{13}}{26}x\right), \quad x \in [x_l, x_r], \tag{54}$$

and the boundary conditions

$$u(x_l,t) = u(x_r,t) = u_x(x_l,t) = u_x(x_r,t) = u_{xx}(x_l,t) = u_{xx}(x_r,t) = 0, \quad t \in [0,T]. \tag{55}$$

Recall that Eqs. (53)–(55) possesses the solitary wave of the form

$$u(x,t) = \frac{15}{19}\operatorname{sech}^4\left(\frac{\sqrt{13}}{26}\left(x - \frac{169}{133}t\right)\right).$$

The numerical simulations are performed by setting $x_l = -50$ and $x_r = 150$. The accuracy of the presented scheme is compared with those FDMs for the usual Rosenua-RLW equation in [20,24,33]. Various space and time step combinations

Table 1
The errors of numerical solutions and rate of convergence at $t = 24$ using $p = 2$, $\tau = h$, $x_l = -50$, and $x_r = 150$.

	Present		Ref. [20]		Ref. [24]		Ref. [33]	
	$\|e^n\|$	Rate	$\|e^n\|$	Rate	$\|e^n\|$	Rate	$\|e^n\|$	Rate
$h = 0.8$	7.78402×10^{-4}	–	2.42851×10^{-1}	–	3.11658×10^{-1}	–	2.03287×10^{-2}	–
$h = 0.4$	4.73034×10^{-5}	4.04050	6.58790×10^{-2}	1.88218	8.62872×10^{-2}	1.85275	4.88759×10^{-3}	2.05632
$h = 0.2$	2.94078×10^{-6}	4.00767	1.68468×10^{-2}	1.96735	2.21942×10^{-2}	1.95896	1.21311×10^{-3}	2.01042
$h = 0.1$	1.83776×10^{-7}	4.00018	4.23946×10^{-3}	1.99052	5.59422×10^{-3}	1.98817	3.02978×10^{-4}	2.00142
	Present		Ref. [20]		Ref. [24]		Ref. [33]	
	$\|e^n\|_\infty$	Rate	$\|e^n\|_\infty$	Rate	$\|e^n\|_\infty$	Rate	$\|e^n\|_\infty$	Rate
$h = 0.8$	3.09410×10^{-4}	–	9.06883×10^{-2}	–	1.16717×10^{-1}	–	7.56362×10^{-3}	–
$h = 0.4$	1.87205×10^{-5}	4.04683	2.48437×10^{-2}	1.88218	3.27045×10^{-2}	2.05632	1.82402×10^{-3}	1.85275
$h = 0.2$	1.16521×10^{-6}	4.00596	6.36404×10^{-3}	1.96735	8.43616×10^{-3}	2.01042	4.52324×10^{-4}	1.95896
$h = 0.1$	7.27778×10^{-8}	4.00095	1.12985×10^{-4}	1.99052	3.02978×10^{-4}	2.00142	2.21651×10^{-3}	1.98817

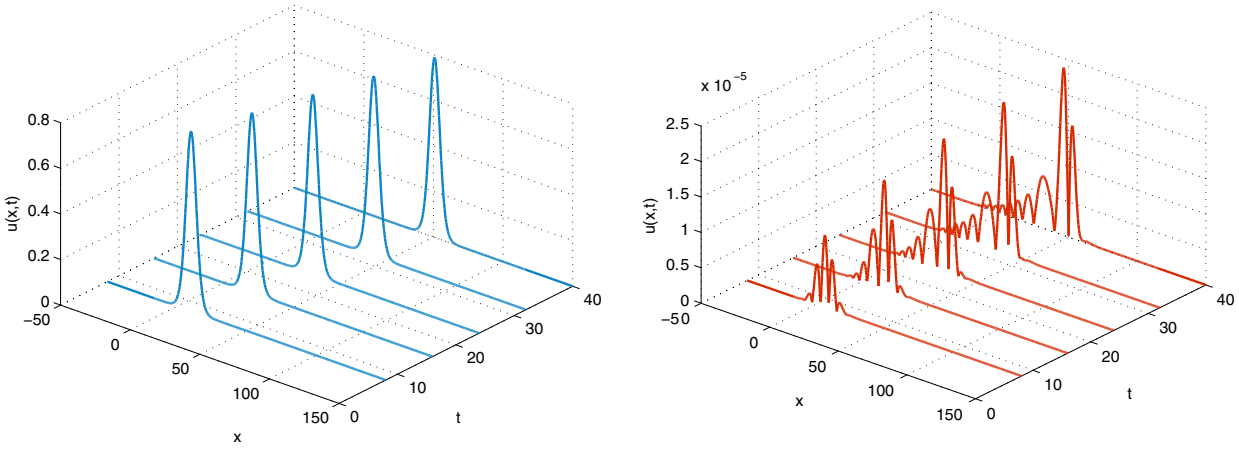

Fig. 1. (Left) Numerical solution using $p = 2$, $\tau = h$ and $x_l = -50$. (Right) Distribution error using $p = 2$, $\tau = h$ and $x_l = -50$.

are investigated and compared with the exact solution. We model a solitary wave with approximately the 0.75 maximum amplitude and present the results of the simulation in Table 1. As seen, the $\|\cdot\|-$ and $\|\cdot\|_\infty-$ error norms stay less than 7.8×10^{-4} at time $t = 24$. The most accurate simulation as obtained from our method is with the choice $\tau = h = 0.1$ for which the $\|\cdot\|-$ and $\|\cdot\|_\infty-$ errors less than 7.3×10^{-8}. According to the results in Table 1, it can be seen that the computational efficiency of the present scheme is clearly better than others, in term of grid point number. Obviously, experimental results agree with the theoretical convergence rate $O(\tau^4 + \tau^2 h^2 + h^4)$ or the fourth-order convergence rate verified in the case $h = \tau$.

The solution profiles are shown in Fig. 1 (Left) at selected time $t \in [0, 40]$. From this figure, it is clear that the peak of solitary waves remains the same during the time simulation. The distribution of absolute errors at selected time $t \in [0, 40]$ is illustrated in Fig. 1 (Right). It seems that the maximum error occurs near the peak amplitude of the solitary wave. Moreover, Fig. 1 (Right) indicates that the error slightly increases as the time is increased.

In the present analysis, there is not only the order of accuracy but also other important factors for improving the efficiency of the numerical method. One of those factors is the preserving invariant property of the method that has the same or perhaps even more impact on numerical results. The proposed method is applied to verify the conservation of the numerical model by tracking the simulation of solitary wave motion run up to $t = 40$, as indicated in Table 2. For a solitary wave, the constant value of the mobility shall be analytically to give $Q = 7.5906342641$. The results show that the mobility constant slightly alters from the exact value by less than $2.1 \times 10^{-9}\%$. Moreover, the invariant E whose exact value is gained as $E = 4.2654202506$ is listed in Table 2 for the simulation period. Likewise, the mobility constant slightly alters from the exact value by less than $2.2 \times 10^{-2}\%$. The result from Table 2 shows discrete mass obtained from Theorem 1 close to the one obtained from the analytical method.

According to the experiment, a waveform at long time should be observed. As in Figs. 2 and 3, the waveforms modeled by the present scheme are illustrated using $h = 0.8$, $\tau = 0.8$, $x_l = -50$, and $x_r = 1300$. The waveforms at $t = 1000$ agree with those at $t = 0$ quite well, which also presents the performance of the scheme. We characterize these results at long time obtained by the second-order finite difference schemes reported by Pan and Zhang [20,24,33] in order to underscore the efficiency of the present scheme. Results obtained by Pan and Zhang [20,24] show lagging of numerical solutions when

Table 2
Quantities Q^n and E^n under different mesh steps $h = \tau = 0.4$ at various time.

	Mass		Energy		Discrete Mass	
	Q^n	$\lvert Q^n - Q(0)\rvert$	E^n	$\lvert E^n - E(0)\rvert$	Q^n_{Thm1}	$\lvert Q^n_{Thm1} - Q(0)\rvert$
Analytical	7.5906342641	–	4.2654202506	–	7.5906342641	–
4	7.5906342641	1.56358×10^{-10}	4.2645011659	9.19091×10^{-4}	7.5906342641	1.55941×10^{-10}
8	7.5906342641	1.55657×10^{-10}	4.2645008939	9.19363×10^{-4}	7.5906342641	1.55491×10^{-10}
12	7.5906342641	1.55242×10^{-10}	4.2645009896	9.19268×10^{-4}	7.5906342641	1.55043×10^{-10}
16	7.5906342641	1.55742×10^{-10}	4.2645009662	9.19291×10^{-4}	7.5906342641	1.55555×10^{-10}
20	7.5906342641	1.56096×10^{-10}	4.2645009588	9.19298×10^{-4}	7.5906342641	1.55933×10^{-10}
24	7.5906342641	1.55834×10^{-10}	4.2645009548	9.19302×10^{-4}	7.5906342641	1.55795×10^{-10}

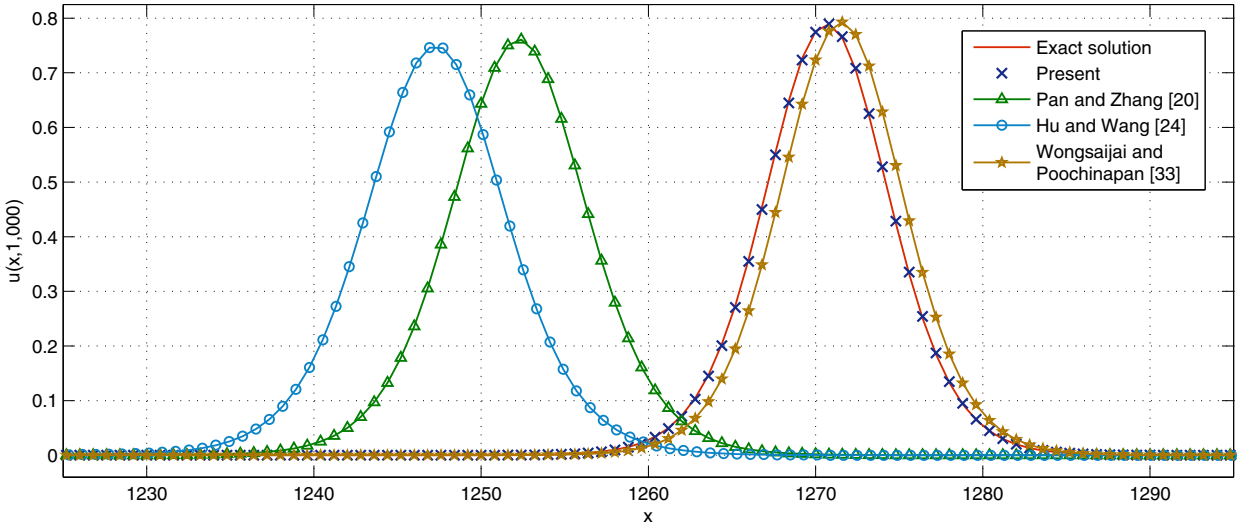

Fig. 2. The long-time behavior of numerical solutions at $t = 1000$ using $p = 2, h = 0.8, \tau = h, x_l = -50,$ and $x_r = 1300$.

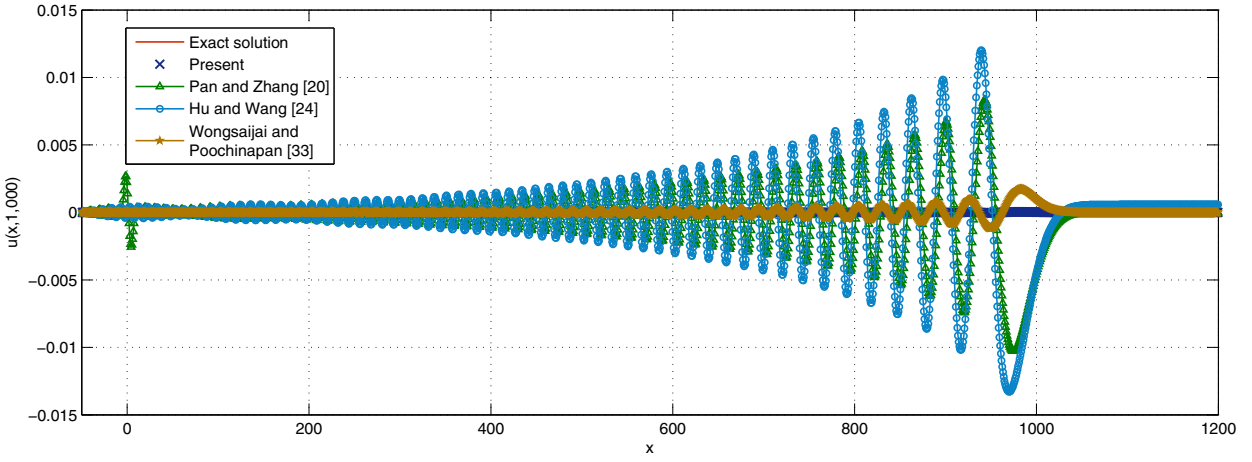

Fig. 3. The left-tail behavior of numerical solutions at $t = 1000$ using $p = 2, h = 0.8, \tau = h, x_l = -50,$ and $x_r = 1300$.

compared to exact solutions. However, results obtained by Wongsaijai and Poochinapan [33] show leading of numerical solutions when compared to exact solutions. Besides, Fig. 3 that illustrates the expanded left-tail figure exhibits the oscillation of numerical approximations on $x \in [-50, 1200]$. As observed, the present method offers the fit resolution of wave structure at left-tail.

Table 3
The errors of numerical solutions and rate of convergence at $t = 24$ using $p = 2$, $\tau = h$, $x_l = -50$, and $x_r = 150$.

	Present		Ref. [17]		Ref. [21]		Ref. [22]	
	$\|e^n\|$	Rate	$\|e^n\|$	Rate	$\|e^n\|$	Rate	$\|e^n\|$	Rate
$h = 0.8$	4.33437×10^{-4}	–	4.33356×10^{-2}	–	2.29013×10^{-1}	–	5.47448×10^{-2}	–
$h = 0.4$	2.59246×10^{-5}	4.06343	1.11909×10^{-2}	1.95323	5.00535×10^{-2}	2.19389	1.29577×10^{-2}	2.07891
$h = 0.2$	1.60587×10^{-6}	4.01289	2.82645×10^{-3}	1.98526	1.21867×10^{-2}	2.03816	3.20256×10^{-3}	2.01652
$h = 0.1$	1.00259×10^{-7}	4.00155	7.09140×10^{-4}	1.99485	3.03019×10^{-3}	2.00783	7.99013×10^{-4}	2.00293
	Present		Ref. [17]		Ref. [21]		Ref. [22]	
	$\|e^n\|_\infty$	Rate	$\|e^n\|_\infty$	Rate	$\|e^n\|_\infty$	Rate	$\|e^n\|_\infty$	Rate
$h = 0.8$	1.73987×10^{-4}	–	1.64873×10^{-2}	–	9.21264×10^{-2}	–	2.03188×10^{-2}	–
$h = 0.4$	1.03213×10^{-5}	4.07528	4.25828×10^{-3}	1.95301	2.01925×10^{-2}	2.18979	4.78559×10^{-3}	2.08604
$h = 0.2$	6.37832×10^{-7}	4.01630	1.07810×10^{-3}	1.98178	4.89501×10^{-3}	2.04444	1.17720×10^{-3}	2.02333
$h = 0.1$	3.97932×10^{-8}	4.00258	2.70375×10^{-4}	1.99546	1.21680×10^{-3}	2.00821	2.93288×10^{-4}	2.00497

Table 4
Quantities Q^n and E^n under different mesh steps $h = \tau = 0.4$ at various time.

	Mass		Energy	
	Q^n	$\|Q^n - Q(0)\|$	E^n	$\|E^n - E(0)\|$
Analytical	6.2658061620	–	2.8676945570	–
4	6.2658061737	1.16998×10^{-8}	2.8667709115	9.23646×10^{-4}
8	6.2658061739	1.19090×10^{-8}	2.8667710721	9.23485×10^{-4}
12	6.2658061725	1.05193×10^{-8}	2.8667710180	9.23539×10^{-4}
16	6.2658061733	1.13092×10^{-8}	2.8667710109	9.23546×10^{-4}
20	6.2658061739	1.19305×10^{-8}	2.8667710076	9.23549×10^{-4}
24	6.2658061736	1.16634×10^{-8}	2.8667710046	9.23552×10^{-4}

Example 2. Consider the following the general Rosenau-RLW equation in the case of $p = 4$, $\alpha = 1$

$$u_t - u_{xxt} + u_{xxxxt} + u_x + (u^4)_x = 0 \tag{56}$$

with initial condition

$$u(x, 0) = u_0(x), \quad x \in [x_l, x_r], \tag{57}$$

and the boundary conditions

$$u(x_l, t) = u(x_r, t) = u_x(x_l, t) = u_x(x_r, t) = u_{xx}(x_l, t) = u_{xx}(x_r, t) = 0, \quad t \in [0, T]. \tag{58}$$

It is known that, the solitary wave solution for Eq. (1) is

$$u(x, t) = e^{\ln\{(p+3)(3p+1)(p+1)/[2(p^2+3)(p^2+4p+7)]\}/(p-1)} \operatorname{sech}^{4/(p-1)}\left[\frac{p-1}{\sqrt{4p^2+8p+20}}(x - ct)\right],$$

where $p \geq 2$ is an integer and $c = (p^4 + 4p^3 + 14p^2 + 20p + 25)/(p^4 + 4p^3 + 10p^2 + 12p + 21)$.

Similar to the Example 1, the motion of a solitary wave is first modeled with the range $x_l = -50$ and $x_r = 150$ with $t = 24$. Table 3 lists the error of the numerical solutions using various τ and h. As seen, the error slightly decreases as τ and h are decreased. The $\|\cdot\|-$ and $\|\cdot\|_\infty-$ error norms stay less than 4.4×10^{-4} at time $t = 24$. The most accurate simulation as obtained from our method is with the choice $\tau = h = 0.1$ for which the $\|\cdot\|-$ and $\|\cdot\|_\infty-$ errors less than 3.98×10^{-8}. As shown in Table 3, the fourth-order convergence of numerical solutions is verified.

Fig. 4(Left) and (Right) illustrate the profile of the solitary wave at times $t = 8, 16, 24, 32, 40$ and the error distribution of the profile, respectively. As in the figures, during the time simulation, the crest of soliton clearly remains the same. As presented in Table 3, we apply the present scheme to verify the conservation of the numerical model by tracking the experiment of soliton motion run up to $t = 40$. The mobility values shall be analytically to give $Q = 6.2658061620$ and $E = 2.8676945570$, as observed in Table 5. The results show that the mobility constants Q^n and E^n slightly change from the exact values by less than $1.9 \times 10^{-7}\%$ and $3.3 \times 10^{-2}\%$, respectively.

We analyze the behavior at long time obtained by the second-order difference methods presented by Pan and Zhang [17,21,22] in order to underscore the efficiency of the proposed scheme. As shown in Fig. 5, results calculated by the methods [17,22] show lagging of predicted solutions when compared to exact solutions. However, results generated by Wongsaijai et al. [21] show leading of approximate solutions when compared to exact solutions. As observed, Fig. 6 that illustrates the expanded left-tail figure exhibits the fluctuation of numerical approximations on $x \in [-50, 1250]$. Furthermore, the present method offers the fit resolution of the wave structure at left-tail.

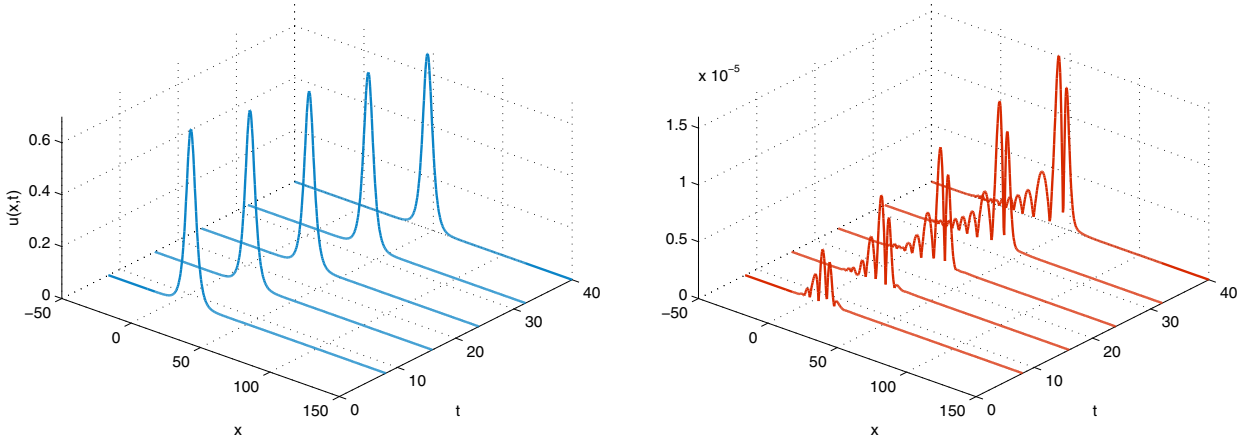

Fig. 4. (Left) Numerical solution using $p = 4, \tau = h$ and $x_l = -50$. (Right) Distribution error using $p = 4, \tau = h$ and $x_l = -50$.

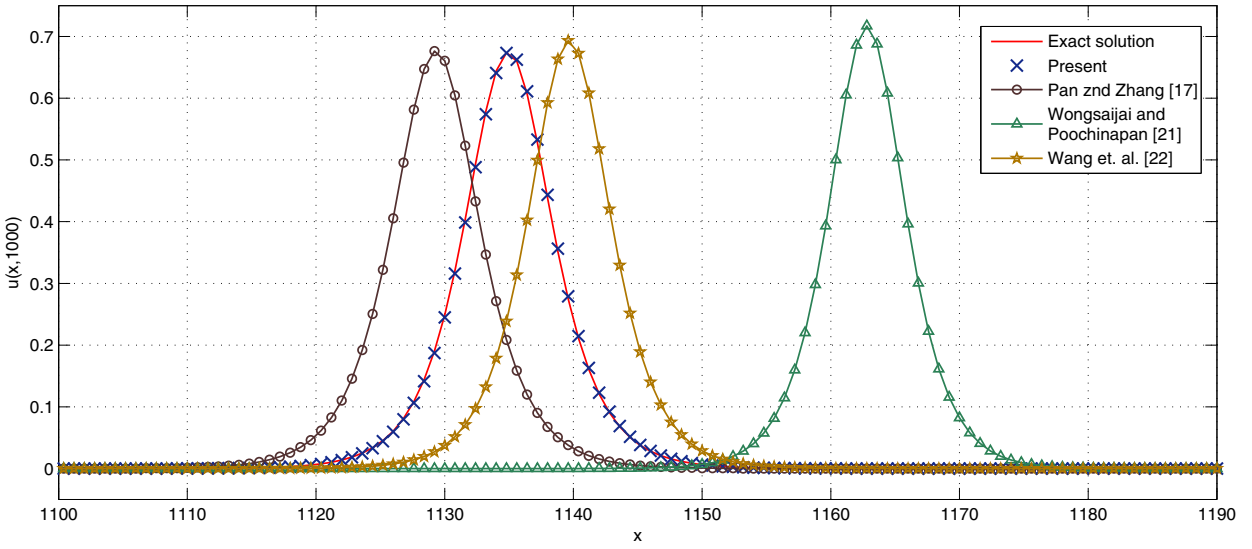

Fig. 5. The long-time behavior of numerical solutions at $t = 1000$ using $p = 4, h = 0.8, \tau = h, x_l = -50$, and $x_r = 1250$.

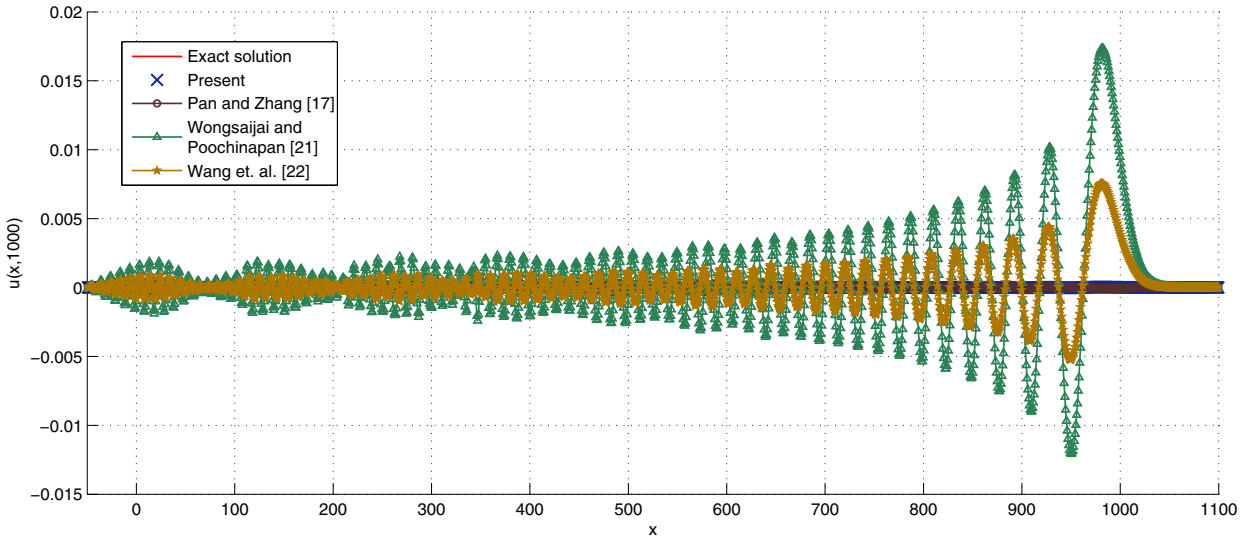

Fig. 6. The left-tail behavior of numerical solutions at $t = 1000$ using $p = 4, h = 0.8, \tau = h, x_l = -50$, and $x_r = 1250$.

8. Conclusions

The method which combines between the nonlinear finite difference and iterative algorithms was introduced and analyzed. Only a regular five-point stencil at higher-time level is required for construction of the compact finite difference scheme, which is similar to the second-order schemes [17,20–22,24,33]. The accuracy and stability of the numerical method to the solution of the Rosenau-RLW equation can be tested by using the exact solution. The scheme was constructed so that it maintains a high-order of accuracy and gives highly accurate results up to four digit better than previous known methods do when $h = 0.1$ is used. An extensive comparison of the present numerical results with the previous benchmark solutions, Figs. 2 and 5, establishes that the use of the compact method at long time results in waveforms to be smoothed out by the type of high-order accuracy. In practice, the existence and uniqueness of the approximate solution are directly obtained from the calculation of a nonlinear system, which can be implemented by using the present iterative algorithm. The numerical simulations indicated that the present method supports the analysis of convergence rate and the invariant properties can be verified by using analytical expressions. Such analysis provided guidelines as to how the method solves the given problem and may also lead to error estimates on the approximate solution.

Acknowledgments

This research was supported by the Thailand Research Funds (TRF) under grant no. MRG5580217, the Commission on Higher Education (CHE), and Chiang Mai University.

References

[1] K. Chunga, T. Toulkeridis, First evidence of paleo-tsunami deposits of a major historic event in ecuador, J. Tsunami Soc. Int. 33 (1) (2014) 55–69.
[2] R.C. Smith, J. Hill, G.S. Collins, M. D. Piggott, S.C. Kramer, S.D. Parkinson, C. Wilson, Comparing approaches for numerical modelling tsunami generation by deformable submarine slides, Ocean Model. 100 (2016) 125–140.
[3] D.J. Korteweg, G. de Vries, On the change of form of long waves advancing in a rectangular canal, and on a new type of long stationary waves, Philos. Mag. 39 (1895) 422–443.
[4] D.H. Peregrine, Calculations of the development of an undular bore, J. Fluid Mech. 25 (1966) 321–330.
[5] D.H. Peregrine, Long waves on a beach, J. Fluid Mech. 27 (1967) 815–827.
[6] P. Rosenau, A quasi-continuous description of a nonlinear transmission line, Phys. Scripta 34 (1986) 827–829.
[7] P. Rosenau, Dynamics of dense discrete systems, Prog. Theor. Phys. 79 (1988) 1028–1042.
[8] A.R. Bahadir, Exponential finite-difference method applied to Korteweg-de Vries equation for small times, Appl. Math. Comput. 160 (3) (2005) 675–682.
[9] S. Ozer, S. Kutluay, An analytical-numerical method for solving the Korteweg-de Vries equation, Appl. Math. Compt. 164 (3) (2005) 789–797.
[10] Y. Cui, D.k. Mao, Numerical method satisfying the first two conservation laws for the kortewegde vries equation, J. Comput. Phys. 227 (2007) 376–399.
[11] M.A. Park, On the rosenau equation, Math. Appl. Comput. 9 (2) (1990) 145–152.
[12] M.A. Park, Pointwise decay estimate of solutions of the generalized rosenau equation, J. Korean Math. Soc. 29 (1992) 261–280.
[13] P.K. Barreta, C.S.Q. Caldas, P. Gamboa, J. Limaco, Existence of solutions to the Rosenau and Benjamin-Bona-Mahony equation in domains with moving boundary, Electron. J. Diff. Equ. 2004 (35) (2004) 1–12.
[14] S.K. Chung, S.N. Ha, Finite element Galerkin solutions for the Rosenau equation, Appl. Anal. 54 (1994) 39–56.
[15] K. Omrani, F. Abidi, T. Achouri, N. Khiari, A new conservative finite difference scheme for the rosenau equation, Appl. Math. Comput. 201 (2008) 35–43.
[16] J.M. Zuo, M. Zhang, T.D. Zhang, F. Chang, A new conservative difference scheme for the general Rosenau-RLW equation, Bound. Value Probl. 2010 (516260) (2010) 13pages.
[17] X. Pan, L. Zhang, Numerical simulation for general Rosenau-RLW equation: an average linearized conservative math, scheme, Probl. Eng. 2012 (517818) (2012) 15pages.
[18] H. Wang, S. Li, J. Wang, A conservative weighted finite difference scheme for the generalized rosenau-RLW equation, Comp. Appl. Math. 36 (2017) 63–78.
[19] X. Pan, K. Zheng, L. Zhang, Finite difference discretization for the Rosenau-RLW equation, Appl. Anal. 92 (12) (2013) 2578–2589.
[20] X. Pan, L. Zhang, On the convergence of a conservative numerical scheme for the usual Rosenau-RLW equation, Appl. Math. Model. 36 (2012) 3371–3378.
[21] B. Wongsaijai, K. Poochinapan, T. Disyadej, A compact finite difference method for solving the general Rosenau-RLW equation, IAENG Int. J. Appl. Math. 44 (4) (2014) 192–199.
[22] H. Wang, J. Wang, S. Li, A new conservative nonlinear high-order compact finite difference scheme for the general Rosenau-RLW equation, Bound. Value Probl. 2015 (77) (2015).
[23] S. Li, Numerical analysis for fourth-order compact conservative difference scheme to solve the 3D Rosenau-RLW equation, Comput. Math. Appl. 72 (9) (2016) 2388–2407.
[24] J. Hu, Y. Wang, A high-accuracy linear conservative difference scheme for Rosenau-RLW equation, Math. Probl. Eng. 2013 (870291) (2013) 8pages.
[25] D.W. Zingg, Comparison of high-accuracy finite-difference methods for linear wave propagation, SIAM J. Sci. Comput. 22 (2) (2000) 476–502.
[26] B. Gustafsson, E. Mossberg, Time compact high order difference methods for wave propagation, SIAM J. Sci. Comput. 26 (2004) 259–271.
[27] G. Berikelashvili, M.M. Gupta, M. Mirianashvili, Convergence of fourth order compact difference schemes for the three-dimensional convection-diffusion equations, SIAM J. Numer. Anal. 45 (2007) 443–455.
[28] H.L. Liao, Z.Z. Sun, Maximum norm error bounds of ADI and compact ADI methods for solving parabolic equations, Numer. Methods Partial Differ. Equ. 26 (2010) 37–60.
[29] K. Poochinapan, B. Wongsaijai, T. Disyadej, Efficiency of high-order accurate difference schemes for the Korteweg-de Vries equation, Math. Probl. Eng. 2014 (862403) (2014) 8pages.
[30] Y. Zhou, Application of Discrete Functional Analysis to the Finite Difference Method, International Academic Publishers, Beijing, 1990.
[31] F.E. Browder, Existence and uniqueness theorems for solutions of nonlinear boundary value problems, Proc. Sympos. Appl. Math. 17 (1965) 24–49.
[32] Z.Z. Sun, Q.D. Zhu, On Tsertsvadze's difference scheme for the Kuramoto-Tsuzuki equation, J. Comput. Appl. Math. 98 (1998) 289–304.
[33] B. Wongsaijai, K. Poochinapan, A three-level average implicit finite difference scheme to solve equation obtained by coupling the Rosenau-KdV equation and the Rosenau-RLW equation, Appl. Math. Comput. 245 (2014) 289–304.

Applied Mathematics and Computation 273 (2016) 809–825

Contents lists available at ScienceDirect

Applied Mathematics and Computation

journal homepage: www.elsevier.com/locate/amc

Numerical implementation for solving the symmetric regularized long wave equation

S. Yimnet, B. Wongsaijai, T. Rojsiraphisal, K. Poochinapan*

Department of Mathematics, Faculty of Science, Chiang Mai University, Chiang Mai 50200, Thailand

ARTICLE INFO

Keywords:
Finite difference method
SRLW equation
Convergence
Stability

ABSTRACT

The paper presents a novel finite difference method for the symmetric regularized long wave equation. The time discretization is performed by using a four-level average difference technique for solving the fluid velocity independently from the density. At this stage, the numerical solution is easily solved by using the presented method since it does not require an extra effort to deal with a nonlinear term and the density. The existence and uniqueness of the numerical solution and the conservation of mass are guaranteed. The stability and convergence of the numerical solution with second-order accuracy on both space and time are also verified. Numerical results are carried out to confirm the accuracy of our theoretical results and the efficiency of the scheme. To illustrate the effectiveness and the advantage of the proposed method, the results at long-time behavior are compared with the ones obtained from previously known methods. Moreover, in the computation, the present method is applied to the collision of solitons under the effect of variable parameters.

1. Introduction

Seyler and Fenstermacher [1] investigated the symmetric regularized long wave (SRLW) equation for describing various nonlinear phenomena such as the propagation of ion acoustic waves, shallow water waves, and solitary waves with bidirectional propagation:

$$u_t - u_{xxt} + \rho_x + uu_x = 0, \tag{1}$$

$$\rho_t + u_x = 0, \tag{2}$$

where u and ρ are the fluid velocity and the density, respectively. The density function can be removed from Eqs. (1) and (2) and then the equations turn to a single nonlinear equation for the velocity function:

$$u_{tt} - u_{xxtt} - u_{xx} + \frac{1}{2}(u^2)_{xt} = 0. \tag{3}$$

The equation is comparable to the regularized long wave (RLW) equation but explicitly symmetry in the x and t derivatives (see [1–7] and references therein).

There are several researches on the system of the SRLW equation using theoretical and numerical techniques [1,8–13]. The hyperbolic secant squared solitary waves have been proposed by Seyler and Fenstermacher [1]. They demonstrated the solution

* Corresponding author. Tel.: +66 816712598.
E-mail address: kanyuta@hotmail.com, k.poochinapan@gmail.com (K. Poochinapan).

http://dx.doi.org/10.1016/j.amc.2015.09.069
0096-3003/

to the SRLW equation for preserving four invariants of motion. Also, the behavior of solitary waves of the SRLW equation is numerically investigated and compared with that of the RLW equation. The existence of the global solution and global attractor to the system of multi-dimensional SRLW equation with periodic conditions has been proved by Shaomei et al. [8]. Zheng et al. [9] applied the Fourier pseudo-spectral method with a restraint operator to approximate a nonlinear term. They proved the generalized stability of the semi-discrete and fully-discrete schemes and gave the optimum error estimate. Later, Shang and Gua [10] applied the Chebyshev pseudo–spectral method for solving the multi-dimensional generalized SRLW equation with homogeneous initial boundary conditions. They constructed the fully-discrete Chebyshev pseudo-spectral scheme and also obtained the optimum error estimate. Wang et al. [11] proposed three conservative finite difference schemes: a coupled two-level nonlinear implicit scheme, a coupled three-level linear implicit scheme, and an uncoupled two-level linear implicit scheme. All schemes are of second-order accuracy in both space and time. They also showed that the energy was preserved for all schemes and the mass was preserved only for the first scheme. Subsequently, Nie [12] proposed an uncoupled three–level linear finite difference scheme for solving this system. The discrete energy and the truncation error of order $O(h^4+\tau^2)$ have been derived by using a five-point stencil. Moreover, Hu et al. [13] developed a coupled conservative three-level implicit scheme with the fourth–order rate of convergence. Obviously, the scheme requires heavy iterative computations because it is nonlinear implicit.

From literature, the numerical methods have been used to study the SRLW equation mostly in the form of system (1) and (2). However, the numerical method for the SRLW equation in the form of Eq. (3) which is independent of the variable ρ has been scarcely studied. In this paper, we consider the SRLW equation (3), with the homogeneous boundary conditions:

$$u(x_L,t)=u(x_R,t)=0,\quad u_x(x_L,t)=u_x(x_R,t)=0,\quad u_{xx}(x_L,t)=u_{xx}(x_R,t)=0,\quad t\in[0,T], \tag{4}$$

where x_L and x_R are left and right endpoints, and the initial conditions:

$$u(x,0)=u_0(x),\quad u_t(x,0)=u_1(x), x\in[x_L,x_R], \tag{5}$$

where $u_0(x)$ and $u_1(x)$ are two known smooth functions. The solution and its derivatives for the solitary wave are supposed to have the following asymptotic values, $u\to 0$ as $x\to\pm\infty$, and for $n\geq 1$, $\frac{\partial^n u}{\partial x^n}\to 0$ as $x\to\pm\infty$. For that reason, if $x_L\ll 0$ and $x_R\gg 0$, the initial-boundary value problem is in agreement with the Cauchy problem of Eq. (3). In addition, the time evolution of the SRLW equation preserves the following physical quantities:

$$I_1(t)=\frac{1}{2}\int_{x_L}^{x_R}u(x,t)dx=\frac{1}{2}\int_{x_L}^{x_R}u_0(x)dx=I_1(0), \tag{6}$$

$$I_2(t)=\frac{1}{2}\int_{x_L}^{x_R}\rho(x,t)dx=\frac{1}{2}\int_{x_L}^{x_R}\rho_0(x)dx=I_2(0), \tag{7}$$

$$I_3(t)=\frac{1}{2}(\|u\|_{L_2}^2+\|u_x\|_{L_2}^2+\|\rho\|_{L_2}^2)=\frac{1}{2}(\|u_0\|_{L_2}^2+\|(u_0)_x\|_{L_2}^2+\|\rho_0\|_{L_2}^2)=I_3(0), \tag{8}$$

where $I_1(t)$, $I_2(t)$, and $I_3(t)$ are called mass of $u(x,t)$, mass of $\rho(x,t)$, and energy at time t, respectively [11].

Scientists in the past have presented many conservative finite difference schemes in order to study solutions for various nonlinear wave equations [14–22]. One of the important properties of fluid or propagating waves is obviously the conservativeness. For example, the accomplishment of a numerical estimation in the long-time behavior is assured by schemes for the conservation of energy and mass. Therefore, a mass-conservative finite difference scheme which can preserves the solution to the SRLW equation is needed. Moreover, a four-level linear implicit finite difference scheme for solving the SRLW equation (3) is created because there is no single method which is most suitable for all aspects. In general, the type of linearization which is used can significantly affect the convergence rate of the iterations to the solution.

The content of this paper is organized as follows. In Section 2, we propose a four-level linear implicit finite difference scheme which guarantees unique solvability for the SRLW equation (3). Discrete norms and some preliminary lemmas are given, and the discrete conservative property of mass is also proved. Section 3 describes complete proofs on the convergence and stability of the finite difference scheme which is second–order accuracy on both space and time. Section 4, presents the results obtained with the proposed numerical model, where our results are compared to available data. Conclusions are finally reported in Section 5.

2. Finite difference scheme

In this section, a finite difference procedure for solving Eq. (3) and conditions (4) and (5) is established. The spatial domain $[x_L, x_R]$ is discretized by using function values on a finite set of the points $\{x_i\}_{i=0}^{M}\subset[x_L,x_R]$, where $h=(x_R-x_L)/M$ is uniform distance between two points. We discretize the time domain uniformly by $t_n=n\tau$. Points can be located according to values of i and n, so difference equations are usually written in term of the point (i,n). We write the notation u_i^n for a value of a function u at the grid point $(x_L+ih,n\tau)$. Denote

$$Z_h^0=\{u=(u_i)\,|\,u_{-1}=u_0=u_1=u_{M-1}=u_M=u_{M+1}=0,\quad i=-1,0,\ldots,M,M+1\}.$$

Throughout this paper, let C be a generic positive constant independent of h and τ, which may have different values in different occurrences. For a nonnegative integer k, let $H^k(\Omega)$ denote the usual Sobolev space of real valued functions defined on Ω. We

define the following Sobolev space:

$$H_0^k(\Omega) = \left\{ u \in H^k(\Omega) \mid \frac{\partial^i u}{\partial x^i} = 0 \text{ on } \partial\Omega, i = 0, 1, \ldots, k-1 \right\}.$$

We define the following notations applied to the grid function u_i^n below:

$$(u_i^n)_x = \frac{u_{i+1}^n - u_i^n}{h}, \quad (u_i^n)_{\bar{x}} = \frac{u_i^n - u_{i-1}^n}{h}, \quad (u_i^n)_{\hat{x}} = \frac{u_{i+1}^n - u_{i-1}^n}{2h},$$
$$(u_i^n)_t = \frac{u_i^{n+1} - u_i^n}{\tau}, \quad (u_i^n)_{\bar{t}} = \frac{u_i^n - u_i^{n-1}}{\tau}, \quad (u_i^n)_{\hat{t}} = \frac{u_i^{n+1} - u_i^{n-1}}{2\tau},$$
$$\bar{u}_i^n = \frac{u_i^{n+1} + u_i^{n-1}}{2}, \quad \langle u^n, v^n \rangle = h \sum_{i=1}^{M-1} u_i^n v_i^n,$$
$$\|u^n\|^2 = \langle u^n, u^n \rangle, \quad \|u^n\|_\infty = \max_{1 \le i \le M-1} |u_i^n|.$$

We use the second-order accurate central difference approximations for linear operators in Eqs. (3)–(5). The second-order accurate backward approximation in time derivative appearing in the nonlinear term of Eq. (3) makes the whole scheme very easy to implement. We provide the formula here. To approximate the nonlinear term $\frac{1}{2}(u^2)_{xt}$ at the point (x_i, t_n), we use the formula

$$\frac{3}{4}[(u_i^n)^2]_{\hat{x}\bar{t}} - \frac{1}{4}[(u_i^{n-1})^2]_{\hat{x}\bar{t}}.$$

Using the Taylor expansion, it can be seen from the above analysis that the approximation has the second–order accuracy in both space and time if the function to be approximated is four times continuously differentiable. Combining these above approximations yields the difference equations

$$(u_i^n)_{t\bar{t}} - (u_i^n)_{x\bar{x}t\bar{t}} - (\bar{u}_i^n)_{x\bar{x}} + \frac{3}{4}[(u_i^n)^2]_{\hat{x}\bar{t}} - \frac{1}{4}[(u_i^{n-1})^2]_{\hat{x}\bar{t}} = 0, 1 \le i \le M-1, \tag{9}$$

$$u_i^0 = u_0(x_i), u_i^1 = u_1(x_i), 0 \le i \le M, \tag{10}$$

$$u_0^n = u_M^n = 0, \quad (u_0^n)_{\hat{x}} = (u_M^n)_{\hat{x}} = 0, \quad (u_0^n)_{x\bar{x}} = (u_M^n)_{x\bar{x}} = 0, 1 \le n \le N. \tag{11}$$

The above scheme can be rewritten as

$$\begin{aligned}
&-\left(\frac{1}{2h^2} + \frac{1}{\tau^2 h^2}\right)u_{i-1}^{n+1} + \left(\frac{1}{\tau^2} + \frac{2}{\tau^2 h^2} + \frac{1}{h^2}\right)u_i^{n+1} - \left(\frac{1}{2h^2} + \frac{1}{\tau^2 h^2}\right)u_{i+1}^{n+1} \\
&= +\left(\frac{1}{2h^2} + \frac{1}{\tau^2 h^2}\right)u_{i-1}^{n-1} - \left(\frac{1}{\tau^2} + \frac{2}{\tau^2 h^2} + \frac{1}{h^2}\right)u_i^{n-1} + \left(\frac{1}{2h^2} + \frac{1}{\tau^2 h^2}\right)u_{i+1}^{n-1} - \frac{2}{\tau^2 h^2}u_{i-1}^n \\
&\quad + \left(\frac{2}{\tau^2} + \frac{4}{\tau^2 h^2}\right)u_i^n - \frac{2}{\tau^2 h^2}u_{i+1}^n + \frac{1}{8\tau h}[(u_{i+1}^{n-1})^2 - (u_{i+1}^{n-2})^2 - (u_{i-1}^{n-1})^2 + (u_{i-1}^{n-2})^2] \\
&\quad - \frac{3}{8\tau h}[(u_{i+1}^n)^2 - (u_{i+1}^{n-1})^2 - (u_{i-1}^n)^2 + (u_{i-1}^{n-1})^2].
\end{aligned}$$

Then we get the linear algebraic system for $n = 2, 3, \ldots, N-1$

$$k_1 u_{i-1}^{n+1} + k_2 u_i^{n+1} + k_1 u_{i+1}^{n+1} = f_i^n, 1 \le i \le M-1, \tag{12}$$

where

$$k_1 = -\frac{1}{2h^2} - \frac{1}{\tau^2 h^2}, \quad k_2 = \frac{1}{\tau^2} + \frac{2}{\tau^2 h^2} + \frac{1}{h^2},$$

and

$$\begin{aligned}
f_i^n = &-\frac{2}{\tau^2 h^2}u_{i-1}^n + \left(\frac{2}{\tau^2} + \frac{4}{\tau^2 h^2}\right)u_i^n - \frac{2}{\tau^2 h^2}u_{i+1}^n + \left(\frac{1}{2h^2} + \frac{1}{\tau^2 h^2}\right)u_{i-1}^{n-1} \\
&- \left(\frac{1}{\tau^2} + \frac{2}{\tau^2 h^2} + \frac{1}{h^2}\right)u_i^{n-1} + \left(\frac{1}{2h^2} + \frac{1}{\tau^2 h^2}\right)u_{i+1}^{n-1} \\
&+ \frac{1}{8\tau h}[(u_{i+1}^{n-1})^2 - (u_{i+1}^{n-2})^2 - (u_{i-1}^{n-1})^2 + (u_{i-1}^{n-2})^2] \\
&- \frac{3}{8\tau h}[(u_{i+1}^n)^2 - (u_{i+1}^{n-1})^2 - (u_{i-1}^n)^2 + (u_{i-1}^{n-1})^2].
\end{aligned}$$

Since $u_0^{n+1} = u_M^{n+1} = 0$, Eq. (12) can be written as $\mathbf{KU} = \mathbf{F}$ where

$$\mathbf{K} = \begin{bmatrix} k_2 & k_1 & 0 & \dots & 0 \\ k_1 & k_2 & k_1 & \dots & 0 \\ \vdots & \vdots & \vdots & \vdots & \vdots \\ 0 & \dots & k_1 & k_2 & k_1 \\ 0 & \dots & 0 & k_1 & k_2 \end{bmatrix}, \quad \mathbf{U} = \begin{bmatrix} u_1^{n+1} \\ u_2^{n+1} \\ \vdots \\ u_{M-2}^{n+1} \\ u_{M-1}^{n+1} \end{bmatrix}, \text{ and } \mathbf{F} = \begin{bmatrix} f_1^n \\ f_2^n \\ \vdots \\ f_{M-2}^n \\ f_{M-1}^n \end{bmatrix}.$$

The coefficient matrix in the above equation depends on constants h and τ and is *strictly diagonally dominant* matrix. This guarantees the existence and uniqueness of our numerical solution. Moreover, the scheme (9)–(11) is linear thus the solution can be easily obtained.

Next, the conservative approximation is developed as follows:

Theorem 1. *Suppose $u_0 \in H_0^1[x_L, x_R]$, then the difference scheme (9)–(11) is conservative in a sense:*

$$Q^n = h\sum_{i=1}^{M-1}(u_i^{n+1} - u_i^n) = Q^{n-1} = \cdots = Q^0. \tag{13}$$

Proof. Multiplying Eq. (9) with h, summing up on i from 1 to $M-1$, we obtain

$$h\sum_{i=1}^{M-1}(u_i^n)_{t\bar{t}} - h\sum_{i=1}^{M-1}(u_i^n)_{x\bar{x}t\bar{t}} - h\sum_{i=1}^{M-1}(\bar{u}_i^n)_{x\bar{x}} + h\sum_{i=1}^{M-1}\left(\frac{3}{4}[(u_i^n)^2]_{\hat{x}\bar{t}} - \frac{1}{4}[(u_i^{n-1})^2]_{\hat{x}\bar{t}}\right) = 0.$$

Considering the boundary conditions (11), we have

$$h\sum_{i=1}^{M-1}(u_i^{n+1} - 2u_i^n + u_i^{n-1}) = 0.$$

Then, Eq. (13) holds. □

The following lemmas play an important role to proof the boundedness, convergence, and stability of our numerical solution.

Lemma 2. *Let $u, v \in Z_h^0$ be any two mesh functions. Then we have*

$$\langle u_{\hat{x}}, v\rangle = -\langle u, v_{\hat{x}}\rangle, \langle u_{x\bar{x}}, v\rangle = -\langle u_x, v_x\rangle,$$

and

$$\langle u_{x\bar{x}}, u\rangle = -\langle u_x, u_x\rangle = -\|u_x\|^2.$$

Lemma 3 (Discrete Poincaré inequality [23])**.** *Let $u \in Z_h^0$ be any mesh functions. Then we have*

$$\left(\frac{2\sin(\pi h/2)}{h}\right)\|u\| \le \|u_{\bar{x}}\|. \tag{14}$$

Lemma 4 (Discrete Sobolev's inequality [24])**.** *There exist two constants C_1 and C_2 such that*

$$\|u^n\|_\infty \le C_1\|u^n\| + C_2\|u_x^n\|. \tag{15}$$

For establishment of the next lemma, we use the boundary conditions (11), discrete Poincaré inequality, and discrete Sobolev's inequality in order to be a tool for proofing the next theorem.

Lemma 5. *Let $u \in Z_h^0$ be any mesh function satisfying $\|u_x^n\| \le C$, then $\|u^n\|_\infty \le C$.*

Proof. Since, $\sup_{0<h<1}\left(\frac{h}{2\sin(\pi h/2)}\right) = \frac{1}{2}$, by using Lemma 3, we have

$$\|u^n\| \le \left[\sup_{0<h<1}\left(\frac{h}{2\sin(\pi h/2)}\right)\right]\|u_{\bar{x}}^n\| = \frac{1}{2}\|u_{\bar{x}}^n\|.$$

From the boundary conditions (11), we have

$$\|u_{\bar{x}}^n\| = \|u_x^n\|. \tag{16}$$

Since $\|u_x^n\| \le C$, thus Eq. (16) leads to

$$\|u^n\| \le C.$$

Using Lemma 4, we obtain

$$\|u^n\|_\infty \le C_1\|u^n\| + C_2\|u_x^n\| \le C.$$

This completes the proof of Lemma 5. □

Lemma 6 (Discrete Gronwall's inequality [24]). *Suppose $\omega(k)$ and $\rho(k)$ are nonnegative functions and $\rho(k)$ is a nondecreasing function. If $C > 0$ and*

$$\omega(k) \le \rho(k) + C\tau\sum_{l=0}^{k-1}\omega(l), \quad \forall k,$$

then

$$\omega(k) \le \rho(k)e^{C\tau k}, \quad \forall k.$$

The following theorem guarantees that the numerical solution obtained from the scheme (9)–(11) is bounded.

Theorem 7. *Suppose $u_0 \in H_0^1[x_L, x_R]$, then there is an approximate solution u^n of the scheme (9)–(11) that satisfying*

$$\|u^n\| \le C, \|u_x^n\| \le C, \|u^n\|_\infty \le C, \text{and} \|u_{\hat{t}}^n\|_\infty \le C. \tag{17}$$

Proof. Using the mathematical induction, we assume

$$\|u_{\hat{t}}^k\| \le C, \|u_{x\bar{t}}^k\| \le C, \|u_x^k\| \le C, \|u^k\| \le C, \tag{18}$$

and

$$\|u_{\hat{t}}^k\|_\infty \le C, \ \|u^k\|_\infty \le C, \tag{19}$$

for $k = 1, 2, \ldots, n$. Taking an inner product between Eq. (9) with $u_{\hat{t}}^n$, we obtain

$$\langle u_{t\bar{t}}^n, u_{\hat{t}}^n\rangle - \langle u_{x\bar{x}t\bar{t}}^n, u_{\hat{t}}^n\rangle - \langle \bar{u}_{x\bar{x}}^n, u_{\hat{t}}^n\rangle = -\frac{3}{4}\langle (u^n)_{\hat{x}\bar{t}}^2, u_{\hat{t}}^n\rangle + \frac{1}{4}\langle (u^{n-1})_{\hat{x}\bar{t}}^2, u_{\hat{t}}^n\rangle. \tag{20}$$

Using Lemma 2, Eq. (20) becomes

$$\frac{1}{2\tau}(\|u_{\hat{t}}^{n+1}\|^2 - \|u_{\hat{t}}^n\|^2) + \frac{1}{2\tau}(\|u_{x\bar{t}}^{n+1}\|^2 - \|u_{x\bar{t}}^n\|^2) + \frac{1}{4\tau}(\|u_x^{n+1}\|^2 - \|u_x^{n-1}\|^2) = -\frac{3}{4}\langle (u^n)_{\hat{x}\bar{t}}^2, u_{\hat{t}}^n\rangle + \frac{1}{4}\langle (u^{n-1})_{\hat{x}\bar{t}}^2, u_{\hat{t}}^n\rangle. \tag{21}$$

From

$$(u_i^n)_{\hat{x}\bar{t}} = \frac{(u_{i+1}^n - u_{i-1}^n)_{\bar{t}}}{2h} = \frac{1}{2\tau h}(u_{i+1}^n - u_{i+1}^{n-1} - u_{i-1}^n + u_{i-1}^{n-1}),$$

we have

$$\begin{aligned}
[(u_i^n)^2]_{\hat{x}\bar{t}} =& \frac{1}{2\tau h}[(u_{i+1}^n)^2 - (u_{i+1}^{n-1})^2 - (u_{i-1}^n)^2 + (u_{i-1}^{n-1})^2] \\
=& \frac{1}{2\tau h}[(u_{i+1}^n - u_{i+1}^{n-1} - u_{i-1}^n + u_{i-1}^{n-1})(u_{i+1}^n + u_{i-1}^{n-1} + u_{i+1}^{n-1} + u_{i-1}^n)] \\
&+ \frac{1}{2\tau h}[2u_{i+1}^{n-1}u_{i+1}^n - 2u_{i+1}^n u_{i-1}^{n-1}] - \frac{1}{2\tau h}[2u_{i+1}^{n-1}u_{i+1}^n - 2u_{i+1}^{n-1}u_{i-1}^n] \\
=& (u_{i+1}^n + u_{i-1}^{n-1} + u_{i+1}^{n-1} + u_{i-1}^n)(u_i^n)_{\hat{x}\bar{t}} + \frac{2}{\tau}[u_{i+1}^n(u_i^{n-1})_{\hat{x}}] - \frac{2}{\tau}[u_{i+1}^{n-1}(u_i^n)_{\hat{x}}] \\
=& (u_{i+1}^n + u_{i-1}^{n-1} + u_{i+1}^{n-1} + u_{i-1}^n)(u_i^n)_{\hat{x}\bar{t}} - 2u_{i+1}^n\left[\frac{(u_i^n)_{\hat{x}} - (u_i^{n-1})_{\hat{x}}}{\tau}\right] + 2(u_i^n)_{\hat{x}}\left[\frac{u_{i+1}^n - u_{i+1}^{n-1}}{\tau}\right] \\
=& (u_{i+1}^n + u_{i-1}^{n-1} + u_{i+1}^{n-1} + u_{i-1}^n)(u_i^n)_{\hat{x}\bar{t}} - 2u_{i+1}^n(u_i^n)_{\hat{x}\bar{t}} + 2(u_i^n)_{\hat{x}}(u_{i+1}^n)_{\bar{t}}\,.
\end{aligned} \tag{22}$$

With the assumption (19), Eq. (22) reaches

$$|[(u_i^n)^2]_{\hat{x}\bar{t}}| = |(u_{i+1}^n + u_{i-1}^{n-1} + u_{i+1}^{n-1} + u_{i-1}^n)(u_i^n)_{\hat{x}\bar{t}} - 2u_{i+1}^n(u_i^n)_{\hat{x}\bar{t}} + 2(u_i^n)_{\hat{x}}(u_{i+1}^n)_{\bar{t}}| \le C|(u_i^n)_{\hat{x}\bar{t}}| + C|(u_i^n)_{\hat{x}}|. \tag{23}$$

Using Eq. (23) and the Cauchy–Schwarz inequality, we get

$$\begin{aligned}
\langle (u^n)_{\hat{x}\bar{t}}^2, u_{\hat{t}}^n\rangle &= h\sum_{i=1}^{M-1}(u_i^n)_{\hat{x}\bar{t}}^2(u_i^n)_{\hat{t}} \le h\sum_{i=1}^{M-1}|(u_i^n)_{\hat{x}\bar{t}}^2||(u_i^n)_{\hat{t}}| \le Ch\sum_{i=1}^{M-1}|(u_i^n)_{\hat{x}\bar{t}}||(u_i^n)_{\hat{t}}| + Ch\sum_{i=1}^{M-1}|(u_i^n)_{\hat{x}}||(u_i^n)_{\hat{t}}| \\
&\le C\|u_{\hat{x}\bar{t}}^n\|\|u_{\hat{t}}^n\| + C\|u_{\hat{x}}^n\|\|u_{\hat{t}}^n\| \le C(\|u_{\hat{x}\bar{t}}^n\|^2 + \|u_{\hat{x}}^n\|^2 + \|u_{\hat{t}}^n\|^2).
\end{aligned} \tag{24}$$

In the same manner, we can obtain

$$\langle (u^{n-1})_{\hat{x}\bar{t}}^2, u_{\hat{t}}^n\rangle \le C(\|u_{\hat{x}\bar{t}}^{n-1}\|^2 + \|u_{\hat{x}}^{n-1}\|^2 + \|u_{\hat{t}}^n\|^2). \tag{25}$$

Furthermore,

$$\|u_{\bar{t}}^n\|^2 = \frac{1}{4}\|u_{\bar{t}}^{n+1} + u_{\bar{t}}^n\|^2 \le \frac{1}{2}(\|u_{\bar{t}}^{n+1}\|^2 + \|u_{\bar{t}}^n\|^2), \tag{26}$$

and using boundary conditions (11), we have

$$\|u_{\hat{x}}^n\|^2 = \frac{1}{4}\|u_x^n + u_{\bar{x}}^n\|^2 \le \frac{1}{2}(\|u_x^n\|^2 + \|u_{\bar{x}}^n\|^2) = \|u_x^n\|^2. \tag{27}$$

Substituting Eqs. (24)–(27) into Eq. (21), we get

$$\begin{aligned}&(\|u_{\bar{t}}^{n+1}\|^2 - \|u_{\bar{t}}^n\|^2) + (\|u_{x\bar{t}}^{n+1}\|^2 - \|u_{x\bar{t}}^n\|^2) + \frac{1}{2}(\|u_x^{n+1}\|^2 - \|u_x^{n-1}\|^2)\\ &\quad\le C\tau(\|u_{x\bar{t}}^n\|^2 + \|u_{x\bar{t}}^{n-1}\|^2 + \|u_{\bar{t}}^{n+1}\|^2 + \|u_{\bar{t}}^n\|^2 + \|u_x^n\|^2 + \|u_x^{n-1}\|^2).\end{aligned} \tag{28}$$

Let

$$B^n \equiv \|u_{\bar{t}}^n\|^2 + \|u_{x\bar{t}}^n\|^2 + \frac{1}{2}\|u_x^n\|^2 + \frac{1}{2}\|u_x^{n-1}\|^2.$$

Using the assumption (18), Eq. (28) can be rewritten as follows:

$$B^{n+1} - B^n \le C\tau(\|u_{x\bar{t}}^n\|^2 + \|u_{\bar{t}}^{n+1}\|^2 + \|u_{\bar{t}}^n\|^2 + \|u_x^n\|^2 + \|u_x^{n-1}\|^2) + C\tau\|u_{x\bar{t}}^{n-1}\|^2 \le C\tau(B^{n+1} + B^n) + C\tau.$$

That is,

$$(1 - C\tau)(B^{n+1} - B^n) \le C\tau B^n + C\tau.$$

If τ is sufficiently small satisfying $1 - C\tau > 0$, then

$$B^{n+1} - B^n \le C\tau B^n + C\tau. \tag{29}$$

Summing up Eq. (29) from 1 to n, we have

$$B^{n+1} - B^1 \le C\tau\sum_{k=1}^{n} B^k + Cn\tau \le C\tau\sum_{k=1}^{n} B^k + CT.$$

From the assumption (18), we get $B^1 \le C$. Hence,

$$B^{n+1} \le C + C\tau\sum_{k=1}^{n} B^k.$$

By Lemma 6, it can immediately obtain $B^{n+1} \le Ce^{Cn\tau} \le Ce^{CT} \le C$. This leads to

$$\|u_{\bar{t}}^{n+1}\| \le C, \quad \|u_{x\bar{t}}^{n+1}\| \le C, \quad \|u_x^{n+1}\| \le C.$$

Finally, by using Lemma 4 and Lemma 5, we get

$$\|u_{\bar{t}}^{n+1}\|_\infty \le C, \quad \|u^{n+1}\|_\infty \le C.$$

This completes the proof of Theorem 7. □

3. Convergence and stability

In this section, the convergence and stability of the scheme (9)–(11) are given. Let $v_i^n = v(x_i, t_n)$ be the solution of Eq. (3) with conditions (4) and (5). Then the truncation error of the difference scheme (9)–(11) can be obtained from

$$r_i^n = (v_i^n)_{t\bar{t}} - (v_i^n)_{x\bar{x}t\bar{t}} - (\bar{v}_i^n)_{x\bar{x}} + \frac{3}{4}[(v_i^n)^2]_{\hat{x}\bar{t}} - \frac{1}{4}[(v_i^{n-1})^2]_{\hat{x}\bar{t}}. \tag{30}$$

By the Taylor expansion, we easily obtain $r_i^n = O(h^2 + \tau^2)$ as $\tau, h \to 0$. The proof is based on the following lemma.

Lemma 8 (Wang et al. [11]). *Suppose $u_0 \in H_0^1[x_L, x_R]$, then the solution of Eq. (3) with conditions (4) and (5) satisfies*

$$\|u\|_{L_2} \le C, \quad \|u_x\|_{L_2} \le C, \text{ and } \|u\|_{L_\infty} \le C, \tag{31}$$

for a constant C.

Theorem 9. *Suppose $u_0 \in H_0^1[x_L, x_R]$, then the solution u^n of scheme (9)–(11) converges to the solution of Eq. (3) with conditions (4) and (5) in the sense of $\|\cdot\|_\infty$ with the rate of convergence of order $O(h^2 + \tau^2)$.*

Proof. Let $e_i^n = v_i^n - u_i^n$, we have

$$r_i^n = (e_i^n)_{t\bar{t}} - (e_i^n)_{x\bar{x}t\bar{t}} - (\bar{e}_i^n)_{x\bar{x}} + \frac{3}{4}[(v_i^n)^2 - (u_i^n)^2]_{\hat{x}\bar{t}} - \frac{1}{4}[(v_i^{n-1})^2 - (u_i^{n-1})^2]_{\hat{x}\bar{t}}. \tag{32}$$

Taking an inner product between Eq. (32) with $e_{\bar{t}}^n$ and using Lemma 2, we obtain

$$\begin{aligned}&(\|e_{\bar{t}}^{n+1}\|^2-\|e_{\bar{t}}^n\|^2)+(\|e_{x\bar{t}}^{n+1}\|^2-\|e_{x\bar{t}}^n\|^2)+\frac{1}{2}(\|e_x^{n+1}\|^2-\|e_x^{n-1}\|^2)\\&\quad=2\tau\langle r^n,e_{\bar{t}}^n\rangle-\frac{3}{2}\tau\langle[(v^n)^2-(u^n)^2]_{\hat{x}\bar{t}},e_{\bar{t}}^n\rangle+\frac{1}{2}\tau\langle[(v^{n-1})^2-(u^{n-1})^2]_{\hat{x}\bar{t}},e_{\bar{t}}^n\rangle.\end{aligned}\tag{33}$$

According to Lemma 2, Theorem 7, Lemma 8, and the Cauchy–Schwarz inequality, we have

$$\begin{aligned}\langle[(v^n)^2-(u^n)^2]_{\hat{x}\bar{t}},e_{\bar{t}}^n\rangle&=-\langle[(v^n)^2-(u^n)^2]_{\bar{t}},e_{\hat{x}\bar{t}}^n\rangle\\&=-h\sum_{i=1}^{M-1}[(v_i^n)^2-(u_i^n)^2]_{\bar{t}}(e_i^n)_{\hat{x}\bar{t}}\\&=-h\sum_{i=1}^{M-1}[v_i^n(e_i^n+u_i^n)-u_i^n(v_i^n-e_i^n)]_{\bar{t}}(e_i^n)_{\hat{x}\bar{t}}\\&=-h\sum_{i=1}^{M-1}(v_i^ne_i^n)_{\bar{t}}(e_i^n)_{\hat{x}\bar{t}}-h\sum_{i=1}^{M-1}(u_i^ne_i^n)_{\bar{t}}(e_i^n)_{\hat{x}\bar{t}}\\&=-h\sum_{i=1}^{M-1}[v_i^n(e_i^n)_{\bar{t}}+e_i^{n-1}(v_i^n)_{\bar{t}}](e_i^n)_{\hat{x}\bar{t}}-h\sum_{i=1}^{M-1}[u_i^n(e_i^n)_{\bar{t}}+e_i^{n-1}(u_i^n)_{\bar{t}}](e_i^n)_{\hat{x}\bar{t}}\\&\le h\sum_{i=1}^{M-1}(|v_i^n||(e_i^n)_{\bar{t}}|+|e_i^{n-1}||(v_i^n)_{\bar{t}}|)|(e_i^n)_{\hat{x}\bar{t}}|+h\sum_{i=1}^{M-1}(|u_i^n||(e_i^n)_{\bar{t}}|+|e_i^{n-1}||(u_i^n)_{\bar{t}}|)|(e_i^n)_{\hat{x}\bar{t}}|\\&\le h\sum_{i=1}^{M-1}(|v_i^n||(e_i^n)_{\bar{t}}|+|e_i^{n-1}||(e_i^n)_{\bar{t}}|+|e_i^{n-1}||(u_i^n)_{\bar{t}}|)|(e_i^n)_{\hat{x}\bar{t}}|\\&\quad+h\sum_{i=1}^{M-1}(|u_i^n||(e_i^n)_{\bar{t}}|+|e_i^{n-1}||(u_i^n)_{\bar{t}}|)|(e_i^n)_{\hat{x}\bar{t}}|\\&\le Ch\sum_{i=1}^{M-1}|(e_i^n)_{\bar{t}}||(e_i^n)_{\hat{x}\bar{t}}|+Ch\sum_{i=1}^{M-1}|e_i^{n-1}||(e_i^n)_{\hat{x}\bar{t}}|\\&\le C\|e_{\bar{t}}^n\|\|e_{\hat{x}\bar{t}}^n\|+C\|e^{n-1}\|\|e_{\hat{x}\bar{t}}^n\|\\&\le C(\|e_{\bar{t}}^n\|^2+\|e^{n-1}\|^2+\|e_{\hat{x}\bar{t}}^n\|^2).\end{aligned}\tag{34}$$

Similarly, it can be easily shown that

$$\langle[(v^{n-1})^2-(u^{n-1})^2]_{\hat{x}\bar{t}},e_{\hat{t}}^n\rangle\le C(\|e_{\bar{t}}^{n-1}\|^2+\|e^{n-2}\|^2+\|e_{\hat{x}\bar{t}}^n\|^2).\tag{35}$$

Furthermore,

$$\langle r^n,e_{\hat{t}}^n\rangle=\left\langle r^n,\frac{1}{2}(e_{\bar{t}}^{n+1}+e_{\bar{t}}^n)\right\rangle\le\frac{1}{2}\|r^n\|^2+\frac{1}{4}(\|e_{\bar{t}}^{n+1}\|^2+\|e_{\bar{t}}^n\|^2).\tag{36}$$

Similarly to Eq. (27), we have $\|e_{\hat{x}\bar{t}}^n\|^2\le\|e_{x\hat{t}}^n\|^2$. Then

$$\|e_{\hat{x}\bar{t}}^n\|^2\le\frac{1}{4}\|e_{x\bar{t}}^{n+1}+e_{x\bar{t}}^n\|^2\le\frac{1}{2}(\|e_{x\bar{t}}^{n+1}\|^2+\|e_{x\bar{t}}^n\|^2).\tag{37}$$

Substituting Eqs. (34)–(37) into Eq. (33), we obtain

$$\begin{aligned}&(\|e_{\bar{t}}^{n+1}\|^2-\|e_{\bar{t}}^n\|^2)+(\|e_{x\bar{t}}^{n+1}\|^2-\|e_{x\bar{t}}^n\|^2)+\frac{1}{2}(\|e_x^{n+1}\|^2-\|e_x^{n-1}\|^2)\\&\quad\le C\tau(\|e_{\bar{t}}^{n+1}\|^2+\|e_{\bar{t}}^n\|^2+\|e_{\bar{t}}^{n-1}\|^2+\|e^{n-1}\|^2+\|e^{n-2}\|^2+\|e_{x\bar{t}}^{n+1}\|^2+\|e_{x\bar{t}}^n\|^2)+\tau\|r^n\|^2.\end{aligned}\tag{38}$$

Let

$$D^n\equiv\|e_{\bar{t}}^n\|^2+\|e_{x\bar{t}}^n\|^2+\frac{1}{2}\|e_x^n\|^2+\frac{1}{2}\|e_x^{n-1}\|^2.$$

Using Lemma 3, Eq. (38) can be rewritten as

$$D^{n+1}-D^n\le C\tau(D^{n+1}+D^n+D^{n-1})+\tau\|r^n\|^2,$$

and obtain

$$(1-C\tau)(D^{n+1}-D^n)\le C\tau(D^n+D^{n-1})+\tau\|r^n\|^2.$$

If τ is sufficiently small satisfying $1 - C\tau > 0$, then

$$D^{n+1} - D^n \le C\tau (D^n + D^{n-1}) + C\tau \|r^n\|^2. \tag{39}$$

Summing up Eq. (39) from 2 to n, we have

$$D^{n+1} - D^2 \le C\tau \sum_{k=1}^{n} D^k + C\tau \sum_{k=2}^{n} \|r^k\|^2. \tag{40}$$

Notice that

$$\tau \sum_{k=2}^{n} \|r^k\|^2 \le (n-1)\tau \max_{2\le k\le n} \|r^k\|^2 \le T \cdot O(h^2 + \tau^2)^2.$$

Since we can approximate u^1 and u^2 using any available second-order accuracy method, thus, it implies u^1 and u^2 are of $O(h^2 + \tau^2)$. From Eq. (40), we obtain

$$D^{n+1} \le O(h^2 + \tau^2)^2 + C\tau \sum_{k=1}^{n} D^k.$$

By Lemma 6, we have

$$D^{n+1} \le O(h^2 + \tau^2)^2 e^{Cn\tau} \le O(h^2 + \tau^2)^2 e^{CT} = O(h^2 + \tau^2)^2.$$

That is,

$$\|e_{\bar{t}}^{n+1}\| \le O(h^2 + \tau^2), \quad \|e_{x\bar{t}}^{n+1}\| \le O(h^2 + \tau^2), \quad \|e_x^{n+1}\| \le O(h^2 + \tau^2).$$

Finally, by using Lemmas 4 and 5, we get

$$\|e_{\bar{t}}^{n+1}\|_\infty \le O(h^2 + \tau^2), \quad \|e^{n+1}\|_\infty \le O(h^2 + \tau^2).$$

This completes the proof of Theorem 9. □

Theorem 10. *Under the conditions of Theorem 9, the solution of scheme (9)–(11) is stable with respect to* $\|\cdot\|_\infty$.

4. Numerical experiments

The exact solitary wave [1] of the SRLW equation (3) has the following form

$$u(x,t) = \frac{3(\upsilon^2 - 1)}{\upsilon} \operatorname{sech}^2\left(\sqrt{\frac{\upsilon^2 - 1}{4\upsilon^2}}(x - \upsilon t)\right). \tag{41}$$

Note that υ is a variable parameter that allows the existence of bidirectional propagation for $\upsilon < -1$ and $\upsilon > 1$ simply refer to left and right traveling solitary waves of the same type, respectively. Recall that the RLW equation possesses solitary waves of the form

$$u(x,t) = 3(1 - \upsilon) \operatorname{sech}^2\left(\sqrt{\frac{\upsilon - 1}{4\upsilon}}(x - \upsilon t)\right), \tag{42}$$

which propagate in both directions. The two branches of solitary waves for the velocity υ in the ranges $\upsilon < 0$ and $\upsilon > 1$ simply refer to left and right traveling solitary waves of different types, respectively. In test problems for the SRLW equation, we use initial conditions with $\upsilon = \sqrt{2}$ associated with this equation, which takes the form [11]

$$u_0(x) = \frac{3\sqrt{2}}{2} \operatorname{sech}^2\left(\frac{\sqrt{2}}{4}x\right), u_1(x) = \frac{3\sqrt{2}}{2} \operatorname{sech}^2\left(\frac{\sqrt{2}}{4}x\right) \tanh\left(\frac{\sqrt{2}}{4}x\right).$$

Since the first–order system of the SRLW equation (1) and (2) which was mentioned in introduction is equivalent to Eq. (3), thus, we can directly calculate the density $\rho(x,t)$ by using the second-order finite difference approximation

$$\rho_i^{n+1} = \frac{-\tau}{h}(u_{i+1}^n - u_{i-1}^n) + \rho_i^{n-1}.$$

It is known that, the exact density [11,12] is

$$\rho(x,t) = \frac{3(\upsilon^2 - 1)}{\upsilon^2} \operatorname{sech}^2\left(\sqrt{\frac{\upsilon^2 - 1}{4\upsilon^2}}(x - \upsilon t)\right).$$

Here we take the initial density associated with this equation, which takes the form

$$\rho_0(x) = \frac{3}{2} \operatorname{sech}^2\left(\frac{\sqrt{2}}{4}x\right).$$

Our study of numerical simulations can be summarized as follows.

Table 1
The error of numerical solutions u_i^n using $\|\cdot\|-$norm at $t = 20$.

Scheme	$h = \tau = 0.1$	$h = \tau = 0.05$	$h = \tau = 0.025$
Scheme 1 [11]	0.0347	0.0087	0.0022
Scheme 2 [11]	0.0735	0.0186	0.0046
Scheme 3 [11]	0.0283	0.0071	0.0018
Present	0.0162	0.0037	0.00088

Table 2
The error of numerical solutions ρ_i^n using $\|\cdot\|-$norm at $t = 20$.

Scheme	$h = \tau = 0.1$	$h = \tau = 0.05$	$h = \tau = 0.025$
Scheme 1 [11]	0.0254	0.0064	0.0016
Scheme 2 [11]	0.0536	0.0136	0.0034
Scheme 3 [11]	0.0201	0.0051	0.0013
Present	0.0151	0.0036	0.00087

Table 3
The error of numerical solutions u_i^n and rate of convergence using $\|\cdot\|-$norm.

	$h = \tau = 0.1$		$h = \tau = 0.05$		$h = \tau = 0.025$	
	$\|e^n\|$	Rate	$\|e^n\|$	Rate	$\|e^n\|$	Rate
$t = 5$	0.00854	–	0.00215	1.9931	0.00054	1.9945
$t = 10$	0.01168	–	0.00285	2.0332	0.00071	2.0136
$t = 15$	0.01371	–	0.00325	2.0777	0.00079	2.0352
$t = 20$	0.01622	–	0.00370	2.1335	0.00088	2.0644

Table 4
The error of numerical solutions u_i^n and rate of convergence using $\|\cdot\|_\infty-$norm.

	$h = \tau = 0.1$		$h = \tau = 0.05$		$h = \tau = 0.025$	
	$\|e^n\|$	Rate	$\|e^n\|$	Rate	$\|e^n\|$	Rate
$t = 5$	0.00515	–	0.00129	1.99781	0.00032	1.99765
$t = 10$	0.00589	–	0.00146	2.01409	0.00036	2.00466
$t = 15$	0.00671	–	0.00163	2.04016	0.00040	2.01781
$t = 20$	0.00782	–	0.00185	2.08044	0.00045	2.03930

Table 5
The error of numerical solutions ρ_i^n and rate of convergence using $\|\cdot\|-$norm.

	$h = \tau = 0.1$		$h = \tau = 0.05$		$h = \tau = 0.025$	
	$\|e^n\|$	Rate	$\|e^n\|$	Rate	$\|e^n\|$	Rate
$t = 5$	0.01192	–	0.00292	2.0301	0.00072	2.0136
$t = 10$	0.01222	–	0.00303	2.0115	0.00076	2.0047
$t = 15$	0.01250	–	0.00301	2.0555	0.00074	2.0250
$t = 20$	0.01509	–	0.00357	2.0804	0.00087	2.0373

4.1. Error and convergence rate

A grid refinement study has been performed to assess the asymptotic error of the present scheme by using $x_L = -20$ and $x_R = 180$. The error has been defined to be discrete $\|\cdot\|-$ and $\|\cdot\|_\infty-$ norms of the difference between the exact and the numerical solutions. We compute the error at the final time $t = 20$ and compare it to the error from methods in [11] to illustrate the accuracy of the scheme. The results obtained by the new scheme show the same significant digits as the ones obtained by the scheme 2 in [11] although the new scheme approximately uses two time larger step size, as presented in Tables 1 and 2. In term of the grid point number, the computational performance of the new scheme is obviously better than that of the schemes in [11]. Also, our scheme can reduce errors from the schemes in [11]. Especially, the present scheme obtains almost two time less error than the scheme 1 does and four time less error than the scheme 2 does. It is clear that results by our scheme show improvement over the previous one reported by [11]. As shown in Tables 3–6, the second-order convergence of numerical solutions is verified.

A more quantitative comparison is presented in Fig. 1, where numerical solutions of the present scheme and the scheme 3 in [11] are compared. For the numerical simulations, we set $x_L = -20$, $x_R = 180$, and $t \in [0, 60]$. In the plot of Fig. 1, we present the error norm of u_i^n versus time. The plots show that the convergence histories computed by using the present scheme and the

Table 6
The error of numerical solutions ρ_i^n and rate of convergence using $\|\cdot\|_\infty$–norm.

	$h = \tau = 0.1$		$h = \tau = 0.05$		$h = \tau = 0.025$	
	$\|e^n\|$	Rate	$\|e^n\|$	Rate	$\|e^n\|$	Rate
$t = 5$	0.00733	–	0.00176	2.05379	0.00043	2.02804
$t = 10$	0.00507	–	0.00127	1.99427	0.00032	1.99945
$t = 15$	0.00523	–	0.00125	2.06439	0.00031	2.03157
$t = 20$	0.00605	–	0.00141	2.10406	0.00034	2.05301

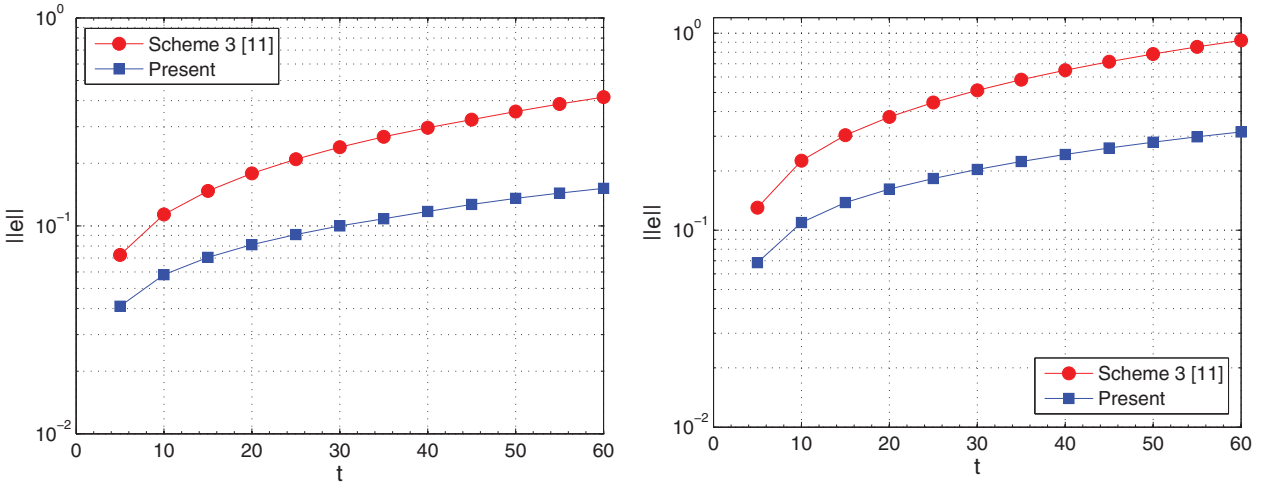

Fig. 1. The error of numerical solutions of $u(x, t)$ using $\|\cdot\|$–norm at $t = 60$ with $h = 0.25$, $\tau = 0.1$ (left) and $h = 0.5$, $\tau = 0.1$ (right).

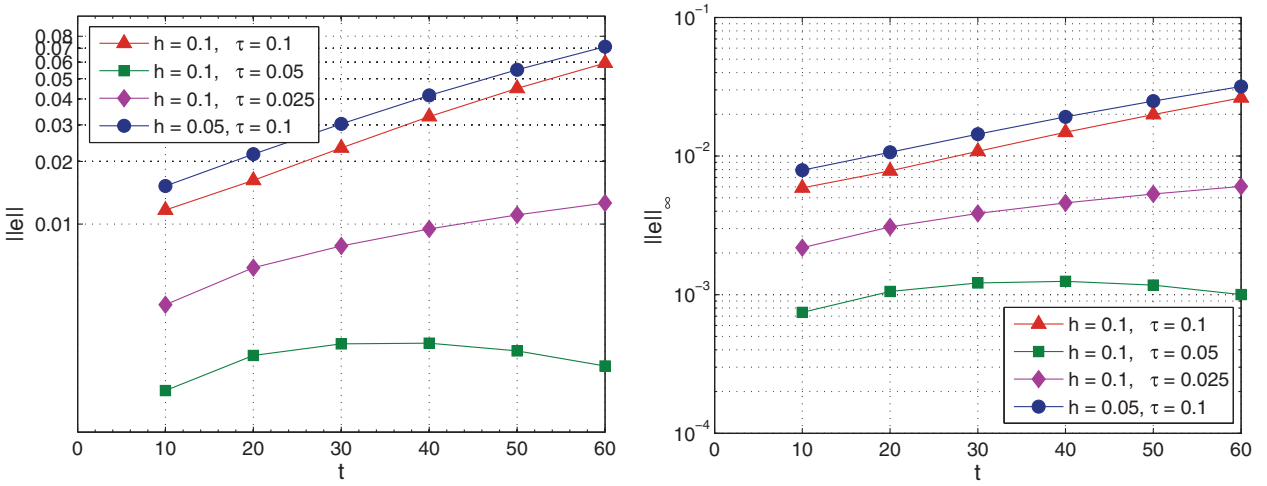

Fig. 2. The error of numerical solutions of $u(x, t)$ using $\|\cdot\|$–norm (left) and $\|\cdot\|_\infty$–norm (right) under different mesh steps h and τ.

scheme 3 in [11] are distinguishable. It is observed that both errors increase with time but the error of the present scheme is less than that of the scheme 3 in [11]. The present scheme behaviors have been obtained using step sizes considerably larger than those employed for the schemes in [11]. Figs. 2 and 3 show error norms obtained by the present scheme as a function of time step and grid spacing. From four cases of simulation, the errors increase almost linearly with time except the case $h = 0.1$ and $\tau = 0.05$. The error slightly increases as the time step is decreased to $\tau = 0.025$, presumably because of the increase in round-off error. This reason is the same as the case that the error slightly increases as the grid spacing is decreased to $h = 0.05$.

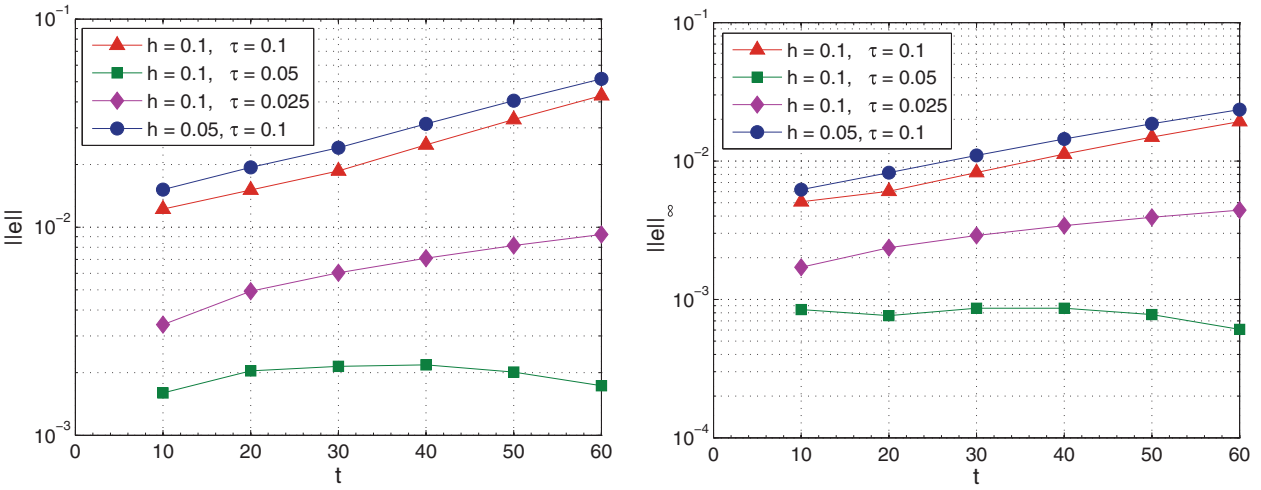

Fig. 3. The error of numerical solutions of $\rho(x, t)$ using $\|\cdot\|$–norm (left) and $\|\cdot\|_\infty$–norm (right) under different mesh steps h and τ.

Table 7
Quantities Q^n under different mesh steps h and τ at various time.

	$h = \tau = 0.1$	$h = 0.1, \tau = 0.05$	$h = 0.1, \tau = 0.025$	$h = 0.05, \tau = 0.1$
$t = 0$	0.0000008532	0.0000004373	0.0000002214	0.0000008384
$t = 10$	0.0000014616	0.0000004730	0.0000002048	0.0000009769
$t = 20$	0.0000053996	−0.0000032166	−0.0000025267	0.0000121037
$t = 30$	−0.0000475892	0.0000045640	0.0000060689	−0.0000651447
$t = 40$	0.0000135275	−0.0000026284	−0.0000018423	0.0000252299
$t = 50$	0.0000109632	−0.0000018509	−0.0000010681	0.0000192928
$t = 60$	−0.0000379896	−0.0000026339	0.0000014097	−0.0000409694

Table 8
Quantities I_1^n under different mesh steps h and τ at various time.

	$h = \tau = 0.1$	$h = 0.1, \tau = 0.05$	$h = 0.1, \tau = 0.025$	$h = 0.05, \tau = 0.1$
Analytical value	5.9999956719	5.9999956719	5.9999956719	5.9999956719
$t = 0$	5.9999955171	5.9999955171	5.9999955171	5.9999955949
$t = 10$	5.9999818987	5.9999883051	5.9999898719	5.9999860981
$t = 20$	5.9998590814	5.9999287900	5.9999500510	5.9999003444
$t = 30$	5.9989594743	6.0004457165	6.0008455686	5.9981872735
$t = 40$	5.9991755664	6.0003288589	6.0007063648	5.9985558260
$t = 50$	5.9996485455	6.0003318057	6.0006334590	5.9990934424
$t = 60$	6.0001680653	6.0003794646	6.0005905238	5.9996447141

4.2. Conservative approximations

Conservative approximation, that is a supplementary constraint, is essential for a suitable difference equation to make a discrete analogue effective to the fundamental conservation properties of the governing equation. Then, we can calculate three conservative approximations by using discrete forms as follows:

$$I_1^n = \frac{h}{2}\sum_{i=1}^{M-1} u_i^n,$$

$$I_2^n = \frac{h}{2}\sum_{i=1}^{M-1} \rho_i^n,$$

$$I_3^n = \frac{h}{2}\sum_{i=1}^{M-1} (u_i^n)^2 + \frac{1}{8h}\sum_{i=1}^{M-1} (u_{i+1}^n - u_{i-1}^n)^2 + \frac{h}{2}\sum_{i=1}^{M-1} (\rho_i^n)^2.$$

In Table 7, it results from the present method, and the values of Q^n at any time $t \in [0, 60]$ coincide with the theory. In this case, the following sets of parameters are chosen for the test problems: $x_L = -20$ and $x_R = 180$. In Tables 8 and 9, the quantities I_1^n and I_2^n are well preserved regardless of the time step and grid spacing. The quantity I_3^n is presented in Table 10. One can easily

Table 9
Quantities I_2^n under different mesh steps h and τ at various time.

	$h = \tau = 0.1$	$h = 0.1, \tau = 0.05$	$h = 0.1, \tau = 0.025$	$h = 0.05, \tau = 0.1$
Analytical value	4.2426376267	4.2426376267	4.2426376267	4.2426376267
$t = 0$	4.2426375172	4.2426375172	4.2426375172	4.2426375723
$t = 10$	4.2426385251	4.2426381201	4.2426379403	4.2426383024
$t = 20$	4.2426388155	4.2426365015	4.2426357062	4.2426391530
$t = 30$	4.2426247708	4.2426409843	4.2426452841	4.2426287753
$t = 40$	4.2426455507	4.2426365856	4.2426351950	4.2426439868
$t = 50$	4.2426444371	4.2426368507	4.2426362331	4.2426429745
$t = 60$	4.2426196418	4.2426356990	4.2426410456	4.2426278958

Table 10
Quantities I_3^n under different mesh steps h and τ at various time.

	$h = \tau = 0.1$	$h = 0.1, \tau = 0.05$	$h = 0.1, \tau = 0.025$	$h = 0.05, \tau = 0.1$
Analytical value	13.5764501988	13.5764501988	13.5764501988	13.5764501988
$t = 0$	13.5754409883	13.5754409883	13.5754409883	13.5761977195
$t = 10$	13.5819388501	13.5770214700	13.5766395403	13.5818774327
$t = 20$	13.5892493371	13.5779107322	13.5767488004	13.5892335547
$t = 30$	13.5966265407	13.5788185645	13.5768622319	13.5966433943
$t = 40$	13.6040284766	13.5797269165	13.5769754293	13.6040790919
$t = 50$	13.6114414174	13.5806353499	13.5770885004	13.6115252098
$t = 60$	13.6188685380	13.5815439746	13.5772014613	13.6189855725

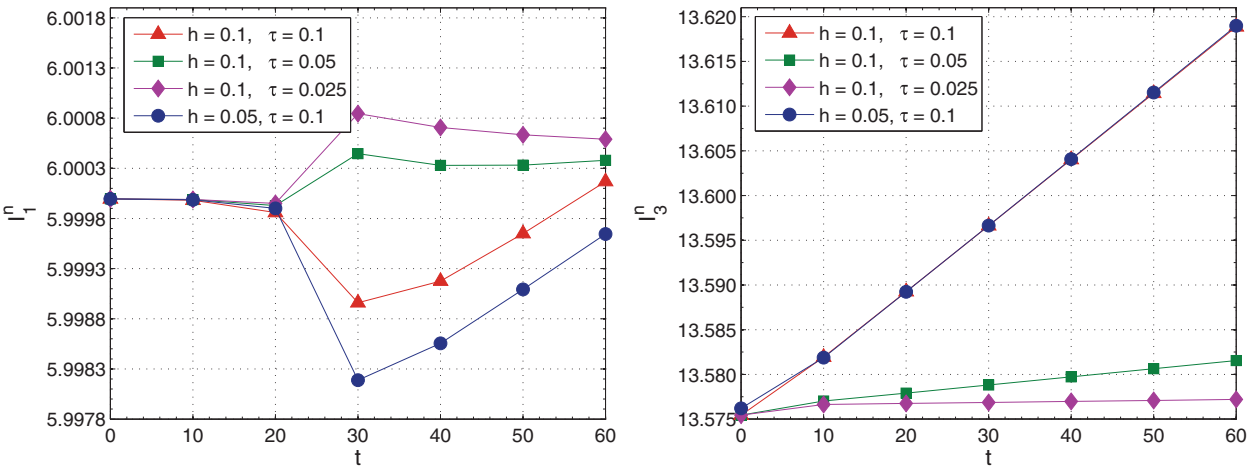

Fig. 4. Discrete mass I_1^n (left) and discrete energy I_3^n (right) under different mesh steps h and τ.

see that the quantity I_3^n slightly increases as the time is increased whereas it slightly decreases as the time step is decreased. As shown in Fig. 4, the quantity I_1^n is independent from the time step, grid spacing, and time. For the quantity I_3^n, it has been found to increase as the time is increased and seems to tend to asymptotic constant values for the case $h = 0.1$ and $\tau = 0.025$.

4.3. Long-time simulations

According to an experiment, at long–time behavior should be observed. The waveforms obtained by the present scheme are plotted in Fig. 5 using $h = 0.25$, $\tau = 0.1$, $x_L = -20$, and $x_R = 180$. The waveforms at $t = 40$ and 80 agree with the waveforms at $t = 0$ quite well, which also shows the accuracy of the scheme. To underscore the efficiency of the present method, we compare these results at long time obtained by using the second-order finite difference method reported by [11]. Clearly, it converges very slowly, and even on the finer grid than the grid used in Fig. 6 (left), it is still far from the converged solution, especially at the peak of amplitude.

The plots of Figs. 7 and 8 show a clear loss of accuracy of the scheme 3 in [11] with the step size $h = 0.5$, $\tau = 0.1$, $x_L = -20$, $x_R = 180$, and $t = 100$. Results obtained by the scheme 3 show lagging of numerical solutions when compared to exact solutions. Moreover, subgraphs of Figs. 7 and 8 which illustrate the expanded left-tail figure show oscillation of numerical approximations on $x \in [40, 120]$. It can be observed that the present scheme provides the well resolution of wave structure at left-tail.

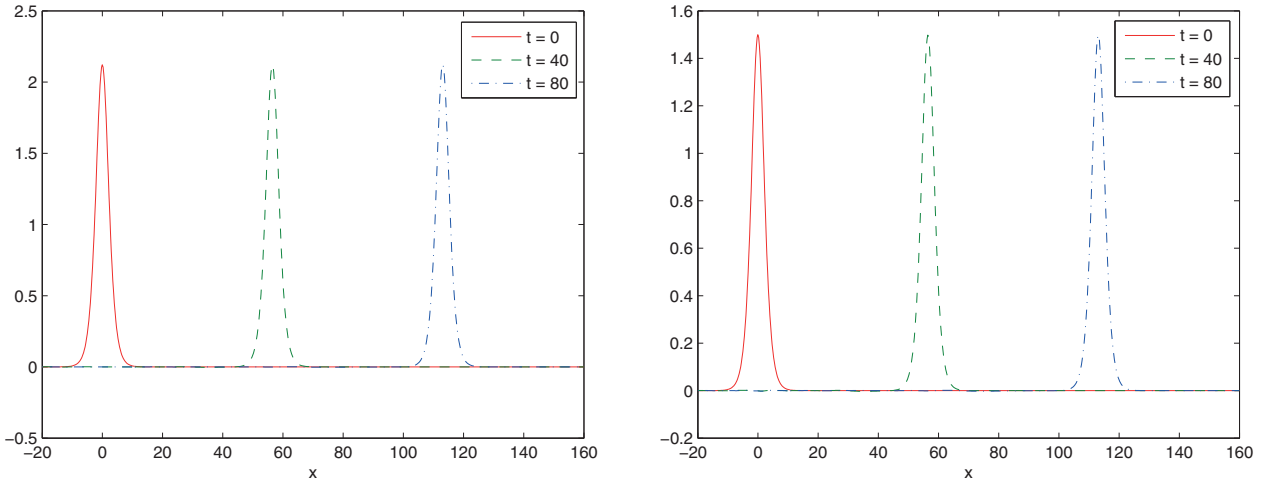

Fig. 5. Numerical solutions of $u(x, t)$ (left) and $\rho(x, t)$ (right) with $h = 0.25$ and $\tau = 0.1$.

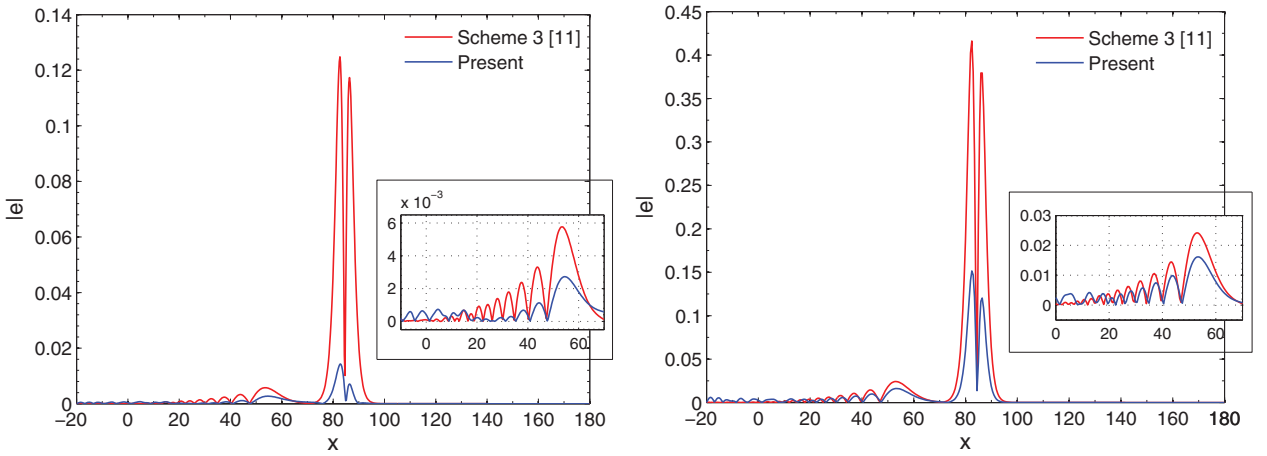

Fig. 6. Comparison absolute error of numerical solutions of $u(x, t)$ at $t = 60$ with $h = 0.25$, $\tau = 0.1$ (left) and $h = 0.5$, $\tau = 0.1$ (right).

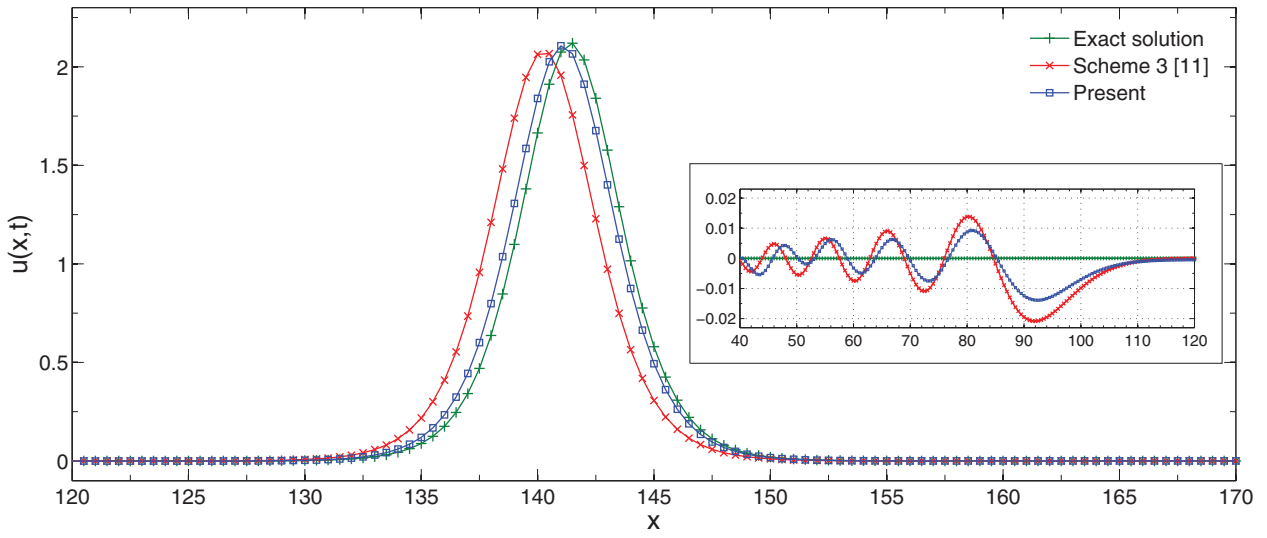

Fig. 7. Numerical solution of $u(x, t)$ at $t = 100$ with $h = 0.5$, $\tau = 0.1$.

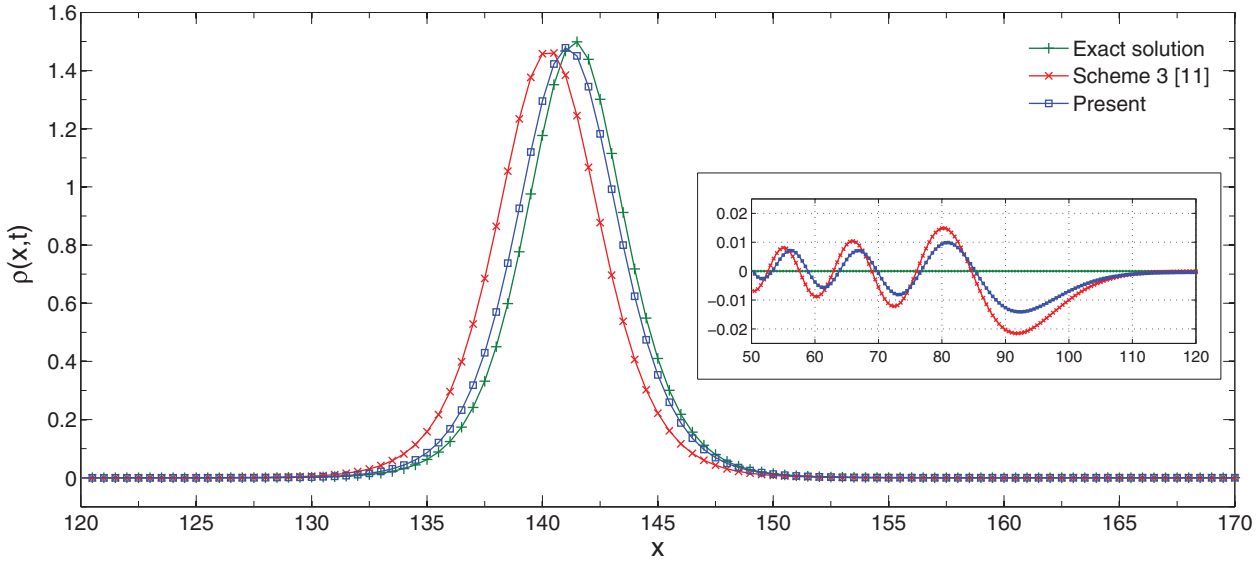

Fig. 8. Numerical solution of $\rho(x, t)$ at $t = 100$ with $h = 0.5, \tau = 0.1$.

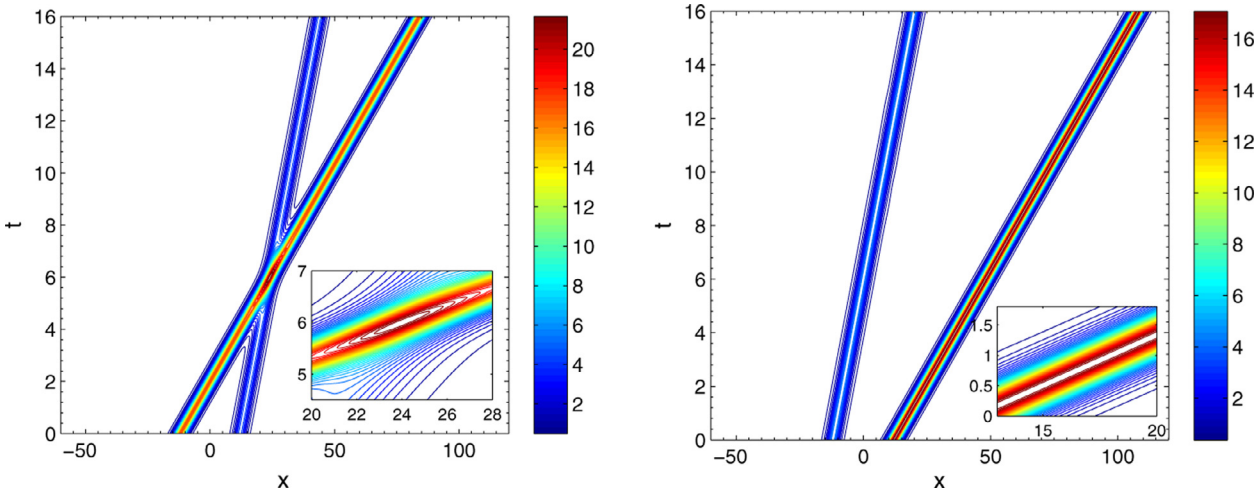

Fig. 9. Overtaking collision of two solitary waves with $h = 0.05$ and $\tau = 0.001$ at $\upsilon_1 = 2, \upsilon_2 = 6, x_0 = 12$, (left) and $\upsilon_1 = 6, \upsilon_2 = 2, x_0 = 12$ (right).

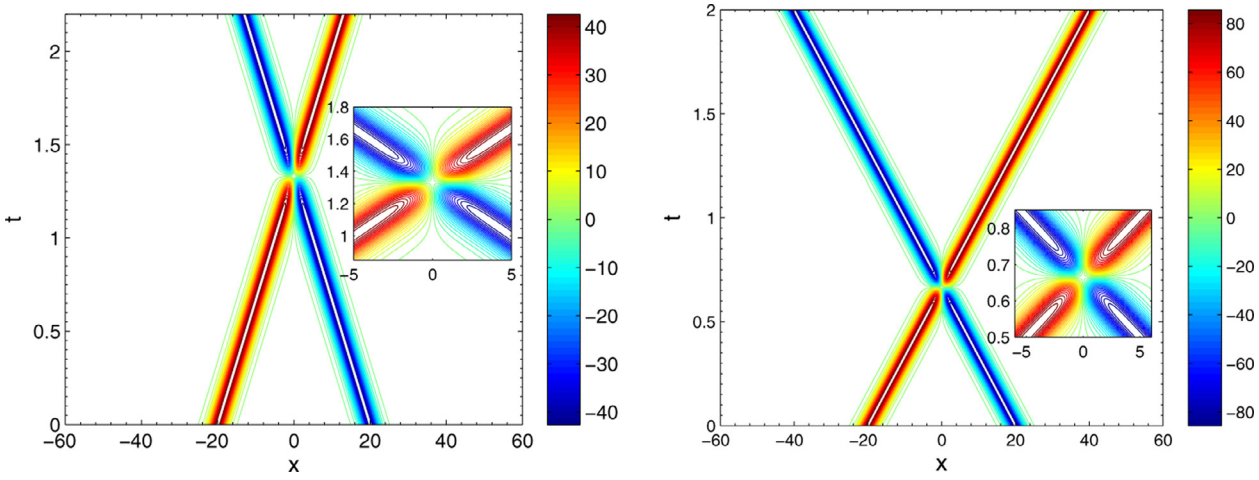

Fig. 10. Head-on collision of two solitary waves with $h = 0.05$ and $\tau = 0.001$ at $\upsilon_1 = -15, \upsilon_2 = 15, x_0 = 20$ (left) and $\upsilon_1 = -30, \upsilon_2 = 30, x_0 = 20$ (right).

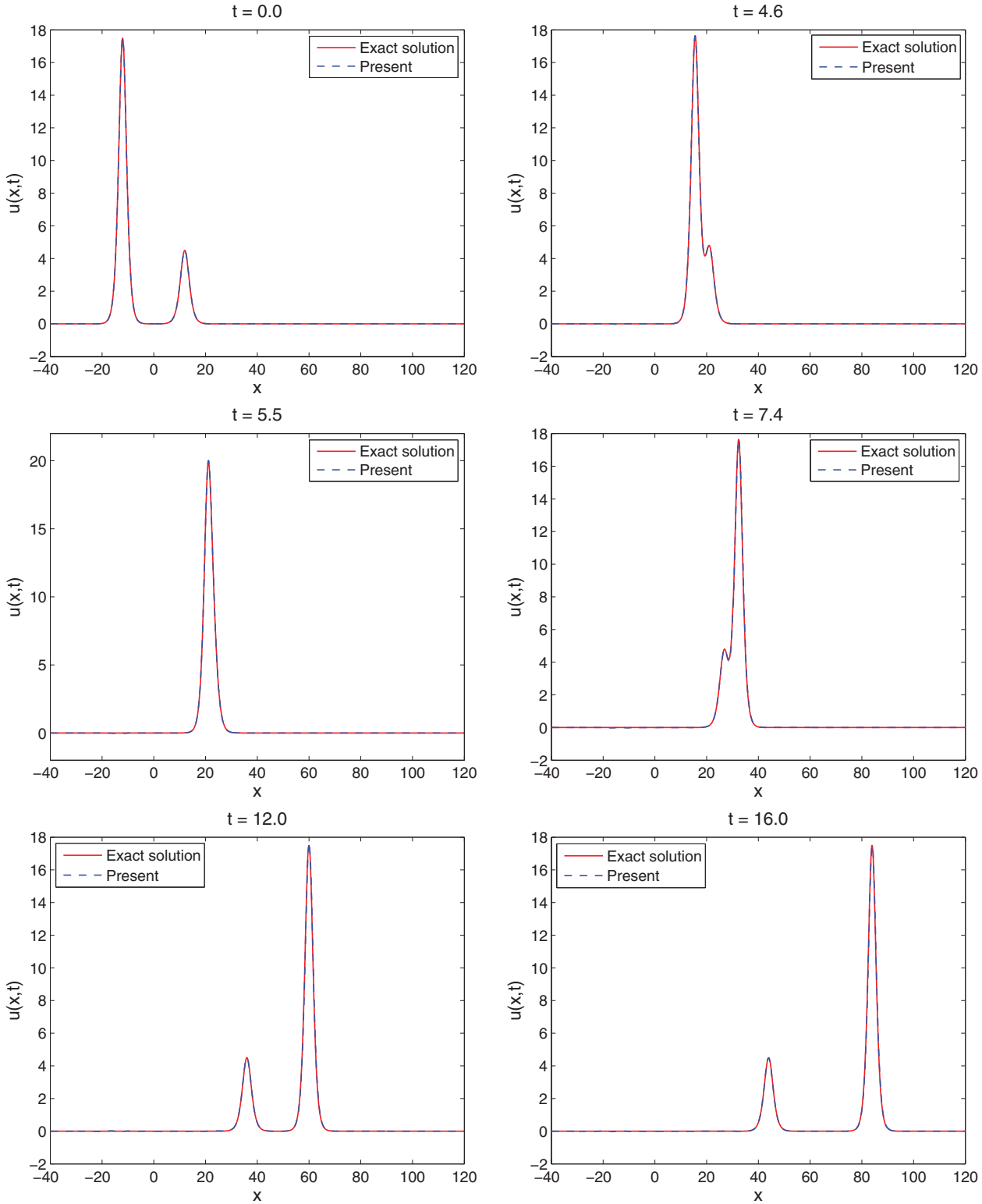

Fig. 11. Overtaking collision of two solitary waves with velocity pair $\upsilon_1 = 2, \upsilon_2 = 6, x_0 = 12, h = 0.05$, and $\tau = 0.001$.

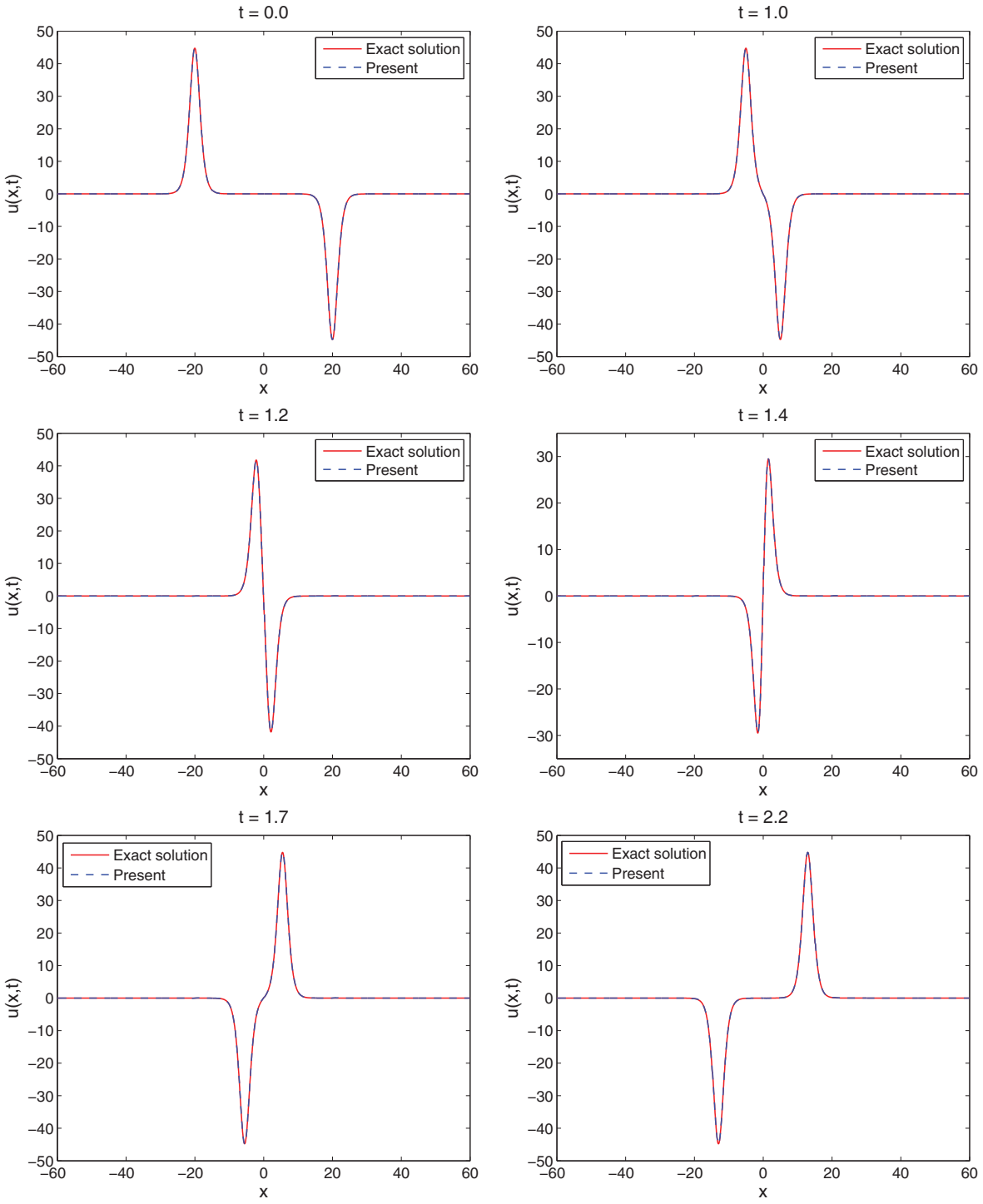

Fig. 12. Head-on collision of two equal–amplitude solitary waves with velocity pair $\upsilon_1 = -15, \upsilon_2 = 15, x_0 = 20, h = 0.05$, and $\tau = 0.001$.

4.4. Collision of two solitons

We next examine the performance of the present scheme for the collision case. Results from a sequence of numerical simulations in cases of copropagating and counterpropagating interactions between two solitons are presented and compared with the

exact solution by using the soliton solution which is in the form

$$u(x,t) = \frac{3({\upsilon_1}^2-1)}{\upsilon_1}\operatorname{sech}^2\left(\sqrt{\frac{{\upsilon_1}^2-1}{4{\upsilon_1}^2}}(x-x_0-\upsilon_1 t)\right) + \frac{3({\upsilon_2}^2-1)}{\upsilon_2}\operatorname{sech}^2\left(\sqrt{\frac{{\upsilon_2}^2-1}{4{\upsilon_2}^2}}(x+x_0-\upsilon_2 t)\right). \tag{43}$$

For numerical experiments, we set $h = 0.05$, $\tau = 0.001$, $x_L = -60$, $x_R = 120$, and $t \in [0, 20]$. Figs. 9 and 10 clearly show that the parameters υ_1 and υ_2 affect the propagation characteristics of collision of two solitons. From Fig. 9, if υ_1 is less than υ_2 and both have the same sign, the overtaking collision will happen. From Fig. 10, however, if two solitons have the different polarity, the head-on collision will happen. The bigger size of υ_1 and υ_2 is, the faster head-on collision occurs.

Fig. 11 shows the results with a time-dependent computation corresponding to the propagation of initial waves $\upsilon_1 = 2$ and $\upsilon_2 = 6$. The initial waves are centered at $x_0 = 12$ and the solutions are computed on step size $h = 0.05$, $\tau = 0.001$, $x_L = -40$, and $x_R = 120$. The soliton with the bigger amplitude overtakes the smaller one, as both with positive polarity are right-going. Fig. 12 shows the results with a time dependent computation corresponding to the propagation of initial waves $\upsilon_1 = -15$ and $\upsilon_2 = 15$. The initial waves are centered at $x_0 = 20$ and the solutions are computed on step size $h = 0.05$, $\tau = 0.001$, $x_L = -60$, and $x_R = 60$. While υ_1 is positive and υ_2 is negative, a head-on collision of different polarity between one right-going soliton and one left-going soliton appears. It can be observed that the sign of υ_i regulates the direction in which the solitons propagate. The velocity and amplitude of each soliton definitely remain the same after both overtaking and head-on collisions.

5. Conclusions

The four-level linear implicit finite difference scheme for the SRLW equation is introduced and analyzed. The existence and uniqueness of the numerical solution are directly obtained from the calculation of a linear system since a coefficient matrix is strictly diagonally dominant. Moreover, the accuracy and stability of the numerical scheme for the solution of the SRLW equation can be tested by using the exact solution. The present method gives an implicit linear system, which can be easily implemented, and also shows the second-order accuracy in time and space. The numerical experiments show that the present method supports the analysis of convergence rate and the invariant properties can be verified by using analytical expressions. It is obvious that the solitary wave obtained by this novel method can be smoothed out, at long time. In addition, overtaking and head-on collisions between two solitons can be dealt with the proposed scheme.

Acknowledgments

This research was supported by Chiang Mai University. The authors appreciate the reviewers for their valuable comments which improved this article.

References

[1] C.E. Seyler, D.L. Fenstermacher, A symmetric regularized-long-wave equation, Phys. Fluids 27 (1) (1984) 4–7.
[2] J.L. Bona, W.G. Pritchard, L.R. Scott, Numerical schemes for a model for nonlinear dispersive waves, J. Comput. Phys. 60 (1985) 167–186.
[3] D. Bhardwaj, R. Shankar, A computational method for regularized long wave equation, Comput. Math. Appl. 40 (2000) 1397–1404.
[4] A. Dogan, Numerical solution of regularized long wave equation using Petrov–Galerkin method, Commun. Numer. Meth. Eng. 17 (2001) 485–494.
[5] A. Dogan, Numerical solution of RLW equation using linear finite elements within Galerkin's method, Appl. Math. Model. 26 (2002) 771–783.
[6] K.R. Raslan, A computational method for the regularized long wave (RLW) equation, Appl. Math. Comput. 167 (2005) 1101–1118.
[7] J. Lin, Z. Xie, J. Zhou, High-order compact difference scheme for the regularized long wave equation, Commun. Numer. Meth. Eng. 23 (2007) 135–156.
[8] F. Shaomei, G. Boling, Q. Hua, The existence of global attractors for a system of multi-dimensional symmetric regularized wave equations, Commun. Nonlinear Sci. Numer. Simul. 14 (2009) 61–68.
[9] Z. Zheng, R. Zhang, B. Guo, The Fourier pseudo–spectral method for the SRLW equation, Appl. Math. Mech. 10 (9) (1989) 843–852.
[10] Y. Shang, B. Gua, Analysis of Chebyshev pseudospectral method for multi-dimensional generalized SRLW equations, Appl. Math. Mech. 24 (10) (2003) 1168–1183.
[11] T. Wang, L. Zhang, F. Chen, Conservative schemes for the symmetric regularized long wave equations, Appl. Math. Comput. 190 (2007) 1063–1080.
[12] T. Nie, A decoupled and conservative difference scheme with fourth–order accuracy for the symmetric regularized long wave equations, Appl. Math. Comput. 219 (2013) 9461–9468.
[13] J. Hu, K. Zheng, M. Zheng, Numerical simulation and convergence analysis of high-order conservative difference scheme for SRLW equation, Appl. Math. Model. 38 (23) (2014) 5573–5581.
[14] S. Li, L. Vu-Quoc, Finite difference calculus invariant structure of a class of algorithms for the nonlinear Klein–Gordon equation, SIAM J. Numer. Anal. 32 (6) (1995) 1839–1875.
[15] F. Zhang, M.P. Victor, V. Luis, Numerical simulation of nonlinear Schrödinger systems: a new conservative scheme, Appl. Math. Comput. 71 (1995) 165–177.
[16] K. Omrani, F. Abidi, T. Achouri, N. Khiari, A new conservative finite difference scheme for the Rosenau equation, Appl. Math. Comput. 201 (2008) 35–43.
[17] T. Wang, B. Guo, L. Zhang, New conservative difference schemes for a coupled nonlinear Schrödinger system, Appl. Math. Comput. 217 (2010) 1604–1619.
[18] Z. Ren, W. Wang, D. Yu, A new conservative finite difference method for the nonlinear regularized long wave equation, Appl. Math. Sci. 5 (42) (2011) 2091–2096.
[19] X. Pan, L. Zhang, On the convergence of a conservative numerical scheme for the usual Rosenau–RLW equation, Appl. Math. Model. 36 (2012) 3371–3378.
[20] J. Hu, Y. Xu, B. Hu, Conservative linear difference scheme for Rosenau–KdV equation, Adv. Math. Phys. 2013 (2013) 7. Article ID 423718.
[21] K. Zheng, J. Hu, High-order conservative Crank–Nicolson scheme for regularized long wave equation, Adv. Differ. Equ. 2013 (2013) 287.
[22] X. Shao, G. Xue, C. Li, A conservative weighted finite difference scheme for regularized long wave equation, Appl. Math. Comput. 219 (2013) 9202–9209.
[23] R.P. Agarwall, Difference Equations an Inequalities, Marcel Dekker Inc., New York, 1992.
[24] Y. Zhou, Application of Discrete Functional Analysis to the Finite Difference Method, International Academic Publishers, Beijing, 1991.

Applied Mathematics and Computation 245 (2014) 289–304

Contents lists available at ScienceDirect

Applied Mathematics and Computation

journal homepage: www.elsevier.com/locate/amc

A three-level average implicit finite difference scheme to solve equation obtained by coupling the Rosenau–KdV equation and the Rosenau–RLW equation

B. Wongsaijai, K. Poochinapan *

Department of Mathematics, Faculty of Science, Chiang Mai University, Chiang Mai 50200, Thailand

ARTICLE INFO

Keywords:
Rosenau–KdV equation
Rosenau–RLW equation
Finite difference method
Convergence
Stability

ABSTRACT

In the present work, a mathematical model to obtain the solution of the nonlinear wave by coupling the Rosenau–KdV equation and the Rosenau–RLW equation is proposed. The solution properties are also derived. A numerical tool is applied to the model by using a three-level average implicit finite difference technique. The fundamental conservative properties of the equation are preserved by the presented numerical scheme, and the existence and uniqueness of the numerical solution are proved. Moreover, the convergence and stability of the numerical solution are also shown. The new method give second-order accurate in time and space. Thus, the presented results can be constructed to demonstrate the viability of the new model.

1. Introduction

A nonlinear wave phenomenon is one of the important areas of scientific research, which many scientists in the past have studied about mathematical models explaining the behavior. There are mathematical models which describe the dynamics of wave behaviors, such as the KdV equation, the RLW equation, the Rosenau equation, and many others [1–17]. The KdV equation has been used in very wide applications, such as magnetic fluid wave, ion sound wave, and longitudinal astigmatic wave [1–4]. The RLW equation, which is first proposed by Peregrine [16,17], provides an explanation on different situations of a nonlinear dispersive wave from the more classical KdV equation. Peregrine developed the RLW equation as a new option of the KdV equation to examine solution behavior and as a model for small-amplitude long waves on the water surface. Furthermore, an interesting property of the RLW equation is that the production of secondary solitary waves or sinusoidal solutions is caused by the collision of two solitary waves. Since the case of wave–wave and wave–wall interactions cannot be described by the KdV equation, Rosenau [6,7] proposed an equation for describing the dynamic of dense discrete systems. It is known as the Rosenau equation:

$$u_t + u_{xxxxt} + u_x + (u^2)_x = 0.$$

The existence and uniqueness of the solution for the Rosenau equation were proved by Park [8,18]. For the further consideration of nonlinear waves, the viscous term u_{xxx} needs to be included in the equation. This equation is usually called the Rosenau–KdV equation [10–15]:

* Corresponding author.
E-mail address: kanyuta@hotmail.com (K. Poochinapan).

http://dx.doi.org/10.1016/j.amc.2014.07.075
0096-3003/

$$u_t + u_{xxxxt} + u_{xxx} + u_x + (u^2)_x = 0.$$

However, a numerical method for the initial-boundary value problem of the Rosenau–KdV equation has not been studied widely. Hu et al. [10] has proposed the second-order conservative finite difference scheme for the approximate solution. On the other hand, to understand another nonlinear behavior of waves, the term $-u_{xxt}$ is included in the equation. This equation is usually called the Rosenua-RLW equation:

$$u_t - u_{xxt} + u_{xxxxt} + u_x + (u^2)_x = 0.$$

The behavior of the solution to the Rosenau–RLW equation with the Cauchy problem has been well studied for the past years [19–24]. The Rosenau–RLW equation has been solved numerically by various methods. Zuo et al. [19] have proposed the Crank–Nicolson finite difference scheme for the equation; the convergence and stability of the proposed method were also discussed. Obviously, the scheme in [19] requires heavy iterative computations because it is nonlinear implicit. Moreover, Pan and Zhang [20,21] developed linearized difference schemes which are three-level and conservative implicit for both Rosenau–RLW and general Rosenau–RLW equations. The second-order accuracy and unconditional stability were also proved.

In this paper, we consider the numerical method of the following initial-boundary value problem for coupling the general Rosenau–RLW equation and the Rosenau–KdV equation (the Rosenau–KdV–RLW equation):

$$u_t - \gamma^{\mathrm{RLW}} u_{xxt} + u_{xxxxt} + \beta^{\mathrm{KdV}} u_{xxx} + u_x + \alpha(u^2)_x = 0, \quad x_l < x < x_r, \quad 0 \leqslant t \leqslant T, \tag{1}$$

with an initial condition

$$u(x,0) = u_0(x), \quad x_l \leqslant x \leqslant x_r, \tag{2}$$

and boundary conditions

$$u(x_l,t) = u(x_r,t) = 0, \quad u_x(x_l,t) = u_x(x_r,t) = 0, \quad u_{xx}(x_l,t) = u_{xx}(x_r,t) = 0, \quad 0 \leqslant t \leqslant T, \tag{3}$$

where $\alpha > 0$ and β^{KdV} and γ^{RLW} are any real number. When $-x_l \gg 0$ and $x_r \gg 0$, the initial-boundary value problem (1)–(3) is consistent, so the boundary condition (3) is reasonable.

By observation, the total accuracy of a specific method is affected by not only the order of accuracy of the numerical method but also other factors. That is, the conservative approximation property of the method is another factor that has the same or possibly even more impact on results. Better solutions can be expected from numerical schemes which have effective conservative approximation properties rather than the ones which have nonconservative properties [10,25]. To create the discretization equation, the finite difference method is applied in the present research since conservative approximation analysis by the mathematical tools has been developing until now.

In this study, the performance of the purposed method is investigated by considering well-known benchmark problems, the Rosenau–KdV equation and the Rosenau–RLW equation. Test cases involve simulating the solitary waves at several parameters and the characteristics of these benchmark problems have been reported by previously known numerical investigations. It will also be shown that our solution is equipped with all mentioned characteristics. Moreover, the test problems have a common experiment approach which is used to check or improve a numerical technique (see for example, [10,11,19–24]).

The content of this paper is organized as follows. In the next section, we present invariant and boundedness properties of solutions. Section 3 describes a conservative implicit finite difference scheme for the Rosenau–KdV–RLW Eq. (1) with the initial and boundary conditions (2) and (3). Some preliminary lemmas and discrete norms are given, and the invariant properties are proved. The solvability of the finite difference scheme is discussed, and the existence and uniqueness of the solution are proven. This section presents complete proofs on the convergence and stability of the proposed method with convergence rate $O(\tau^2 + h^2)$. The results on validation of the finite difference scheme are presented in Section 4, where we make a detailed comparison with available data, to confirm and illustrate our theoretical analysis. Finally, we finish our paper by concluding remarks in the last section.

2. Solution properties

In order to make a discrete analogue effective to the fundamental conservation properties (mass and energy) of the governing equation, discrete conservation, which is an supplementary restriction, is necessary for a suitable difference equation. For a conservative governing equation, the analytic results are evaluated in this section. By assumptions, the solitary wave solution and its derivatives have the following asymptotic values, $u \to 0$ as $x \to \pm\infty$, and for $n \geqslant 1$, $\frac{\partial^n u}{\partial x^n} \to 0$ as $x \to \pm\infty$. Therefore, we obtain the solution properties as follows:

Theorem 1. *Suppose $u_0 \in H_0^2[x_l, x_r]$, then the solution of Eqs. (1)–(3) satisfies:*

$$Q(t) = \int_{x_l}^{x_r} u(x,t)dx = \int_{x_l}^{x_r} u_0(x,0)dx = Q(0).$$

Theorem 2. *Suppose $u_0 \in H_0^2[x_l, x_r]$, then the solution of Eqs. (1)–(3) satisfies:*

$$E(t) = \|u\|_{L_2}^2 + \gamma^{\mathrm{RLW}}\|u_x\|_{L_2}^2 + \|u_{xx}\|_{L_2}^2 = E(0).$$

Proof. Consider $u_t - \gamma^{\mathrm{RLW}}u_{xxt} + u_{xxxxt} = -u_x - \beta^{\mathrm{KdV}}u_{xxx} - \alpha(u^2)_x$, we have

$$\begin{aligned}
\frac{dE(t)}{dt} &= 2\int_{x_l}^{x_r} uu_t dx + 2\gamma^{\mathrm{RLW}}\int_{x_l}^{x_r} u_x u_{xt} dx + 2\int_{x_l}^{x_r} u_{xx}u_{xxt} dx \\
&= 2\int_{x_l}^{x_r} uu_t dx - 2\gamma^{\mathrm{RLW}}\int_{x_l}^{x_r} uu_{xxt} dx - 2\int_{x_l}^{x_r} u_x u_{xxxt} dx + 2\left(\gamma^{\mathrm{RLW}}uu_{xt} + u_x u_{xxt}\right)\Big|_{x_l}^{x_r} \\
&= 2\int_{x_l}^{x_r} uu_t dx - 2\gamma^{\mathrm{RLW}}\int_{x_l}^{x_r} uu_{xxt} dx + 2\int_{x_l}^{x_r} uu_{xxxxt} dx - 2uu_{xxxt}\Big|_{x_l}^{x_r} = 2\int_{x_l}^{x_r} u\left(u_t - \gamma^{\mathrm{RLW}}u_{xxt} + u_{xxxxt}\right)dx \\
&= 2\int_{x_l}^{x_r} u\left(-u_x - \beta^{\mathrm{KdV}}u_{xxx} - \alpha 2uu_x\right)dx = -2\int_{x_l}^{x_r}\left(uu_x + \beta^{\mathrm{KdV}}uu_{xxx} + \alpha 2u^2u_x\right)dx = -2\beta^{\mathrm{KdV}}\int_{x_l}^{x_r} uu_{xxx} dx \\
&= 2\beta^{\mathrm{KdV}}\int_{x_l}^{x_r} u_x u_{xx} dx - 2\beta^{\mathrm{KdV}}uu_{xx}\Big|_{x_l}^{x_r} = 0.
\end{aligned}$$

Therefore, $E(t)$ is a constant function, that is

$$E(t) = \|u\|_{L_2}^2 + \gamma^{\mathrm{RLW}}\|u_x\|_{L_2}^2 + \|u_{xx}\|_{L_2}^2 = E(0). \qquad \square$$

Theorem 3. *Suppose that $u_0 \in H_0^2[x_l, x_r]$, then the solution of Eqs. (1)–(3) satisfies $\|u\|_{L_2} \leqslant C$, $\|u_{xx}\|_{L_2} \leqslant C$ which yields $\|u\|_{L_\infty} \leqslant C$.*

Proof. From Theorem 2, we have

$$\|u\|_{L_2} \leqslant C \quad \text{and} \quad \|u_{xx}\|_{L_2} \leqslant C.$$

Using the Hölder inequality and the Cauchy–Schwarz inequality yields

$$\|u_x\|_{L_2}^2 = \int_{x_l}^{x_r} (u_x)^2 dx = -\int_{x_l}^{x_r} uu_{xx} dx \leqslant \|u\|_{L_2}\|u_{xx}\|_{L_2} \leqslant \frac{1}{2}\left(\|u\|_{L_2}^2 + \|u_{xx}\|_{L_2}^2\right).$$

Then,

$$\|u_x\|_{L_2}^2 \leqslant \frac{1}{2}\left(\|u\|_{L_2}^2 + \|u_{xx}\|_{L_2}^2\right) \leqslant C.$$

By the Sobolev's inequality, we get $\|u\|_\infty \leqslant C$. $\square$

3. Numerical technique

In this section, we present a complete description of our finite difference scheme and an algorithm for the formulation of the problem (1)–(3). We first describe our solution domain and its grid. The solution domain is defined to be $\Omega = \{(x,t) | \, x_l \leqslant x \leqslant x_r,\ 0 \leqslant t \leqslant T\}$, which is covered by a uniform grid $\Omega_h = \{(x_i, t_n) | \, x_i = x_l + ih,\ t_n = n\tau,\ i = 0, \ldots, M,\ n = 0, \ldots, N\}$, with spacings $h = (x_r - x_l)/M$ and $\tau = T/N$. Denote $u_i^n \approx u(x_l + ih, n\tau)$ and $Z_h^0 = \{u = (u_i) | \, u_{-1} = u_0 = u_M = u_{M+1} = 0,\ i = -1, 0, 1, \ldots, M, M+1\}$. We use the following notations for the simplicity:

$$\begin{aligned}
&u_i^{n+\frac{1}{2}} = \frac{u_i^{n+1} + u_i^n}{2}, \quad \bar{u}_i^n = \frac{u_i^{n+1} + u_i^{n-1}}{2}, \\
&(u_i^n)_t = \frac{u_i^{n+1} - u_i^n}{\tau}, \quad (u_i^n)_{\hat{t}} = \frac{u_i^{n+1} - u_i^{n-1}}{2\tau}, \\
&(u_i^n)_x = \frac{u_{i+1}^n - u_i^n}{h}, \quad (u_i^n)_{\bar{x}} = \frac{u_i^n - u_{i-1}^n}{h}, \quad (u_i^n)_{\dot{x}} = \frac{u_{i+1}^n - u_{i-1}^n}{2h}, \\
&(u^n, v^n) = h\sum_{i=1}^{M-1} u_i^n v_i^n, \quad \|u^n\|^2 = (u^n, u^n), \quad \|u^n\|_\infty = \max_{1 \leqslant i \leqslant M-1} |u_i^n|.
\end{aligned}$$

In the paper, $C = C(\theta)$ denotes a general positive constant, which may have different values in different occurrences. Since $(u^2)_x = 2\theta u u_x + (1-\theta)(u^2)_{\bar{x}}$, where $\theta \in \mathbb{R}$ is a real constant, we employ second-order central-difference approximations for the operators in Eqs. (1) and (3). The system of difference equations becomes

$$(u_i^n)_{\hat{t}} - \gamma^{\mathrm{RLW}}(u_i^n)_{x\bar{x}\hat{t}} + (u_i^n)_{x\bar{x}\bar{x}\hat{t}} + \beta^{\mathrm{KdV}}(\bar{u}_i^n)_{x\bar{x}\hat{x}} + (u_i^n)_{\hat{x}} + \varphi_\theta(u_i^n, \bar{u}_i^n) = 0, \quad 1 \leqslant i \leqslant M-1, \quad 1 \leqslant n \leqslant N-1, \tag{4}$$

where

$$\varphi_\theta(u_i^n, \bar{u}_i^n) = \alpha\left[2\theta u_i^n (\bar{u}_i^n)_{\hat{x}} + (1-\theta)(u_i^n \bar{u}_i^n)_{\hat{x}}\right],$$

$$u_i^0 = u_0(x_i), \quad 0 \leqslant i \leqslant M, \tag{5}$$

$$u_0^n = u_M^n = 0, \quad (u_0^n)_{\hat{x}} = (u_M^n)_{\hat{x}} = 0, \quad (u_0^n)_{x\bar{x}} = (u_M^n)_{x\bar{x}} = 0, \quad 1 \leqslant n \leqslant N. \tag{6}$$

The three-step method is used for time discretization of the above described scheme. The matrix system of the Eqs. (4) and (6) is banded with penta-diagonal. The nonlinear term of Eq. (1) is handled by using the linear implicit approximation. Therefore, the algebraic system of equations is solved easily by using the presented method since it does not require extra effort to deal with a nonlinear term.

The following lemmas are some properties of the above finite difference scheme which can be obtained directly from the definition. They are essential for existence, uniqueness, convergence, and stability of our numerical solution.

Lemma 4. *For any two mesh functions u, $v \in Z_h^0$, we have*

$$(u_{\hat{x}}, v) = -(u, v_{\hat{x}}), \quad (u_x, v) = -(u, v_{\bar{x}}), \quad (u_{x\bar{x}}, v) = -(u_x, v_x),$$

$$(u, u_{x\bar{x}}) = -(u_x, u_x) = -\|u_x\|^2.$$

Furthermore, if $(u_0)_{x\bar{x}} = (u_M)_{x\bar{x}} = 0$, it implies

$$(u, u_{xx\bar{x}\bar{x}}) = \|u_{x\bar{x}}\|^2.$$

Lemma 5. *For any two mesh functions $u \in Z_h^0$, we have*

$$(u_{\hat{x}}, u) = 0, (u_{x\bar{x}\hat{x}}, u) = 0.$$

Lemma 6 (Discrete Sobolev's inequality [26]). *There exist two constants C_1 and C_2 such that*

$$\|u^n\|_\infty \leqslant C_1\|u^n\| + C_2\|u_x^n\|.$$

Theorem 7. *Suppose $u_0 \in H_0^2[x_l, x_r]$, then there is an estimated solution of the difference scheme (4)–(6) satisfying $\|u^n\| \leqslant C, \|u_{x\bar{x}}^n\| \leqslant C$ which yield $\|u^n\|_\infty \leqslant C$.*

Proof. To prove the theorem, we proceed by the mathematical induction. We assume that

$$\|u^k\| \leqslant C, \quad \|u_{x\bar{x}}^k\| \leqslant C, \quad \|u^k\|_\infty \leqslant C, \quad k = 0, 1, 2, 3, \ldots, n. \tag{7}$$

After computing the inner product of Eq. (4) and $2\bar{u}^n$(i.e.$u^{n+1} + u^{n-1}$), according to Lemma 4, we have

$$\frac{1}{2\tau}\left(\|u^{n+1}\|^2 - \|u^{n-1}\|^2\right) + \frac{1}{2\tau}\gamma^{\mathrm{RLW}}\left(\|u_x^{n+1}\|^2 - \|u_x^{n-1}\|^2\right) + \frac{1}{2\tau}\left(\|u_{x\bar{x}}^{n+1}\|^2 - \|u_{x\bar{x}}^{n-1}\|^2\right) + \beta^{\mathrm{KdV}}(\bar{u}_{x\bar{x}\hat{x}}^n, 2\bar{u}^n)$$
$$+ (u_{\hat{x}}^n, 2\bar{u}^n) + (\varphi_\theta(u^n, \bar{u}^n), 2\bar{u}^n) = 0, \tag{8}$$

where

$$\varphi_\theta(u_i^n, \bar{u}_i^n) = \alpha\left[2\theta u_i^n (\bar{u}_i^n)_{\hat{x}} + (1-\theta)(u_i^n \bar{u}_i^n)_{\hat{x}}\right].$$

By the Cauchy–Schwarz inequality, boundary conditions, and Lemma 4, we obtain

$$(\bar{u}_{x\bar{x}\hat{x}}^n, 2\bar{u}^n) = 0, \tag{9}$$

$$\|u_{\hat{x}}^n\|^2 \leqslant \|u_x^n\|^2 \leqslant \frac{1}{2}\|u^n\|^2 + \frac{1}{2}\|u_{x\bar{x}}^n\|^2, \tag{10}$$

$$(u_{\hat{x}}^n, 2\bar{u}^n) \leqslant \|u_x^n\|^2 + \frac{1}{2}\|u^{n-1}\|^2 + \frac{1}{2}\|u^{n+1}\|^2. \tag{11}$$

From boundary conditions (6), then

$$2h\sum_{i=1}^{M-1}\left[u_i^n\left(\bar{u}_i^n\right)_{\hat{x}}+\left(u_i^n\bar{u}_i^n\right)_{\hat{x}}\right]\bar{u}_i^n=\sum_{i=1}^{M-1}\left[u_i^n\left(\bar{u}_{i+1}^n-\bar{u}_{i-1}^n\right)+u_{i+1}^n\bar{u}_{i+1}^n-u_{i-1}^n\bar{u}_{i-1}^n\right]\bar{u}_i^n$$
$$=\sum_{i=1}^{M-1}\left(u_i^n\bar{u}_{i+1}^n\bar{u}_i^n-u_{i-1}^n\bar{u}_i^n\bar{u}_{i-1}^n\right)-\sum_{i=1}^{M-1}\left(u_i^n\bar{u}_i^n\bar{u}_{i-1}^n-u_{i+1}^n\bar{u}_{i+1}^n\bar{u}_i^n\right)=0, \tag{12}$$

by the Schwarz inequality and Eq. (7), we obtain

$$\left(\varphi_\theta(u^n,\bar{u}^n),2\bar{u}^n\right)=2\alpha h\sum_{i=1}^{M-1}\left[2\theta u_i^n\left(\bar{u}_i^n\right)_{\hat{x}}+(1-\theta)\left(u_i^n\bar{u}_i^n\right)_{\hat{x}}\right]\bar{u}_i^n$$
$$=2\alpha(1-\theta)h\sum_{i=1}^{M-1}\left[u_i^n\left(\bar{u}_i^n\right)_{\hat{x}}+\left(u_i^n\bar{u}_i^n\right)_{\hat{x}}\right]\bar{u}_i^n+2\alpha h\sum_{i=1}^{M-1}(3\theta-1)u_i^n\left(\bar{u}_i^n\right)_{\hat{x}}\bar{u}_i^n=2\alpha h\sum_{i=1}^{M-1}(3\theta-1)u_i^n\left(\bar{u}_i^n\right)_{\hat{x}}\bar{u}_i^n$$
$$\leqslant Ch\sum_{i=1}^{M-1}\left|\left(\bar{u}_i^n\right)_{\hat{x}}\right|\left|\bar{u}_i^n\right|\leqslant C\left(\left\|\bar{u}^n\right\|^2+\left\|\bar{u}_x^n\right\|^2\right)\leqslant C\left(\left\|u^{n+1}\right\|^2+\left\|u^{n-1}\right\|^2+\left\|u_x^{n+1}\right\|^2+\left\|u_x^{n-1}\right\|^2\right)$$
$$\leqslant C\left(\left\|u^{n+1}\right\|^2+\left\|u^{n-1}\right\|^2+\left\|u_{x\bar{x}}^{n+1}\right\|^2+\left\|u_{x\bar{x}}^{n-1}\right\|^2\right). \tag{13}$$

Substituting Eqs. (9)–(13) into Eq. (8), we obtain

$$\left(\left\|u^{n+1}\right\|^2-\left\|u^{n-1}\right\|^2\right)+\gamma^{\mathrm{RLW}}\left(\left\|u_x^{n+1}\right\|^2-\left\|u_x^{n-1}\right\|^2\right)+\left(\left\|u_{x\bar{x}}^{n+1}\right\|^2-\left\|u_{x\bar{x}}^{n-1}\right\|^2\right)$$
$$\leqslant C\tau\left(\left\|u^{n-1}\right\|^2+\left\|u^n\right\|^2+\left\|u^{n+1}\right\|^2+\left\|u_{x\bar{x}}^{n-1}\right\|^2+\left\|u_{x\bar{x}}^n\right\|^2+\left\|u_{x\bar{x}}^{n+1}\right\|^2\right). \tag{14}$$

Let

$$B^n=\left(\left\|u^n\right\|^2+\left\|u^{n-1}\right\|^2\right)+\gamma^{\mathrm{RLW}}\left(\left\|u_x^n\right\|^2+\left\|u_x^{n-1}\right\|^2\right)+\left(\left\|u_{x\bar{x}}^n\right\|^2+\left\|u_{x\bar{x}}^{n-1}\right\|^2\right),$$

then Eq. (14) can be rewritten as follows:

$$B^{n+1}-B^n\leqslant C\tau\left(B^{n+1}+B^n\right).$$

If τ is sufficiently small which satisfies $\tau\leqslant\frac{k-2}{kC}$ and $k>2$, then

$$B^{n+1}\leqslant\frac{(1+\tau C)}{(1-\tau C)}B^n\leqslant(1+\tau kC)B^n\leqslant(1+\tau kC)^nB^1\leqslant\exp(kCT)B^1.$$

Hence $\left\|u^{n+1}\right\|\leqslant C$, $\left\|u_x^{n+1}\right\|\leqslant C$, and $\left\|u_{x\bar{x}}^{n+1}\right\|\leqslant C$, then yield $\left\|u^{n+1}\right\|_\infty\leqslant C$ by Lemma 6. □

3.1. Discrete conservation

Now, the conservative approximations are developed for discrete conservation of mass which is guaranteed for all a parameter $\theta\in\mathbb{R}$. However, for discrete energy, we can guarantee $\theta=\frac{1}{3}$ only.

Theorem 8. *Suppose $u_0\in H_0^2[x_l,x_r]$, then the finite difference scheme (4)–(6) is conservative for discrete mass in sense:*

$$Q^n=\frac{h}{2}\sum_{i=1}^{M-1}\left(u_i^{n+1}+u_i^n\right)+\alpha\theta\tau h\sum_{i=1}^{M-1}u_i^n\left(u_i^{n+1}\right)_{\hat{x}}=Q^{n-1}=\ldots=Q^0. \tag{15}$$

Proof. By multiplying Eq. (4) by τh , summing up for i from 1to $M-1$, and considering the boundary conditions (6) together with Lemma 4, we obtain

$$\frac{h}{2}\sum_{i=1}^{M-1}\left(u_i^{n+1}-u_i^{n-1}\right)+\alpha\theta\tau h\sum_{i=1}^{M-1}\left[u_i^n\left(u_i^{n+1}\right)_{\hat{x}}-u_i^{n-1}\left(u_i^n\right)_{\hat{x}}\right]=0.$$

Then, this gives Eq. (15). □

Theorem 9. *Suppose $u_0\in H_0^2[x_l,x_r]$ and $\theta=\frac{1}{3}$, then the finite difference scheme (4)–(6) is conservative for discrete energy in sense:*

$$E^n=\left(\frac{1}{2}\left\|u^{n+1}\right\|^2+\left\|u^n\right\|^2\right)+\frac{\gamma^{\mathrm{RLW}}}{2}\left(\left\|u_x^{n+1}\right\|^2+\left\|u_x^n\right\|^2\right)+\frac{1}{2}\left(\left\|u_{x\bar{x}}^{n+1}\right\|^2+\left\|u_{x\bar{x}}^n\right\|^2\right)+h\tau\sum_{i=1}^{M-1}u_i^{n+1}\left(u_i^n\right)_{\hat{x}}=E^{n-1}=\ldots=E^0. \tag{16}$$

Proof. After computing the inner product of Eq. (4) and $2\bar{u}^n$ (i.e. $u^{n+1}+u^{n-1}$), according to Lemmas 4 and 5, we have

$$\frac{1}{2\tau}\left(\|u^{n+1}\|^2-\|u^{n-1}\|^2\right)+\frac{1}{2\tau}\gamma^{\mathrm{RLW}}\left(\|u_x^{n+1}\|^2-\|u_x^{n-1}\|^2\right)+\frac{1}{2\tau}\left(\|u_{x\bar{x}}^{n+1}\|^2-\|u_{x\bar{x}}^{n-1}\|^2\right)+(u_{\hat{x}}^n,2\bar{u}^n)+\left(\varphi_{\frac{1}{3}}(u^n,\bar{u}^n),2\bar{u}^n\right)=0. \tag{17}$$

From Eq. (12), we obtain

$$\left(\varphi_{\frac{1}{3}}(u^n,\bar{u}^n),2\bar{u}^n\right)=\frac{4}{3}h\sum_{i=1}^{M-1}\left[u_i^n(\bar{u}_i^n)_{\hat{x}}+(u_i^n\bar{u}_i^n)_{\hat{x}}\right]\bar{u}_i^n=0.$$

By Lemma 4, it gives

$$(u_{\hat{x}}^n,2\bar{u}^n)=2h\sum_{i=1}^{M-1}(u_i^n)_{\hat{x}}\bar{u}_i^n=h\sum_{i=1}^{M-1}(u_i^n)_{\hat{x}}u_i^{n+1}-h\sum_{i=1}^{M-1}(u_i^n)_{\hat{x}}u_i^{n-1}.$$

Then, Eq. (17) can be rewritten as

$$\frac{1}{2\tau}\left(\|u^{n+1}\|^2-\|u^{n-1}\|^2\right)+\frac{1}{2\tau}\gamma^{\mathrm{RLW}}\left(\|u_x^{n+1}\|^2-\|u_x^{n-1}\|^2\right)+\frac{1}{2\tau}\left(\|u_{x\bar{x}}^{n+1}\|^2-\|u_{x\bar{x}}^{n-1}\|^2\right)+h\sum_{i=1}^{M-1}(u_i^n)_{\hat{x}}u_i^{n+1}-h\sum_{i=1}^{M-1}(u_i^n)_{\hat{x}}u_i^{n-1}=0.$$

Finally, this gives Eq. (16), which completes the proof of theorem. □

A conservative approximation confirms that the energy would not increase in time, which allows to make the scheme stable for the case $\theta=\frac{1}{3}$ only.

Remark 10. In the case $\theta=\frac{1}{3}$, the approximation of the nonlinear term of the scheme (4) is the same as that of the scheme [10] for the Rosenau–KdV equation, where $\gamma^{RLW}=0$, and that of the schemes [19–22] for the Rosenau–RLW equation, where $\beta^{KdV}=0$. Moreover, the same approximation of the nonlinear term as the scheme (4) is widely used for the RLW equation [9,27], the RLW-Burgers equation [28], the Rosenau equation [29,30], and the Rosenau–Burgers equation [31–33].

3.2. Existence and uniqueness

In this part, we prove the solvability of solutions for the scheme (4)–(6). This guarantees the existence and uniqueness of our numerical solution.

Theorem 11. *The finite difference scheme (4)–(6) is uniquely solvable.*

Proof. To prove the Theorem, we proceed by the mathematical induction. We assume that $u^0,u^1,\ldots,u^n$ satisfy the difference scheme (4)–(6) for $1\leqslant n\leqslant N-1$. Indeed, u^1 can be computed by an available second-order method (such as the Crank–Nicolson method). Next, we prove that there exists u^{n+1} satisfied Eq. (4). We first consider

$$\frac{1}{2\tau}u_i^{n+1}-\frac{1}{2\tau}\gamma^{\mathrm{RLW}}(u_i^{n+1})_{x\bar{x}}+\frac{1}{2\tau}(u_i^{n+1})_{x\bar{x}x\bar{x}}+\frac{1}{2}\beta^{\mathrm{KdV}}(u_i^{n+1})_{x\bar{x}\hat{x}}+\frac{1}{2}\varphi_\theta(u_i^n,u_i^{n+1})=0, \tag{18}$$

where

$$\varphi_\theta(u_i^n,u_i^{n+1})=\alpha\left[2\theta u_i^n(u_i^{n+1})_{\hat{x}}+(1-\theta)(u_i^nu_i^{n+1})_{\hat{x}}\right].$$

By taking the inner product of Eq. (18) with u^{n+1}, we obtain

$$\frac{1}{2\tau}\|u^{n+1}\|^2+\frac{1}{2\tau}\gamma^{\mathrm{RLW}}\|u_x^{n+1}\|^2+\frac{1}{2\tau}\|u_{x\bar{x}}^{n+1}\|^2+\frac{1}{2}(\varphi_\theta(u^n,u^{n+1}),u^{n+1})=0.$$

Since

$$\begin{aligned}\sum_{i=1}^{M-1}\left[u_i^n(u_i^{n+1})_{\hat{x}}+(u_i^nu_i^{n+1})_{\hat{x}}\right]&=\sum_{i=1}^{M-1}\left[u_i^n(u_{i+1}^{n+1}-u_{i-1}^{n+1})+u_{i+1}^nu_{i+1}^{n+1}-u_{i-1}^nu_{i-1}^{n+1}\right]u_i^{n+1}\\&=\sum_{i=1}^{M-1}\left[u_i^nu_{i+1}^{n+1}u_i^{n+1}-u_{i-1}^nu_{i-1}^{n+1}u_i^{n+1}\right]-\sum_{i=1}^{M-1}\left[u_i^nu_{i-1}^{n+1}u_i^{n+1}-u_{i+1}^nu_{i+1}^{n+1}u_i^{n+1}\right]=0.\end{aligned} \tag{19}$$

By the Cauchy–Schwarz inequality, Theorem 7, Eqs. (19) and (10), we obtain

$$\begin{aligned}(\varphi_\theta(u^n,u^{n+1}),u^{n+1}) &= \alpha h\sum_{i=1}^{M-1}\left[2\theta u_i^n\left(u_i^{n+1}\right)_{\hat{x}}+(1-\theta)\left(u_i^n u_i^{n+1}\right)_{\hat{x}}\right]u_i^{n+1}\\ &= \alpha(1-\theta)h\sum_{i=1}^{M-1}\left[u_i^n\left(u_i^{n+1}\right)_{\hat{x}}+\left(u_i^n u_i^{n+1}\right)_{\hat{x}}\right]\bar{u}_i^n+2\alpha h\sum_{i=1}^{M-1}(3\theta-1)u_i^n\left(u_i^{n+1}\right)_{\hat{x}}u_i^{n+1}\\ &= \alpha h\sum_{i=1}^{M-1}(3\theta-1)u_i^n\left(u_i^{n+1}\right)_{\hat{x}}u_i^{n+1}\leqslant Ch\sum_{i=1}^{M-1}\left|\left(u_i^{n+1}\right)_{\hat{x}}\right|\left|u_i^{n+1}\right|\leqslant C\left(\left\|u^{n+1}\right\|^2+\left\|u_x^{n+1}\right\|^2\right)\\ &\leqslant C\left(\left\|u^{n+1}\right\|^2+\left\|u_{x\bar{x}}^{n+1}\right\|^2\right).\end{aligned}$$

Therefore,

$$\left\|u^{n+1}\right\|^2+\gamma^{\mathrm{RLW}}\left\|u_x^{n+1}\right\|^2+\left\|u_{x\bar{x}}^{n+1}\right\|^2\leqslant 2\tau C\left(\left\|u^{n+1}\right\|^2+\left\|u_{x\bar{x}}^{n+1}\right\|^2\right).$$

If τ is sufficiently small, which satisfies $1-2C\tau>0$, then

$$\left\|u^{n+1}\right\|=0\quad\text{and}\quad\left\|u_{x\bar{x}}^{n+1}\right\|=0.$$

This implies that there uniquely exists the trivial solution satisfying Eq. (4). Hence, u^{n+1} is uniquely solvable, and this completes the proof of the theorem. □

3.3. Convergence and stability

Now, we prove the convergence and stability of the scheme (4)–(6). Let $e_i^n=v_i^n-u_i^n$, where v_i^n and u_i^n are the solutions of Eqs. (1)–(6), respectively. We then obtain the following error equations

$$\begin{aligned}r_i^n &= \left(e_i^n\right)_{\hat{t}}-\gamma^{\mathrm{RLW}}\left(e_i^n\right)_{x\bar{x}\hat{t}}+\left(e_i^n\right)_{xx\bar{x}\hat{t}}+\beta^{\mathrm{KdV}}\left(\bar{e}_i^n\right)_{x\bar{x}\hat{x}}+\left(e_i^n\right)_{\hat{x}}+\alpha\left[2\theta v_i^n\left(\bar{v}_i^n\right)_{\hat{x}}+(1-\theta)\left(v_i^n\bar{v}_i^n\right)_{\hat{x}}\right]\\ &\quad-\alpha\left[2\theta u_i^n\left(\bar{u}_i^n\right)_{\hat{x}}+(1-\theta)\left(u_i^n\bar{u}_i^n\right)_{\hat{x}}\right],\end{aligned}\tag{20}$$

where r_i^n denotes the truncation error. By using Taylor expansion, we easily obtain that $r_i^n=O(\tau^2+h^2)$ holds as $\tau,\ h\to 0$.

The following lemmas and theorem play important roles for the proof of convergence and stability.

Lemma 12 (Discrete Gronwall's inequality [26]). *Suppose that $\omega(k)$ and $\rho(k)$ are nonnegative functions and $\rho(k)$ is a nondecreasing function. If $C>0$ and*

$$\omega(k)\leqslant\rho(k)+C\tau\sum_{l=0}^{k-1}\omega(l),\quad\forall k,$$

then

$$\omega(k)\leqslant\rho(k)e^{C\tau k},\quad\forall k.$$

The following theorem grantees the convergence of the scheme (4)–(6) with the convergence rate $O(\tau^2+h^2)$.

Theorem 13. *Suppose $u_0\in H_0^2[x_l,x_r]$, then the solution u^n of the scheme (4)–(6) converges to the solution of the problem (1)–(3) in the sense of $\|\cdot\|_\infty$, and the rate of convergence is $O(\tau^2+h^2)$.*

Proof. By taking the inner product of Eq. (20) and $2\bar{e}^n$ (i.e. $e^{n+1}+e^{n-1}$), and using Lemma 4, we obtain

$$\begin{aligned}&\frac{1}{2\tau}\left(\left\|e^{n+1}\right\|^2-\left\|e^{n-1}\right\|^2\right)-\frac{1}{2\tau}\gamma^{\mathrm{RLW}}\left(\left\|e_x^{n+1}\right\|^2-\left\|e_x^{n-1}\right\|^2\right)+\left(\left\|e_{x\bar{x}}^{n+1}\right\|^2-\left\|e_{x\bar{x}}^{n-1}\right\|^2\right)\\ &\quad=\left(r^n,2\bar{e}^n\right)-\left(e_{\hat{x}}^n,2\bar{e}^n\right)-\left(M_1+M_2,2\bar{e}^n\right),\end{aligned}\tag{21}$$

where

$$\begin{aligned}M_1&=2\alpha\theta\left[v_i^n\left(\bar{v}_i^n\right)_{\hat{x}}-u_i^n\left(\bar{u}_i^n\right)_{\hat{x}}\right],\\ M_2&=\alpha(1-\theta)\left[\left(v_i^n\bar{v}_i^n\right)_{\hat{x}}-\left(u_i^n\bar{u}_i^n\right)_{\hat{x}}\right].\end{aligned}$$

According to Lemma 4, Theorems 7 and 3, and the Cauchy–Schwarz inequality, we have

$$(M_1, 2e^n) = 2\alpha\theta h\sum_{i=1}^{M-1}[v_i^n(\bar{v}_i^n)_{\hat{x}} - u_i^n(\bar{u}_i^n)_{\hat{x}}]\bar{e}_i^n = 2\alpha\theta h\sum_{i=1}^{M-1}v_i^n(\bar{e}_i^n)_{\hat{x}}\bar{e}_i^n + 2\alpha\theta h\sum_{i=1}^{M-1}e_i^n(\bar{u}_i^n)_{\hat{x}}\bar{e}_i^n \leqslant C\left(\|\bar{e}_{\hat{x}}^n\|^2 + \|\bar{e}^n\|^2 + \|e^n\|^2\right)$$
$$\leqslant C\left(\|e_{\hat{x}}^{n+1}\|^2 + \|e_{\hat{x}}^{n-1}\|^2 + \|e^{n+1}\|^2 + \|e^n\|^2 + \|e^{n-1}\|^2\right). \tag{22}$$

Similar to the proof of Eq. (22), we also have

$$(M_2, 2e^n) \leqslant C\left(\|\bar{e}_{\hat{x}}^n\|^2 + \|\bar{e}^n\|^2 + \|e^n\|^2\right) \leqslant C\left(\|e_{\hat{x}}^{n+1}\|^2 + \|e_{\hat{x}}^{n-1}\|^2 + \|e^{n+1}\|^2 + \|e^n\|^2 + \|e^{n-1}\|^2\right). \tag{23}$$

Furthermore,

$$\|e_{\hat{x}}^n\|^2 \leqslant \|e_x^n\|^2 \leqslant \frac{1}{2}\left(\|e^n\|^2 + \|e_{x\bar{x}}^n\|^2\right), \tag{24}$$
$$(e_{\hat{x}}^n, 2\bar{e}^n) \leqslant \|e_x^n\|^2 + \frac{1}{2}\left(\|e^{n+1}\|^2 + \|e^{n-1}\|^2\right), \tag{25}$$
$$(r^n, 2e^n) \leqslant \|r^n\|^2 + \frac{1}{2}\left(\|e^{n+1}\|^2 + \|e^{n-1}\|^2\right). \tag{26}$$

Substituting Eqs. (22)–(24), (26) into Eq. (19), we obtain

$$\left(\|e^{n+1}\|^2 - \|e^{n-1}\|^2\right) + \gamma^{\mathrm{RLW}}\left(\|e_x^{n+1}\|^2 - \|e_x^{n-1}\|^2\right) + \left(\|e_{x\bar{x}}^{n+1}\|^2 - \|e_{x\bar{x}}^{n-1}\|^2\right)$$
$$\leqslant C\tau\left(\|e_x^{n+1}\|^2 + \|e_x^{n-1}\|^2 + \|e^n\|^2 + \|e^{n+1}\|^2 + \|e^{n-1}\|^2 + \|e^n\|^2\right) + 2\tau\|r^n\|^2. \tag{27}$$

Let

$$B^n = \left(\|e^n\|^2 + \|e^{n-1}\|^2\right) + \gamma^{\mathrm{RLW}}\left(\|e_x^n\|^2 + \|e_x^{n-1}\|^2\right) + \left(\|e_{x\bar{x}}^n\|^2 + \|e_{x\bar{x}}^{n-1}\|^2\right).$$

Then Eq. (27) can be rewritten as

$$B^{n+1} - B^n \leqslant 2\tau\|r^n\|^2 + \tau C(B^{n+1} + B^n).$$

Hence,

$$(1 - C\tau)(B^{n+1} - B^n) \leqslant 2\tau\|r^n\|^2 + 2C\tau B^n.$$

If τ is sufficiently small, which satisfies $1 - C\tau > 0$, then

$$B^{n+1} - B^n \leqslant C\tau\|r^n\|^2 + \tau C B^n. \tag{28}$$

By summing Eq. (28) from 1 to n, we have

$$B^{n+1} \leqslant B^1 + C\tau\sum_{k=1}^{n}\|r^k\|^2 + C\tau\sum_{k=1}^{n}B^k. \tag{29}$$

Notice that

$$\tau\sum_{k=1}^{n}\|r^k\|^2 \leqslant n\tau\max_{1\leqslant k\leqslant n}\|r^k\|^2 \leqslant T\cdot O\left(\tau^2 + h^2\right)^2$$

and $e^0 = 0$. We then have $B^1 = O\left(\tau^2 + h^2\right)^2$. Hence,

$$B^{n+1} \leqslant O(\tau^2 + h^2)^2 + C\tau\sum_{k=1}^{n}B^k.$$

According to Lemma 12, we get $B^n \leqslant O(\tau^2 + h^2)^2$. That is

$$\|e^{n+1}\|^2 \leqslant O\left(\tau^2 + h^2\right)^2 \quad \text{and} \quad \|e_{x\bar{x}}^{n+1}\|^2 \leqslant O\left(\tau^2 + h^2\right)^2.$$

It follows from Eq. (24) that

$$\|e_x^{n+1}\| \leqslant O(\tau^2 + h^2).$$

By using Lemma 6, we have

$$\|e^{n+1}\|_\infty \leqslant O(\tau^2 + h^2).$$

Therefore, the solution u^n of the scheme (4)–(6) converges to the solution of the problem (1)–(3) in the sense of $\|\cdot\|_\infty$ with the rate $O(\tau^2 + h^2)$. □

Theorem 14. *Under the conditions of Theorem 13, the solution u^n of the scheme (4)–(6) is stable in the sense of $\|\cdot\|_\infty$.*

4. Numerical experiments

In this section, some numerical experiments to verify the correction of our theoretical analysis were computed. As a test problem for the scheme proposed here, we chose three test problems for which exact solution or numerical solutions have been reported previously. For the Rosenau–KdV and Rosenau–RLW equations, the parameters used by other researchers [10,22] to obtain their results were taken as guiding principle for our computations.

In order to apply the three-level linear scheme, u^1 needs to be accurately approximated. To approximate u^1, therefore we have to develop another two-level finite difference scheme which satisfies desired invariant properties

$$(u_i^0)_t - \gamma^{\mathrm{RLW}}(u_i^0)_{x\bar{x}t} + (u_i^0)_{xx\bar{x}\bar{x}t} + \beta^{\mathrm{KdV}}(u_i^{1/2})_{x\bar{x}\hat{x}} + (u_i^0)_{\hat{x}} + \varphi_\theta\left(u_i^0, u_i^{1/2}\right) = 0,$$

where

$$\varphi_\theta\left(u_i^0, u_i^{1/2}\right) = \alpha\left[2\theta u_i^0\left(u_i^{1/2}\right)_{\hat{x}} + (1-\theta)\left(u_i^0 u_i^{1/2}\right)_{\hat{x}}\right],$$

$$u_i^0 = u_0(x_i), \quad 0 \leqslant i \leqslant M.$$

By using $\|\cdot\|$ and $\|\cdot\|_\infty$ norm, the accuracy of the new method is measured by the comparison of numerical solutions with the exact solutions as well as other numerical solutions from methods in the literatures.

4.1. The Rosenau–KdV equation

Consider the Rosenau–KdV equation with the initial condition

$$u_0(x) = \left(-\frac{35}{24} + \frac{35}{312}\sqrt{313}\right)\mathrm{sech}^4\left[\left(\frac{1}{24}\sqrt{-26+2\sqrt{313}}\right)x\right],$$

and the boundary conditions

$$u(x_l,t) = u(x_r,t) = 0, \quad u_x(x_l,t) = u_x(x_r,t) = 0, \quad u_{xx}(x_l,t) = u_{xx}(x_r,t) = 0, \quad 0 \leqslant t \leqslant T.$$

It is know that, the solitary wave solution [10,15] is

$$u(x,t) = \left(-\frac{35}{24} + \frac{35}{312}\sqrt{313}\right)\mathrm{sech}^4\left[\frac{1}{24}\sqrt{-26+2\sqrt{313}}\left(x - \left(\frac{1}{2} + \frac{1}{26}\sqrt{313}\right)t\right)\right].$$

The results in term of errors at the time $T = 20$ by using $\gamma^{RLW} = 0$, $\beta^{KdV} = 1$, $\alpha = \frac{1}{2}$, $x_l = -70$, and $x_r = 100$ are reported in Tables 1–4. According to the results in Tables 1 and 3, even though the present method uses approximately two time larger step size than the method [10] does, the present method obtains the same significant digits. It can be seen that the computational efficiency of the present method is slightly better than that of the method [10], in term of grid point number. As shown in Tables 2 and 4, the second-order convergence of the numerical solutions is verified.

We continue with the examination of the soliton profile in Fig. 1. The patterns are in excellent agreement with the exact solutions.

4.2. The Rosenau–RLW equation

Consider the Rosenau–RLW equation with the initial condition

$$u(x,0) = \frac{15}{19}\mathrm{sech}^4\left[\frac{\sqrt{13}}{26}x\right],$$

and the boundary conditions

$$u(x_l,t) = u(x_r,t) = 0, \quad u_{xx}(x_l,t) = u_{xx}(x_r,t) = 0, \quad 0 \leqslant t \leqslant T.$$

Table 1
Comparison of errors using L_2-norm at $T = 20$.

Scheme	$\tau = h = 0.2$	$\tau = h = 0.1$	$\tau = h = 0.05$	$\tau = h = 0.025$
Scheme [10]	–	3.045414E−03	7.631169E−04	1.905450E−04
Scheme (4) $\theta = -1/3$	2.63759E−03	6.57830E−04	1.64418E−04	4.11082E−05
Scheme (4) $\theta = 1/3$	1.77798E−03	4.43965E−04	1.10984E−04	2.77477E−05

Table 2
Rate of convergence using L_2-norm at $T = 20$.

Scheme	$\tau = h = 0.2$	$\tau = h = 0.1$	$\tau = h = 0.05$	$\tau = h = 0.025$
Scheme [10]	–	–	1.996662	2.001772
Scheme (4) $\theta = -1/3$	–	2.003433	2.000347	1.999870
Scheme (4) $\theta = 1/3$	–	2.001721	2.000094	1.999912

Table 3
Comparison of errors using L_∞-norm at $T = 20$.

Scheme	$\tau = h = 0.2$	$\tau = h = 0.1$	$\tau = h = 0.05$	$\tau = h = 0.025$
Scheme [10]	–	1.131442E−03	2.835874E−04	7.097948E−05
Scheme (4) $\theta = -1/3$	1.01916E−03	2.54116E−04	6.35011E−05	1.58769E−05
Scheme (4) $\theta = 1/3$	4.95101E−04	1.23727E−04	3.09342E−05	7.73365E−06

Table 4
Rate of convergence using L_∞-norm at $T = 20$.

Scheme	$\tau = h = 0.2$	$\tau = h = 0.1$	$\tau = h = 0.05$	$\tau = h = 0.025$
Scheme [10]	–	–	1.996297	1.998319
Scheme (4) $\theta = -1/3$	–	2.003821	2.000634	1.999852
Scheme (4) $\theta = 1/3$	–	2.000563	1.999886	1.999981

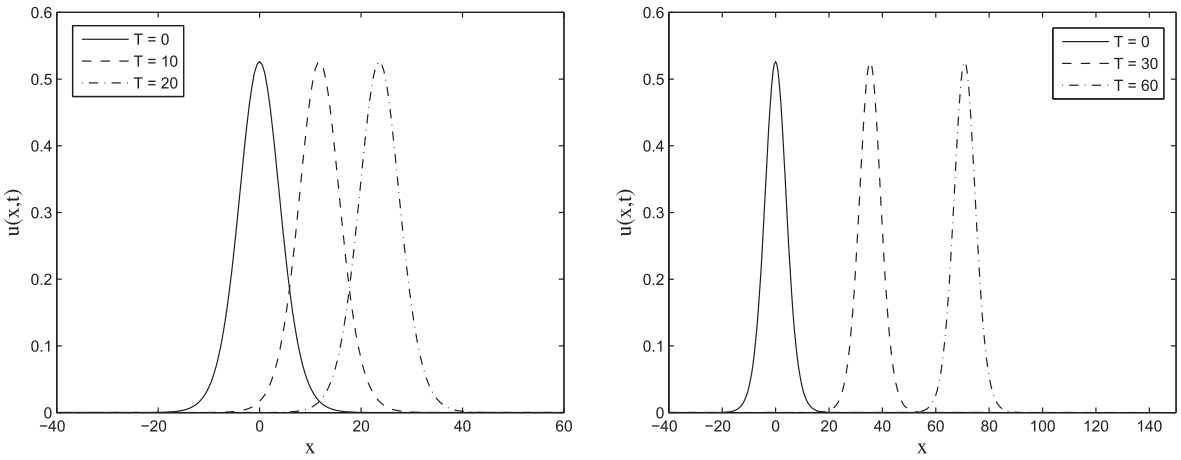

Fig. 1. Numerical solutions of the Rosenau–KdV equation with $\tau = h = 0.25,\ x_l = -40,\ x_r = 60$ (left) and $x_l = -40,\ x_r = 150$ (right).

Table 5
Comparison of errors using L_2-norm at $T = 20$.

Scheme	$\tau = h = 0.4$	$\tau = h = 0.2$	$\tau = h = 0.1$	$\tau = h = 0.05$
Scheme I [22]	2.85546E−02	7.27247E−03	1.82699E−03	4.57348E−04
Scheme II [22]	2.43622E−02	6.17910E−03	1.55040E−03	3.87952E−04
Scheme (4) $\theta = -1/3$	4.25934E−03	1.05710E−03	2.64073E−04	6.60383E−05
Scheme (4) $\theta = 1/3$	1.50201E−02	3.80043E−03	9.54178E−04	2.38950E−04

The exact solitary wave solution [22] has the following form:

$$u(x,t) = \frac{15}{19}\operatorname{sech}^4\left[\frac{\sqrt{13}}{26}\left(x - \frac{169}{133}t\right)\right].$$

Table 6
Rate of convergence using L_2-norm at $T = 20$.

Scheme	$\tau = h = 0.4$	$\tau = h = 0.2$	$\tau = h = 0.1$	$\tau = h = 0.05$
Scheme I [22]	–	1.973206	1.992977	1.998104
Scheme II [22]	–	1.979176	1.994756	1.998690
Scheme (4) $\theta = -1/3$	–	2.010518	2.001103	1.999562
Scheme (4) $\theta = 1/3$	–	1.982660	1.993832	1.997550

Table 7
Comparison of errors using L_∞- norm at $T = 20$.

Scheme	$\tau = h = 0.4$	$\tau = h = 0.2$	$\tau = h = 0.1$	$\tau = h = 0.05$
Scheme I [22]	1.09079E−02	2.78947E−03	7.01120E−04	1.75565E−04
Scheme II [22]	9.45747E−03	2.40611E−03	6.04189E−04	1.51212E−04
Scheme (4) $\theta = -1/3$	1.60697E−03	3.98895E−04	9.96138E−05	2.49119E−05
Scheme (4) $\theta = 1/3$	5.04081E−03	1.27673E−03	3.20501E−04	8.02614E−05

Table 8
Rate of convergence using L_∞-norm at $T = 20$.

Scheme	$\tau = h = 0.4$	$\tau = h = 0.2$	$\tau = h = 0.1$	$\tau = h = 0.05$
Scheme I [22]	–	1.967310	1.992258	1.997656
Scheme II [22]	–	1.974752	1.993631	1.998427
Scheme (4) $\theta = -1/3$	–	2.010262	2.001592	1.999511
Scheme (4) $\theta = 1/3$	–	1.981202	1.994053	1.997551

The numerical results in term of errors obtained by scheme (4) are reported in Tables 5–8 by using $\gamma^{RLW} = 1,\ \beta^{KdV} = 0,\ \alpha = \frac{1}{2},\ x_l = -40$, and $x_r = 60$. The results of numerical experiments compare quantitatively very well with the case presented in [22]. It is clear from Tables 5 and 7 that results by our method show improvement over the previous one reported by [22], especially for the case $\theta = -\frac{1}{3}$. From Tables 6 and 8, we get the second-order accurate scheme which is as accurate as [22].

The solitary waves by the scheme (4) are plotted in Fig. 2 with $\tau = h = 0.25$. The solitons at $t = 10,\ 20,\ 30$, and 60 agree with the soliton at $t = 0$ quite well, which also shows the accuracy of the scheme.

4.3. The Rosenau–KdV–RLW equation

Now, we present a brief description of solving the Rosenau–KdV–RLW Eq. (1) by using the sine–cosine method. In order to obtain the solitary wave solution of the Rosenau–KdV–RLW equation, after making transformation $u(x,t) = u(\xi),\ \xi = x - ct$ where c is constant to be determined later, Eq. (1) becomes

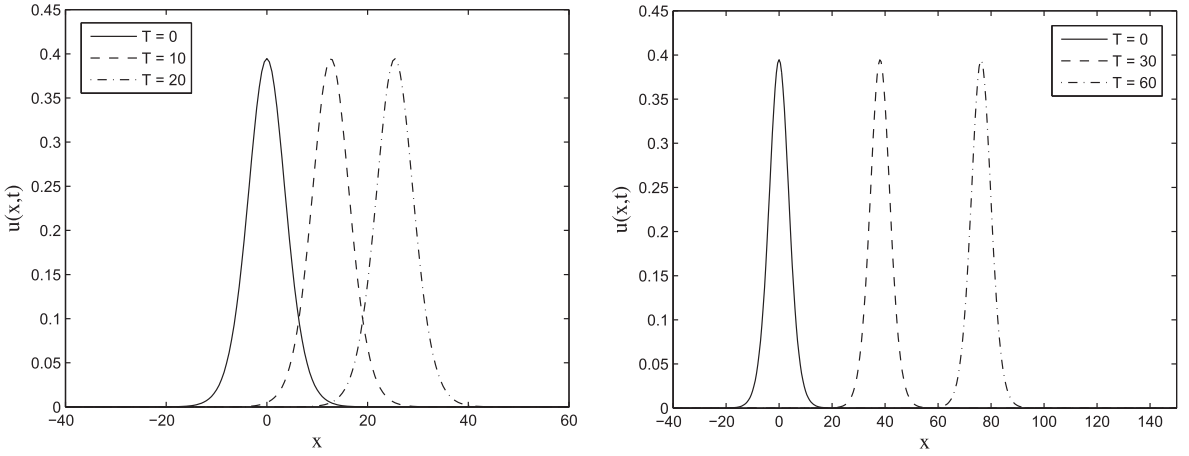

Fig. 2. Numerical solutions of the Rosenau–RLW equation with $\tau = h = 0.25,\ x_l = -40,\ x_r = 60$ (left) and $x_l = -40,\ x_r = 150$ (right).

$$(1-c)u+\alpha u^2+\left(\beta^{\mathrm{KdV}}+c\gamma^{\mathrm{RLW}}\right)u_{\xi\xi}-cu_{\xi\xi\xi\xi}=0. \tag{30}$$

Using the method mentioned above, we may choose the solution of reduced ODE (30) in the form

$$u(\xi)=\begin{cases}\lambda\cos^{\eta}(\mu\xi), & |\xi|\leqslant\frac{\pi}{2\mu}\\ 0, & \text{otherwise},\end{cases} \tag{31}$$

or in the form

$$u(\xi)=\begin{cases}\lambda\sin^{\eta}(\mu\xi), & |\xi|\leqslant\frac{\pi}{2\mu}\\ 0, & \text{otherwise},\end{cases} \tag{32}$$

where λ, ξ, and η are parameters which are determined. It is easy to reduce that

$$u''=\lambda\eta(\eta-1)\mu^2\cos^{\eta-2}(\mu\xi)-\lambda\eta^2\mu^2\cos^{\eta}(\mu\xi) \tag{33}$$

and

$$u^{(4)}=\lambda\mu^4\eta(\eta-1)(\eta-2)(\eta-3)\cos^{\eta-4}(\mu\xi)-2\lambda\mu^4\eta(\eta-1)\left(\eta^2-2\eta+2\right)\cos^{\eta-2}(\mu\xi)+\lambda\mu^4\eta^4\cos^{\eta}(\mu\xi), \tag{34}$$

where similar equations can be obtained for the sine assumption. By applying Eqs. (31)–(34) into Eq. (30), we find

$$\begin{aligned}&\lambda\left(1-c-\left(\beta^{\mathrm{KdV}}+c\gamma^{\mathrm{RLW}}\right)\eta^2\mu^2-c\mu^4\eta^4\right)\cos^{\eta}(\mu\xi)-c\lambda\mu^4\eta(\eta-1)(\eta-2)(\eta-3)\cos^{\eta-4}(\mu\xi)\\&\quad+\lambda\left(\left(\beta^{\mathrm{KdV}}+c\gamma^{\mathrm{RLW}}\right)\eta(\eta-1)\mu^2+c2\mu^4\eta(\eta-1)\left(\eta^2-2\eta+2\right)\right)\cos^{\eta-2}(\mu\xi)+\alpha\lambda^2\cos^{2\eta}(\mu\xi)=0.\end{aligned} \tag{35}$$

Balancing $cos^{2\eta}(\mu\xi)$ with $cos^{\eta-4}(\mu\xi)$ in Eq. (35) gives $\eta=-4$. Substituting $\eta=-4$ into Eq. (35) and setting each coefficients of $cos^{j}(\mu\xi)$ to zero yield a set of equation for μ, λ, and c

$$\begin{aligned}&\lambda(\alpha\lambda-840c\mu^4)=0,\\&\lambda\left(20\left(\beta^{\mathrm{KdV}}+c\gamma^{\mathrm{RLW}}\right)\mu^2+1040c\mu^4\right)=0,\\&\lambda\left(1-c-16\left(\beta^{\mathrm{KdV}}+c\gamma^{\mathrm{RLW}}\right)\mu^2-256c\mu^4\right)=0.\end{aligned} \tag{36}$$

In case $\beta^{\mathrm{KdV}}=\gamma^{\mathrm{RLW}}=1$ and $\alpha=0.5$, system (36) gives

$$\begin{aligned}&\frac{1}{2}\lambda(\lambda-1680c\mu^4)=0,\\&\lambda(20(1+c)\mu^2+1040c\mu^4)=0,\\&\lambda(1-c-16(1+c)\mu^2-256c\mu^4)=0.\end{aligned} \tag{37}$$

Solving the system (37) leads to the following sets of solutions

$$\begin{aligned}&\mu=\pm i\frac{1}{\sqrt{288}}\sqrt{-13+\sqrt{457}},\\&c=\frac{241+13\sqrt{457}}{266},\\&\lambda=\frac{5}{456}\left(-25+13\sqrt{457}\right),\end{aligned} \tag{38}$$

and

$$\begin{aligned}&\mu=\pm\frac{1}{\sqrt{288}}\sqrt{13+\sqrt{457}},\\&c=\frac{241-13\sqrt{457}}{266},\\&\lambda=\frac{5}{456}\left(-25-13\sqrt{457}\right).\end{aligned} \tag{39}$$

By using the results of Eqs. (38) and (39), we obtain solutions of Eq. (1)

$$u(x,t)=\frac{5}{456}\left(-25+13\sqrt{457}\right)\operatorname{sech}^4\left[\frac{1}{\sqrt{288}}\sqrt{-13+\sqrt{457}}\left(x-\left(\frac{241+13\sqrt{457}}{266}\right)t\right)\right]$$

Table 9
Errors of numerical solutions at $T = 30$.

$\tau = h$	$\|e\|$	rate	$\|e\|_\infty$	rate
$\theta = -1$				
0.5	2.57844E+00		9.86753E−01	
0.25	5.56190E−01	2.21285	2.14488E−01	2.20179
0.125	1.34741E−01	2.04539	5.19201E−02	2.04653
0.0625	3.34447E−02	2.01034	1.28858E−02	2.01051
$\theta = -1/3$				
0.5	4.14324E−01		1.72860E−01	
0.25	9.17596E−02	2.17483	3.83521E−02	2.17222
0.125	2.23327E−02	2.03871	9.34197E−03	2.03751
0.0625	5.54842E−03	2.00901	2.32074E−03	2.00914
$\theta = 0$				
0.5	6.02160E−01		2.43684E−01	
0.25	1.50948E−01	1.99610	6.06169E−02	2.00722
0.125	3.78126E−02	1.99711	1.51770E−02	1.99783
0.0625	9.46327E−03	1.99845	3.79653E−03	1.99913
$\theta = 1/3$				
0.5	1.45901E+00		5.57917E−01	
0.25	3.72110E−01	1.97119	1.42175E−01	1.97238
0.125	9.34897E−02	1.99285	3.56991E−02	1.99371
0.0625	2.34123E−02	1.99754	8.93944E−03	1.99763
$\theta = 1$				
0.5	2.94337E+00		1.08501E+00	
0.25	8.05629E−01	1.86928	3.00424E−01	1.85264
0.125	2.05276E−01	1.97255	7.66547E−02	1.97055
0.0625	5.15696E−02	1.99297	1.92614E−02	1.99266

and

$$u(x,t) = \frac{5}{456}\left(25 - 13\sqrt{457}\right)\operatorname{csch}^4\left[\frac{1}{\sqrt{288}}\sqrt{-13+\sqrt{457}}\left(x - \left(\frac{241+13\sqrt{457}}{266}\right)t\right)\right].$$

In test problems for the Rosenau–KdV–RLW equation, we use the initial condition associated with this equation, which takes the form

$$u_0(x) = \frac{5}{456}\left(-25 + 13\sqrt{457}\right)\operatorname{sech}^4\left[\left(\frac{1}{\sqrt{288}}\sqrt{-13+\sqrt{457}}\right)x\right].$$

As shown in Table 9, for a particular choice of parameters $x_l = -40$ and $x_r = 100$, the estimated rates of convergence are close the theoretically predicted second-order rate of convergence. We can also say that when we use smaller time and space steps, numerical solutions are almost the same as the exact solutions. In Tables 10 and 11, it results from the present method, and the values of Q^n and E^n at any time $t \in [0, 60]$ coincide with the theory. The quantities Q^n and E^n seem to be conserved on the average, i.e. they are contained in a small interval but there are fluctuations. In this case, the following sets of parameters are chosen for the test problems: $\tau = h = 0.25,\ x_l = -40$, and $x_r = 160$.

Table 10
Invariant of motion Q^n.

T	$\theta = -1$	$\theta = -1/3$	$\theta = 0$	$\theta = 1/3$	$\theta = 1$
0	21.6792584430	21.6792584430	21.6792584430	21.6792584430	21.6792584430
15	21.6825770313	21.6798772354	21.6792585207	21.6791001829	21.6801606811
30	21.6826412754	21.6798843150	21.6792488984	21.6790824977	21.6801763808
45	21.6834261714	21.6805287614	21.6798420932	21.6796348051	21.6802663552
60	21.6746253679	21.6728367822	21.6726648091	21.6729484047	21.6749016262

Table 11
Invariant of motion E^n.

T	$\theta = -1$	$\theta = -1/3$	$\theta = 0$	$\theta = 1/3$	$\theta = 1$
0	43.7085514657	43.7085514657	43.7085514657	43.7085514657	43.7085514657
15	43.7265201536	43.7147171789	43.7112854772	43.7093907612	43.7099637500
30	43.7266422849	43.7148001553	43.7113467696	43.7094288659	43.7099530153
45	43.7266440914	43.7148018420	43.7113480338	43.7094288529	43.7099016523
60	43.7266440850	43.7148021240	43.7113484031	43.7094296146	43.7099281613

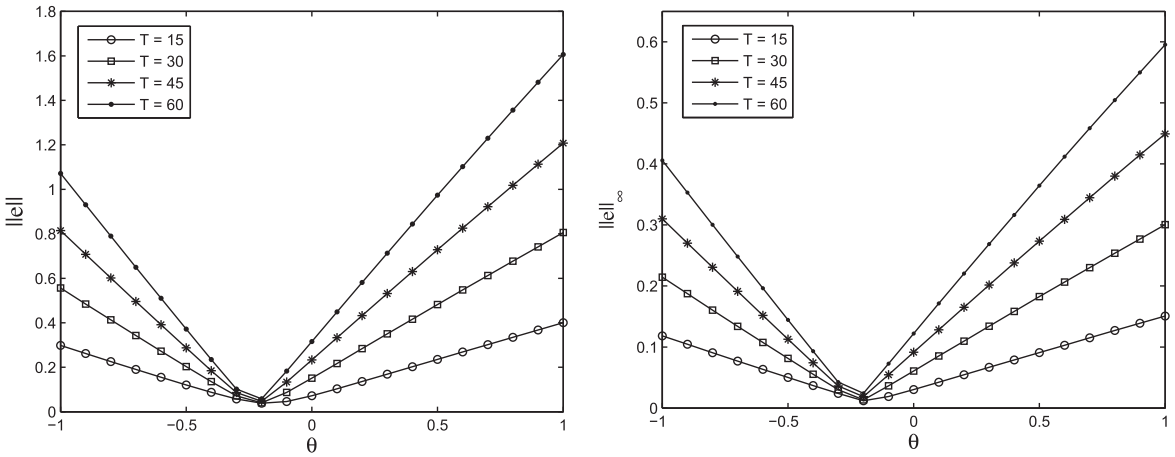

Fig. 3. Impact of the parameter θ with $\tau = h = 0.25,\ x_l = -40$, and $x_r = 160$.

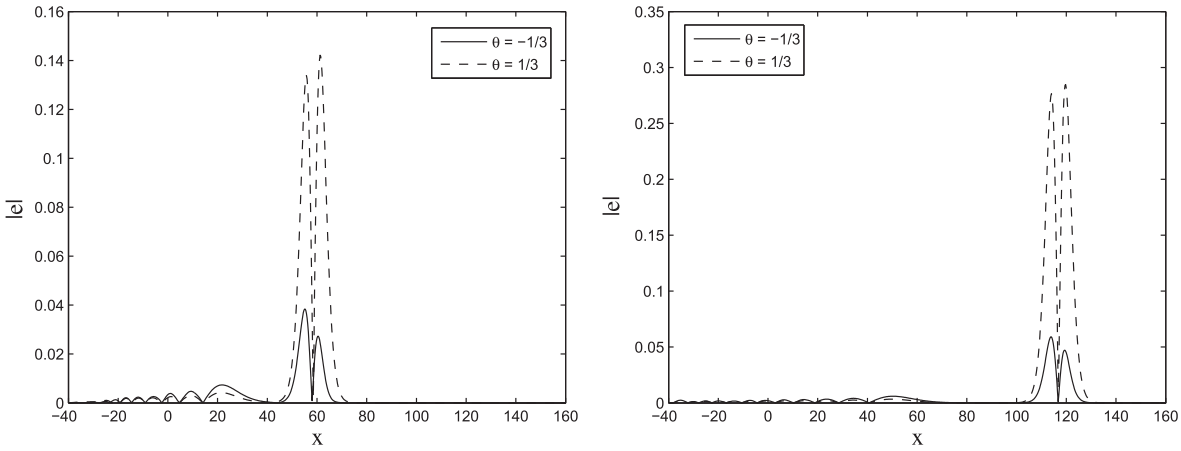

Fig. 4. Absolute error distribution at $T = 30$ (left) and $T = 60$ (right).

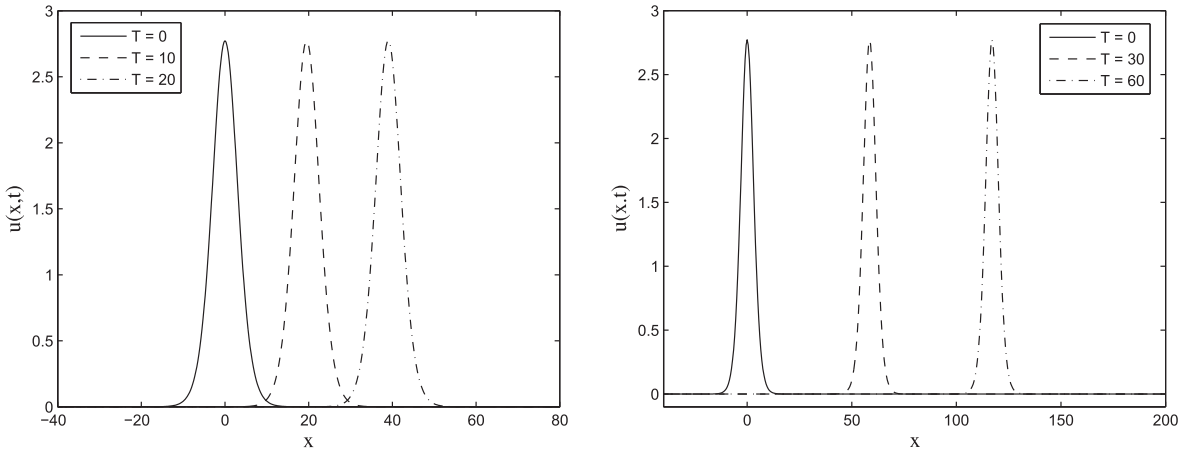

Fig. 5. Numerical solutions of the Rosenau–KdV–RLW equation with $\tau = h = 0.25,\ x_l = -40,\ x_r = 80$ (left) and $x_l = -40,\ x_r = 200$ (right).

We then study the impact of the parameter θ to the error of our numerical solution. The results are shown in the Fig. 3 where the errors of the numerical solutions are plotted versus θ for different sets of parameters. One can easily see that the variation of θ in the range of $[-1, 1]$ affects the approximate quantities; hence, the truncation error is improved. Absolute error distributions with $\tau = h = 0.25$ are drawn at $t = 30$ and $t = 60$ in Fig. 4, respectively. It can be easily observed that the maximum error is taken place around the peak amplitude of solitary waves. Finally, Fig. 5 presents numerical results from $t = 0$ to $t = 60$, which are close to exact values. The present method can be well used to study a solitary wave at long time.

The results of this section suffice to claim that both the new formulation and its numerical implementation offer a valid approach toward the numerical investigation of a nonlinear wave phenomena.

5. Conclusion

The new formulation for a nonlinear wave proposed by coupling the Rosenau–KdV equation and the Rosenau–RLW equation is implemented numerically. The impact on the results of the actual value of a small parameter θ in a nonlinear term is judiciously evaluated by numerical experiments and show that, for $\theta \in (-1, 1)$, the results are correct with the same significant digits as the truncation error. The new numerical model is applied to the Rosenau–KdV equation and the Rosenau–RLW equation. We show that the new technique performs robustly and allows one to follow accurately of the soliton patterns. The results are in good quantitative agreement with [10,22] in the common ranges of the parameters.

Moreover, the accuracy and stability of the numerical scheme for the solutions of the Rosenau–KdV–RLW equation can be tested by using the exact solution. The present method gives an implicit linear system, which can be easily implemented. This method shows the second-order accurate in time and space. The numerical experiments show that the present method supports the analysis of convergence rate and the invariant properties can be verified by using the analytical expression.

The present paper shows that the Rosenau–KdV–RLW equation is a viable approach to a model of a nonlinear wave and can serve as a basis for efficient numerical models.

Acknowledgments

This research was supported by the Department of Mathematics, Faculty of Science, Chiang Mai University.

References

[1] S. Zhu, J. Zhao, The alternating segment explicit–implicit scheme for dispersive equation, Appl. Math. Lett. 14 (6) (2001) 657–662.
[2] A.R. Bahadir, Exponential finite-difference method applied to Korteweg–de Vries equation for small times, Appl. Math. Comput. 160 (3) (2005) 675–682.
[3] S. Ozer, S. Kutluay, An analytical–numerical method applied to Korteweg–de Vries equation, Appl. Math. Comput. 164 (3) (2005) 789–797.
[4] Y. Cui, D.-K. Mao, Numerical method satisfying the first two conservation laws for the Korteweg–de Vries equation, J. Comput. Phys. 227 (2007) 376–399.
[5] J.I. Ramos, Explicit finite difference methods for the EW and RLW equations, Appl. Math. Comput. 179 (2006) 622–638.
[6] P. Rosenau, A quasi-continuous description of a nonlinear transmission line, Phys. Scr. 34 (1986) 827–829.
[7] P. Rosenau, Dynamics of dense discrete systems, Prog. Theor. Phys. 79 (1988) 1028–1042.
[8] M.A. Park, On the Rosenau equation, Math. Aplicada a Comput. 9 (2) (1990) 145–152.
[9] L. Zhang, A finite difference scheme for generalized regularized long-wave equation, Appl. Math. Comput. 168 (2) (2005) 962–972.
[10] J. Hu, Y. Xu, B. Hu, Conservative linear difference scheme for Rosenau–KdV equation, Adv. Math. Phys. 2013 (2013) 7. Article ID 423718.
[11] J.-M. Zuo, Solitons and periodic solutions for the Rosenau–KdV and Rosenau–Kawahara equations, Appl. Math. Comput. 215 (2) (2009) 835–840.
[12] A. Saha, Topological 1-soliton solutions for the generalized Rosenau–KdV equation, Fund. J. Math. Phys. 2 (1) (2012) 19–25.
[13] G. Ebadi, A. Mojaver, H. Triki, A. Yildirim, A. Biswas, Topological solitons and other solutions of the Rosenau–KdV equation with power law nonlinearity, Rom. J. Phys. 58 (2013) 3–14.
[14] P. Razborova, H. Triki, A. Biswas, Perturbation of dispersive shallow water waves, Ocean Eng. 63 (2013) 1–7.
[15] A. Esfahani, Solitary wave solutions for generalized Rosenau–KdV equation, Commun. Theor. Phys. 63 (2013) 1–7.
[16] D.H. Peregrine, Calculations of the development of an undular bore, J. Fluid Mech. 25 (1996) 321–330.
[17] D.H. Peregrine, Long waves on a beach, J. Fluid Mech. 27 (1997) 815–827.
[18] M.A. Park, Pointwise decay estimate of solutions of the generalized Rosenau equation, J. Korean Math. Soc. 29 (1992) 261–280.
[19] J.-M. Zuo, Y.-M. Zhang, T.-D. Zhang, F. Chang, A new conservative difference scheme for the general Rosenau–RLW equation, Boundary Value Prob. 2010 (2010) 13. Article ID 516260.
[20] X. Pan, L. Zhang, On the convergence of a conservative numerical scheme for the usual Rosenau–RLW equation, Appl. Math. Model. 36 (2012) 3371–3378.
[21] X. Pan, L. Zhang, Numerical simulation for general Rosenau–RLW equation: an average linearized conservative scheme, Math. Prob. Eng. 2012 (2012) 15. Article ID 517818.
[22] X. Pan, K. Zheng, L. Zhang, Finite difference discretization of the Rosenau–RLW equation, Appl. Anal. 92 (12) (2013) 2578–2589.
[23] N. Atouani, K. Omrani, Galerkin finite element method for the Rosenau–RLW equation, Comput. Math. Appl. 66 (2013) 289–303.
[24] R.C. Mittal, R.K. Jain, Numerical solution of general Rosenau–RLW equation using quintic B-splines collocation method, Commun. Numer. Anal. (2012) 16. Article ID cna-00129.
[25] F.E. Ham, F.S. Lien, A.B. Strong, A fully conservative second-order finite difference scheme for incompressible flow on nonuniform grids, J. Comput. Phys. 177 (2002) 117–133.
[26] Y. Zhou, Application of Discrete Functional Analysis to the Finite Difference Method, International Academy Publishers, Beijing, 1990.
[27] Z. Ren, W. Wang, D. Yu, A new conservative finite difference method for the nonlinear regularized long wave equation, Appl. Math. Sci. 5 (42) (2011) 2091–2096.
[28] X. Zhao, D. Li, D. Shi, A finite difference scheme for RLW-Burgers equation, J. Appl. Math. Inform. 26 (2008) 573–581.
[29] K. Omrani, F. Abidi, T. Achour, N. Khiari, A new conservative finite difference scheme for Rosenau equation, Appl. Math. Comput. 201 (2008) 35–43.
[30] M. Wang, D. Li, P. Cui, A new conservative finite difference scheme for generalized Rosenau equation, Int. J. Pure Appl. Math. 71 (4) (2011) 539–549.

[31] X. Pan, L. Zhang, A new finite difference scheme for Rosenau–Burgers equation, Appl. Math. Comput. 218 (2012) 8917–8924.
[32] J. Hu, B. Hu, Y. Xu, Average implicit linear difference scheme for generalized Rosenau–Burgers equation, Int. J. Pure Appl. Math. 217 (2011) 7557–7563.
[33] J. Janwised, B. Wongsaijai, T. Mouktonglang, K. Poochinapan, A modified three-level average linear-implicit finite difference method for the Rosenau–Burgers equation, Adv. Math. Phys. 2014 (2014) 11. Article ID 734067.

Hindawi Publishing Corporation
Mathematical Problems in Engineering
Volume 2014, Article ID 862403, 8 pages
http://dx.doi.org/10.1155/2014/862403

Research Article

Efficiency of High-Order Accurate Difference Schemes for the Korteweg-de Vries Equation

Kanyuta Poochinapan,[1] Ben Wongsaijai,[1] and Thongchai Disyadej[2]

[1]*Department of Mathematics, Faculty of Science, Chiang Mai University, Chiang Mai 50200, Thailand*
[2]*Electricity Generating Authority of Thailand, Phitsanulok 65000, Thailand*

Correspondence should be addressed to Kanyuta Poochinapan; kanyuta@hotmail.com

Received 5 August 2014; Accepted 2 November 2014; Published 8 December 2014

Academic Editor: Igor Andrianov

Two numerical models to obtain the solution of the KdV equation are proposed. Numerical tools, compact fourth-order and standard fourth-order finite difference techniques, are applied to the KdV equation. The fundamental conservative properties of the equation are preserved by the finite difference methods. Linear stability analysis of two methods is presented by the Von Neumann analysis. The new methods give second- and fourth-order accuracy in time and space, respectively. The numerical experiments show that the proposed methods improve the accuracy of the solution significantly.

1. Introduction

Researchers in the past have worked on mathematical models explaining the behavior of a nonlinear wave phenomenon which is one of the significant areas of applied research. Derived by Korteweg and de Vries [1], the Korteweg-de Vries eqaution (KdV equation) is one of the mathematical models which are used to study a nonlinear wave phenomenon. The KdV equation has been used in very wide applications, such as magnetic fluid waves, ion sound waves, and longitudinal astigmatic waves.

The KdV equation has been solved numerically by various methods, such as the collocation method [2–4], the finite element method [5, 6], the Galerkin method [7–10], the spectral method [11, 12], and the finite difference method [13–18]. To create a numerical tool, the finite difference method for the KdV equation is developed until now. Zhu [13] solved the KdV equation using the implicit difference method. The scheme is unconditionally linearly stable and has a truncation error of order $O(\tau + h^2)$. Qu and Wang [14] developed the alternating segment explicit-implicit (ASE-I) difference scheme consisting of four asymmetric difference schemes, a classical explicit scheme, and an implicit scheme, which is unconditionally linearly stable by the analysis of linearization procedure. Wang et al. [15] have proposed an explicit finite difference scheme for the KdV equation. The scheme is more stable than the Zabusky-Kruskal (Z-K) scheme [16] when it is used to simulate the collisions of multisoliton. The stability of the method in [15] was also discussed by using the frozen coefficient Von Neumann analysis method. The time step limitation of the method in [15] is twice looser than that of the Z-K method. Moreover, Kolebaje and Oyewande [17] investigated the behavior of solitons generated from the KdV equation that depends on the nature of the initial condition, by using the Goda method [18], the Z-K method, and the Adomian decomposition method.

The stability, accuracy, and efficiency, which are in conflict with each other, are the desired properties of the finite difference scheme. Implicit approximation is requested in order to reach the stability of the finite difference scheme. A high-order accuracy in the spatial discretization is desired in various problems. The stencil becomes wider with increasing order of accuracy for a high-order method of a conventional scheme. Furthermore, using an implicit method results in the solution of an algebraic system for equations with extensive bandwidth. It is required to improve schemes that have a broad range of stability and high order of accuracy. Additionally, this leads to the solution of the system for linear

equations with a pentadiagonal matrix, that is, the system of linear equations arising from a standard second-order discretization of a boundary value problem. A method to conquer the conflict between stability, accuracy, and computational cost is the development of a high-order compact scheme.

In recent decades, many scientists concentrated upon the difference method that makes a discrete analogue effective in the fundamental conservation properties. This causes us to create finite difference schemes which preserve the mass and energy of solutions for the KdV equation. In this paper, two fourth-order difference schemes are constructed for the one dimensional KdV equation:

$$u_t + \alpha u_{xxx} + \gamma \left(u^2\right)_x = 0, \quad x_L < x < x_R, \ 0 \le t \le T, \tag{1}$$

with an initial condition

$$u(x,0) = u_0(x), \quad x_L \le x \le x_R, \tag{2}$$

and boundary conditions

$$\begin{aligned} &u(x_L,t) = u(x_R,t) = 0,\\ &u_x(x_L,t) = u_x(x_R,t) = 0,\\ &u_{xx}(x_L,t) = u_{xx}(x_R,t) = 0,\\ &\qquad 0 \le t \le T, \end{aligned} \tag{3}$$

where α and γ are any real number. When $-x_L \gg 0$ and $x_R \gg 0$, the initial-boundary value problem (1)–(3) is consistent, so the boundary condition (3) is reasonable. By assumptions, the solitary wave solution and its derivatives have the following asymptotic values, $u \to 0$ as $x \to \pm\infty$, and for $n \ge 1$, $\partial^n u/\partial x^n \to 0$ as $x \to \pm\infty$. Moreover, we obtain the solution properties as follows [19]:

$$\begin{aligned} I_1 &= \int_{x_L}^{x_R} u(x,t)\,dx,\\ I_2 &= \int_{x_L}^{x_R} u(x,t)^2\,dx,\\ I_3 &= \int_{x_L}^{x_R} \left[2\gamma u(x,t)^3 - 3\alpha \left[u(x,t)_x\right]^2\right]. \end{aligned} \tag{4}$$

The content of this paper is organized as follows. In the next section, we create fourth-order finite difference schemes for the KdV equation with the initial and boundary conditions. The stability of finite difference schemes is discussed and the conservative approximations are also given. The results on validation of finite difference schemes are presented in Section 3, where we make a detailed comparison with available data, to confirm and illustrate our theoretical analysis. Finally, we finish our paper by conclusions in the last section.

2. Difference Schemes

We start the discussion of finite difference schemes by defining a grid of points in the (x,t) plane. For simplicity, we use a uniform grid for a discrete process with states identified by $x_j = x_L + jh$ which the grid size is $h = (x_R - x_L)/M$, where M is the number of grid points. Therefore, the grid will be the points $(x_j, t_n) = (x_L + jh, n\tau)$ for arbitrary integers j and n. Here τ is a time increment (time step length). We write the notation u_j^n for a value of a function u at the grid point $(x_L + jh, n\tau)$.

In this paper, we give a complete description of our finite difference schemes and an algorithm for the formulation of the problem (1)–(3). We use the following notations for simplicity:

$$\begin{aligned} &\overline{u}_j^n = \frac{u_j^{n+1} + u_j^{n-1}}{2}, \qquad \left(u_j^n\right)_{\hat{t}} = \frac{u_j^{n+1} - u_j^{n-1}}{2\tau},\\ &\left(u_j^n\right)_{\overline{x}} = \frac{u_j^n - u_{j-1}^n}{h}, \qquad \left(u_j^n\right)_x = \frac{u_{j+1}^n - u_j^n}{h},\\ &\left(u_j^n\right)_{\hat{x}} = \frac{u_{j+1}^n - u_{j-1}^n}{2h}, \qquad \left(u_j^n\right)_{\ddot{x}} = \frac{u_{j+2}^n - u_{j-2}^n}{4h},\\ &\left(u^n, v^n\right) = h\sum_{j=1}^{M-1} u_j^n v_j^n, \qquad \left\|u^n\right\|^2 = \left(u^n, u^n\right),\\ &\left\|u^n\right\|_\infty = \max_{1\le j\le M-1} \left|u_j^n\right|. \end{aligned} \tag{5}$$

As introduced in the following subsections, the techniques for determining the value of numerical solution to (1) are used.

2.1. Compact Fourth-Order Finite Difference Scheme. By setting $w = -\alpha u_{xxx} - \gamma(u^2)_x$, (1) can be written as $w = u_t$. By the Taylor expansion, we obtain

$$w_j^n = \left(\partial_t u\right)_j^n = \left(u_j^n\right)_{\hat{t}} + O\left(\tau^2\right), \tag{6}$$

$$\begin{aligned} w_j^n = &-\alpha\left[\left(u_j^n\right)_{x\overline{x}\hat{x}} - \frac{h^2}{4}\left(\partial_x^5 u\right)_j^n\right]\\ &- \gamma\left[\left[\left(u_j^n\right)^2\right]_{\hat{x}} - \frac{h^2}{6}\left(\partial_x^3 u^2\right)_j^n\right] + O\left(h^4\right). \end{aligned} \tag{7}$$

From (6), we have

$$\alpha\left(\partial_x^5 u\right)_j^n = -\gamma\left(\partial_x^3 u^2\right)_j^n - \left(\partial_x^2 w\right)_j^n. \tag{8}$$

Substituting (8) into (7), we get

$$\begin{aligned} w_j^n = &-\alpha\left(u_j^n\right)_{x\overline{x}\hat{x}} - \frac{h^2}{4}\left(\partial_x^2 w\right)_j^n - \gamma\left[\left(u_j^n\right)^2\right]_{\hat{x}}\\ &- \frac{h^2}{12}\gamma\left(\partial_x^3 u^2\right)_j^n + O\left(h^4\right). \end{aligned} \tag{9}$$

Using second-order accuracy for approximation, we obtain

$$\begin{aligned} \left(\partial_x^3 u^2\right)_j^n &= \left[\left(u_j^n\right)^2\right]_{x\overline{x}\hat{x}} + O\left(h^2\right),\\ \left(\partial_x^2 w\right)_j^n &= \left(w_j^n\right)_{x\overline{x}} + O\left(h^2\right). \end{aligned} \tag{10}$$

The following method is the proposed compact finite difference scheme to solve the problem (1)–(3):

$$\left(u_j^n\right)_{\hat{t}} + \frac{h^2}{4}\left(u_j^n\right)_{x\bar{x}\hat{t}} + \alpha\left(\overline{u}_j^n\right)_{x\bar{x}\hat{x}} + \gamma\left[\left(u_j^n\right)\left(\overline{u}_j^n\right)\right]_{\hat{x}} + \frac{\gamma h^2}{12}\left[\left(u_j^n\right)\left(\overline{u}_j^n\right)\right]_{x\bar{x}\hat{x}} = 0, \tag{11}$$

where

$$u_j^0 = u_0\left(x_j\right), \quad 0 \le j \le M. \tag{12}$$

Since the boundary conditions are homogeneous, they give

$$u_0^n = u_M^n = 0, \quad \left(u_0^n\right)_{\hat{x}} = \left(u_M^n\right)_{\hat{x}} = 0, \quad 1 \le n \le N. \tag{13}$$

At this time, let $e_j^n = v_j^n - u_j^n$ where v_j^n and u_j^n are the solution of (1)–(3) and (11)–(13), respectively. Then, we obtain the following error equation:

$$r_j^n = \left(e_j^n\right)_{\hat{t}} + \frac{h^2}{4}\left(e_j^n\right)_{x\bar{x}\hat{t}} + \alpha\left(\overline{e}_j^n\right)_{x\bar{x}\hat{x}} + \gamma\left[\left(v_j^n\right)\left(\overline{v}_j^n\right)\right]_{\hat{x}} - \gamma\left[\left(u_j^n\right)\left(\overline{u}_j^n\right)\right]_{\hat{x}} + \frac{\gamma h^2}{12}\left[\left(v_j^n\right)\left(\overline{v}_j^n\right)\right]_{x\bar{x}\hat{x}} - \frac{\gamma h^2}{12}\left[\left(u_j^n\right)\left(\overline{u}_j^n\right)\right]_{x\bar{x}\hat{x}}, \tag{14}$$

where r_j^n denotes the truncation error. By using the Taylor expansion, it is easy to see that $r_j^n = O(\tau^2 + h^4)$ holds as $\tau, h \to 0$.

The Von Neumann stability analysis of (11) with $u_j^n = \xi^n e^{ikjh}$, where $i^2 = -1$ and k is a wave number, gives the following the amplification factor:

$$\xi^2 = \frac{A - i\tau B}{A + i\tau B}, \tag{15}$$

where

$$A = 6h^3\left(\cos\left(kh\right) + 1\right), \quad B = 12\alpha\left(\sin\left(2kh\right) - 2\sin\left(kh\right)\right) + \gamma h^2\left(u_j^n\right)\left(\sin\left(4kh\right) + 10\sin\left(2kh\right)\right). \tag{16}$$

The amplification factor which is a complex number has its modulus equal to one; therefore the compact finite difference scheme is unconditionally stable.

Theorem 1. *Suppose $u(x,t)$ is smooth enough, then the scheme (11)–(13) is conservative in a sense:*

$$I_1^n = \frac{h}{2}\sum_{j=1}^{M-1}\left(u_j^{n+1} + u_j^n\right) = I_1^{n-1} = \cdots = I_1^0, \tag{17}$$

under assumptions $u_1 = u_{M-1} = 0$.

Proof. By multiplying (11) by h, summing up for j from 1 to $M-1$, and considering the boundary condition and assuming $u_1 = u_{M-1} = 0$, we get

$$\frac{h}{2\tau}\sum_{j=1}^{M-1}\left(u_j^{n+1} - u_j^{n-1}\right) = 0. \tag{18}$$

Then, this gives (17). □

2.2. Standard Fourth-Order Finite Difference Scheme. By the fact $(u^2)_x = (2/3)[uu_x + (u^2)_x]$ and using an implicit finite difference method, we propose a standard seven-point implicit difference scheme for the problem (1)–(3):

$$\left(u_j^n\right)_{\hat{t}} + \alpha\left(\frac{3}{2}\left(\overline{u}_j^n\right)_{x\bar{x}\hat{x}} - \frac{1}{2}\left(\overline{u}_j^n\right)_{x\bar{x}\ddot{x}}\right) + 2\gamma\left[\frac{4}{9}\left(\left(u_j^n\overline{u}_j^n\right)_{\hat{x}} + u_j^n\left(\overline{u}_j^n\right)_{\hat{x}}\right) - \frac{1}{9}\left(\left(u_j^n\overline{u}_j^n\right)_{\ddot{x}} + u_j^n\left(\overline{u}_j^n\right)_{\ddot{x}}\right)\right] = 0, \tag{19}$$

where

$$u_j^0 = u_0\left(x_j\right), \quad 0 \le j \le M. \tag{20}$$

Since the boundary conditions are homogeneous, we obtain

$$u_0^n = u_M^n = 0, \tag{21}$$

$$4\left(u_0^n\right)_{\hat{x}} - \left(u_0^n\right)_{\ddot{x}} = 4\left(u_M^n\right)_{\hat{x}} - \left(u_M^n\right)_{\ddot{x}} = 0, \tag{22}$$

$$-\left(u_{-1}^n\right)_{x\bar{x}} + 14\left(u_0^n\right)_{x\bar{x}} - \left(u_1^n\right)_{x\bar{x}} = -\left(u_{M-1}^n\right)_{x\bar{x}} 14\left(u_M^n\right)_{x\bar{x}} - \left(u_{M+1}^n\right)_{x\bar{x}} = 0, \quad 1 \le n \le N. \tag{23}$$

u, u_x, and u_{xx} are required by the standard fourth-order technique to be zero at the upstream and downstream boundaries because the method utilizes a seven-point finite difference scheme for the approximation of solution u. Through the analytical technique of contrasting, (11) requires two homogeneous boundary conditions only.

Now, let $e_j^n = v_j^n - u_j^n$ where v_j^n and u_j^n are the solution of (1)–(3) and (19)–(22), respectively. Then, we obtain the following error equation:

$$\left(e_j^n\right)_{\hat{t}} + \alpha\frac{3}{2}\left(\overline{e}_j^n\right)_{x\bar{x}\hat{x}} - \alpha\frac{1}{2}\left(\overline{e}_j^n\right)_{x\bar{x}\ddot{x}} + \frac{8\gamma}{9}\left[\left(\left(v_j^n\overline{v}_j^n\right)_{\hat{x}} + v_j^n\left(\overline{v}_j^n\right)_{\hat{x}}\right) - \left(\left(u_j^n\overline{u}_j^n\right)_{\hat{x}} + u_j^n\left(\overline{u}_j^n\right)_{\hat{x}}\right)\right] - \frac{2\gamma}{9}\left[\left(\left(v_j^n\overline{v}_j^n\right)_{\ddot{x}} + v_j^n\left(\overline{v}_j^n\right)_{\ddot{x}}\right) - \left(\left(u_j^n\overline{u}_j^n\right)_{\ddot{x}} + u_j^n\left(\overline{u}_j^n\right)_{\ddot{x}}\right)\right] = 0, \tag{24}$$

where r_j^n denotes the truncation error. By using the Taylor expansion, it is easy to see that $r_j^n = O(\tau^2 + h^4)$ holds as $\tau, h \to 0$.

The Von Neumann stability analysis of (19) with $u_j^n = \xi^n e^{ikjh}$ gives the following amplification factor:

$$\xi^2 = \frac{36h^3 - i\tau A}{36h^3 + i\tau A}, \tag{25}$$

where

$$\begin{aligned} A = {} & 4\gamma h^2 \left(u_j^n\right)(-\sin(4kh) + 7\sin(2kh) + 8\sin(kh)) \\ & + 9\alpha(-\sin(3kh) + 8\sin(2kh) - 13\sin(kh)). \end{aligned} \tag{26}$$

The amplification factor which is a complex number has its modulus equal to one; therefore the finite difference scheme is unconditionally stable.

Theorem 2. *Suppose $u(x,t)$ is smooth enough, then the scheme (11)–(13) is conservative in a sense:*

$$\begin{aligned} I_1^n = {} & \frac{h}{2}\sum_{j=1}^{M-1}\left(u_j^{n+1} + u_j^n\right) \\ & + \tau h\gamma \sum_{j=1}^{M-1}\left[\frac{4}{9}u_j^n\left(u_j^{n+1}\right)_{\hat{x}} - \frac{1}{9}u_j^n\left(u_j^{n+1}\right)_{\ddot{x}}\right] \\ = {} & I_1^{n-1} = \cdots = I_1^0, \end{aligned} \tag{27}$$

under assumptions $u_1 = u_2 = u_{M-2} = u_{M-1} = 0$. Moreover, the scheme (19)–(22) is conservative in a sense:

$$I_2^n = \frac{1}{2}\left\|u^n\right\|^2 + \frac{1}{2}\left\|u^{n+1}\right\|^2 = I_2^{n-1} = \cdots = I_2^0. \tag{28}$$

Proof. By multiplying (11) by h, summing up for j from 1 to $M-1$, and considering the boundary condition and assuming $u_1 = u_2 = u_{M-2} = u_{M-1} = 0$, we have

$$\begin{aligned} & \tau h\sum_{j=1}^{M-1}\left[\frac{8}{9}\left(u_j^n\left(\overline{u}_j^n\right)_{\hat{x}}\right) - \frac{2}{9}\left(u_j^n\left(\overline{u}_j^{n+1}\right)_{\ddot{x}}\right)\right] \\ & = \tau h\sum_{j=1}^{M-1}\left[\frac{4}{9}\left(u_j^n\left(u_j^{n+1}\right)_{\hat{x}} - u_j^{n-1}\left(u_j^n\right)_{\hat{x}}\right)\right. \\ & \qquad \left. -\frac{1}{9}\left(u_j^n\left(u_j^{n+1}\right)_{\ddot{x}} - u_j^{n-1}\left(u_j^n\right)_{\ddot{x}}\right)\right]. \end{aligned} \tag{29}$$

As a result, we have

$$\begin{aligned} & \frac{h}{2}\sum_{j=1}^{M-1}\left(u_j^{n+1} - u_j^{n-1}\right) \\ & + \gamma\tau h\sum_{j=1}^{M-1}\left[\frac{4}{9}\left(u_j^n\left(u_j^{n+1}\right)_{\hat{x}} - u_j^{n-1}\left(u_j^n\right)_{\hat{x}}\right)\right. \\ & \qquad \left. -\frac{1}{9}\left(u_j^n\left(u_j^{n+1}\right)_{\ddot{x}} - u_j^{n-1}\left(u_j^n\right)_{\ddot{x}}\right)\right] = 0. \end{aligned} \tag{30}$$

Then, this gives (27). We then take an inner product between (19) and $2\overline{u}^n$. We obtain

$$\begin{aligned} & \frac{1}{2\tau}\left(\left\|u^{n+1}\right\|^2 - \left\|u^{n-1}\right\|^2\right) + \frac{3\alpha}{2}\left(\left(\overline{u}^n\right)_{x\bar{x}\hat{x}}, \left(\overline{u}^n\right)\right) \\ & \quad - \frac{\alpha}{2}\left(\left(\overline{u}^n\right)_{x\bar{x}\ddot{x}}, \left(\overline{u}^n\right)\right) + 2\gamma\left(\varphi^n\left(u^n, \overline{u}^n\right), \overline{u}^n\right) = 0, \end{aligned} \tag{31}$$

where

$$\begin{aligned} \varphi^n\left(u_j^n, \overline{u}_j^n\right) = {} & \frac{4}{9}\left(\left(u_j^n\overline{u}_j^n\right)_{\hat{x}} + u_j^n\left(\overline{u}_j^n\right)_{\hat{x}}\right) \\ & - \frac{1}{9}\left(\left(u_j^n\,\overline{u}_i^n\right)_{\ddot{x}} + u_j^n\left(\overline{u}_j^n\right)_{\ddot{x}}\right), \end{aligned} \tag{32}$$

by considering the boundary condition (13). According to

$$\begin{aligned} \left(\overline{u}_{x\bar{x}\hat{x}}^n, \overline{u}^n\right) = 0, \\ \left(\overline{u}_{x\bar{x}\ddot{x}}^n, \overline{u}^n\right) = 0, \end{aligned} \tag{33}$$

indeed,

$$\begin{aligned} & \left(\varphi^n\left(u^n, \overline{u}^n\right), \overline{u}^n\right) \\ & = \frac{4h}{9}\sum_{j=1}^{M-1}\left[u_j^n\left(u_j^{n+1}\right)_{\hat{x}} + \left(u_j^n u_j^{n+1}\right)_{\hat{x}}\right]u_j^{n+1} \\ & \quad - \frac{h}{9}\sum_{j=1}^{M-1}\left[u_j^n\left(u_j^{n+1}\right)_{\ddot{x}} + \left(u_j^n u_j^{n+1}\right)_{\ddot{x}}\right]u_j^{n+1} \\ & = \frac{2}{9}\sum_{j=1}^{M-1}\left[\left(u_j^n u_j^{n+1}u_{j+1}^{n+1} - u_{j-1}^n u_{j-1}^{n+1}u_j^{n+1}\right)\right. \\ & \qquad \left. + \left(u_{j+1}^n u_j^{n+1}u_{j+1}^{n+1} - u_j^n u_{j-1}^{n+1}u_j^{n+1}\right)\right] \\ & \quad - \frac{1}{36}\sum_{j=1}^{M-1}\left[\left(u_j^n u_j^{n+1}u_{j+2}^{n+1} - u_{j-2}^n u_{j-2}^{n+1}u_j^{n+1}\right)\right. \\ & \qquad \left. + \left(u_{j+2}^n u_j^{n+1}u_{j+2}^{n+1} - u_j^n u_{j-2}^{n+1}u_j^{n+1}\right)\right] \\ & = 0. \end{aligned} \tag{34}$$

Therefore,

$$\frac{1}{2\tau}\left(\left\|u^{n+1}\right\|^2 - \left\|u^{n-1}\right\|^2\right) = 0. \tag{35}$$

Then, this gives (28). □

A conservative approximation confirms that the energy would not increase in time, which allows making the scheme stable.

3. Numerical Experiments

In this section, we present numerical experiments on the classical KdV equation when $\alpha = 1$ and $\gamma = 3$ with both difference schemes. The accuracy of the methods is measured

Table 1: Error and convergence rate of the compact finite difference scheme (11) at $t = 60$, $h = 0.5$, and $\tau = 0.25$.

	τ, h	$\tau/4, h/2$	$\tau/16, h/4$
$\|e\|$	1.39538×10^{-2}	7.15872×10^{-4}	4.49013×10^{-5}
Rate	—	4.28481	3.99487
$\|e\|_\infty$	7.64991×10^{-3}	3.32024×10^{-4}	2.08869×10^{-5}
Rate	—	4.52608	3.99062

Table 2: Error and convergence rate of the standard fourth-order finite difference scheme (19) at $t = 60$, $h = 0.5$, and $\tau = 0.25$.

	τ, h	$\tau/4, h/2$	$\tau/16, h/4$
$\|e\|$	1.59924×10^{-1}	9.79739×10^{-3}	6.09352×10^{-4}
Rate	—	4.02885	4.00705
$\|e\|_\infty$	8.63999×10^{-2}	5.33149×10^{-3}	3.33067×10^{-4}
Rate	—	4.01842	4.00066

Table 3: Invariants of I_1, I_2, and I_3 of the compact fourth-order finite difference scheme (11).

t	I_1	I_2	I_3
0	2.0000000000	0.6666666667	1.2058836346
10	1.9999449243	0.6666680888	1.2059201473
20	2.0001106778	0.6666680896	1.2059186978
30	1.9999055324	0.6666679386	1.2059155167
40	2.0001880153	0.6666680804	1.2059193791
50	1.9999670401	0.6666680255	1.2059262538
60	1.9998768932	0.6666679688	1.2059162036

by the comparison of numerical solutions with the exact solutions as well as other numerical solutions from methods in the literatures, by using $\|\cdot\|$ and $\|\cdot\|_\infty$ norm. The initial conditions for each problem are chosen in such a way that the exact solutions can be explicitly computed. In case $\alpha = 1$ and $\gamma = 3$, the KdV equation has the analytical solution as

$$u(x,t) = 0.5\,\mathrm{sech}^2\left(0.5\,(x-t)\right). \tag{36}$$

Therefore, the initial condition of (1) takes the form

$$u_0(x) = 0.5\,\mathrm{sech}^2\left(0.5\,(x)\right). \tag{37}$$

For these particular experiments, we set $x_L = -40$, $x_R = 100$, and $T = 60$. We make a comparison between the compact fourth-order finite difference scheme (11) and the standard fourth-order finite difference scheme (19). So, the results on this experiment in terms of errors at the time $t = 60$ is reported in Tables 1 and 2, respectively. It is clear that the results obtained by the compact fourth-order difference scheme (11) are more accurate than the ones obtained by the standard fourth-order difference scheme but the estimation of the rate of convergence for both schemes is close to the theoretically predicted fourth-order rate of convergence. It can be seen that the computational efficiency of the scheme (11) is better than that of the scheme (19), in terms of error.

Conservative approximation, that is a supplementary constraint, is essential for a suitable difference equation to make a discrete analogue effective to the fundamental conservation properties of the governing equation. Then, we can calculate three conservative approximations by using discrete forms as follows:

$$\begin{aligned} I_1 &\approx \frac{h}{2}\sum_{j=1}^{M}\left(u_j^{n+1} + u_j^n\right), \\ I_2 &\approx \frac{h}{2}\sum_{j=1}^{M}\left[\left(u_j^{n+1}\right)^2 + \left(u_j^n\right)^2\right], \\ I_3 &\approx h\sum_{j=1}^{M}\left[2\gamma\left(\frac{\left(u_j^{n+1}\right)^3 + \left(u_j^n\right)^3}{2}\right)\right. \\ &\qquad \left. -3\alpha\left(\frac{\left(u_j^{n+1}\right)_{\hat{x}}^2 + \left(u_j^n\right)_{\hat{x}}^2}{2}\right)\right]. \end{aligned} \tag{38}$$

Here, we take $h = 0.25$ and $\tau = h^2$ at $t \in [0, 60]$ for the compact fourth-order finite difference scheme (11) and the standard fourth-order finite difference scheme (19) and results are presented in Tables 3 and 4, respectively. The numerical results show that both two schemes can preserve the discrete conservation properties.

The second-order explicit scheme (Z-K scheme) and the second-order implicit scheme (Goda scheme) are used for testing the numerical performance of the new schemes. In Figure 1, we see that the Z-K scheme computes reasonable solutions using $h = 0.1$ and $\tau = 0.01$, except that the approximate solution at $t = 0.1$ does not maintain the shape of the exact solution. Similar calculations at $t = 0.1$ and $t = 0.11$

Table 4: Invariants of I_1, I_2, and I_3 of the standard fourth-order finite difference scheme (19).

t	I_1	I_2	I_3
0	2.0000000000	0.6666666667	1.2058836346
10	2.0000527573	0.6666666667	1.2059115241
20	2.0000219448	0.6666666667	1.2059125783
30	1.9999931738	0.6666666667	1.2059105915
40	2.0001264687	0.6666666667	1.2059099477
50	1.9999456225	0.6666666667	1.2059116281
60	1.9998875333	0.6666666667	1.2059106816

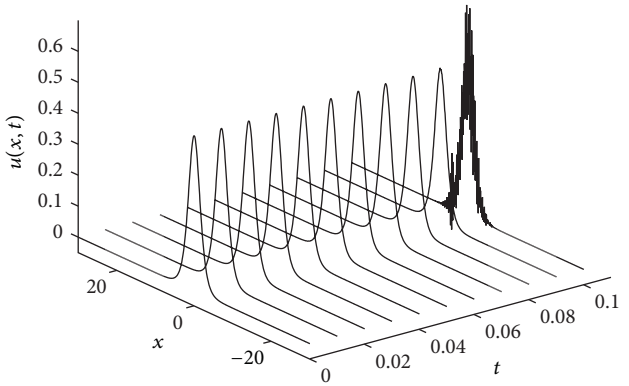

Figure 1: Explicit solutions using the Z-K scheme at $t \in [0, 0.1]$, $x_L = -40$, $x_R = 100$, $h = 0.1$, and $\tau = 0.01$.

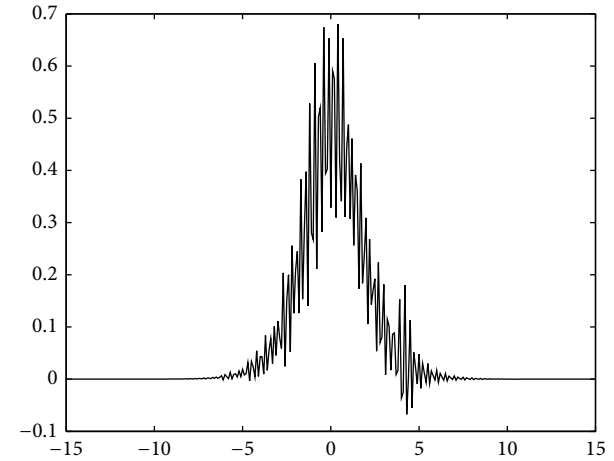

Figure 2: Explicit solution using the Z-K scheme at 10 time steps, $x_L = -40$, $x_R = 100$, $h = 0.1$, and $\tau = 0.01$.

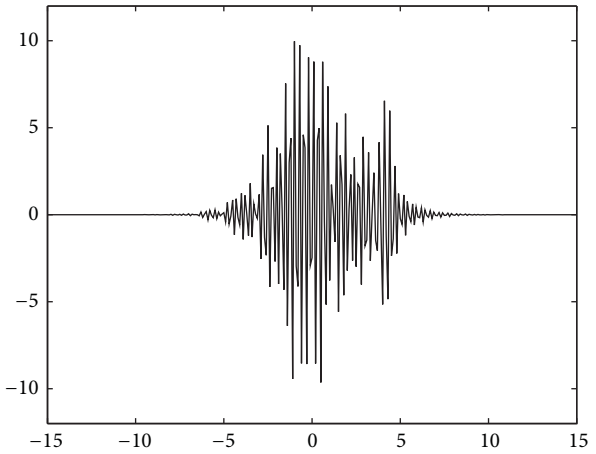

Figure 3: Explicit solution using the Z-K scheme at 11 time steps, $x_L = -40$, $x_R = 100$, $h = 0.1$, and $\tau = 0.01$.

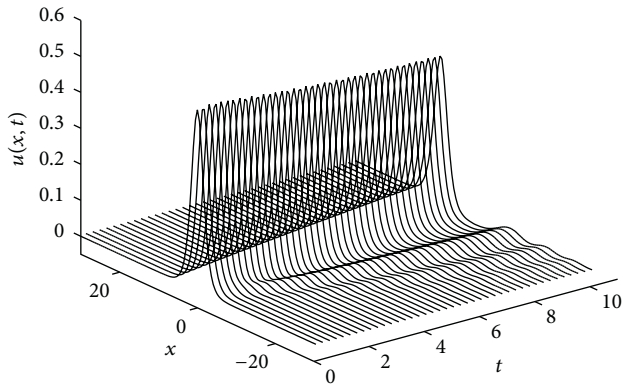

Figure 4: Implicit solutions using the Goda scheme at $t \in [0, 10]$, $x_L = -40$, $x_R = 100$, $h = 0.5$, and $\tau = 0.25$.

are demonstrated in Figures 2 and 3, respectively. The figures show that numerical waveforms begin to oscillate at $t = 0.1$ and show a blowup when $t = 0.11$. According to the results, the Z-K scheme is numerically unstable, regardless of how small time increment is.

As shown in Figure 2, the results of the Z-K scheme are greatly fluctuating at 10 time steps. Therefore, It can not be used to predict the behavior of the solution at long time. Figures 4 and 5 present the numerical solutions by using the Goda scheme. We see that the Goda scheme can run very well at $h = 0.5$ and $\tau = 0.25$. However, the result is still slightly oscillate at the left side of the solution.

Using the same parameters as the Goda scheme, Figures 6 and 7 present waveforms with $t \in [0, 10]$. The result obtained by the fourth-order difference schemes is greatly improved, compared to that obtained by the second-order schemes.

Figure 8 shows the numerical solution at $t = 200$. The result from the compact fourth-order difference scheme (11) is almost perfectly sharp. From the point of view for the long

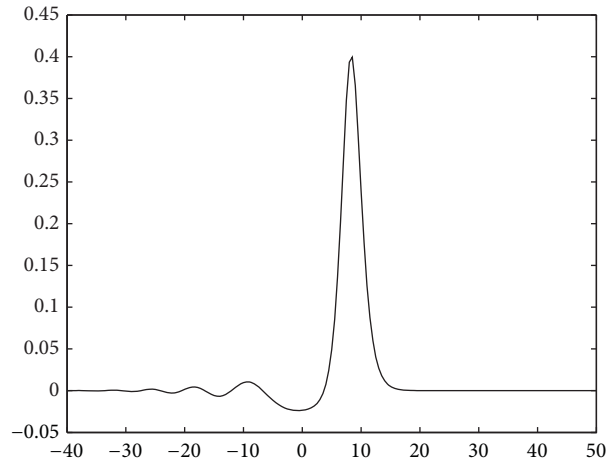

Figure 5: Implicit solution using the Goda scheme at $t = 10$, $x_L = -40$, $x_R = 100$, $h = 0.5$, and $\tau = 0.25$.

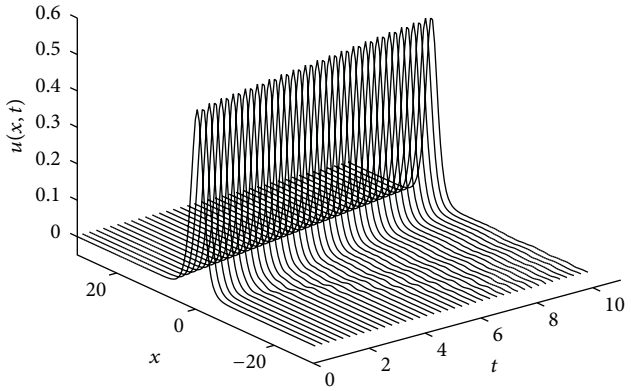

Figure 6: Numerical solutions using the scheme (11) at $t \in [0, 10]$, $x_L = -40$, $x_R = 100$, $h = 0.5$, and $\tau = 0.25$.

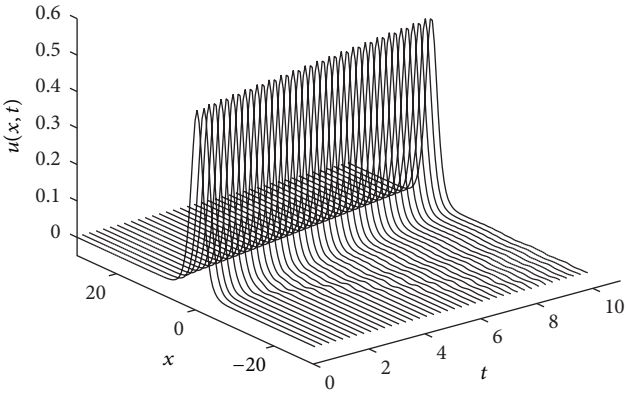

Figure 7: Numerical solutions using the scheme (19) at $t \in [0, 10]$, $x_L = -40$, $x_R = 100$, $h = 0.5$, and $\tau = 0.25$.

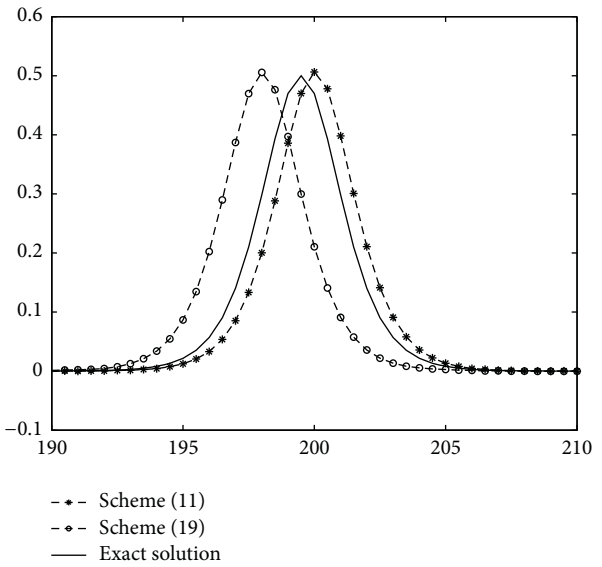

Figure 8: Numerical solutions at $t = 200$, $x_L = -40$, $x_R = 300$, $h = 0.5$, and $\tau = 0.25$.

time behavior of the resolution, the compact fourth-order difference scheme (11) can be seen to be much better than the standard implicit fourth-order scheme (19).

The results of this section suffice to claim that both numerical implementations offer a valid approach toward the numerical investigation of a solution of the KdV equation, especially for the compact finite difference method.

4. Conclusion

Two conservative finite difference schemes for the KdV equation are introduced and analyzed. The construction of the compact finite difference scheme (11) requires only a regular five-point stencil at higher time level, which is similar to the standard second-order Crank-Nicolson scheme, the explicit scheme [16], and the implicit scheme [18]. However, the construction of the standard fourth-order scheme (19) requires a seven-point stencil at higher time level. The accuracy and stability of the numerical schemes for the solutions of the KdV equation can be tested by using the exact solution. In the paper, the numerical experiments show that the present methods support the analysis of convergence rate. The performance of the fourth-order schemes is well efficient at long time by comparing with the second-order schemes [16, 18].

Conflict of Interests

The authors declare that there is no conflict of interests regarding the publication of this paper.

Acknowledgment

This research was supported by Chiang Mai University.

References

[1] D. J. Korteweg and G. de Vries, "On the change of form of long waves advancing in a rectangular canal and on a new type of

long stationary wave," *Philosophical Magazine*, vol. 39, pp. 422–449, 1895.

[2] D. Pavoni, "Single and multidomain Chebyshev collocation methods for the Korteweg-de Vries equation," *Calcolo*, vol. 25, no. 4, pp. 311–346, 1988.

[3] A. A. Soliman, "Collocation solution of the Korteweg-de Vries equation using septic splines," *International Journal of Computer Mathematics*, vol. 81, no. 3, pp. 325–331, 2004.

[4] H. Kalisch and X. Raynaud, "On the rate of convergence of a collocation projection of the KdV equation," *Mathematical Modelling and Numerical Analysis*, vol. 41, no. 1, pp. 95–110, 2007.

[5] G. F. Carey and Y. Shen, "Approximations of the KdV equation by least squares finite elements," *Computer Methods in Applied Mechanics and Engineering*, vol. 93, no. 1, pp. 1–11, 1991.

[6] L. R. T. Gardner, G. A. Gardner, and A. H. A. Ali, "Simulations of solitons using quadratic spline finite elements," *Computer Methods in Applied Mechanics and Engineering*, vol. 92, no. 2, pp. 231–243, 1991.

[7] M. E. Alexander and J. L. Morris, "Galerkin methods applied to some model equations for non-linear dispersive waves," *Journal of Computational Physics*, vol. 30, no. 3, pp. 428–451, 1979.

[8] S. R. Barros and J. W. Cárdenas, "A nonlinear Galerkin method for the shallow-water equations on periodic domains," *Journal of Computational Physics*, vol. 172, no. 2, pp. 592–608, 2001.

[9] H. Ma and W. Sun, "A Legendre-Petrov-Galerkin and Chebyshev collocation method for third-order differential equations," *SIAM Journal on Numerical Analysis*, vol. 38, no. 5, pp. 1425–1438, 2000.

[10] J. Shen, "A new dual-Petrov-Galerkin method for third and higher odd-order differential equations: application to the KDV equation," *SIAM Journal on Numerical Analysis*, vol. 41, no. 5, pp. 1595–1619, 2003.

[11] W. Heinrichs, "Spectral approximation of third-order problems," *Journal of Scientific Computing*, vol. 14, no. 3, pp. 275–289, 1999.

[12] Y. Maday and A. Quarteroni, "Error analysis for spectral approximation of the Korteweg-de Vries equation," *Modélisation Mathématique et Analyse numérique*, vol. 22, no. 3, pp. 499–529, 1988.

[13] S. Zhu, "A scheme with a higher-order discrete invariant for the KdV equation," *Applied Mathematics Letters*, vol. 14, no. 1, pp. 17–20, 2001.

[14] F.-l. Qu and W.-q. Wang, "Alternating segment explicit-implicit scheme for nonlinear third-order KdV equation," *Applied Mathematics and Mechanics. English Edition*, vol. 28, no. 7, pp. 973–980, 2007.

[15] H.-P. Wang, Y.-S. Wang, and Y.-Y. Hu, "An explicit scheme for the KdV equation," *Chinese Physics Letters*, vol. 25, no. 7, pp. 2335–2338, 2008.

[16] N. J. Zabusky and M. D. Kruskal, "Interaction of "solitons" in a collisionless plasma and the recurrence of initial states," *Physical Review Letters*, vol. 15, no. 6, pp. 240–243, 1965.

[17] O. Kolebaje and O. Oyewande, "Numerical solution of the Korteweg-de Vries equation by finite differenece an d adomain decomposition method," *International Journal of Basic and Applied Sciences*, vol. 1, no. 3, pp. 321–335, 2012.

[18] K. Goda, "On stability of some finite difference schemes for the Korteweg-de Vries equation," *Journal of the Physical Society of Japan*, vol. 39, no. 1, pp. 229–236, 1975.

[19] S. Hamdi, W. H. Enright, W. E Schiesser, and J. J. Gottlieb, "Exact solutions and conservation laws for coupled generalized Korteweg-de Vries and quintic regularized long wave equations," *Nonlinear Analysis, Theory, Methods and Applications*, vol. 63, no. 5–7, pp. e1425–e1434, 2005.

Hindawi Publishing Corporation
Advances in Mathematical Physics
Volume 2014, Article ID 734067, 11 pages
http://dx.doi.org/10.1155/2014/734067

Research Article

A Modified Three-Level Average Linear-Implicit Finite Difference Method for the Rosenau-Burgers Equation

Jiraporn Janwised, Ben Wongsaijai, Thanasak Mouktonglang, and Kanyuta Poochinapan

Department of Mathematics, Faculty of Science, Chiang Mai University, Chiang Mai 50200, Thailand

Correspondence should be addressed to Kanyuta Poochinapan; kanyuta@hotmail.com

Received 23 January 2014; Accepted 16 March 2014; Published 17 April 2014

Academic Editor: Pavel Kurasov

We introduce a new technique, a three-level average linear-implicit finite difference method, for solving the Rosenau-Burgers equation. A second-order accuracy on both space and time numerical solution of the Rosenau-Burgers equation is obtained using a five-point stencil. We prove the existence and uniqueness of the numerical solution. Moreover, the convergence and stability of the numerical solution are also shown. The numerical results show that our method improves the accuracy of the solution significantly.

1. Introduction

A nonlinear wave phenomenon is the important area of scientific research. There are mathematical models which describe the dynamic of wave behaviors such as the KdV equation, the Rosenau equation, and many others. The KdV equation cannot explain the wave-wave and wave-wall interactions for the model of the dynamics of compact discrete systems. Therefore, Rosenau [1, 2] presented the novel model, which is more suitable than the KdV equation, as follows:

$$u_t + u_{xxxxt} + u_x + uu_x = 0. \tag{1}$$

The existence and uniqueness of the solution for this equation were proved by Park [3]. Many methods have been applied to find a numerical solution of the Rosenau equation such as a discontinuous Galerkin method [4], a finite element Galerkin method [5], and a finite difference method [6–8]. Numerical solutions and error estimates in $\|\cdot\|$ and $\|\cdot\|_\infty$ norms were obtained for the Rosenau equation in one space variable [9].

As for Burgers' equation,

$$u_t - u_{xx} + uu_x = 0, \tag{2}$$

this equation has been studied in the evolution equation describing a wave propagation. Moreover, the simulation for Burgers' equation was the very first step of conceptual understanding of the method for the computations of complex flow. The existence and uniqueness of the generalized Burgers' equation have been shown with certain conditions.

In this paper, we consider the following initial-boundary value problem of the generalized Rosenau-Burgers equation:

$$u_t + u_{xxxxt} - \alpha u_{xx} + \beta u_x + \left(u^p\right)_x = 0, \quad 0 \le x \le 1, \quad 0 \le t \le T, \tag{3}$$

with an initial condition

$$u(x,0) = u_0(x), \quad 0 \le x \le 1, \tag{4}$$

and boundary conditions

$$u(0,t) = u(1,t) = 0, \qquad u_{xx}(0,t) = u_{xx}(1,t) = 0, \quad 0 \le t \le T, \tag{5}$$

where $\alpha > 0$, $\beta \in \mathbb{R}$, and $p \ge 2$ is an integer.

This equation was proposed in 1989 to describe the wave in shallow water. It differs from Burgers' equation by an additional strongly dissipative term u_{xxxxt}. The behavior of the solution to the Rosenau-Burgers equation with the Cauchy problem has been well studied for the past years [10–13]. Several second-order accuracy finite difference methods in space were used for finding numerical solutions on both linear and nonlinear terms [14–20].

Hu et al. [14] have proposed the Crank-Nicolson difference scheme, nonlinear scheme, for the Rosenau-Burgers equation. Hu et al. [18] have proposed a three-level average implicit finite difference scheme for the Rosenau-Burgers equation. The schemes are obviously implicit and require a heavy calculation for each iteration. Pan and Zhang [20] have proposed a three-level linear-implicit difference scheme. The schemes, we have mentioned above, are second-order accuracy on both time and space.

In this paper, we propose a modified three-level average linear-implicit finite difference method for the Rosenau-Burgers equation. By comparing with the existence second-order accuracy finite difference scheme on a test problem, our new technique gives a better maximal error of the numerical solutions. A second-order accuracy on both space and time numerical solution of the equation is obtained using a five-point stencil.

This paper is organized into 7 sections. In Section 2, we describe our modified finite different scheme. In Section 3, we discuss the solvability of our scheme. The existence and uniqueness are also proven in this section. In Section 4, we give complete proofs on the convergence and stability of the finite difference scheme which is second-order accuracy on both space and time. The numerical results are given in Section 5 to confirm and illustrate our theoretical analysis. Then we finish our paper by concluding remarks.

2. Modified Finite Difference Scheme

In this section, we give a complete description of our modified finite difference scheme and an algorithm for the formulation of the problem (3)–(5). We first describe our solution domain and its grid. We define the solution domain to be $Q = \{(x,t) \mid 0 \le x \le 1,\ 0 \le t \le T\}$, which is covered by a uniform grid $Q_h = \{(x_i,t_n) \mid x_i = ih,\ t_n = n\tau,\ i = 0,\dots,J,\ n = 0,\dots,N\}$, with spacings $h = 1/J$ and $\tau = T/N$. Denote $u_i^n \approx u(ih, n\tau)$ and $Z_h^0 = \{u = (u_i) \mid u_0 = u_J = 0,\ i = -1, 0,\dots,J, J+1\}$. Throughout this paper, we will denote C as a generic constant independent of step sizes τ and h. For nonnegative integer k, let $H^k(\Omega)$ denote the usual Sobolev space of real-valued functions defined on Ω. We define the following Sobolev space:

$$H_0^k(\Omega) = \left\{ u \in H^k(\Omega) : \frac{\partial^i u}{\partial u^i} = 0 \ \text{ on } \ \partial\Omega,\ i = 0, 1, \dots, k-1 \right\}. \tag{6}$$

We use the following notations for the simplicity:

$$\overline{u}_i^n = \frac{u_i^{n+1} + u_i^{n-1}}{2}, \qquad \left(u_i^n\right)_{\hat{t}} = \frac{u_i^{n+1} - u_i^{n-1}}{2\tau},$$
$$\left(u_i^n\right)_x = \frac{u_{i+1}^n - u_i^n}{h}, \qquad \left(u_i^n\right)_{\bar{x}} = \frac{u_i^n - u_{i-1}^n}{h},$$
$$\left(u_i^n\right)_{\hat{x}} = \frac{u_{i+1}^n - u_{i-1}^n}{2h}, \qquad \left(u_i^n\right)_{x\bar{x}} = \frac{u_{i+1}^n - 2u_i^n + u_{i-1}^n}{h^2},$$
$$\left(u^n, v^n\right) = h\sum_{i=1}^{J-1} u_i^n v_i^n, \qquad \left\|u^n\right\|^2 = \left(u^n, u^n\right),$$
$$\left\|u^n\right\|_\infty = \max_{1\le i\le J-1} \left|u_i^n\right|. \tag{7}$$

Since $(u^p)_x = p/(p+1)[u^{p-1}u_x + (u^p)_x]$, the following finite difference scheme solves the problem (3)–(5):

$$\left(u_i^n\right)_{\hat{t}} + \frac{h^2}{6}\left(u_i^n\right)_{x\bar{x}\hat{t}} - \frac{\alpha h^2}{12}\left(\overline{u}_i^n\right)_{xx\bar{x}\bar{x}} + \left(u_i^n\right)_{xx\bar{x}\bar{x}\hat{t}} - \alpha\left(\overline{u}_i^n\right)_{x\bar{x}} + \beta\left(\overline{u}_i^n\right)_{\hat{x}} + \psi\left(u_i^n, \overline{u}_i^n\right) = 0, \quad 1 \le i \le J-1, \tag{8}$$

$$u_0^n = u_J^n = 0, \quad \left(u_0^n\right)_{x\bar{x}} = \left(u_J^n\right)_{x\bar{x}} = 0, \quad 1 \le n \le N, \tag{9}$$

$$u_i^0 = u_0\left(x_i\right), \tag{10}$$

where

$$\psi\left(u_i^n, \overline{u}_i^n\right) = \frac{p}{p+1}\left[\left(u_i^n\right)^{p-1}\left(\overline{u}_i^n\right)_{\hat{x}} + \left(\left(u_i^n\right)^{p-1}\overline{u}_i^n\right)_{\hat{x}}\right]. \tag{11}$$

The following lemmas are some properties of the above finite difference scheme which can be obtained directly from the definition. They are essential for existence, uniqueness, convergence, and stability of our numerical solution.

Lemma 1 (Hu et al. [14]). *For any two mesh functions $u, v \in Z_h^0$, we have*

$$\left(u_x, v\right) = -\left(u, v_{\bar{x}}\right), \qquad \left(v, u_{x\bar{x}}\right) = -\left(v_x, u_x\right),$$
$$\left(u, u_{x\bar{x}}\right) = -\left(u_x, u_x\right) = -\left\|u_x\right\|^2. \tag{12}$$

Furthermore, if $(u_0)_{x\bar{x}} = (u_J)_{x\bar{x}} = 0$, then

$$\left(u, u_{xx\bar{x}\bar{x}}\right) = \left\|u_{x\bar{x}}\right\|^2. \tag{13}$$

Lemma 2 (discrete Sobolev's inequality [9]). *There exist constants C_1 and C_2 such that*

$$\left\|u^n\right\|_\infty \le C_1\left\|u^n\right\| + C_2\left\|u_x^n\right\|. \tag{14}$$

The following theorem guarantees that the numerical solution obtained from scheme (8)-(9) is bounded.

Theorem 3. *Suppose $u_0 \in H_0^2[0,L]$. Then there is an estimation for the solution u^n of the scheme (8)-(9) that satisfies*

$$\left\|u^n\right\| \le C, \qquad \left\|u_{x\bar{x}}^n\right\| \le C \tag{15}$$

which imply $\|u^n\|_\infty \le C$ for some $C \in \mathbb{R}$.

Proof. Consider the inner product between (8) and $2\overline{u}^n \equiv (u^{n+1} + u^{n-1})$. According to Lemma 1, we have

$$\frac{1}{2\tau}\left(\left\|u^{n+1}\right\|^2 - \left\|u^{n-1}\right\|^2\right) - \frac{h^2}{12\tau}\left(\left\|u_x^{n+1}\right\|^2 - \left\|u_x^{n-1}\right\|^2\right) - \frac{\alpha h^2}{6}\left\|\overline{u}_{x\bar{x}}^n\right\|^2 + \frac{1}{2\tau}\left(\left\|u_{x\bar{x}}^{n+1}\right\|^2 - \left\|u_{x\bar{x}}^{n-1}\right\|^2\right) + 2\alpha\left\|\overline{u}_x^n\right\|^2 + \beta\left(\overline{u}_{\hat{x}}^n, 2\overline{u}^n\right) + \left(\psi\left(u^n, \overline{u}^n\right), 2\overline{u}^n\right) = 0. \tag{16}$$

By a direct calculation and the boundary condition (9), we have

$$\begin{aligned}\left(\overline{u}_{\bar{x}}^{n}, 2\overline{u}^{n}\right) &= 2h\sum_{i=1}^{J-1}\left[\frac{1}{2h}\left(\overline{u}_{i+1}^{n}-\overline{u}_{i-1}^{n}\right)\overline{u}_{i}^{n}\right] \\ &= \sum_{i=1}^{J-1}\overline{u}_{i}^{n}\overline{u}_{i+1}^{n}-\sum_{i=1}^{J-1}\overline{u}_{i-1}^{n}\overline{u}_{i}^{n}=0.\end{aligned} \tag{17}$$

Furthermore, by using the definition of the inner product

$$\begin{aligned}&\left(\psi\left(u^{n},\overline{u}^{n}\right),2\overline{u}^{n}\right) \\ &= \frac{2p}{p+1}h\sum_{i=1}^{J-1}\left[\left(u_{i}^{n}\right)^{p-1}\left(\overline{u}_{i}^{n}\right)_{\hat{x}}+\left(\left(u_{i}^{n}\right)^{p-1}\overline{u}_{i}^{n}\right)_{\hat{x}}\right]\overline{u}_{i}^{n} \\ &= \frac{p}{p+1}\sum_{i=1}^{J-1}\left[\left(u_{i}^{n}\right)^{p-1}\left(\overline{u}_{i+1}^{n}-\overline{u}_{i-1}^{n}\right)+\left(u_{i+1}^{n}\right)^{p-1}\overline{u}_{i+1}^{n}\right. \\ &\qquad \left.-\left(u_{i-1}^{n}\right)^{p-1}\overline{u}_{i-1}^{n}\right]\overline{u}_{i}^{n} \\ &= \frac{p}{p+1}\sum_{i=1}^{J-1}\left[\left(u_{i}^{n}\right)^{p-1}\overline{u}_{i+1}^{n}\overline{u}_{i}^{n}-\left(u_{i-1}^{n}\right)^{p-1}\overline{u}_{i}^{n}\overline{u}_{i-1}^{n}\right] \\ &\quad -\frac{p}{p+1}\sum_{i=1}^{J-1}\left[\left(u_{i}^{n}\right)^{p-1}\overline{u}_{i}^{n}\overline{u}_{i-1}^{n}-\left(u_{i+1}^{n}\right)^{p-1}\overline{u}_{i+1}^{n}\overline{u}_{i}^{n}\right]=0.\end{aligned} \tag{18}$$

From (17) and (18), (16) can be rewritten as

$$\begin{aligned}&\frac{1}{2\tau}\left(\left\|u^{n+1}\right\|^{2}-\left\|u^{n-1}\right\|^{2}\right)-\frac{h^{2}}{12\tau}\left(\left\|u_{x}^{n+1}\right\|^{2}-\left\|u_{x}^{n-1}\right\|^{2}\right) \\ &\quad -\frac{\alpha h^{2}}{6}\left\|\overline{u}_{x\bar{x}}^{n}\right\|^{2}+\frac{1}{2\tau}\left(\left\|u_{x\bar{x}}^{n+1}\right\|^{2}-\left\|u_{x\bar{x}}^{n-1}\right\|^{2}\right) \\ &\quad +2\alpha\left\|\overline{u}_{x}^{n}\right\|^{2}=0.\end{aligned} \tag{19}$$

Therefore,

$$\begin{aligned}&\left(\left\|u^{n+1}\right\|^{2}-\left\|u^{n-1}\right\|^{2}\right)-\frac{h^{2}}{6}\left(\left\|u_{x}^{n+1}\right\|^{2}-\left\|u_{x}^{n-1}\right\|^{2}\right) \\ &\quad +\left(\left\|u_{x\bar{x}}^{n+1}\right\|^{2}-\left\|u_{x\bar{x}}^{n-1}\right\|^{2}\right)\le\frac{\alpha\tau h^{2}}{6}\left(\left\|u_{x\bar{x}}^{n+1}\right\|^{2}+\left\|u_{x\bar{x}}^{n-1}\right\|^{2}\right).\end{aligned} \tag{20}$$

We now define

$$\begin{aligned}E^{n}\equiv&\left(\left\|u^{n}\right\|^{2}+\left\|u^{n-1}\right\|^{2}\right)-\frac{h^{2}}{6}\left(\left\|u_{x}^{n}\right\|^{2}+\left\|u_{x}^{n-1}\right\|^{2}\right) \\ &+\left(\left\|u_{x\bar{x}}^{n}\right\|^{2}+\left\|u_{x\bar{x}}^{n-1}\right\|^{2}\right).\end{aligned} \tag{21}$$

Then inequality (20) can be rewritten as follows:

$$E^{n+1}-E^{n}\le\tau C\left(E^{n+1}+E^{n}\right). \tag{22}$$

If τ is sufficiently small which satisfies $\tau\le(k-2)/kC$ and $k>2$, then

$$\begin{aligned}E^{n+1}&\le\frac{(1+\tau C)}{(1-\tau C)}E^{n}\le(1+\tau kC)E^{n}\le(1+\tau kC)^{n}E^{1} \\ &\le\exp(kCT)E^{1}.\end{aligned} \tag{23}$$

Hence,

$$\begin{aligned}&\left(\left\|u^{n+1}\right\|^{2}+\left\|u^{n}\right\|^{2}\right)-\frac{h^{2}}{6}\left(\left\|u_{x}^{n+1}\right\|^{2}+\left\|u_{x}^{n}\right\|^{2}\right) \\ &\quad +\left(\left\|u_{x\bar{x}}^{n+1}\right\|^{2}+\left\|u_{x\bar{x}}^{n}\right\|^{2}\right)\le C.\end{aligned} \tag{24}$$

By using Lemma 1 and the Cauchy-Schwarz inequality, we arrive at

$$\left\|u_{x}^{n}\right\|^{2}\le\frac{1}{2}\left(\left\|u^{n}\right\|^{2}+\left\|u_{x\bar{x}}^{n}\right\|^{2}\right). \tag{25}$$

Then, we get

$$\left(1-\frac{h^{2}}{12}\right)\left[\left(\left\|u^{n+1}\right\|^{2}+\left\|u^{n}\right\|^{2}\right)+\left(\left\|u_{x\bar{x}}^{n+1}\right\|^{2}+\left\|u_{x\bar{x}}^{n}\right\|^{2}\right)\right]\le C. \tag{26}$$

If h is sufficiently small in which $(1-h^{2}/12)>0$, we arrive at that

$$\left\|u^{n+1}\right\|\le C,\qquad\left\|u_{x\bar{x}}^{n+1}\right\|\le C. \tag{27}$$

From (25), it follows that $\|u_{x}^{n+1}\|\le C$. By Lemma 2, it is obvious that $\|u^{n+1}\|_{\infty}\le C$ and that completes the proof. □

3. Solvability

In this section, we prove the solvability of a solution for scheme (8). This guarantees the existence and uniqueness of our numerical solution.

Theorem 4. *The finite difference scheme* (8)–(10) *is uniquely solvable.*

Proof. To prove the theorem, we proceed by the mathematical induction. We assume that $u^{0},u^{1},\ldots,u^{n}$ satisfy the difference scheme (8). Indeed, u^{1} can be computed by an available second-order accuracy method. Next we prove that there exists u^{n+1} which satisfied (8). Consider

$$\begin{aligned}&\frac{1}{2\tau}u_{i}^{n+1}-\left(\frac{\alpha}{2}-\frac{h^{2}}{12\tau}\right)\left(u_{i}^{n+1}\right)_{x\bar{x}}+\left(\frac{1}{2\tau}-\frac{\alpha h^{2}}{24}\right)\left(u_{i}^{n+1}\right)_{xx\bar{x}\bar{x}} \\ &\quad +\frac{\beta}{2}\left(u_{i}^{n+1}\right)_{\hat{x}}+\frac{1}{2}\psi\left(u_{i}^{n},u_{i}^{n+1}\right)=0,\quad 1\le i\le J-1,\end{aligned} \tag{28}$$

where

$$\psi\left(u_{i}^{n},u_{i}^{n+1}\right)=\frac{p}{p+1}\left[\left(u_{i}^{n}\right)^{p-1}\left(u_{i}^{n+1}\right)_{\hat{x}}+\left(\left(u_{i}^{n}\right)^{p-1}u_{i}^{n+1}\right)_{\hat{x}}\right]. \tag{29}$$

By taking the inner product of (28) with u^{n+1} and using Lemma 1, we obtain

$$\begin{aligned}&\frac{1}{2\tau}\left\|u^{n+1}\right\|^{2}+\left(\frac{\alpha}{2}-\frac{h^{2}}{12\tau}\right)\left\|u_{x}^{n+1}\right\|^{2}+\left(\frac{1}{2\tau}-\frac{\alpha h^{2}}{24}\right)\left\|u_{x\bar{x}}^{n+1}\right\|^{2} \\ &\quad +\frac{1}{2}\left(\psi\left(u^{n},u^{n+1}\right),u^{n+1}\right)=0.\end{aligned} \tag{30}$$

Notice that

$$\begin{aligned}
&\left(\psi\left(u^n, u^{n+1}\right), u^{n+1}\right) \\
&= \frac{hp}{p+1}\sum_{i=1}^{J-1}\left[\left(u_i^n\right)^{p-1}\left(u_i^{n+1}\right)_{\hat{x}} + \left(\left(u_i^n\right)^{p-1}u_i^{n+1}\right)_{\hat{x}}\right]u_i^{n+1} \\
&= \frac{p}{2(p+1)}\sum_{i=1}^{J-1}\left[\left(u_i^n\right)^{p-1}\left(u_{i+1}^{n+1} - u_{i-1}^{n+1}\right)\right. \\
&\qquad \left. + \left(u_{i+1}^n\right)^{p-1}u_{i+1}^{n+1} - \left(u_{i-1}^n\right)^{p-1}u_{i-1}^{n+1}\right]u_i^{n+1} \\
&= \frac{p}{2(p+1)}\sum_{i=1}^{J-1}\left[\left(u_i^n\right)^{p-1}u_{i+1}^{n+1}u_i^{n+1} - \left(u_{i-1}^n\right)^{p-1}u_{i-1}^{n+1}u_i^{n+1}\right] \\
&\quad - \frac{p}{2(p+1)}\sum_{i=1}^{J-1}\left[\left(u_i^n\right)^{p-1}u_{i-1}^{n+1}u_i^{n+1} - \left(u_{i+1}^n\right)^{p-1}u_{i+1}^{n+1}u_i^{n+1}\right] = 0.
\end{aligned} \tag{31}$$

Hence,

$$\left\|u^{n+1}\right\|^2 + \left(\alpha\tau - \frac{h^2}{6}\right)\left\|u_x^{n+1}\right\|^2 + \left(1 - \frac{\alpha\tau h^2}{12}\right)\left\|u_{x\bar{x}}^{n+1}\right\|^2 = 0. \tag{32}$$

Similar to the proof of inequality (25), (32) can be rewritten as

$$\left(1 - \frac{h^2}{12}\right)\left(\left\|u^{n+1}\right\|^2 + \left\|u_{x\bar{x}}^{n+1}\right\|^2\right) \le \frac{\alpha\tau h^2}{12}\left\|u_{x\bar{x}}^{n+1}\right\|^2. \tag{33}$$

For h and τ are sufficiently small which satisfies $1-(h^2/12)(1-\alpha\tau) > 0$, we obtain

$$\left\|u^{n+1}\right\|^2 + \left\|u_{x\bar{x}}^{n+1}\right\|^2 \le 0. \tag{34}$$

It follows that

$$\left\|u^{n+1}\right\|^2 = \left\|u_{x\bar{x}}^{n+1}\right\|^2 = 0. \tag{35}$$

This implies that there uniquely exists a trivial solution satisfying (8)–(10). Hence, u^{n+1} is uniquely solvable. This completes the proof. □

4. Convergence and Stability

In this section, the second-order rate of convergence and stability of scheme (8)-(9) are guaranteed and explicitly proved. Let $e_i^n = v_i^n - u_i^n$, where v_i^n and u_i^n are the solutions of the problem (3)–(5) and the problem (8)-(9), respectively. We arrive at the following error equation:

$$\begin{aligned}
r_i^n &= \left(e_i^n\right)_{\hat{t}} + \frac{h^2}{6}\left(e_i^n\right)_{x\bar{x}\hat{t}} - \frac{\alpha h^2}{12}\left(\bar{e}_i^n\right)_{xx\bar{x}\bar{x}} + \left(e_i^n\right)_{xx\bar{x}\bar{x}\hat{t}} - \alpha\left(\bar{e}_i^n\right)_{x\bar{x}} \\
&\quad + \beta\left(\bar{e}_i^n\right)_{\hat{x}} + \frac{p}{p+1}\left[\left(v_i^n\right)^{p-1}\left(\bar{v}_i^n\right)_{\hat{x}} + \left(\left(v_i^n\right)^{p-1}\bar{v}_i^n\right)_{\hat{x}}\right] \\
&\quad - \frac{p}{p+1}\left[\left(u_i^n\right)^{p-1}\left(\bar{u}_i^n\right)_{\hat{x}} + \left(\left(u_i^n\right)^{p-1}\bar{u}_i^n\right)_{\hat{x}}\right],
\end{aligned} \tag{36}$$

where r_i^n denotes the truncation error. By the Taylor expansion, we easily obtain that $r_i^n = O(\tau^2 + h^2)$ holds as $\tau, h \to 0$. The following lemmas are well known and useful for the proofs of the convergence and stability.

Lemma 5 (Zheng and Hu [16]). *Suppose that $u \in H_0^2[0, L]$. Then the solution of the initial-boundary value problem (3)–(5) satisfies*

$$\|u\|_{L_2} \le C, \qquad \|u_{xx}\|_{L_2} \le C, \qquad \|u\|_{L_\infty} \le C, \tag{37}$$

for a constant C.

Lemma 6 (discrete Gronwall inequality [9]). *Suppose $w(k)$, $\rho(k)$ are nonnegative mesh functions and $\rho(k)$ is a nondecreasing function. If $C > 0$ and*

$$w(k) \le \rho(k) + C\tau\sum_{l=0}^{k-1} w(l), \quad \forall k, \tag{38}$$

then

$$w(k) \le \rho(k)\, e^{C\tau k}, \quad \forall k. \tag{39}$$

The following theorem guarantees the convergence of our scheme with the convergence rate of $O(\tau^2 + h^2)$.

Theorem 7. *Suppose $u_0 \in H_0^2[0, L]$. Then the solution u^n of scheme (8)-(9) converges to the solution of the problem (3)–(5) in the sense of $\|\cdot\|_\infty$ and the rate of convergence is $O(\tau^2 + h^2)$.*

Proof. By taking the inner product of (8) and $2\bar{e}^n \equiv e^{n+1} + e^{n-1}$ and using the fact that $(e_{\hat{x}}^n, 2\bar{e}^n) = 0$, we get

$$\begin{aligned}
&\frac{1}{2\tau}\left(\left\|e^{n+1}\right\|^2 - \left\|e^{n-1}\right\|^2\right) - \frac{h^2}{12\tau}\left(\left\|e_x^{n+1}\right\|^2 - \left\|e_x^{n-1}\right\|^2\right) \\
&\qquad - \frac{\alpha h^2}{6}\left\|\bar{e}_{x\bar{x}}^n\right\|^2 + \frac{1}{2\tau}\left(\left\|e_{x\bar{x}}^{n+1}\right\|^2 - \left\|e_{x\bar{x}}^{n-1}\right\|^2\right) + 2\alpha\left\|\bar{e}_x^n\right\|^2 \\
&\qquad = \left(r^n, 2\bar{e}^n - \left(M_1 + M_2, 2\bar{e}^n\right)\right),
\end{aligned} \tag{40}$$

where

$$\begin{aligned}
M_1 &= \frac{p}{p+1}\left[\left(v^n\right)^{p-1}\left(\bar{v}^n\right)_{\hat{x}} - \left(u^n\right)^{p-1}\left(\bar{u}^n\right)_{\hat{x}}\right], \\
M_2 &= \frac{p}{p+1}\left[\left(\left(v^n\right)^{p-1}\bar{v}^n\right)_{\hat{x}} - \left(\left(u^n\right)^{p-1}\bar{u}^n\right)_{\hat{x}}\right].
\end{aligned} \tag{41}$$

According to Lemma 5, Theorem 3, and the Cauchy-Schwartz inequality, we have

$$\begin{aligned}
&\left(M_1, 2\bar{e}^n\right) \\
&= \frac{2p}{p+1}h\sum_{i=1}^{J-1}\left[\left(v_i^n\right)^{p-1}\left(\bar{v}_i^n\right)_{\hat{x}} - \left(u_i^n\right)^{p-1}\left(\bar{u}_i^n\right)_{\hat{x}}\right]\bar{e}_i^n \\
&= \frac{2p}{p+1}h\sum_{i=1}^{J-1}\left[\left(v_i^n\right)^{p-1}\left(\bar{e}_i^n\right)_{\hat{x}}\bar{e}_i^n\right] \\
&\quad + \frac{2p}{p+1}h\sum_{i=1}^{J-1}\left[\left(v_i^n\right)^{p-1} - \left(u_i^n\right)^{p-1}\right]\left(\bar{u}_i^n\right)_{\hat{x}}\bar{e}_i^n
\end{aligned}$$

$$
\begin{aligned}
&= \frac{2p}{p+1}h\sum_{i=1}^{J-1}\left[(v_i^n)^{p-1}(\overline{e}_i^n)_{\hat{x}}\overline{e}_i^n\right] \\
&\quad + \frac{2p}{p+1}h\sum_{i=1}^{J-1}\left[e_i^n\sum_{k=0}^{p-2}(v_i^n)^{p-2-k}(u_i^n)^k\right](\overline{u}_i^n)_{\hat{x}}\overline{e}_i^n \\
&\le C\left(\left\|\overline{e}_{\hat{x}}^n\right\|^2 + \left\|\overline{e}^n\right\|^2 + \left\|e^n\right\|^2\right) \\
&\le C\left(\left\|e_{\hat{x}}^{n+1}\right\|^2 + \left\|e_{\hat{x}}^{n-1}\right\|^2 + \left\|e^{n+1}\right\|^2 + \left\|e^n\right\|^2 + \left\|e^{n-1}\right\|^2\right).
\end{aligned} \tag{42}
$$

Similar to the proof of (42), we have also

$$
\begin{aligned}
(M_2, 2\overline{e}^n) &\le C\left(\left\|\overline{e}_{\hat{x}}^n\right\|^2 + \left\|\overline{e}^n\right\|^2 + \left\|e^n\right\|^2\right) \\
&\le C\left(\left\|e_{\hat{x}}^{n+1}\right\|^2 + \left\|e_{\hat{x}}^{n-1}\right\|^2\right. \\
&\quad \left. + \left\|e^{n+1}\right\|^2 + \left\|e^n\right\|^2 + \left\|e^{n-1}\right\|^2\right).
\end{aligned} \tag{43}
$$

Furthermore,

$$
\left\|e_{\hat{x}}^n\right\|^2 \le \left\|e_x^n\right\|^2 \le \frac{1}{2}\left(\left\|e^n\right\|^2 + \left\|e_{x\overline{x}}^n\right\|^2\right), \tag{44}
$$

$$
(r^n, 2\overline{e}^n) \le \left\|r^n\right\|^2 + \frac{1}{2}\left(\left\|e^{n+1}\right\|^2 + \left\|e^{n-1}\right\|^2\right). \tag{45}
$$

By substituting (42)–(45) into (40), we obtain

$$
\begin{aligned}
&\frac{1}{2\tau}\left(\left\|e^{n+1}\right\|^2 - \left\|e^{n-1}\right\|^2\right) \\
&\quad - \frac{h^2}{12\tau}\left(\left\|e_x^{n+1}\right\|^2 - \left\|e_x^{n-1}\right\|^2\right) - \frac{\alpha h^2}{6}\left\|\overline{e}_{x\overline{x}}^n\right\|^2 \\
&\quad + \frac{1}{2\tau}\left(\left\|e_{x\overline{x}}^{n+1}\right\|^2 - \left\|e_{x\overline{x}}^{n-1}\right\|^2\right) + 2\alpha\left\|\overline{e}_x^n\right\|^2 \\
&\le \left\| r^n\right\|^2 + C\left(\left\|e_{x\overline{x}}^{n+1}\right\|^2 + \left\|e_{x\overline{x}}^n\right\|^2 + \left\|e_{x\overline{x}}^{n-1}\right\|^2\right. \\
&\quad \left. + \left\|e^{n+1}\right\|^2 + \left\|e^n\right\|^2 + \left\|e^{n-1}\right\|^2\right).
\end{aligned} \tag{46}
$$

Hence,

$$
\begin{aligned}
&\left(\left\|e^{n+1}\right\|^2 - \left\|e^{n-1}\right\|^2\right) - \frac{h^2}{6}\left(\left\|e_x^{n+1}\right\|^2 - \left\|e_x^{n-1}\right\|^2\right) \\
&\quad + \left(\left\|e_{x\overline{x}}^{n+1}\right\|^2 - \left\|e_{x\overline{x}}^{n-1}\right\|^2\right) \le 2\tau\left\|r^n\right\|^2 \\
&\quad + C\tau\left(\left\|e_{x\overline{x}}^{n+1}\right\|^2 + \left\|e_{x\overline{x}}^n\right\|^2 + \left\|e_{x\overline{x}}^{n-1}\right\|^2\right. \\
&\quad \left. + \left\|e^{n+1}\right\|^2 + \left\|e^n\right\|^2 + \left\|e^{n-1}\right\|^2\right).
\end{aligned} \tag{47}
$$

Let

$$
\begin{aligned}
E^n &= \left(\left\|e^n\right\|^2 + \left\|e^{n-1}\right\|^2\right) - \frac{h^2}{6}\left(\left\|e_x^n\right\|^2 + \left\|e_x^{n-1}\right\|^2\right) \\
&\quad + \left(\left\|e_{x\overline{x}}^n\right\|^2 + \left\|e_{x\overline{x}}^{n-1}\right\|^2\right), \\
B^n &= \left(\left\|e^n\right\|^2 + \left\|e^{n-1}\right\|^2\right) + \left(\left\|e_{x\overline{x}}^n\right\|^2 + \left\|e_{x\overline{x}}^{n-1}\right\|^2\right).
\end{aligned} \tag{48}
$$

From (44), then (47) can be rewritten as

$$
E^{n+1} - E^n \le 2\tau\left\|r^n\right\|^2 + \tau C\left(E^{n+1} + E^n\right). \tag{49}
$$

That is,

$$
(1 - C\tau)\left(E^{n+1} - E^n\right) \le 2\tau\left\|r^n\right\|^2 + 2C\tau E^n. \tag{50}
$$

If τ is sufficiently small which satisfies $1 - C\tau > 0$, then

$$
E^{n+1} - E^n \le C\tau\left\|r^n\right\|^2 + C\tau E^n. \tag{51}
$$

Summing up from 1 to n, we have

$$
E^{n+1} - E^1 \le C\tau\sum_{k=1}^{n}\left\|r^k\right\|^2 + C\tau\sum_{k=1}^{n}E^k. \tag{52}
$$

Then

$$
E^{n+1} \le E^1 + C\tau\sum_{k=1}^{n}\left\|r^k\right\|^2 + C\tau\sum_{k=1}^{n}E^k. \tag{53}
$$

Using (44), we obtain that

$$
\frac{1}{2}B^n \le E^n \le B^n. \tag{54}
$$

Equations (53) and (54) yield

$$
\frac{1}{2}B^{n+1} \le B^1 + C\tau\sum_{k=1}^{n}\left\|r^k\right\|^2 + C\tau\sum_{k=1}^{n}B^k, \tag{55}
$$

which is equivalent to

$$
B^{n+1} \le 2B^1 + C\tau\sum_{k=1}^{n}\left\|r^k\right\|^2 + C\tau\sum_{k=1}^{n}B^k. \tag{56}
$$

Notice that

$$
\tau\sum_{k=1}^{n}\left\|r^k\right\|^2 \le n\tau\max_{1\le k\le n}\left\|r^k\right\|^2 \le T\cdot O\left(\tau^2 + h^2\right)^2. \tag{57}
$$

Since we can approximate u^1 using any available second-order accuracy method, we have $B^1 = O(\tau^2 + h^2)^2$. Hence

$$
B^{n+1} \le O\left(\tau^2 + h^2\right)^2 + C\tau\sum_{k=1}^{n}B^k. \tag{58}
$$

According to Lemma 6, $B^{n+1} \le O(\tau^2 + h^2)^2$ implies

$$
\left\|e^{n+1}\right\| \le O\left(\tau^2 + h^2\right), \qquad \left\|e_{x\overline{x}}^{n+1}\right\| \le O\left(\tau^2 + h^2\right). \tag{59}
$$

It follows from (44) that

$$
\left\|e_x^{n+1}\right\| \le O\left(\tau^2 + h^2\right). \tag{60}
$$

By using Lemma 2, we have

$$
\left\|e^{n+1}\right\|_\infty \le O\left(\tau^2 + h^2\right). \tag{61}
$$

This completes the proof of Theorem 7. □

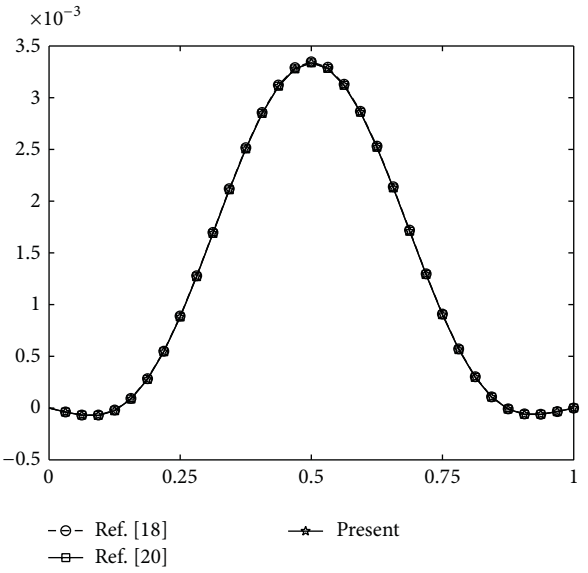

Figure 1: Numerical solutions at $t = 10$, $h = 1/32$, $\tau = 0.1$, $\beta = 1$, $\alpha = 2$, and $p = 4$.

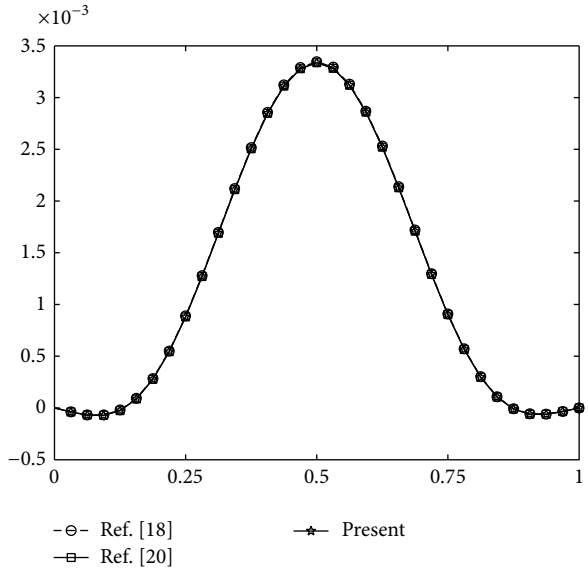

Figure 2: Numerical solutions at $t = 10$, $h = 1/32$, $\tau = 0.1$, $\beta = 1$, $\alpha = 2$, and $p = 8$.

Theorem 8. *Under the conditions of Theorem 7, the solution of scheme* (8)-(9) *is stable with respect to* $\|\cdot\|_\infty$.

5. Numerical Experiments

In this section, we present numerical experiments on a test problem

$$u_t + u_{xxxxt} - \alpha u_{xx} + \beta u_x + \left(u^p\right)_x = 0, \quad 0 \le x \le 1, \quad 0 \le t \le 10, \tag{62}$$

with an initial condition

$$u(x,0) = u_0(x) = x^4(1-x)^4, \quad 0 \le x \le 1, \tag{63}$$

and boundary conditions

$$u(0,t) = u(1,t) = 0, \qquad u_{xx}(0,t) = u_{xx}(1,t) = 0, \quad 0 \le t \le 10, \tag{64}$$

to confirm and illustrate the accuracy of our method. Since the exact solution is not known, the finest grid ($h = 1/256$) is used as a reference solution (pseudoanalytical solution). We make comparisons between schemes proposed in [18, 20] with our scheme (8), which is also second-order in space and time. The errors from the three schemes are presented in Tables 1, 2, and 3. For $p = 2, 4$, and 8, it is clear that our scheme gives better approximation than both schemes proposed in [18, 20].

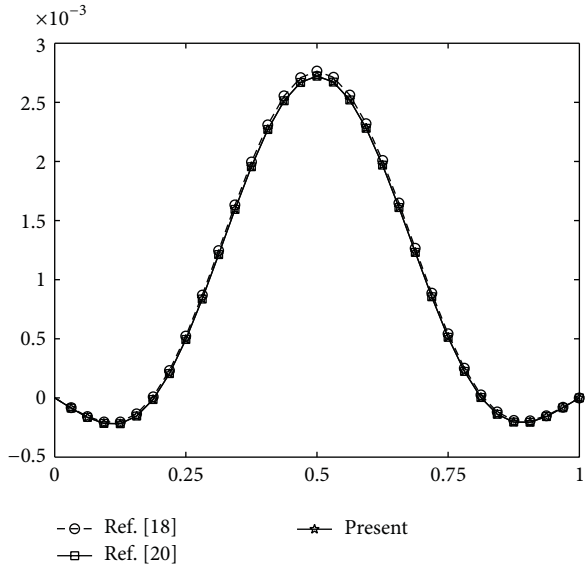

Figure 3: Numerical solutions at $t = 10$, $h = 1/32$, $\tau = 0.1$, $\beta = 1$, $\alpha = 4$, and $p = 4$.

The corresponding errors with respect to $\|\cdot\|$ and $\|\cdot\|_\infty$-norm are listed in Tables 4, 5, and 6 for $p = 2, 4$, and 8. The rate of convergence is computed using two grids according to the formula

$$\text{rate} = \log_2 \frac{\|e_h\|}{\|e_{h/2}\|}. \tag{65}$$

Since we have five grids, we can get four different estimations of the convergent rates. As shown in Tables 4, 5, and 6 for one particular choice of the parameters, the three numerically estimated rates are presented and they are close to the

Table 1: The maximal errors of numerical solutions at $t = 10$, $\tau = 0.1$, $\beta = 1$, $\alpha = 2$, and $p = 2$.

Methods	$h = 1/16$	$h = 1/32$	$h = 1/64$	$h = 1/128$
[18]	$5.319866e-4$	$1.276895e-4$	$3.018276e-5$	$6.026481e-6$
[20]	$4.483472e-5$	$1.110691e-5$	$2.644709e-6$	$5.290243e-7$
Scheme (8)	$3.831638e-5$	$9.264042e-6$	$2.207048e-6$	$4.408479e-7$

Table 2: The maximal errors of numerical solutions at $t = 10$, $\tau = 0.1$, $\beta = 1$, $\alpha = 2$, and $p = 4$.

Methods	$h = 1/16$	$h = 1/32$	$h = 1/64$	$h = 1/128$
[18]	$5.319788e-4$	$1.276876e-4$	$3.018218e-5$	$6.026111e-6$
[20]	$4.482287e-5$	$1.110366e-5$	$2.644021e-6$	$5.288865e-7$
Scheme (8)	$3.830394e-5$	$9.261242e-6$	$2.206324e-6$	$4.407013e-7$

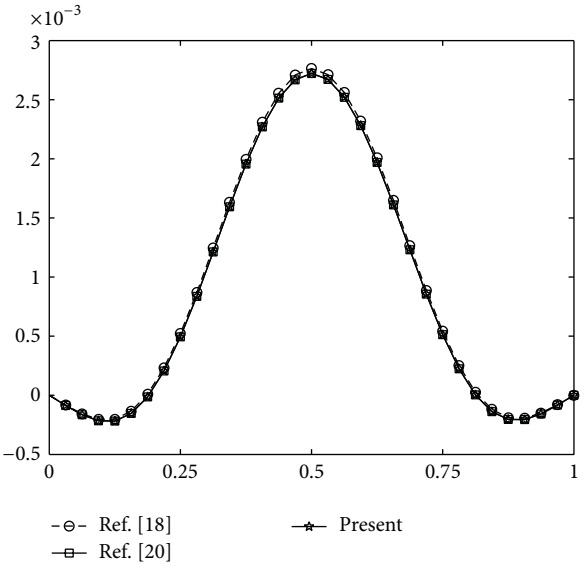

Figure 4: Numerical solutions at $t = 10$, $h = 1/32$, $\tau = 0.1$, $\beta = 1$, $\alpha = 4$, and $p = 8$.

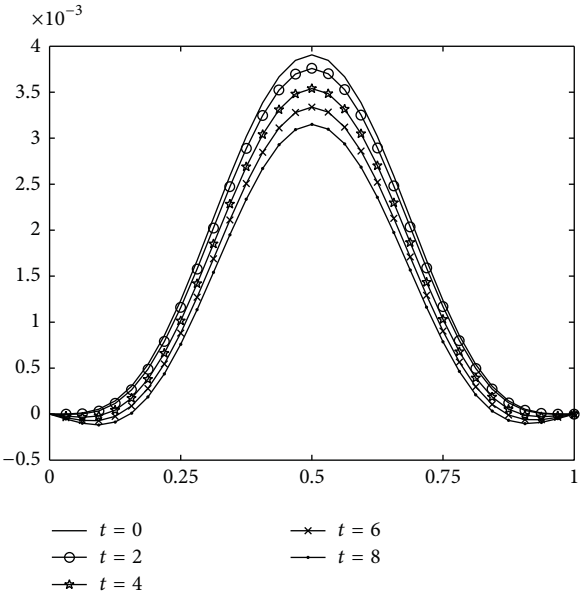

Figure 5: Numerical solutions at different time with $h = 1/32$, $\tau = 0.1$, $\beta = 1$, $\alpha = 2$, and $p = 4$.

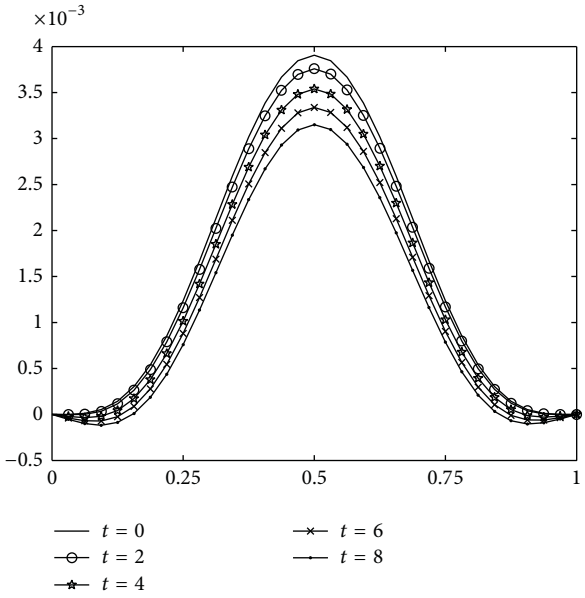

Figure 6: Numerical solutions at different time with $h = 1/32$, $\tau = 0.1$, $\beta = 1$, $\alpha = 2$, and $p = 8$.

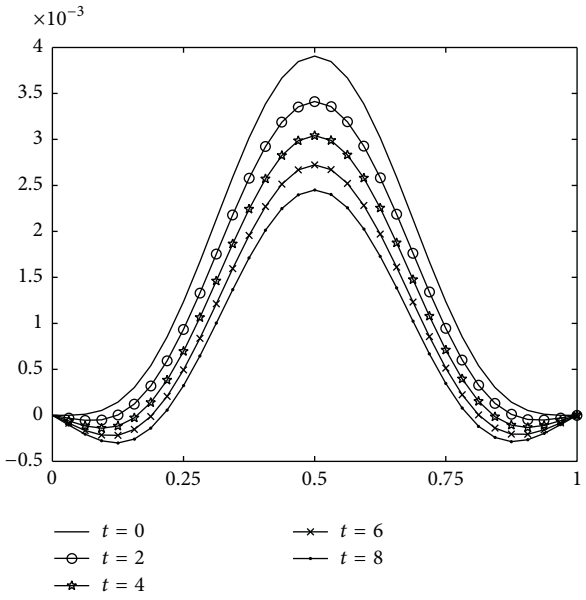

Figure 7: Numerical solutions at different time with $h = 1/32$, $\tau = 0.1$, $\beta = 1$, $\alpha = 4$, and $p = 4$.

Table 3: The maximal errors of numerical solutions at $t = 10$, $\tau = 0.1$, $\beta = 1$, $\alpha = 2$, and $p = 8$.

Methods	$h = 1/16$	$h = 1/32$	$h = 1/64$	$h = 1/128$
[18]	$5.319785e-4$	$1.276873e-4$	$3.018188e-5$	$6.025843e-6$
[20]	$4.482286e-5$	$1.110366e-5$	$2.644016e-6$	$5.288811e-7$
Scheme (8)	$3.830394e-5$	$9.261242e-6$	$2.206324e-6$	$4.407013e-7$

Table 4: The errors of numerical solutions at $t = 10$, $\tau = 0.1$, $\beta = 1$, $\alpha = 2$, and $p = 2$.

h	$\|e\|_\infty$	Rate	$\|e\|$	Rate
1/8	$1.674577e-4$	—	$9.800635e-5$	—
1/16	$3.831638e-5$	2.127764	$2.291144e-5$	2.096807
1/32	$9.264042e-6$	2.048248	$5.554049e-6$	2.044456
1/64	$2.207048e-6$	2.069524	$1.315895e-6$	2.077495
1/128	$4.408479e-7$	2.323765	$2.628915e-7$	2.323505

Table 5: The errors of numerical solutions at $t = 10$, $\tau = 0.1$, $\beta = 1$, $\alpha = 2$, and $p = 4$.

h	$\|e\|_\infty$	Rate	$\|e\|$	Rate
1/8	$1.673863e-4$	—	$9.800669e-5$	—
1/16	$3.830394e-5$	2.127617	$2.291161e-5$	2.096801
1/32	$9.261242e-6$	2.048215	$5.554093e-6$	2.044456
1/64	$2.206324e-6$	2.069561	$1.315904e-6$	2.077497
1/128	$4.407013e-7$	2.323772	$2.628917e-7$	2.323514

Table 6: The errors of numerical solutions at $t = 10$, $\tau = 0.1$, $\beta = 1$, $\alpha = 2$, and $p = 8$.

h	$\|e\|_\infty$	Rate	$\|e\|$	Rate
1/8	$1.673863e-4$	—	$9.800669e-5$	—
1/16	$3.830394e-5$	2.127617	$2.291161e-5$	2.096801
1/32	$9.261242e-6$	2.048215	$5.554093e-6$	2.044456
1/64	$2.206324e-6$	2.069561	$1.315905e-6$	2.077496
1/128	$4.407013e-7$	2.323772	$2.628922e-7$	2.323512

theoretically predicted ones which are second-order rates of convergence.

Figures 1, 2, 3, and 4 show the numerical solutions at $t = 10$ with $p = 4$ and 8. The graphs of the numerical solutions of Hu et al. [18], Pan and Zhang [20] schemes, and the proposed scheme are presented. It is to confirm that the approximated solutions are coinciding.

Figures 5, 6, 7, and 8 present the numerical solutions computed by the finite difference scheme (8) with $\tau = 0.1$, $h = 1/32$ at $t = 0, 2, 4, 6$, and 8 when $\alpha = 2$ and 4, respectively. It is clear that the amplitude of the numerical solution decreases over time. In Figures 9, 10, 11, and 12, numerical solutions are presented for a fixed set of h, τ, and t with different values of β and α, respectively. The graph shows that β does not contribute to the height of the amplitude of the numerical solution. On the other hand, the larger the value of α, the smaller the amplitude of the numerical solution.

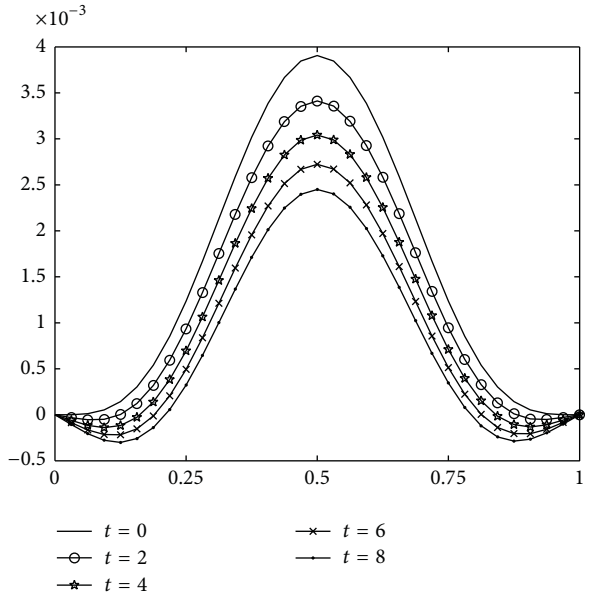

Figure 8: Numerical solutions at different time with $h = 1/32$, $\tau = 0.1$, $\beta = 1$, $\alpha = 4$, and $p = 8$.

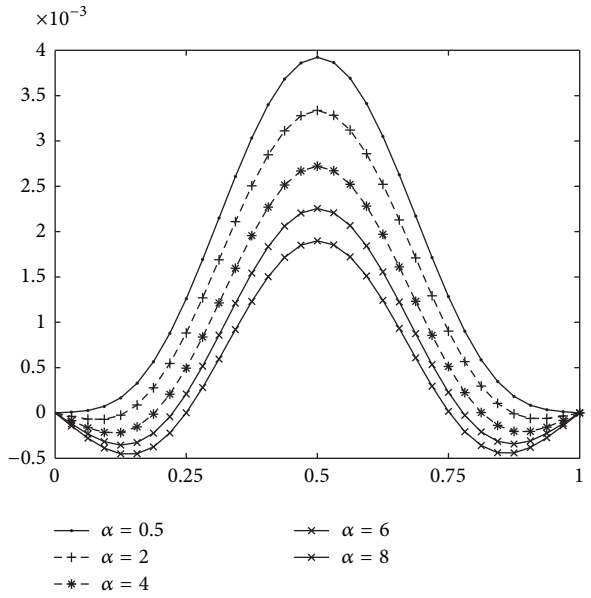

Figure 9: Numerical solutions at different α with $h = 1/32$, $\tau = 0.1$, $\beta = 1$, and $p = 4$.

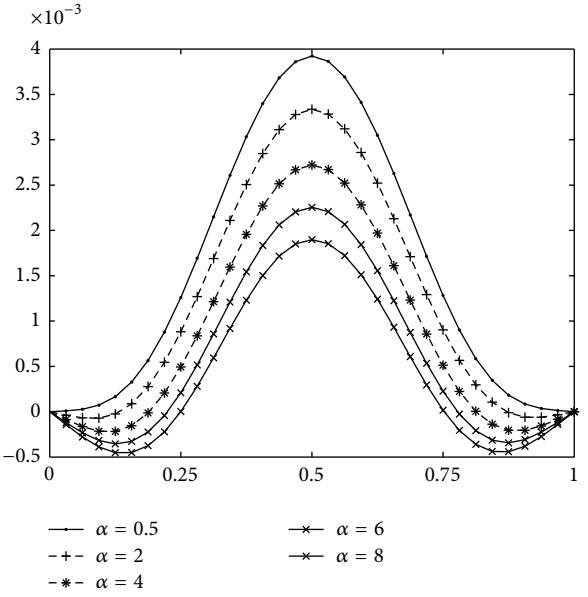

Figure 10: Numerical solutions at different α with $h = 1/32$, $\tau = 0.1$, $\beta = 1$, and $p = 8$.

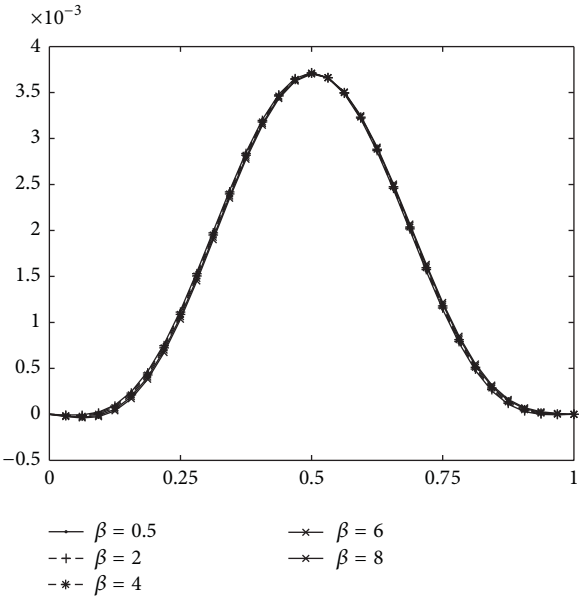

Figure 11: Numerical solutions at different β with $h = 1/32$, $\tau = 0.1$, $\alpha = 1$, and $p = 4$.

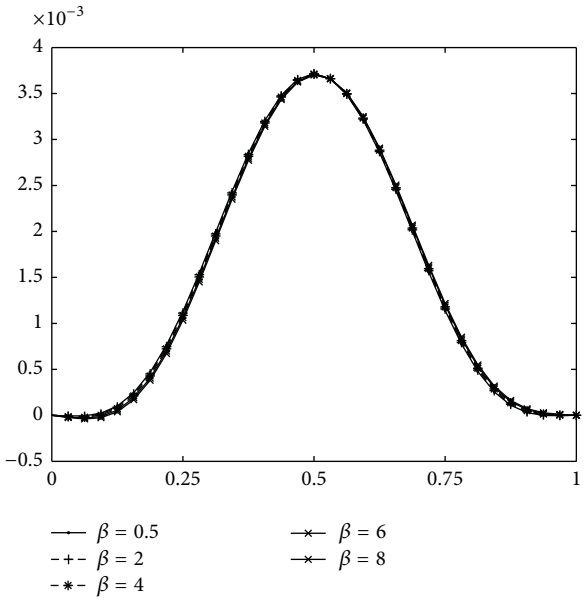

Figure 12: Numerical solutions at different β with $h = 1/32$, $\tau = 0.1$, $\alpha = 1$, and $p = 8$.

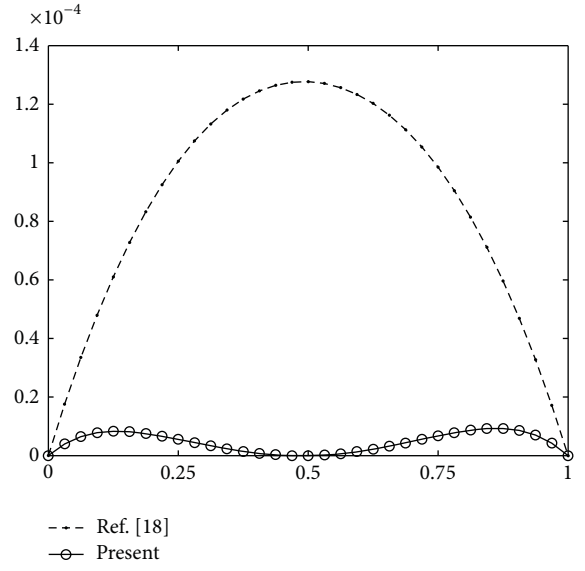

Figure 13: Absolute error distribution at $h = 1/32$, $\tau = 0.1$, $\beta = 1$, $\alpha = 2$, $p = 4$, and $t = 10$.

Absolute error distributions for the three methods are plotted at $t = 10$ in Figures 13, 14, 15, and 16. Clearly, our proposed method gives a better approximate solution than the schemes proposed in [18, 20], especially at the peak of the solution. As the results in some of the applications where the characterization of the solution at the peak needs to be precise our proposed method is highly recommended.

6. Concluding Remarks

We introduce a three-level average linear-implicit finite difference method for solving the Rosenau-Burgers equation. We prove the existence and uniqueness of the numerical

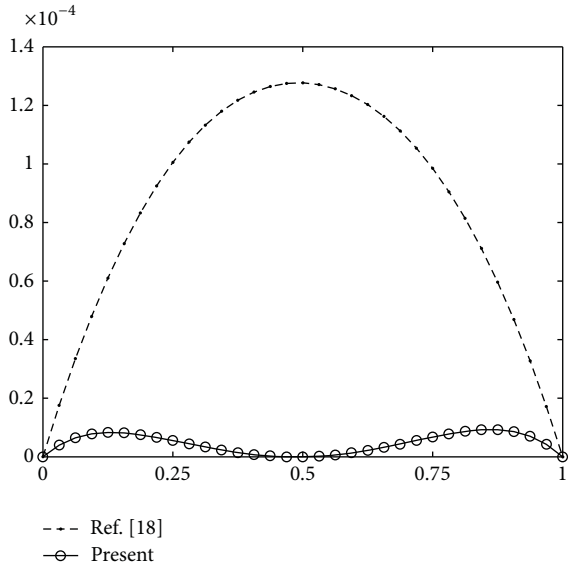

Figure 14: Absolute error distribution at $h = 1/32$, $\tau = 0.1$, $\beta = 1$, $\alpha = 2$, $p = 8$, and $t = 10$.

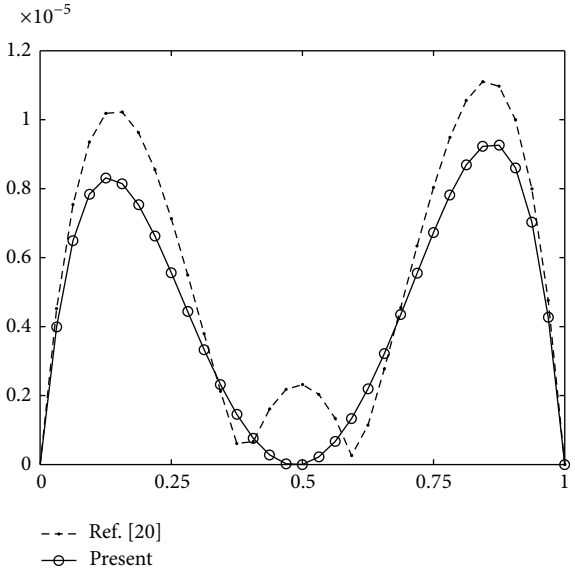

Figure 15: Absolute error distribution at $h = 1/32$, $\tau = 0.1$, $\beta = 1$, $\alpha = 2$, $p = 4$, and $t = 10$.

solution. The convergence and stability of the numerical solution are also shown. The quantitative comparison of the numerical results from previously known methods shows that our method improves the accuracy of the solution significantly. In addition, our results provide the most precise peak amplitude.

Conflict of Interests

The authors declare that there is no conflict of interests regarding the publication of this paper.

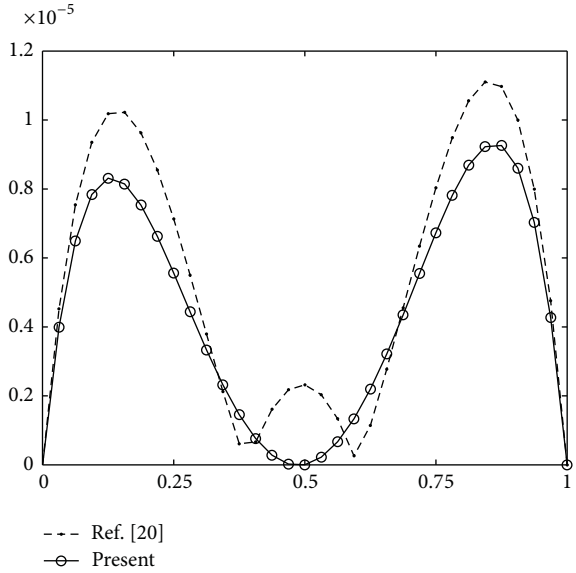

Figure 16: Absolute error distribution at $h = 1/32$, $\tau = 0.1$, $\beta = 1$, $\alpha = 2$, $p = 8$, and $t = 10$.

Acknowledgment

This research was supported by Chiang Mai University.

References

[1] P. Rosenau, "A quasi continuous description of a nonlinear transmission line," *Physica Scripta*, vol. 34, pp. 827–829, 1986.

[2] P. Rosenau, "Dynamics of dense discrete systems," *Progress of Theoretical Physics*, vol. 79, pp. 1028–1042, 1988.

[3] M. A. Park, "On the Rosenau equation," *Applied Mathematics and Computation*, vol. 9, pp. 145–152, 1990.

[4] S. M. Choo, S. K. Chung, and K. I. Kim, "A discontinuous Galerkin method for the Rosenau equation," *Applied Numerical Mathematics*, vol. 58, no. 6, pp. 783–799, 2008.

[5] H. Y. Lee, M. R. Ohm, and J. Y. Shin, "Finite element Galerkin solutions for the Rosenau equation," *Applicable Analysis*, vol. 2, pp. 153–160, 1997.

[6] K. Omrani, F. Abidi, T. Achouri, and N. Khiari, "A new conservative finite difference scheme for the Rosenau equation," *Applied Mathematics and Computation*, vol. 201, no. 1-2, pp. 35–43, 2008.

[7] K. Zheng and J. Hu, "Two conservative difference schemes for the generalized rosenau equation," *Boundary Value Problems*, vol. 2010, Article ID 543503, 2010.

[8] M. Wang, D. Li, and P. Cui, "A conservative finite difference scheme for the generalized rosenau equation," *International Journal of Pure and Applied Mathematics*, vol. 71, no. 4, pp. 539–549, 2011.

[9] Y. Zhou, *Application of Discrete Functional Analysis to the Finite Difference Method*, International Academic Publisherss, Beijing, China, 1990.

[10] M. Mei, "Long-time behavior of solution for Rosenau-Burgers equation (I)," *Applicable Analysis*, vol. 63, pp. 315–330, 1996.

[11] M. Mei, "Long-time behavior of solution for Rosenau-Burgers equation (II)," *Applicable Analysis*, vol. 68, pp. 333–356, 1998.

[12] L. Liu and M. Mei, "A better asymptotic profile of Rosenau-Burgers equation," *Applied Mathematics and Computation*, vol. 131, no. 1, pp. 147–170, 2002.

[13] L. Liu, M. Mei, and Y. S. Wong, "Asymptotic behavior of solutions to the Rosenau-Burgers equation with a periodic initial boundary," *Nonlinear Analysis: Theory, Methods and Applications*, vol. 67, no. 8, pp. 2527–2539, 2007.

[14] B. Hu, Y. Xu, and J. Hu, "Crank-Nicolson finite difference scheme for the Rosenau-Burgers equation," *Applied Mathematics and Computation*, vol. 204, no. 1, pp. 311–316, 2008.

[15] D. Li, Z. Wang, Y. Wu, and Y. Lu, "A finite difference simulation for Rosenau-Burgers equation," in *Proceedings of the International Conference on Information Engineering and Computer Science (ICIECS '09)*, pp. 1–4, Wuhan, China.

[16] K. Zheng and J. Hu, "Crank-Nicolson difference scheme for the generalized Rosenau-Burgers equation," *International Journal of Mathematics and Computer Science*, vol. 5, no. 4, 2009.

[17] W. Ma, A. Yang, and Y. Wang, "A second-order accurate linearized difference scheme for the Rosenau-Burgers equation," *Journal of Information and Computational Science*, vol. 7, no. 8, pp. 1793–1800, 2010.

[18] J. Hu, B. Hu, and Y. Xu, "Average implicit linear difference scheme for generalized Rosenau-Burgers equation," *Applied Mathematics and Computation*, vol. 217, no. 19, pp. 7557–7563, 2011.

[19] M. O. Korpusov, "On the blow-up of solutions of the Benjamin-Bona-Mahony-Burgers and Rosenau-Burgers equations," *Nonlinear Analysis: Theory, Methods and Applications*, vol. 75, no. 4, pp. 1737–1743, 2012.

[20] X. Pan and L. Zhang, "A new finite difference scheme for the Rosenau-Burgers equation," *Applied Mathematics and Computation*, vol. 218, no. 17, pp. 8917–8924, 2012.

A Compact Finite Difference Method for Solving the General Rosenau–RLW Equation

Ben Wongsaijai, Kanyuta Poochinapan*, and Thongchai Disyadej

***Abstract*—In this paper, a compact finite difference method to solve the Rosenau–RLW equation is proposed. A numerical tool is applied to the model by using a three–level average implicit finite difference technique. The fundamental conservative property of the equation is preserved by the presented numerical scheme, and the existence and uniqueness of the numerical solution are proved. Moreover, the convergence and stability of the numerical solution are also shown. The new method gives second– and fourth–order accuracy in time and space, respectively. The algorithm uses five–point stencil to approximate the derivatives for the space discretization. The numerical experiments show that the proposed method improves the accuracy of the solution significantly.**

***Index Terms*—finite difference method, Rosenau–RLW equation.**

I. Introduction

A nonlinear wave phenomenon is the important area of scientific research, which many scientists in the past have studied about mathematical models explaining the wave behavior. There are mathematical models which describe the dynamic of wave behaviors–for example, the KdV equation, the RLW equation, the Rosenau equation, and many others [1]–[10]. The KdV equation has been used in very wide applications, such as magnetic fluid waves, ion sound waves, and longitudinal astigmatic waves [4]–[6]. The RLW equation, which was first proposed by Peregrine [7], [8] provides an explanation on a different situation of a nonlinear dispersive wave from the more classical KdV equation. The RLW equation is one of models which are encountered in many areas, e.g. ion–acoustic plasma waves, magnetohydrodynamic plasma waves, and shallow water waves. Since the case of wave–wave and wave–wall interactions cannot be described by the KdV equation, Rosenau [9], [10] proposed an equation for describing the dynamic of dense discrete systems; it is known as the Rosenue equation. The existence and uniqueness of the solution for the Rosenau equation were proved by Park [11], [12]. For the further consideration of the nonlinear wave, a viscous term u_{xxt} needs to be included:

$$u_t - u_{xxt} + u_{xxxxt} + u_x + (u^p)_x = 0, \tag{1}$$

where $p \geq 2$ is an integer and $u_0(x)$ is a known smooth function. This equation is usually called the Rosenua–RLW equation. If $p = 2$, then Eq. (1) is called the usual Rosenau–RLW equation. Moreover, if $p = 3$, then Eq. (1) is called the modified Rosenau–RLW equation. The behavior of the solution to the Rosenau–RLW equation with the Cauchy problem has been well studied for the past years [13]–[18]. It is known that the solitary wave solution for Eq. (1) is

$$u(x,t) = e^{ln\{(p+3)(3p+1)(p+1)/[2(p^2+3)(p^2+4p+7)]\}/(p+1)} \times \operatorname{sech}^{4/(p+1)}\left[\frac{p-1}{\sqrt{4p^2+8p+20}}(x-ct)\right],$$

where $p \geq 2$ is an integer and $c = (p^4+4p^3+14p^2+20p+25)/(p^4+4p^3+10p^2+12p+21)$.

The Rosenau–RLW equation has been solved numerically by various methods (for example, see [13]–[18]). Zuo et al. [13] have proposed the Crank–Nocolson finite difference scheme for the equation. The convergence and stability of the proposed method were also discussed. Obviously, the scheme in [13] requires heavy iterative computations because the scheme is nonlinear implicit. Pan and Zhang [14], [15] developed linearized difference schemes which are three–level and conservative implicit for both the usual Rosenau–RLW ($p = 2$) and the general Rosenau–RLW ($p \geq 2$) equations. The second–order accuracy and unconditional stability were also proved.

In this paper, we consider the following initial–boundary value problem of the general Rosenau–RLW equation with an initial condition:

$$u(x,0) = u_0(x), \quad (x_l \leq x \leq x_r), \tag{2}$$

and boundary conditions

$$\begin{aligned} &u(x_l,t) = u(x_r,t) = 0, \\ &u_{xx}(x_l,t) = u_{xx}(x_r,t) = 0, \quad (0 \leq t \leq T). \end{aligned} \tag{3}$$

The initial–boundary value problem possesses the following conservative properties:

$$Q(t) = \int_{x_l}^{x_r} u(x,t)dx = \int_{x_l}^{x_r} u_0(x,0)dx = Q(0),$$

and

$$E(t) = \|u\|_{L_2}^2 + \|u_x\|_{L_2}^2 + \|u_{xx}\|_{L_2}^2 = E(0).$$

When $-x_l \gg 0$ and $x_r \gg 0$, the initial–boundary value problem (1)–(3) is consistent, so the boundary condition (3) is reasonable.

By observation, the total accuracy of a specific method is affected by not only the order of accuracy of the numerical method but also other factors. That is, the conservative approximation property of the method is another factor that has the same or possibly even more impact on results. Better solutions can be expected from numerical schemes which have effective conservative approximation properties rather than the ones which have nonconservative properties [19], [20]. To create the discretization equation, a finite difference

*Kanyuta Poochinapan, Corresponding Author, Department of Mathematics, Faculty of Science, Chiang Mai University, Chiang Mai 50200, Thailand (email: kanyuta@hotmail.com, k.poochinapan@gmail.com)

Ben Wongsaijai, Department of Mathematics, Faculty of Science, Chiang Mai University, Chiang Mai 50200, Thailand (email: ben.wongsaijai@gmail.com)

Thongchai Disyadej, Electricity Generating Authority of Thailand, Phitsanulok 65000, Thailand (e-mail: thongchai.d@egat.co.th)

method is applied in the present research since conservative approximation analysis by the mathematical tools has been developing until now.

The content of this paper is organized as follows. In the next section, we describe a conservative implicit finite difference scheme for the general Rosenau–RLW equation (1) with the initial and boundary conditions (2)–(3). Some preliminary lemmas and discrete norms are given and the invariant property Q^n is proved. We discuss about the solvability of the finite difference scheme, and the existence and uniqueness of the solution are also proved in the Section 3. Section 4 presents complete proofs on the convergence and stability of the proposed method with convergence rate $O(\tau^2+h^4)$. The results of validation for the finite difference scheme are presented in Section 5, where we make a detailed comparison with available data, to confirm and illustrate our theoretical analysis. Finally, we finish our paper by concluding remarks in Section 6.

II. Finite Difference Scheme

In this section, we introduce a finite difference scheme for the formulation of Eqs. (1)–(3). The solution domain $\Omega = \{(x,t)|\ x_l \le x \le x_r,\ 0 \le t \le T\}$ is covered by a uniform grid:

$$\Omega_h = \{(x_i,t_n)|\ x_i = x_l + ih,\ t_n = n\tau, 0 \le i \le M, \\ 0 \le n \le N\},$$

with spacings $h = (x_r - x_l)/M$ and $\tau = T/N$. Denote $u_i^n \approx u(x_i,t_n)$,

$$\bar{\Omega}_h = \{(x_i,t_n)|\ x_i = x_l+ih,\ t_n = n\tau,\ -1 \le i \le M+1, \\ 0 \le n \le N\},$$

and $Z_h^0 = \{u^n = (u_i^n)|\ u_0 = u_M = 0,\ -1 \le i \le M+1\}$. We use the following notations for simplicity:

$$u_i^{n+\frac{1}{2}} = \frac{u_i^{n+1}+u_i^n}{2}, \qquad \bar{u}_i^n = \frac{u_i^{n+1}+u_i^{n-1}}{2},$$
$$(u_i^n)_t = \frac{u_i^{n+1}-u_i^n}{\tau}, \qquad (u_i^n)_{\hat{t}} = \frac{u_i^{n+1}-u_i^{n-1}}{2\tau},$$
$$(u_i^n)_x = \frac{u_{i+1}^n-u_i^n}{h}, \qquad (u_i^n)_{\bar{x}} = \frac{u_i^n-u_{i-1}^n}{h},$$
$$(u_i^n)_{\hat{x}} = \frac{u_{i+1}^n-u_{i-1}^n}{2h}, \qquad (u^n,v^n) = h\sum_{i=1}^{M-1} u_i^n v_i^n,$$
$$\|u^n\|^2 = (u^n,u^n), \qquad \|u^n\|_\infty = \max_{1\le i\le M-1}|u_i^n|.$$

By setting $w = u_{xxt} - u_x - u_{xxxxt} - (u^p)_x$, Eq. (1) can be written as $w = u_t$. By the Taylor expansion, we obtain

$$w_i^n = (\partial_t u)_i^n = (u_i^n)_{\hat{t}} + O\left(\tau^2\right), \tag{4}$$

and

$$w_i^n = \left[(u_i^n)_{x\bar{x}\hat{t}} - \frac{h^2}{12}\left(\partial_x^4\partial_t u\right)_i^n\right] - \left[(u_i^n)_{\hat{x}} - \frac{h^2}{6}\left(\partial_x^3 u\right)_i^n\right] \\ - \left[(u_i^n)_{xx\bar{x}\bar{x}\hat{t}} - \frac{h^2}{6}\left(\partial_x^6\partial_t u\right)_i^n\right] \\ - \left[[(u_i^n)^p]_{\hat{x}} - \frac{h^2}{6}\left(\partial_x^3 u^p\right)_i^n\right] + O\left(h^4\right). \tag{5}$$

From Eq. (4), we have

$$\left(\partial_x^6\partial_t u\right)_i^n = \left(\partial_x^4\partial_t u\right)_i^n - \left(\partial_x^3 u\right)_i^n - \left(\partial_x^3 u^p\right)_i^n - \left(\partial_x^2 w\right)_i^n. \tag{6}$$

Then,

$$w_i^n = \left[(u_i^n)_{x\bar{x}\hat{t}} - \frac{h^2}{12}\left(\partial_x^4\partial_t u\right)_i^n\right] - \left[(u_i^n)_{\hat{x}} - \frac{h^2}{6}\left(\partial_x^3 u\right)_i^n\right] \\ - \left[[(u_i^n)^p]_{\hat{x}} - \frac{h^2}{6}\left(\partial_x^3 u^p\right)_i^n\right] - \Bigg[(u_i^n)_{xx\bar{x}\bar{x}\hat{t}} \\ - \frac{h^2}{6}\left[\left(\partial_x^4\partial_t u\right)_i^n - \left(\partial_x^3 u\right)_i^n - \left(\partial_x^3 u^p\right)_i^n - \left(\partial_x^2 w\right)_i^n\right]\Bigg] \\ + O\left(h^4\right). \tag{7}$$

This implies that

$$w_i^n = (u_i^n)_{x\bar{x}\hat{t}} + \frac{h^2}{12}\left(\partial_x^4\partial_t u\right)_i^n - (u_i^n)_{\hat{x}} - [(u_i^n)^p]_{\hat{x}} \\ - (u_i^n)_{xx\bar{x}\bar{x}\hat{t}} - \frac{h^2}{6}\left(\partial_x^2 w\right)_i^n + O\left(h^4\right). \tag{8}$$

Using second–order accuracy for approximation, we obtain

$$\left(\partial_x^4 u\right)_i^n = (u_i^n)_{xx\bar{x}\bar{x}} + O\left(h^2\right),$$

$$\left(\partial_x^2 w\right)_i^n = (w_i^n)_{x\bar{x}} + O\left(h^2\right).$$

The following method is a proposed finite difference scheme to solve the problem (1)–(3):

$$(u_i^n)_{\hat{t}} - \left(1-\frac{h^2}{6}\right)(u_i^n)_{x\bar{x}\hat{t}} + \left(1-\frac{h^2}{12}\right)(u_i^n)_{xx\bar{x}\bar{x}\hat{t}} \\ + (u_i^n)_{\hat{x}} + [(u_i^n)^p]_{\hat{x}} = 0; \\ 1 \le i \le M-1,\ 1 \le n \le N-1, \tag{9}$$

where

$$u_i^0 = u_0(x_i), \quad 0 \le i \le M, \tag{10}$$

$$u_0^n = u_M^n = 0, \ \ (u_0^n)_{x\bar{x}} = (u_M^n)_{x\bar{x}} = 0, \quad 1 \le n \le N. \tag{11}$$

A three–step method is used for the time discretization of the above described scheme. After the new time discretization of Eq. (9) is performed, three– and five–point stencils approximating the derivatives for the space discretization are used to obtain an algebraic system. The matrix system of Eq. (9) is banded with penta–diagonals and we use a standard routine of the MATLAB to solve the system (9)–(11). The nonlinear term of Eq. (1) is handled by using the linear implicit scheme. Therefore, the equations are solved easily by using the presented method since it does not require extra effort to deal with the nonlinear term.

Lemma 1: (Pan and Zhang [15]) For any two mesh functions $u, v \in Z_h^0$, we have

$$(u_{\hat{x}}, v) = -(u, v_{\hat{x}}),$$
$$(u_x, v) = -(u, v_{\bar{x}}),$$
$$(v, u_{x\bar{x}}) = -(v_x, u_x),$$
$$(u, u_{x\bar{x}}) = -(u_x, u_x) = -\|u_x\|^2.$$

Furthermore, if $(u_0^n)_{x\bar{x}} = (u_M^n)_{x\bar{x}} = 0$, then it implies

$$(u, u_{xx\bar{x}\bar{x}}) = \|u_{x\bar{x}}\|^2.$$

Theorem 2: Suppose that $u_0 \in H_0^2$, then the scheme (9)–(11) is conservative in sense:

$$Q^n = \frac{h}{2}\sum_{i=1}^{M-1}\left(u_i^{n+1}+u_i^n\right) = Q^{n-1} = \ldots = Q^0, \quad (12)$$

under assumptions $u_{-1} = u_1 = 0$ and $u_{M-1} = u_{M+1} = 0$.

Proof: By multiplying Eq. (9) by h, summing up for i from 0 to $M-1$, considering the boundary conditions, and assuming $u_{-1} = u_1 = 0$ and $u_{M-1} = u_{M+1} = 0$, we get

$$\frac{h}{2}\sum_{i=1}^{M-1}\left(u_i^{n+1}-u_i^{n-1}\right) = 0.$$

Then, this gives Eq. (12). ■

Lemma 3: (Discrete Sobolev's inequality [21]) There exist two constants C_1 and C_2 such that

$$\|u^n\|_\infty \le C_1\|u^n\| + C_2\|u_x^n\|.$$

Theorem 4: Suppose $u_0 \in H_0^2[x_l, x_r]$, then the solution u^n satisfies $\|u^n\| \le C$ and $\|u_{xx}^n\| \le C$, which yields $\|u^n\|_\infty \le C$.

Proof: It follows from the initial condition (10) that $u^0 \le C$. The first level u^1 is computed by the fourth–order method. Hence, the following estimates are gotten about $\left\|u^1\right\| \le C$ and $\left\|u^1\right\|_\infty \le C$. Now, we use the induction argument to prove the estimate. We assume that

$$\left\|u^k\right\|_\infty \le C \text{ for } k = 0, 1, 2, \ldots, n. \quad (13)$$

Taking the inner product of Eq. (9) with $2\bar{u}^n$ and using Lemma 1, we obtain

$$\begin{aligned}\left\|u^{n+1}\right\|^2 - \left\|u^{n-1}\right\|^2 + \left(1-\frac{h^2}{6}\right)\left(\left\|u_x^{n+1}\right\|^2 - \left\|u_x^{n-1}\right\|^2\right) \\ + \left(1-\frac{h^2}{12}\right)\left(\left\|u_{x\bar{x}}^{n+1}\right\|^2 - \left\|u_{x\bar{x}}^{n-1}\right\|^2\right) \\ = -2\tau\left((u^n)_{\hat{x}}, 2\bar{u}^n\right) - 2\tau\left([(u^n)^p]_{\hat{x}}, 2\bar{u}^n\right).\end{aligned}$$

According to the Cauchy–Schwarz inequality and direct calculation, it gives

$$\|u_{\hat{x}}^n\| \le \|u_x^n\|,$$

and

$$\left((u^n)_{\hat{x}}, 2\bar{u}^n\right) \le \left(\|u_x^n\|^2 + \frac{1}{2}\left\|u^{n+1}\right\|^2 + \frac{1}{2}\left\|u^{n-1}\right\|^2\right).$$

From Eq. (13), the Cauchy–Schwarz inequality, and Lemma 1, we get

$$\begin{aligned}\left([(u^n)^p]_{\hat{x}}, 2\bar{u}^n\right) &= -h\sum_{i=1}^{M-1}(u_i^n)^p\left(u_i^{n+1}+u_i^{n-1}\right)_{\hat{x}} \\ &\le C\left(\|u^n\|^2 + \frac{1}{2}\left\|u_x^{n+1}\right\|^2 + \frac{1}{2}\left\|u_x^{n-1}\right\|^2\right).\end{aligned}$$

Setting

$$\begin{aligned}B^n = \|u^n\|^2 + \left\|u^{n-1}\right\|^2 + \left(1-\frac{h^2}{6}\right)\left(\|u_x^n\|^2 + \left\|u_x^{n-1}\right\|^2\right) \\ + \left(1-\frac{h^2}{12}\right)\left(\|u_{x\bar{x}}^n\|^2 + \left\|u_{x\bar{x}}^{n-1}\right\|^2\right),\end{aligned}$$

then

$$B^{n+1} - B^n \le \tau C\left(B^{n+1} + B^n\right).$$

If τ is sufficiently small, which satisfies $\tau \le \dfrac{k-2}{kC}$ and $k > 2$, then

$$B^{n+1} \le \frac{(1+\tau C)}{(1-\tau C)}B^n \le (1+\tau kC)\,B^n \le \exp(kCT)\,B^0.$$

Hence $\left\|u^{n+1}\right\| \le C$, $\left\|u_x^{n+1}\right\| \le C$, and $\left\|u_{x\bar{x}}^{n+1}\right\| \le C$, which yield $\left\|u^{n+1}\right\|_\infty \le C$ by Lemma 3. ■

III. Solvability

In this section, we prove the existence and uniqueness of our proposed scheme that implies the unique solvability.

Theorem 5: The finite difference scheme (9)–(11) is uniquely solvable.

Proof: By using the mathematical induction, we can determine u^0 uniquely by an initial condition and then choose a fourth–order method to compute u^1. Now, suppose $u^0, u^1, u^2, ..., u^n$ to be solved uniquely. By considering Eq. (9) for u^{n+1}, we have

$$\begin{aligned}\frac{1}{2\tau}u_i^{n+1} - \frac{1}{2\tau}\left(1-\frac{h^2}{6}\right)\left(u_i^{n+1}\right)_{x\bar{x}} + \\ \frac{1}{2\tau}\left(1-\frac{h^2}{12}\right)\left(u_i^{n+1}\right)_{xx\bar{x}\bar{x}} = 0. \quad (14)\end{aligned}$$

By taking an inner product of Eq. (14) with u^{n+1}, we obtain

$$\begin{aligned}\frac{1}{2\tau}\left\|u^{n+1}\right\|^2 - \frac{1}{2\tau}\left(1-\frac{h^2}{6}\right)\left\|u_x^{n+1}\right\|^2 \\ + \frac{1}{2\tau}\left(1-\frac{h^2}{12}\right)\left\|u_{x\bar{x}}^{n+1}\right\|^2 = 0.\end{aligned}$$

By the Cauchy–Schwarz inequality and Lemma 1, we have

$$\left\|u_x^{n+1}\right\|^2 = (u^{n+1}, u_{x\bar{x}}^{n+1}) \le \frac{1}{2}\left\|u^{n+1}\right\|^2 + \frac{1}{2}\left\|u_{x\bar{x}}^{n+1}\right\|^2.$$

Then,

$$\frac{1}{2}\left\|u^{n+1}\right\|^2 + \left(\frac{1}{2}-\frac{h^2}{12}\right)\left\|u_{x\bar{x}}^{n+1}\right\|^2 = 0.$$

Therefore, Eq. (14) has the only one solution and Eq. (9) u^{n+1} is uniquely solvable. This completes the proof of Theorem 5. ■

IV. Convergence and stability

In this section, we prove the convergence and stability of the scheme (9)–(11). Let $e_i^n = v_i^n - u_i^n$, where v_i^n and u_i^n are the solutions of (1)–(3) and (9)–(11), respectively. Then, we obtain the following error equations:

$$\begin{aligned}r_i^n = (e_i^n)_{\hat{t}} - \left(1-\frac{h^2}{6}\right)(e_i^n)_{x\bar{x}\hat{t}} + \left(1-\frac{h^2}{12}\right)(e_i^n)_{xx\bar{x}\bar{x}\hat{t}} \\ + (e_i^n)_{\hat{x}} + [(v_i^n)^p]_{\hat{x}} - [(u_i^n)^p]_{\hat{x}}, \quad (15)\end{aligned}$$

where r_i^n denotes the truncation error. By using the Taylor expansion, it is easy to see that $r_i^n = O(\tau^2 + h^4)$ holds as $\tau, h \to 0$. The following lemmas are essential for the proof of convergence and stability of our scheme.

Lemma 6: (Discrete Gronwall's inequality [21]) Suppose that $\omega(k)$ and $\rho(k)$ are nonnegative functions and $\rho(k)$ is nondecreasing. If $C > 0$ and

$$\omega(k) \le \rho(k) + C\tau\sum_{l=0}^{k-1}\omega(l), \quad \forall k,$$

then

$$\omega(k) \le \rho(k)e^{C\tau k}, \ \ \forall k.$$

Lemma 7: (Pan and Zhang [15]) Suppose that $u_0 \in H_0^2[x_l, x_r]$, then the solution u^n of Eqs. (1)–(3) satisfies

$$\|u\|_{L_2} \le C, \qquad \|u_x\|_{L_2} \le C,$$
$$\|u_{xx}\|_{L_2} \le C, \qquad \|u\|_{L_\infty} \le C.$$

The following theorem shows that our scheme converges to the solution with convergence rate $O(\tau^2 + h^4)$.

Theorem 8: Suppose $u_0 \in H_0^2[x_l, x_r]$, then the solution u^n converges to the solution for the problem in the sense of $\|\cdot\|_\infty$ and the rate of convergence is $O(\tau^2 + h^4)$.

Proof: By taking an inner product on both sides of Eq. (15) with $2\bar{e}^n \equiv (e^{n+1} + e^{n-1})$, we get

$$\left(\left\|e^{n+1}\right\|^2 - \left\|e^{n-1}\right\|^2\right) + \left(1 - \frac{h^2}{6}\right)\left(\left\|e_x^{n+1}\right\|^2 - \left\|e_x^{n-1}\right\|^2\right) + \left(1 - \frac{h^2}{12}\right)\left(\left\|e_{x\bar{x}}^{n+1}\right\|^2 - \left\|e_{x\bar{x}}^{n-1}\right\|^2\right) = 2\tau\left(r^n, 2\bar{e}^n\right) - 2\tau\left(e_{\hat{x}}^n, 2\bar{e}^n\right) - 2\tau\left([(v^n)^p]_{\hat{x}} - [(u^n)^p]_{\hat{x}}, 2\bar{e}^n\right). \quad (16)$$

According to the Schwarz inequality, Lemma 1, Theorem 2, and Lemma 7, we obtain

$$\begin{aligned}
&\left([(v^n)^p]_{\hat{x}} - [(u^n)^p]_{\hat{x}}, 2\bar{e}^n\right) \\
&= 2h\sum_{i=1}^{M-1}\left[[(v_i^n)^p]_{\hat{x}} - [(u_i^n)^p]_{\hat{x}}\right]\bar{e}_i^n \\
&= -2h\sum_{i=1}^{M-1}\left[(v_i^n)^p - (u_i^n)^p\right](\bar{e}_i^n)_{\hat{x}} \\
&= 2h\sum_{i=1}^{M-1}\left[e_i^n\sum_{k=1}^{p-2}(v_i^n)^{p-k-2}(u_i^n)^k\right](\bar{e}_i^n)_{\hat{x}} \\
&\le C\left(\|e^n\|^2 + \|\bar{e}_{\hat{x}}^n\|^2\right) \\
&\le C\left(\|e^n\|^2 + \left\|e_{\hat{x}}^{n-1}\right\|^2 + \left\|e_{\hat{x}}^{n+1}\right\|^2\right). \quad (17)
\end{aligned}$$

By the Cauchy–Schwarz inequality, Lemma 1, and a direct calculation, we obtain

$$\|e_{\hat{x}}^n\| \le \|e_x^n\|, \quad (18)$$

$$\|e_x^n\| = -\left(e^n, e_{x\bar{x}}^n\right) \le \frac{1}{2}\left(\|e^n\|^2 + \|e_{x\bar{x}}^n\|^2\right), \quad (19)$$

$$\left(e_{\hat{x}}^n, 2\bar{e}^n\right) \le \|e_{\hat{x}}^n\|^2 + \frac{1}{2}\left(\left\|e^{n+1}\right\|^2 + \left\|e^{n-1}\right\|^2\right), \quad (20)$$

$$\left(r^n, 2\bar{e}^n\right) \le \|r^n\|^2 + \frac{1}{2}\left(\left\|e^{n+1}\right\|^2 + \left\|e^{n-1}\right\|^2\right). \quad (21)$$

From Eqs.(16)–(21), they yield

$$\begin{aligned}
&\left(\left\|e^{n+1}\right\|^2 - \left\|e^{n-1}\right\|^2\right) \\
&\quad + \left(1 - \frac{h^2}{6}\right)\left(\left\|e_x^{n+1}\right\|^2 - \left\|e_x^{n-1}\right\|^2\right) \\
&\quad + \left(1 - \frac{h^2}{12}\right)\left(\left\|e_{x\bar{x}}^{n+1}\right\|^2 - \left\|e_{x\bar{x}}^{n-1}\right\|^2\right) \\
&\le 2\tau\|r^n\|^2 + \tau C\left(\left\|e^{n-1}\right\|^2 + \|e^n\|^2 + \left\|e^{n+1}\right\|^2\right. \\
&\quad \left. + \left\|e_x^{n-1}\right\|^2 + \|e_x^n\|^2 + \left\|e_x^{n+1}\right\|^2\right). \quad (22)
\end{aligned}$$

Setting

$$E^n = \|e^n\|^2 + \left\|e^{n-1}\right\|^2 + \left(1 - \frac{h^2}{6}\right)\left(\|e_x^n\|^2 + \left\|e_x^{n-1}\right\|^2\right) + \left(1 - \frac{h^2}{12}\right)\left(\|e_{x\bar{x}}^n\|^2 + \left\|e_{x\bar{x}}^{n-1}\right\|^2\right),$$

then Eq. (22) can be rewritten as

$$E^{n+1} - E^n \le 2\tau\|r^n\|^2 + \tau C\left(E^{n+1} + E^n\right),$$

and

$$(1 - 2\tau C)\left(E^{n+1} - E^n\right) \le \tau\|r^n\|^2 + 2\tau C E^n.$$

If τ is sufficiently small, which satisfies $1 - 2C\tau > 0$, then

$$E^{n+1} - E^n \le \tau C\|r^n\|^2 + \tau C E^n. \quad (23)$$

Summing up Eq. (23) from 1 to n, we have

$$E^{n+1} \le E^1 + C\tau\sum_{k=1}^{n}\left\|r^k\right\|^2 + C\tau\sum_{k=1}^{n}E^k. \quad (24)$$

Thus, we can use a fourth–order method to compute u^1 such that

$$E^1 \le O(\tau^2 + h^4)^2,$$

and

$$\tau\sum_{k=1}^{n}\left\|r^k\right\|^2 \le n\tau\max_{0\le l\le n-1}\left\|r^l\right\|^2 \le T\cdot O(\tau^2 + h^4)^2.$$

By Lemma 6, we obtain $E^n \le O(\tau^2 + h^4)^2$, that is

$$\|e^n\| \le O(\tau^2 + h^4), \quad \|e_{x\bar{x}}^n\| \le O(\tau^2 + h^4).$$

From Eq. (20), we obtain

$$\|e^n\| \le O(\tau^2 + h^4), \ \|e_x^n\| \le O(\tau^2 + h^4),$$

and

$$\|e_{x\bar{x}}^n\| \le O(\tau^2 + h^4).$$

By Lemma 3,

$$\|e^n\|_\infty \le O(\tau^2 + h^4).$$

This completes the proof. ■

Theorem 9: Under the conditions of Theorem 8, the solution u^n of Eqs. (9)–(11) is stable in norm $\|\cdot\|_\infty$.

V. Numerical Experiments

In this section, we present numerical experiments on a test problem to confirm and illustrate the accuracy of our proposed method. The accuracy of the method is measured by the comparison of numerical solutions with exact solutions as well as other numerical solutions from the method in the literature [15] by using $\|\cdot\|$ and $\|\cdot\|_\infty$ norm. The initial condition associated for the Rosenau–RLW equation takes the form:

$$u_0(x) = e^{ln\{(p+3)(3p+1)(p+1)/[2(p^2+3)(p^2+4p+7)]\}/(p+1)}\times \operatorname{sech}^{4/(p+1)}\left[\frac{p-1}{\sqrt{4p^2+8p+20}}(x)\right].$$

TABLE I
COMPARISON OF ERRORS WITH $\tau = 0.1$, $h = 0.25$, $x_l = -60$, AND $x_r = 120$ AT $t = 40$.

	$\|e\| \times 10^{-2}$		$\|e\|_\infty \times 10^{-3}$	
p	Present	Pan&Zhang	Present	Pan&Zhang
2	0.23608	0.78777	0.88670	2.88972
4	0.47254	1.73066	1.81252	6.47969
8	0.46713	1.80583	1.75739	6.66740
16	0.38438	1.37857	1.30630	5.05919

TABLE II
COMPARISON OF ERRORS WITH $\tau = 0.1$, $h = 0.5$, $x_l = -60$, AND $x_r = 120$ AT $t = 40$.

	$\|e\| \times 10^{-2}$		$\|e\|_\infty \times 10^{-2}$	
p	Present	Pan&Zhang	Present	Pan&Zhang
2	0.230294	3.25288	0.086284	1.19460
4	0.447881	7.45173	0.171122	2.78712
8	0.431841	8.03730	0.161891	2.95337
16	0.357253	6.13044	0.118759	2.25471

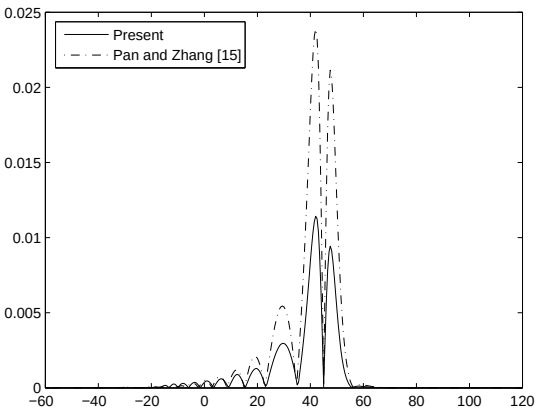

Fig. 1. Absolute error distribution at $p = 4, h = 0.5, \tau = h^2$, and $t = 40$.

For u^1, we employ a two–level method to estimate the solution by

$$(u_i^n)_t - \left(1 - \frac{h^2}{6}\right)(u_i^n)_{x\bar{x}t} + \left(1 - \frac{h^2}{12}\right)(u_i^n)_{xx\bar{x}\bar{x}t} + \left(u_i^{n+\frac{1}{2}}\right)_{\hat{x}} + [(u_i^n)^p]_{\hat{x}} = 0; \quad 1 \le i \le M-1, \ \ 1 \le n \le N-1. \quad (25)$$

We make a comparison between the scheme (9)–(11) and the scheme proposed in [15]. The rate of convergence is computed using two grids, according to the formula:

$$\text{Rate} = \log_2 \frac{\|e_h\|}{\|e_{h/2}\|}.$$

The results in term of errors at $t = 40$, $\tau = 0.1$, and different p, by using $x_l = -60$ and $x_r = 120$, with $h = 0.25$ and $h = 0.5$ are reported in Tables I and II. It is clear that the results obtained by the scheme (9)–(11) are more accurate than the ones obtained by the scheme in [15].

Absolute error distributions for the two methods with $\tau = 0.25, h = 0.5$, and $t = 40$ are drawn at $p = 4$ and 8 in Figs. 1 and 2, respectively. The results obtained by the scheme (9)–(11) are greatly improved when compared to those by the scheme in [15]. It can be easily observed that the maximum

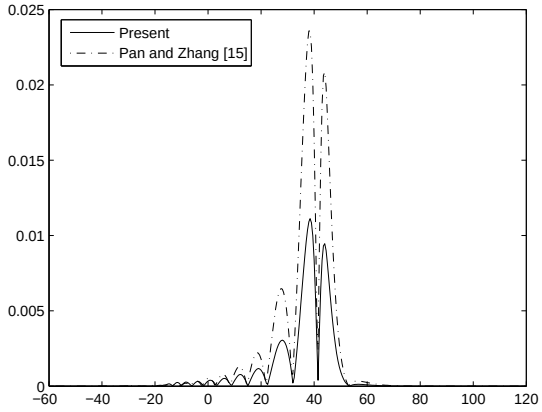

Fig. 2. Absolute error distribution at $p = 8, h = 0.5, \tau = h^2$, and $t = 40$.

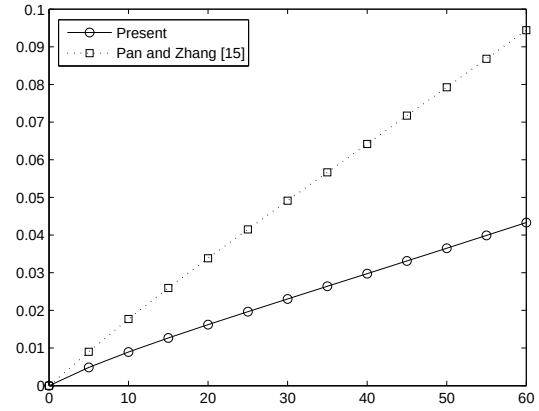

Fig. 3. Error $\|e\|$ versus t at $p = 4, h = 0.5$, and $\tau = h^2$.

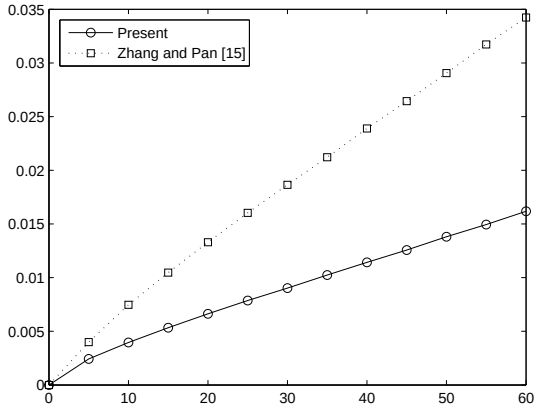

Fig. 4. Error $\|e\|_\infty$ versus t at $p = 4, h = 0.5$, and $\tau = h^2$.

error is taken place around the peak amplitude of the solitary wave and then the scheme (9)–(11) is applied in this area.

Figs. 3–6 show errors at $t \in [0, 60]$ with $\tau = 0.25$, $h = 0.5$, and $p = 4, 8$ by comparing with the Pan&Zhang method [15]. It is observed that both errors increase with time quite linearly but the error of the present method is less than that of the Pan&Zhang method [15].

As shown in Tables III and IV, on one particular choice of the parameters, the estimated rate is close to the theoretically

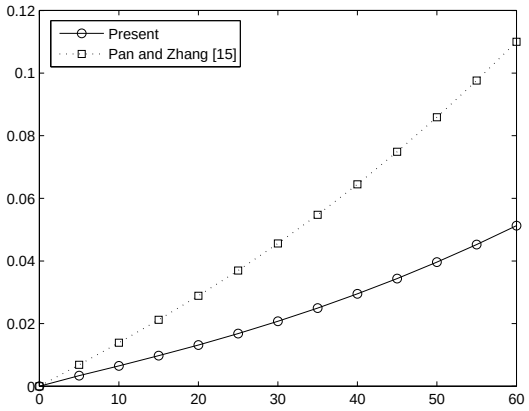

Fig. 5. Error $\|e\|$ versus t at $p = 8, h = 0.5$, and $\tau = h^2$.

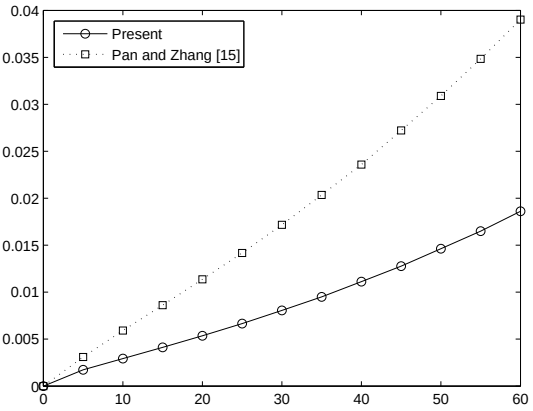

Fig. 6. Error $\|e\|_\infty$ versus t at $p = 8, h = 0.5$, and $\tau = h^2$.

predicted fourth–order rate of convergence. We can also say that when we use smaller time and space steps, numerical values are almost the same as exact values. The CPU time for two methods are listed in Tables III and IV. It can be seen that the computational efficiency of the present method are slightly better than that of Pan&Zhang method [15], in term of CPU time. However, the construction of the novel scheme requires only a regular five–point stencil at a higher time level, which is similar to the standard second–order Crank–Nicolson scheme and Pan&Zhang scheme [15].

As in Tables V and VI, the values of Q^n and E^n at any time $t \in [0, 40]$, which results from the present method, coincide with the theory. The quantities Q^n and E^n seem to be conserved on the average, i.e. they are contained in a small interval but there are fluctuations.

Figs. 7 and 8 show numerical solutions at $t = 200$ with $p = 4$ and 8. The results from the Pan&Zhang method [15] are slightly oscillate at the left side of the solitary wave in case of $p = 8$. However, the results from the present method are almost perfectly sharp in both cases $p = 4$ and 8. From the point of view for the long time behavior of the resolution, the present method can be seen to be much better than the method in [15].

The solitary waves obtained by the present scheme are plotted in Figs. 9 and 10 using $\tau = 0.25, h = 0.5, x_l = -60, x_r = 200$, and $p = 4, 8$. The solitons at $t = 60$ and 120 agree with the soliton at $t = 0$ quite well, which also shows the accuracy of the scheme.

TABLE III
RATE OF CONVERGENCE AND CPU TIME WITH $p = 4$ AND $t = 40$.

	$\tau = 0.25,\ h = 0.5$		
	τ, h	$\frac{\tau}{4}, \frac{h}{2}$	$\frac{\tau}{16}, \frac{h}{4}$
Present			
$\|e\| \times 10^{-2}$	3.20548	0.197080	0.0123084
Rate		4.02369	4.00106
$\|e\|_\infty \times 10^{-2}$	1.22483	0.0752290	0.00469781
Rate		4.02515	4.00123
CPU time (s)	1.153389	12.866165	155.967273
Pan&Zhang			
$\|e\| \times 10^{-2}$	6.41825	1.85385	0.479643
Rate		1.79165	1.95050
$\|e\|_\infty \times 10^{-2}$	2.38960	0.696030	0.180409
Rate		1.77955	1.94788
CPU time (s)	1.251865	13.534488	157.561488

TABLE IV
RATE OF CONVERGENCE AND CPU TIME WITH $p = 8$ AND $t = 40$.

	$\tau = 0.25,\ h = 0.5$		
	τ, h	$\frac{\tau}{4}, \frac{h}{2}$	$\frac{\tau}{16}, \frac{h}{4}$
Present			
$\|e\| \times 10^{-2}$	3.18080	0.194284	0.0121337
Rate		4.03315	4.00108
$\|e\|_\infty \times 10^{-2}$	1.19513	0.0727869	0.00454621
Rate		4.03734	4.00094
CPU time	1.21464	13.868260	174.397644
Pan&Zhang			
$\|e\| \times 10^{-2}$	6.44908	1.99919	0.525426
Rate		1.68968	1.92785
$\|e\|_\infty \times 10^{-2}$	2.35870	0.739615	0.194938
Rate		1.67314	1.92376
CPU time	1.371416	14.862871	175.068007

TABLE V
DISCRETE MASS Q^n.

	$\tau = 0.25,\ h = 0.5$	
t	$p = 4$	$p = 8$
$t = 10$	6.26580620079700	9.74208591413665
$t = 20$	6.26580620078861	9.74208595412127
$t = 30$	6.26580619948382	9.74208578472995
$t = 40$	6.26580617252808	9.74208558745239
$Q(0)$	6.26580620079328	9.74208618205024

TABLE VI
DISCRETE ENERGY E^n.

	$\tau = 0.25,\ h = 0.5$	
t	$p = 4$	$p = 8$
$t = 10$	2.86723006370139	4.73479863443071
$t = 20$	2.86725271321602	4.73481771538282
$t = 30$	2.86726739317968	4.73483391314363
$t = 40$	2.86727839480750	4.73485101919594
$E(0)$	2.86718872840474	4.73477831492679

VI. CONCLUSIONS

The new conservative finite difference scheme for the Rosenau–RLW equation is introduced and analyzed. The present method gives an implicit linear system, which can be easily implemented. This method shows the second– and fourth–order accuracy in time and space, respectively. In

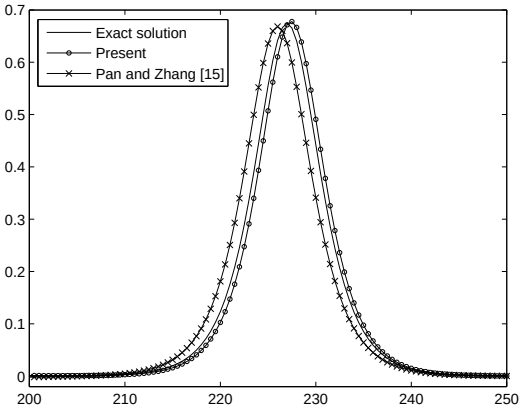

Fig. 7. Numerical solutions at $p = 4, x_l = -60, x_r = 300, h = 0.5$, $\tau = h^2$, and $t = 200$.

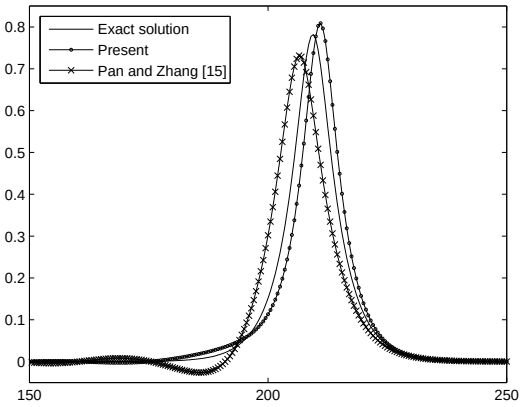

Fig. 8. Numerical solutions at $p = 8, x_l = -60, x_r = 300, h = 0.5$, $\tau = h^2$, and $t = 200$.

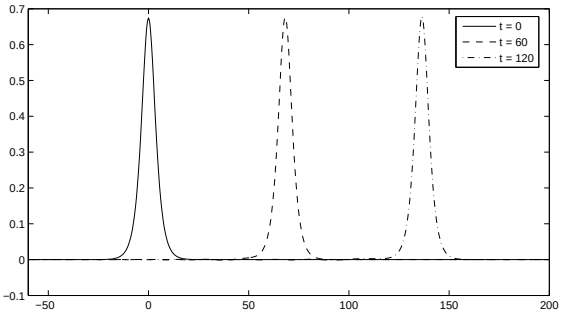

Fig. 9. Numerical solutions at $p = 4$.

addition, the numerical experiments show that the present method supports the analysis of convergence rate.

It is obvious from numerical experiments that the present method, the scheme (9)–(11), gives the well resolution for the Rosenau–RLW equation. It is possible that the solitary wave obtained by this novel method can be smoothed out, at long time, by type of the high–order accuracy.

ACKNOWLEDGMENT

This research was supported by Chiang Mai University.

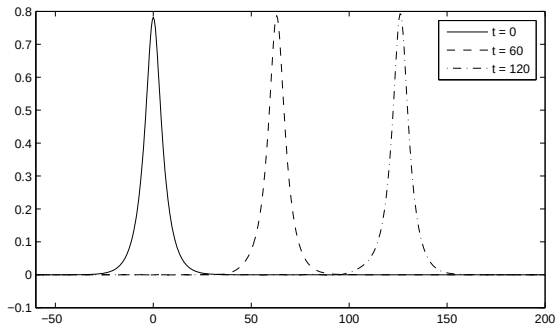

Fig. 10. Numerical solutions at $p = 8$.

REFERENCES

[1] K. Mohammed, "New Exact Travelling Wave Solutions of the (3+1) Dimensional Kadomtsev–Petviashvili (KP) Equation," *IAENG International Jounal of Applied Mathematics*, vol. 37, no. 1, pp. 17–19, 2007.

[2] J.V. Lambers, "An Explicit, Stable, High–Order spectral Method for the Wave Equation Based on Block Gaussian Quadrature," *IAENG International Jounal of Applied Mathematics*, vol. 38, no. 4, pp. 233–248, 2008.

[3] JC Chen and W. Chen, "Two–Dimensional Nonlinear Wave Dynamics in Blasius Boundary Layer Flow Using Combined Compact Difference Methood," *IAENG International Jounal of Applied Mathematics*, vol. 41, no. 2, pp. 162–171, 2011.

[4] A.R. Bahadir, "Exponential Finite–Difference Method Applied to Korteweg–de Vries Equation for Small Times," *Applied Mathematics and Computation*, vol. 160, no. 3, pp. 675–682, 2005.

[5] S. Ozer and S. Kutluay, "An Analytical–Numerical Method Applied to Korteweg–de Vries Equation," *Applied Mathematics and Computation*, vol. 164, no. 3, pp. 789–797, 2005.

[6] Y. Cui and D.-k. Mao, "Numerical Method Satisfying the First Two Conservation Laws for the Korteweg–de Vries Equation," *Journal of Computational Physics*, vol. 227, pp. 376–399, 2007.

[7] D.H. Peregrine, "Calculations of the Development of an Undular Bore," *Journal of Fluid Mechanics*, vol. 25, pp. 321–330, 1996.

[8] D.H. Peregrine, "Long Waves on a Beach," *Journal of Fluid Mechanics*, vol. 27, pp. 815–827, 1997.

[9] P. Rosenau, "A Quasi–Continuous Description of a Nonlinear Transmission Line," *Physica Scripta*, vol. 34, pp. 827–829, 1986.

[10] P. Rosenau, " Dynamics of Dense Discrete Systems," *Progress of Theoretical Physics*, vol. 79, pp. 1028–1042, 1988.

[11] M.A. Park, "On the Rosenau Equation," *Mathematica Aplicada e Computacional*, vol. 9, no. 2, pp. 145–152, 1990.

[12] M.A. Park, "Pointwise Decay Estimate of Solutions of the Generalized Rosenau Equation," *Journal of the Korean Mathematical Society*, vol. 29, pp. 261–280, 1992.

[13] J.-M. Zuo, Y.-M. Zhang, T.-D. Zhang, and F. Chang, "A New Conservative Difference Scheme for the General Rosenau–RLW Equation," *Boundary Value Problems*, vol. 2010, Article ID 516260, 13 pages, 2010.

[14] X. Pan and L. Zhang, "On the Convergence of a Conservative Numerical Scheme for the Usual Rosenau–RLW Equation," *Applied Mathematical Modelling*, vol. 36, pp. 3371–3378, 2012.

[15] X. Pan and L. Zhang, "Numerical Simulation for General Rosenau–RLW Equation: An Average Linearized Conservative Scheme," *Mathematical Problems in Engineering*, vol. 2012, Article I517818, 15 pages, 2012.

[16] X. Pan, K. Zheng, and L. Zhang, " Finite Difference Discretization of the Rosenau–RLW Equation," *Applicable Analysis*, vol. 92, no. 12, pp. 2578–2589, 2013.

[17] N. Atouani and K. Omrani, "Galerkin Finite Element Method for the Rosenau–RLW Equation," *Computers and Mathermatics with Applications*, vol. 66, pp. 289–303, 2013.

[18] R.C. Mittal and R.K. Jain, " Numerical Solution of General Rosenau–RLW Equation Using Quintic B–Splines Collocation Method," *Communication in Numerical Analysis*, vol. 2012, Article ID cna-00129, 16 pages, 2012.

[19] J. Hu, Y. Xu, and B. Hu, "Conservative Linear Difference Scheme for Rosenau–KdV Equation," *Advances in Mathematical Physics* , vol. 2013, Article ID 423718, 7 pages, 2013.

[20] F.E. Ham, F.S. Lien, and A.B. Strong, "A Fully Conservative Second–Order Finite Difference Scheme for Incompressible Flow on Nonuniform Grids," *Journal of Computational Physics*, vol. 177, pp. 117–133, 2002.
[21] Y. Zhou, "Application of Discrete Functional Analysis to the Finite Difference Method," *Inter. Acad. Publishers*, Beijing, 1990.